

THE VICTORIA UNIVERSITY OF MANCHESTER

INSTITUTE OF SCIENCE AND TECHNOLOGY

ULTRASONIC INSPECTION OF CONCRETE STRUCTURES TO DETECT
THE CONDITION OF EMBEDDED STEEL COMPONENTS

BY WALID TAHA DAMAJ

A THESIS SUBMITTED TO

THE VICTORIA UNIVERSITY OF MANCHESTER

FOR THE DEGREE OF

DOCTOR OF PHILOSOPHY

DEPARTMENT OF CIVIL AND STRUCTURAL ENGINEERING

UNIVERSITY OF MANCHESTER

INSTITUTE OF SCIENCE AND TECHNOLOGY

JUNE, 1990

TO MY WIFE NADA AND MY CHILDREN RAYAN AND TAHA

ABSTRACT

Analytical and laboratory studies of stress wave propagation have been carried out to develop a basis for a nondestructive test method to detect corrosion and flaws in embedded steel components in reinforced and prestressed concrete. The technique, which is referred to as the indirect method or the pitch-catch technique, involves introducing an ultrasonic signal into a test object by an ultrasonic transducer, and monitoring the reflections of the signal from internal or external boundaries such as bar/concrete or concrete/air interfaces or from defects such as corrosion or flaws, using other ultrasonic receivers located close to the radiator.

A ray tracing model using computer synthesis has been developed to simulate basic aspects of the effect of the embedded bar or component size, its depth in the material, surface condition i.e. sound, corroded, or cracked, and transducer frequency, on the signals received from the reinforcement embedded in concrete. The model has been verified by comparison with experiments from water and concrete samples. This study demonstrates the power of using computer modelling for prediction of the amplitude of the reflected signals from bars of different sizes and surface conditions embedded in a material.

Equations have been derived to predict the attenuation of signals from bars embedded in concrete with different surface conditions and sizes. Moreover the attenuation of ultrasonic signals in concrete has been studied. An equation has been derived from experimental results to estimate the attenuation loss due to scattering and absorption for high strength concrete.

Laboratory results have been presented. Successes achieved in the laboratory suggest that the pitch-catch method has the potential to become a reliable field technique for detecting corrosion and flaws within concrete structures.

The development (instrumentation and signal processing) of an experimental pitch-catch technique for finding corrosion and flaws within reinforced concrete has been described. This enabled proposals for a prototype testing system to be put forward. The key features of the technique are as follows:

- 1- Five rolling transducers, pulser, and a signal analyser are required.
- 2- Application of the digital filtering technique where the received time signals from a scan carried out on a concrete beam are transformed to the frequency domain, then application of a brick-wall filter on the FFT to leave a chosen frequency bandwidth, and then IFFT of the filtered signal. The energy trend of the scan after filtering is carried out.

ACKNOWLEDGEMENTS

The work described in this thesis was carried out in the Structural Assessment Group, Department of Civil and structural Engineering of the University of Manchester, Institute of Science and Technology.

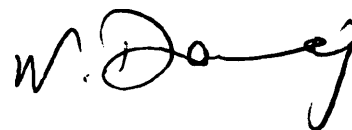
I would like to express my sincere gratitude to my supervisor Professor F.M.Burdekin for his advice, guidance, and encouragement during the process of this work.

The author wishes to thank Dr. P.Gaydecki for his help and with whom he had constructive discussions.

The author would like to thank Mrs. Grieve Mkandawire for her help in typing this thesis.

DECLARATION

No portion of the work referred to in this thesis has been submitted in support of an application for another degree or qualification of this or any other university or other institution of learning.

A handwritten signature in black ink, appearing to read 'W. T. Damaj', written in a cursive style.

W.T. DAMAJ

June, 1990.

CONTENTS

	Page
ABSTRACT	i
ACKNOWLEDGEMENTS	ii
DECLARATION	iii
CONTENTS	iv
<u>CHAPTER 1: INTRODUCTION</u>	<u>1</u>
1.1- GENERAL	1
1.2- PRODUCTION OF WIRE AND STRAND	2
1.2.1- Chemical composition of the Steel	3
1.2.2- Heat Treatment-The Patenting Process	4
1.2.3- Wiredrawing	5
1.2.4- Production of Bar	7
1.3- REVIEW OF TYPES OF DESIGN	7
1.4- FORMS OF CORROSION OF STEEL IN CONCRETE	8
1.4.1- Reports on Bridge Corrosion	8
1.4.2- Corrosion	12
1.4.3- Causes of Reinforcement Corrosion in Bridges	17
1.5- OBJECTIVES AND SCOPE OF RESEARCH	22
1.5.1- Objectives	22
1.5.2- Scope	23
<u>CHAPTER 2: NONDESTRUCTIVE TESTING TECHNIQUES</u>	<u>30</u>
2.1- INTRODUCTION	30
2.2- MAGNETIC METHODS	31
2.3- ELECTROCHEMICAL METHODS OR IMPEDANCE MEASUREMENTS	33
2.4- CHEMICAL METHODS	41
2.5- RADIOGRAHIC TECHNIQUES	42
2.6- SURFACE INSPECTION	42
2.7- RADAR	43
2.8- THERMOGRAPHY	44
2.9- EDDY CURRENT METHODS	45

	v
2.10- VIBRATION MONITORING TECHNIQUES	45
2.11- STRESS WAVE METHODS	46
2.11.1- Introduction	46
2.11.2- Test Methods	47
2.11.3- Through-Transmission Method	48
2.11.4- Echo methods	48
2.11.5- Resonance Method	49
2.11.6- Past Applications	50
2.12- ACOUSTIC EMISSION	60
2.13- OTHER TECHNIQUES	61
2.14- SUMMARY	63
<u>CHAPTER 3: BACKGROUND TO WAVE PROPAGATION IN SOLIDS</u>	72
3.1- INTRODUCTION	72
3.2- BASIC PRINCIPLES OF ELASTIC WAVE PROPAGATION	72
3.2.1- Wave Types	72
3.2.2- Wave Velocity	73
3.3- REFLECTION AND REFRACTION	75
3.3.1- Diffraction at a Crack Tip	81
3.3.2- Attenuation and Divergence	82
3.4- TRANSDUCERS FOR TRANSMITTING AND RECEIVING WAVES IN ULTRASONICS	84
<u>CHAPTER 4: TECHNIQUES USED FOR SIGNAL PROCESSING</u>	97
4.1- INTRODUCTION	97
4.2- PAST APPLICATIONS OF SIGNAL PROCESSING	99
4.3- TIME DOMAIN FUNCTIONS	104
4.3.1- Squaring	104
4.3.2- Differentiation	105
4.3.3- Phase Shifting or Delay	105
4.3.4- RMS, Energy, and Mean Calculations	105
4.3.5- Addition, Subtraction, and Multiplication of Two or Group of Signals	106
4.3.6- Signal Averaging or Noise Reduction	107
4.3.7- Correlation	109
4.4- FREQUENCY DOMAIN ANALYSIS	111
4.4.1- Fast Fourier Transform and its Inverse	112
4.5- DIGITAL FILTERS	114
4.5.1- Brick-Wall Filter	115
4.6- SUMMARY	115

<u>CHAPTER 5: ATTENUATION OF WAVES IN RODS</u>	127
5.1- INTRODUCTION	127
5.2- VARIATIONS OF ULTRASONIC PULSE VELOCITIES IN CYLINDRICAL RODS	128
5.3- ATTENUATION OF WAVES IN BARS	131
5.4- EXPERIMENTAL INVESTIGATION	133
5.4.1- High Frequency Testing	133
5.4.2- Low-Frequency Testing	136
5.5- MECHANICAL ANALYSIS	140
5.6- SUMMARY	142
<u>CHAPTER 6: ATTENUATION OF SOUND IN CONCRETE</u>	153
6.1- INTRODUCTION	153
6.2- ATTENUATION OF ULTRASONIC WAVES IN CONCRETE	153
6.2.1- Scattering	154
6.2.2- Absorption	156
6.2.3- Summary	158
6.3- EXPERIMENTAL ATTENUATION ANALYSIS	159
6.3.1- Group One Experiments	160
6.3.2- Group Two Experiments	163
6.4- SUMMARY	166
<u>CHAPTER 7: ACOUSTIC SCATTERING BY CYLINDRICAL BARS EMBEDDED IN CONCRETE</u>	171
7.1- INTRODUCTION	171
7.2- SIGNAL LOSSES	172
7.3- ESTIMATED SIGNAL ATTENUATION FROM A BACK-WALL ECHO	174
7.4- ESTIMATED SIGNAL ATTENUATION FOR A SOUND CYLINDRICAL BAR EMBEDDED IN CONCRETE	176
7.5- ESTIMATED SIGNAL LOSSES FOR A CORRODED BAR EMBEDDED IN CONCRETE	178
7.6- DISCUSSION	182
7.7- COMPARISON WITH EXPERIMENTS	184
7.8- SUMMARY	185

<u>CHAPTER 8: COMPUTER MODEL USING RAY ACOUSTICS</u>	196
8.1- INTRODUCTION	196
8.2- REVIEW OF SOME OF THE METHODS USED IN COMPUTER MODELLING OF ULTRASONIC WAVES IN SOLIDS	197
8.3- APPLICATION OF THE RAY THEORY	199
8.4- RAY ACOUSTICS	204
8.5- GOVERNING EQUATIONS	205
8.6- APPROACH	209
8.6.1- Estimation of the Amplitude of the Back-Wall Echo	210
8.6.2- Estimation of the Amplitude of the Bar Echo	211
8.6.3- Construction of the Time Signal	214
8.7- RESULTS	214
8.7.1- Material with No Embedded/ Immersed Steel Bars	215
a- Water Model	215
b- Concrete Beam Model	216
8.7.2- Beam with Reinforcement	217
a- Sound Bar Immersed in Water	218
b- Sound Bar Embedded in Concrete	219
c- Corroded Bar Embedded in Concrete	221
d- Cracked Bar Embedded in Concrete	222
8.8- CONCLUSIONS	223
 <u>CHAPTER 9: EXPERIMENTAL DETAILS</u>	 246
9.1- INTRODUCTION	246
9.2- MATERIALS	246
9.3- TEST SPECIMENS	248
9.4- MIXING	252
9.5- TYPE OF MIXES	253
9.6- COMPACTION	253
9.7- CURING	253
9.8- WORKABILITY	254
9.9- TECHNIQUES USED IN TESTING	254
a- The Impact Technique	254
b- Pulse-Echo Technique	255
c- Laser-Generation Acoustic Waveforms	259
d- Transit-Time or Pitch-Catch Method	261
9.10- FREQUENCIES USED IN THIS RESEARCH	262
9.11- PULSERS	264

9.12- SCOPES USED	265
9.13- AMPLIFIER	267
9.14- DATA STORAGE AND COMPUTER PROGRAM FOR SIGNAL PROCESSING	267
9.15- THE ANALOGIC WAVEFORM ANALYSER, MODEL 6100	271
9.16- SUMMARY	272

CHAPTER 10: WATER MODEL 285

10.1- INTRODUCTION	285
10.2- EXPERIMENTATION	285
10.3- MODES OF ANALYSIS	288
10.4- DISCUSSION	289
10.4.1- Good Steel v Steel Cut between Transmitter and Channel B	289
10.4.2- Good Steel v Steel Cut under Right hand Edge of the Transmitter	290
10.4.3- Good Steel v Cut and Axially Rotated through 90°, Midway between Transmitter and Channel B	291
10.4.4- Good Steel v Force-Corroded bar	291
10.4.5- Good Steel v Naturally Corroded Bar	292
10.4.6- Scanning of the Corroded Bar	293
10.4.7- Water with Aggregate alone	294
10.4.8- Clear Water with Good Bar v Water with Aggregate and Good Bar	294
10.4.9- Scanning of Force-Corroded Bar with Aggregate	295
10.4.10- 4-Channel System in Water	295
10.4.11- Low Frequency Analysis	296
10.5- SUMMARY	297

**CHAPTER 11: IMPLEMENTATION OF THE INDIRECT METHOD FOR
DETECTION DEFECTS IN REINFORCEMENT EMBEDDED
IN CONCRETE** 314

11.1- INTRODUCTION	314
11.2- DEVELOPMENT OF A MEASUREMENT TECHNIQUE	314
11.2.1- Transducers and Frequency Aspects	314
11.2.2- Pulsers	316
11.2.3- Oscilloscopes	316
11.2.4- Analyser	316
11.2.5- Concrete Specimens	317
11.2.6- Amplification	317
11.2.7- Multiplexer	318
11.2.8- Signal Acquisition and Processing	318
11.3- EXPERIMENTATION ON MORTAR SAMPLES	320
11.3.1- Summary	324

11.4-	EXPERIMENTATION ON CONCRETE	324
11.5-	EXPERIMENTATION ON SLABS WITH AND WITHOUT SIMULATED CRACK	333
11.6-	EXPERIMENTATION ON DUCTED SAMPLES	334
11.7-	CONCLUSIONS FROM SMALL-SCALE LABORATORY TESTS	336
11.8-	APPLICATION OF DIGITAL FILTERING TECHNIQUES TO A SYSTEM FOR FLAW AND CORROSION DETECTION	338
11.9-	EXPERIMENTAL WORK USING MULTIPLE RECEIVING TRANSDUCERS	341
11.9.1-	Scanning the Large Scale Test Beam	341
11.10-	EXPERIMENTAL WORK USING THE DIGITAL FILTERING TECHNIQUE	344
11.10.1-	Detection of Steel Bar in a Concrete beam	344
11.10.2-	Detection of Steel Bar in a Grouted Duct	345
11.10.3-	Detection of a Void in a Ducted Concrete Beam	346
11.10.4-	Detection of a Flaw in the Large Scale Test Beam	347
11.10.5-	Using Rolling Transducers to Scan the Test Beam	349
11.11-	PROPOSAL OF A SYSTEM FOR FLAW AND CORROSION DETECTION	353
11.12-	CONCLUSIONS	355
<u>CHAPTER 12: SUMMARY, CONCLUSIONS, AND FUTURE RESEARCH</u>		390
12.1-	SUMMARY	390
12.2-	CONCLUSIONS	392
12.2.1-	Theoretical Studies	392
12.2.2-	Experimental Studies	394
12.3-	FUTURE RESEARCH	396
REFERENCES		399

CHAPTER 1

INTRODUCTION

1.1- GENERAL

Reinforced concrete for main structural bridge members, such as girders and pilings, has been in use as a standard construction material since the earliest rural highway bridges. Prestressed concrete, a comparatively recent innovation, has found increasing use over the past 35 years or so. The widespread use of prestressed concrete construction and the fact that instances have been reported in which the prestressing steel has deteriorated thereby critically affecting the structural strength has placed increasing emphasis on the implementation of adequate, routine inspection of these structures. Since present methods for examining and ascertaining the condition of the reinforcing steel are at best marginal and many times completely inadequate (1), therefore this research was aimed at developing a basis for a nondestructive test method for finding flaws caused by corrosion within concrete and for detecting deterioration in the steel of reinforced and prestressed concrete bridge members using stress waves. Proposals for a prototype testing system are put forward based on digital filtering technique at the end of this work.

Corrosion can arise in most parts of a bridge substructure or superstructure and often results from the use of de-icing salts in countries where subzero temperatures occur in winter.

Substructure corrosion is often associated with leaking joints, faulty drainage or salt spray from traffic. In reinforced concrete bridges, corroding reinforcement has been found in decks, soffits, beams, parapets and columns. In columns, piers, beams, parapets and soffits, corrosion is usually of the type designated as general; general corrosion occurs continually over substantial areas of reinforcement with metal loss evenly distributed over the circumference of the bar and the corroding area. General corrosion often produces extensive rust staining in the concrete as a consequence of the large total metal loss and the properties of the corrosion product, i.e. hydrated ferride oxide ($\text{Fe}_2\text{O}_3 \cdot x\text{H}_2\text{O}$) (2).

Localized corrosion may occur in bridge decks and in substructure concrete near leaking expansion joints. This is characterized with occurrence of uncorroded and pitted reinforcement. The substantial reduction in cross section of the bars can sometimes be as high as 100%.

1.2- PRODUCTION OF WIRE AND STRAND

The production of prestressing wire started in the UK in the early 1940s and the first prestressing strand was made in 1953 (3).

The stages of production are shown schematically in fig.1.1. The raw material is hot-rolled carbon steel rod in diameters between 5.5 and 13.5mm. The object of the wire manufacturer is to heat

treat and cold work this material to achieve a combination of properties which will be most suitable for the purpose for which the wire is to be used. This result is obtained by an appropriate combination of three factors:

-The chemical composition of the steel, particularly the carbon content.

-The heat treatment and quench given to the rod before drawing, to achieve a metallurgical structure which will yield the best possible combination of properties in the final product.

-The amount of cold work, that is the total reduction in area from the rod or last heat treatment stage to the final wire size.

These factors are common to any carbon steel wire production, but for prestressing wire there is an additional requirement of a final treatment to enhance elastic properties.

Prestressing strand is manufactured by spinning together a number of wires and the production of the wires is governed by the same three factors, taking into account the properties which will exist after (a) the mechanical deformation of the stranding process and (b) the effect of the final treatment of the whole strand. A point should be made that prestressing strand is not made from prestressing wire.

1.2.1- Chemical composition of the Steel

The requirements of strength determine the composition of steel, as far as the carbon content is concerned, which should be at

least 0.6%. Alloying elements may be useful for certain desirable properties. Manganese is naturally present in the ore and small additions of this element can bring it to the desired level and will enhance the strength of steel. Therefore, all prestressing steel which usually contains about 0.7% of manganese should be classified as high-carbon, low-alloy steel, and steel containing only carbon and a nominal percentage of manganese is referred to as a carbon steel. Even with proper ingredients steels do not have the desired high strength in their annealed state, there are two ways to increase their strength- heat treatment and cold working, most high strength steels are made by combination of these two processes. Steel recommended by British Standards (BS) for prestressing wires has the following chemical composition:

carbon	0.72-0.93 %
manganese	0.42-1.1 %
phosphorus	0.04 max
sulphur	0.05 max
silicon	0.10-0.35 %

1.2.2- Heat Treatment-The Patenting Process

The initial heat treatment process is universally known as patenting. It consists in heating the rod to a sufficiently high temperature to obtain a homogeneous mixture or solid solution of the iron carbide and iron, described as austenite. When the steel is cooled under controlled condition, the constituents of the structure will separate from the austenite in a fine condition. Although the manganese and residual alloy content have some

effect on the structure, in relation to the sizes of material considered here, it is sufficient to consider only the carbon content. As shown in the simplified phase diagram (fig.1.2) as the steel cools slowly ferrite (iron) first separates from austenite and at a temperature of about 720°C the remaining austenite is transformed into pearlite, consisting of alternate plates of iron and iron carbide. With a carbon content of about 0.86 per cent there is no ferrite at the grain boundaries, but as the carbon content falls increasing amounts of ferrite appear until complete envelopes exist around the pearlite grains. The thinner the plates of iron carbide the better is the strength and the ductility in cold working. The cooling of the steel at an appropriate rate is therefore a critical part of the patenting process. A sufficiently rapid rate of small sizes of rod may be achieved in air, when the process is known as air patenting. With large size rods, used in the production of prestressing steel the required structure is obtained by rapid cooling to a temperature of about 500°C followed by a delay in further cooling until the desired metallurgical transformation has occurred (3). This is achieved by quenching in molten lead or molten salt baths. The former is called lead patenting.

1.2.3- Wiredrawing

The third factor in achieving strength and desired properties is the cold working process of wiredrawing. In this the rod is drawn through a hard metal die (tungsten carbide), specially shaped to squeeze the steel in a uniform manner down to a smaller size. The traction of wiredrawing is provided by a capstan on to which

the wire is wound after leaving the die.

As already indicated, the tensile strength of the wire increases significantly as wire drawing proceeds. An average relationship for high carbon steels is given in table 1.1, and table 1.2 gives the specifications for different wire and strand diameters.

The production so far described is generally applicable to any class of carbon steel wire; but there are some further aspects specific to prestressing wire. The work which takes place in wire drawing generates a considerable amount of heat. The dies are therefore contained in water-cooled jackets, the capstans on which the wire is wound have internal water cooling and air passes over the outside. The best combination of all mechanical properties is obtained when the wire is kept as cool as possible. Wire is straightened by mechanical deformation or by a hot stretching process. The straightness and final heat treatment lead to high elastic properties and reduce relaxation.

For many uses under adverse conditions, carbon steel wire is coated with zinc, either by running through a bath of molten zinc or an electrolytic cell to provide a plated coating. Greased and plastics coated tendons are finding increasing use in certain applications. An adherent grease is applied to the wire or strand and the whole finally covered with a plastic sheath by an extrusion process.

1.2.4- Production of Bar

The raw material is steel in billet form. After inspection the billets are reheated to a controlled temperature and hot rolled, with the rolling conditions designed so that as the bar leaves the last rolls the temperature is at the correct stage in the cooling cycle to give a fine pearlite structure.

The bars are next cold worked by stretching to approximate e.g. 90% of the characteristic load. The stretching machine is equipped with a load cell and means of measuring the elongation. Finally, the bars are inspected for surface finish and rolling defects, and then they are machined at each end for a length slightly greater than that required for the thread.

1.3- REVIEW OF TYPES OF DESIGN

The principles of reinforced and prestressed concrete design are shown in fig.1.3. Pre-stressed concrete bridge decks may be divided into two basic categories: pre-tensioned and post-tensioned. In each case the deck may be a variety of cross-sectional shapes and those comprising post-tensioned structures may include multiple spans.

Pre-tensioned beams are widely used throughout the world as standard factory made pre-cast units in which the tendons are stressed between fixed anchorages and the concrete beam is then cast around them and allowed to harden before the external stressing force is removed. As the tendons attempt to contract on

removal of the external force, the concrete is compressed. In this kind of prestressing, the tendons are mainly placed at the bottom of the beam cross section, and additional steel reinforcement is added to carry any shear or lateral tension forces. Different shapes of pre-tensioned beams are used such as rectangular, I, or T shapes.

In post-tensioned beams, ducts are cast into the concrete beam following the required tendon profile, which depends on the bending moment. When the concrete has hardened, tendons are threaded through the ducts, tensioned by external jacks, and the full tension force of the tendons is tensioned by external jacks. The full tension force of the tendons is locked off at the end anchorages, and then, usually cement grout is pumped into the ducts to encase the stressed tendon totally when the grout hardens.

1.4- FORMS OF CORROSION OF STEEL IN CONCRETE

1.4.1- Reports on Bridge Corrosion

Prestressed concrete is an extremely durable material. A survey of some 14000 prestressed concrete bridges in the USA (4) showed that only ten exhibited any evidence of steel tendon corrosion. The half dozen or so isolated failures which first caused concern about the susceptibility of prestressing wire to stress corrosion (hydrogen embrittlement) were reviewed (5) in 1965. It was established that this type of failure occurred due to the combination of tensile stress with a flaw in the steel in a

corrosive environment. It was thought that, as the fracture is of a progressive inter-crystalline type starting from micro-cracking, the coarser grained quenched and tempered steels were more susceptible than patented wires, or more generally pearlitic steel. Another analysis of 63 cases of damage reported from various countries (6), gave the following principal conclusions:

-Fracture of the tendon occurred in 55 cases, 40 of them being of the brittle type.

-In 38 cases the wire fractured within one year, 28 of them before concreting.

-In very few cases could damage be attributed to one cause alone, the most corrosive substances were chlorides and sulphur compounds.

-In 13 cases there was some defect in the steel. Of these, two were in wire tensioned through a die on site and four were quenched and tempered steel which is not produced in the UK.

Out of 110 000 structures recorded in a survey for the FIP Durability Commission (7), the incidents reported by the UK included:

5 wire corrosion due to insufficient cover

50 end block failures

10 of corrosion due to incomplete grouting

20 due to frost damage.

The 42 cases of damage to Canadian bridges were all attributed to de-icing salts.

Vassie (8) carried out an investigation on the grouting of twelve post-tensioned prestressed concrete bridges built between 1958 and 1977. Ten of these structures were examined in-situ and the other two had been demolished. Voids were found in ten of the bridges including the most recently built structure. It was showed that some ducts were not completely sealed from the atmosphere.

Other cases reported where corrosion was the cause of deterioration are:

-Thana Creek, India: Thana creek is north of Bombay, it was built between 1963 and 1972. The deck is precast prestressed concrete T-beams, jointed longitudinally and transversely prestressed. The beams are 35m long to give 362m spans, increased by using V-piers in the navigation area. During an inspection of the bridge in 1981 it was noticed that some of the beams had developed longitudinal cracks with spalling of the concrete in places. The prestressing tendons had corroded and some wires had broken. It was not possible to determine the residual strength of the beams but strengthening and repair work was carried out as a precaution using epoxy resin and external cables.

-Somerset, Watford, Bermuda: A bridge was built in 1967 as a replacement for the existing steel superstructure. It consisted of seven simply supported spans, maximum length 21.5m of precast prestressed concrete T-beams with the flanges forming the road slab. The beams were post-tensioned longitudinally using

preformed steel-sheathed cables in a parabolic profile and transversely by straight cables in the flanges. After about 15 years, the steel tendons and reinforcement of one span, where the beams were continually splashed by sea water, had corroded very badly and since it was not possible to determine how many tendons were still intact, the bridge had to be closed to traffic. It was eventually replaced completely.

-Suspension bridge, USA: A suspension bridge in the USA with a main span of 488m carries both road and rail traffic. It was opened in 1903. The main cables are formed from parallel 5mm diameter high tensile steel wires, not galvanised but originally canvas wrapped and infilled with a graphite oil compound. By 1918 the wire had begun to rust and between 1918 and 1922 the canvas was replaced by wire wrapping but corrosion has continued since. At present the whole of the superstructure is in poor condition and although investigations have been carried out, the present safe capacity of the 500mm approximate diameter main cables is not known precisely.

-Braidley Road Bridge, England: This is a post-tensioned concrete box girder bridge built between 1970 and 1972 with the stressing provided by 121-19 wires/28mm diameter tendons. These are described as being external because they lie beside and not within the decks of the nine longitudinal webs. Within a year of the bridge being opened individual broken wires were discovered and the deterioration subsequently accelerated leading to complete failure of one 19 wire tendon. Metallographic examination of fractured wires identified stress corrosion as the

cause of failure.

-Ynsyguas Bridge, Wales (9): Most recently the sudden collapse, in Nov. 1985 of the Ynsyguas bridge, South Wales, UK (built 1955), caused concern and emergency checks to be made of the 600 pre- or post-tensioned bridge structures built during the past 20 years in the UK. The main break was at mid span and was attributed to corrosion by de-icing salt of the post-tensioning cables which linked together the nine precast I sections forming the main longitudinal structural members. Each beam was post-tensioned by 5 cables using the Freyssinet system of tensioning.

-Taff Fawr Bridge, Wales (9): Taff Fawr bridge, built 1960-1965 crosses the river Taff at height of 110 feet and has an overall length of 470 feet. Construction of the bridge deck is continuous over 3 spans. The deck is in the form of a multicell box girder with precast webs and cast-in-situ top and bottom slabs. Joints between the pre-cast units were prestressed together by single 1 inch diameter strands. Strands were also provided in the top of the deck to counteract hogging and in the bottom of the deck to counteract sagging live loads. Severe corrosion of the pre-stressing tendons due to the penetration of the concrete cover by de-icing salt led to gross weakening of the 21 year old structure. Damage was so extensive that demolition of the entire bridge including supporting piers was considered.

1.4.2- Corrosion

Corrosion is usually defined as the loss of metal by chemical or

electrochemical reaction with its environment. Various types of corrosion have been recognized and are classified in several ways. A simple way to classify corrosion is by the effect on the metal, as general or localized.

-General Corrosion

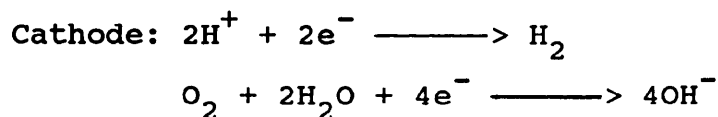
This is the uniform diminution of a metal by chemical attack. Such attack requires that ideally every atom in the exposed surface be equally sensitive to the corrosive environment and that the medium have uniform access to all surface atoms.

-Localized Corrosion

As the surface of metals and corrosive environments are seldom homogeneous, the attack will usually not be uniform but will be localized. For example in the corrosion of steel:

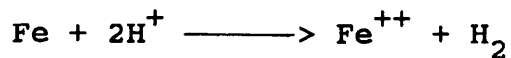


Fe is the iron atom, Fe^{++} the iron ion and 2e^{-} represents two electrons which are freed. The iron ions pass into solution and the electrons, the negative product of ionization, flow along the metallic connection to the cathode until equilibrium is achieved or the circuit is broken. Therefore there is loss of metal from the anode. Two important reactions may occur at a cathode:

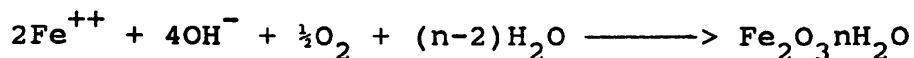


Both of these make use of the electrons and both render the electrolyte more alkaline in the vicinity of the cathode.

The first reaction (fig.1.4.a) requires a supply of hydrogen ions and therefore occurs mainly in an acid electrolyte. The hydrogen ions H^+ are protons and can penetrate steel especially at high temperatures or where the steel is under high tensile stress. When they associate with electrons to form molecular hydrogen there is an increase in volume with the tendency to disrupt or blister the steel. This is the phenomenon known as hydrogen embrittlement which is one particular form of stress corrosion, It is a complex phenomenon and not fully understood (10). The reaction can be written as:



The second reaction (fig.1.4.b) which is perhaps the most common reaction encountered in the rusting of steel occurs mainly in alkaline conditions and is set up by a local concentration of oxygen, for example, in a crevice or under a deposit on the metal. This is known as an oxygen cell. Oxygen at a cathode accelerates corrosion but oxygen at an anode tends to form an insoluble layer of iron oxide (rust) which arrests corrosion. This reaction can be written:



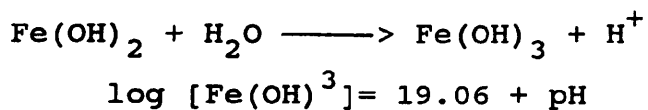
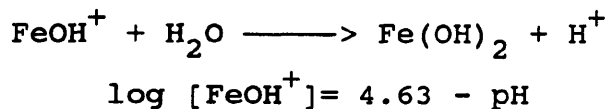
The metal surface is then said to be passivated. In the alkaline

environment (pH about 12) provided by good dense concrete or grout, embedded steel develops a passive layer which protects it against corrosion.

Two diagrams are usually used to show the corrosion behaviour:

1) The Pourbaix Diagrams (fig.1.5): The corrosion behaviour of a metal depends on electrical potential and may be affected by passivity, Pourbaix diagrams show how this behaviour depends on the potential E and pH together.

pH may be regarded as a definition of environment, pH=7 is neutral, pH<7 is increasingly acid, pH>7 is more alkaline, and electrode potential as an indication of the circumstances of exposure. More positive values of electrode potential arise under more oxidizing conditions or by contact with metals that are more corrosion resistant. However, reducing conditions such as lack of dissolved oxygen or contact with a more easily corroded metal bring a change of potential in a negative condition. In the highly alkaline environment of the steel/cement interface the corresponding reactions of interest and their respective pH dependences on solubility are (11):



2) Tafel Diagrams (fig.1.6): In active cells, a net corrosion current flows at each electrode surface. In this case potential-current (often known as potential-log(i)) diagrams known as Polarization diagrams or Tafel diagrams are used. Fig.1.6 illustrates the typical behaviour of a metal.

The situations described above occur as a result of inhomogeneities in the steel, the concrete or the grout or due to the presence of chloride or other salts in solution. Chloride, sulphide, sulphate and carbonate tend to lower the alkalinity of the concrete ($\text{pH} < 7$) and make electrolyte action possible.

Other examples of localized corrosion in concrete:

-Stress differences may be sufficient to provide a potential difference and in the presence of an electrolyte a cell is produced.

-Similar conditions may exist because of a difference in environment at adjacent zones in a length of steel, for example liquid/air interface or even a liquid/solid interface. The implications of this in a badly grouted duct are obvious.

-With steel under high stress the attack may be extremely localized and probably because the stress opens the corrosion pits, there may be very rapid penetration of the steel, encouraged by a potential difference within the developing crack due to stress differences and environment variation between top and bottom (12).

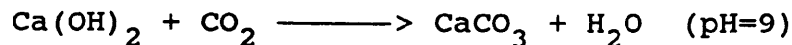
1.4.3- Causes of Reinforcement Corrosion in Bridges

The causes of reinforcement corrosion can be subdivided into chemical and physical effects. The most important substances which depassivate steel in concrete are chloride salts and carbon dioxide.

-Carbonation

Concrete in bridges is exposed to atmospheric carbon dioxide and also near industrialized regions to sulphur dioxide. With water, these form acidic gases which neutralize the alkalis in the concrete from exposed surfaces. The neutralization reaction lowers the concrete pH from about 13 to 9, and this depassivates the steel in concrete affected so that corrosion can proceed at a rate limited only by the access of moisture and/or oxygen through the concrete matrix.

The reaction is:



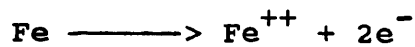
The rate of this reaction depends mainly on the permeability of the concrete.

-Chlorides

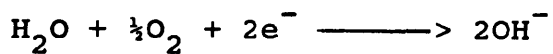
The main source of the chloride found in bridges is rock salt used for de-icing roads. Winds carrying chlorides at marine sites

are another source. In some older concrete construction, chlorides (calcium chlorides) were added as agent accelerating hardening, particularly for precast units, but this now banned. Reinforcement corrosion occurs when the passivation film over the steel surface is destabilised by the presence of chloride ions, which reduce its pH level. In addition, the concentration of these chloride ions is likely to vary, thus producing electropotential differences, the basis of an active electrochemical cell. In this cell, the concrete acts as the electrolyte, with current flowing from those parts of the steel at highest potential to those lowest. The more anodic steel corrodes, while the more cathodic does not.

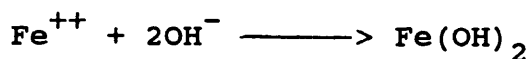
The anodic (oxidation) part of corrosion takes the form of the reaction



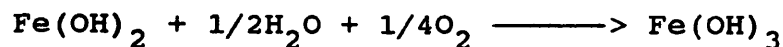
Since the medium is exposed to the atmosphere it contains dissolved oxygen. Water and seawater are nearly neutral, and thus the cathodic (reduction) part of the reaction is:



Remembering that chloride ions do not participate in the reaction, the overall reaction is:



Ferrous hydroxide precipitates from solution. However this compound is unstable in oxygenated solutions and is oxidized to the ferric salts:



And finally cracking and spalling of the concrete occurs which is caused by hoop stresses due to the buildup of solid corrosion products in the concrete adjacent to the metal surface (13).

-Macro-cells

A complication for steel components in concrete is that the steel is situated in a non-uniform environment. For example, for steel tendons in ducts, the ducts may be non-uniformly filled with grout, hence inducing zones where different moisture and oxygen levels can occur. For steel tendons embedded directly into pre-tensioned slabs, the depth of carbonation or chloride penetration may not be uniform across the whole slab. In these cases macro-cells are easily set up where a small anodic area, where the steel is preferentially oxidised, is driven by a much larger cathodic area, where the oxygen reduction process predominates. In these cases even though there is only limited oxygen reduction or moisture available, the macro-cell effect can cause severe corrosion in small areas. This is often observed as macro pitting i.e. intensive corrosion in local areas on wire rods or tendons, at the interface between different environmental conditions. For tendons in ducts the corrosion will occur at areas where there is little or no grout, acting as anodes, with the oxygen reaction

occurring in the areas which are fully grouted, acting as cathode.

-Concrete Cracking

Cracks in concrete arise from numerous causes and include plastic shrinkage a few hours after casting, long term thermal cracks and shrinkage, loading in service, corrosion and alkali-aggregate reactions. However, when cracks develop, the stress in the concrete at the crack sides decreases to zero whilst the stress in the reinforcement increases. In the case of cyclic loading, this could initiate corrosion fatigue in the steel. Cracks in concrete can increase the possibility of corrosion of embedded steel, by acting as a path for ingress of atmospheric carbon dioxide or marine/de-icing salts which may penetrate locally to the steel surface. In addition, cracks can act as a local point on the steel which could become anodic in a macro-cell.

-Stress Corrosion Cracking

Stress corrosion cracking of high strength steels has been observed in many environments (9) including marine and industrial atmospheres. Cracking and failure can occur very rapidly. It is widely accepted that this type of cracking in steels results from hydrogen embrittlement. The corrosion process can supply atomic hydrogen as part of the cathodic reaction.

In the concrete environment, it appears that oxygen reduction is the favoured cathodic reaction and hence the prestressing steel

should not be subject to stress corrosion cracking, even when passivity breaks down. However, there is some concern if aggressive macro-cells develop since this may lead to local hydrogen evolution. A risk of cracking may also occur with moisture penetration to steel in areas where there is no alkalinity e.g. with carbonated concrete, non-cementitious grout, or steel not in contact with concrete.

-Corrosion Fatigue

Fatigue properties of steel can be significantly influenced by corrosion. For high strength steels in aqueous conditions it is normally accepted that hydrogen embrittlement is responsible for lower fatigue life, therefore the same comments made concerning stress corrosion cracking apply for corrosion fatigue.

-Related Physical Factors

The physical factors that increase the probability of corrosion of reinforcement are porous concrete, low depth cover, leaking joints, faulty drainage, absence of waterproofing membranes and intensity of freeze-thaw cycles (14). All these facilitate access of water, carbon dioxide and chlorides to the reinforcement.

1.5- OBJECTIVES AND SCOPE OF RESEARCH

1.5.1- Objectives

Concrete bridges form a vital part of the highway network in many countries. These structures are subject to ever-increasing loading with the rise in both traffic flow and maximum permissible weights for commercial vehicles (15). In addition the introduction of de-icing salts during cold spells has left a corrosive environment, therefore concrete, not surprisingly, shows signs of defects and deterioration. Hence inspection is required to identify cracking and corrosion of embedded steel in highway structures. At the present time, there are no commercial nondestructive methods which can detect the physical condition of corroding steel components embedded in concrete.

The objectives of this research are:

-To study the wave propagation in concrete i.e.the attenuation of signals in a such heterogeneous material as concrete.

-To study the attenuation of signals of bars embedded in concrete.

-To estimate the energy reflected from a sound and corroded wires embedded in concrete.

-To develop a computer model for the problem to predict the signal amplitude after passing through concrete and wire.

-To gain understanding of stress wave propagation in concrete containing corroded reinforcement and flaws.

-To develop a method (testing technique and signal processing) for finding corroded wires or strands or flaws within hardened concrete which is based on the generation and reception of ultrasonic signals.

1.5.2- Scope

Chapter 2 presents a review of the previous applications of nondestructive techniques, specially stress wave propagation techniques for evaluating concrete structures.

Chapter 3 presents a review of the basic principles of elastic wave propagation. Values for wave speeds, reflection and transmission coefficients are given for different interfaces or boundaries, attenuation of waves in concrete is discussed, and the wave physics of the sound field i.e. the sound beam are reviewed.

Chapter 4 presents a literature survey about the past application of signal processing in the field of NDT, and the techniques used for signal processing.

Chapter 5 presents an examination of attenuation of different frequency signals of rods embedded in concrete when a pulse is applied to one end of a rod and received at the same end.

Chapter 6 presents a study of the attenuation of sound in concrete due to its composition i.e. , cement, water, sand, and gravel.

Chapter 7 presents a theoretical approach and a model analysis is given for the estimation of signal strength expected from a back-wall echo, sound bar, and corroded bar embedded in concrete when a pulse-echo system is used i.e. one transducer mounted on the surface of the concrete used to transmit and receive the signal.

Chapter 8 presents a discussion and review of computer-based numerical modelling and a description of the model developed. The predictions are compared with experimental results for the variations in detected echo amplitude as the probes scan over a water tank or a concrete beam containing steel components with and without defects.

Chapter 9 gives information about materials and specimens, in addition, descriptions about instruments used and computer programs written for signal processing are included.

Chapter 10 presents experimental results of modelling tests to examine different samples of steel rods in a water tank.

Chapter 11 presents the signal processing techniques used for finding corroded wires or strands or flaws within hardened concrete. A proposed system for testing is presented. A key

feature of the technique is the application of the digital filtering technique.

Chapter 12 gives summary, conclusions, and future work.

Table 1.1- An Average Relation between the Increase in Tensile Strength and the Reduction in Area (12).

Total reduction in area of wire	Increase in tensile strength
40 %	18 %
60	30
70	36
80	51
94	100

Table 1.2- Specifications of Strands, Wire, and Bars (12).

Type	Nominal Dia. mm	Characteristic Tensile Strength N/mm ²	Characteristic Breaking Load kN
Drawn Strand	18	1700	380
Drawn strand	15.2	1820	300
Drawn strand	12.7	1870	209
Standard strand	15.2	1640	227
Standard strand	12.5	1750	165
Standard strand	9.3	1790	93.5
Wire	7	1570	60.4
	5	1570	30.8
	4	1720	21.7
	3.25	1720	14.3
Bar	40	1000	1250
	32	1000	800
	25	1000	500
	20	1000	325

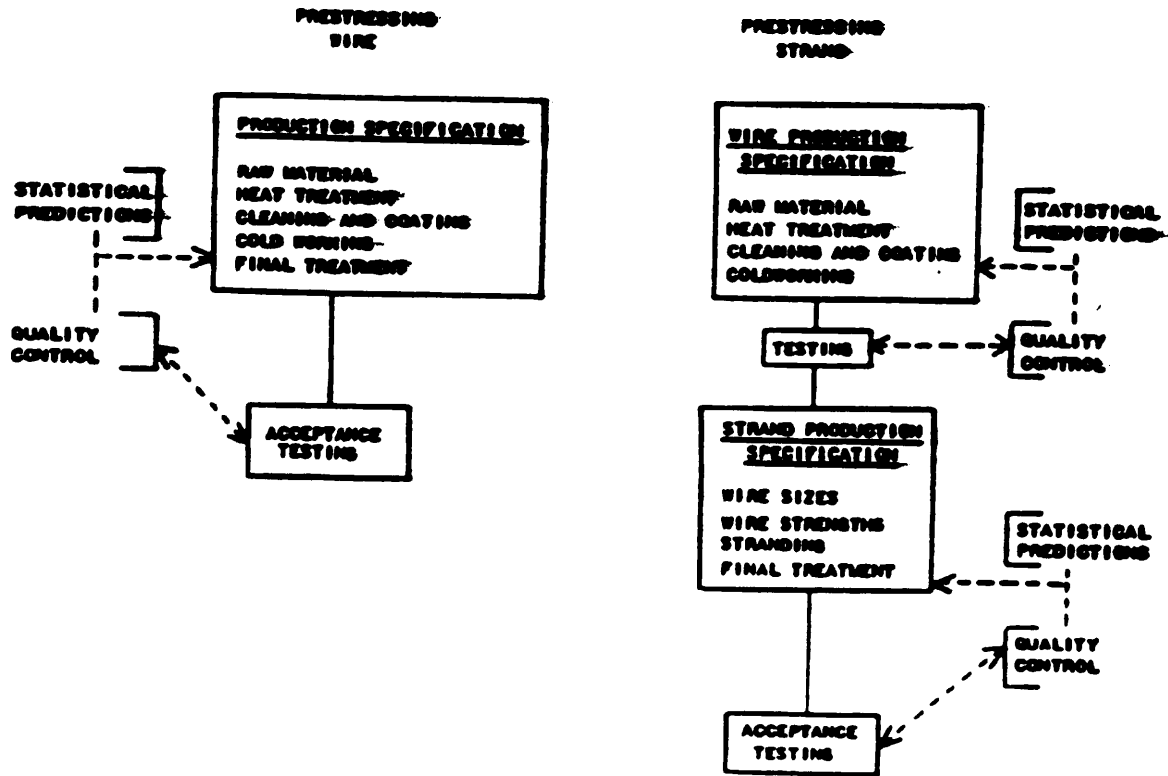


Fig.1.1- The stages of production of prestressing wires and bars (12).

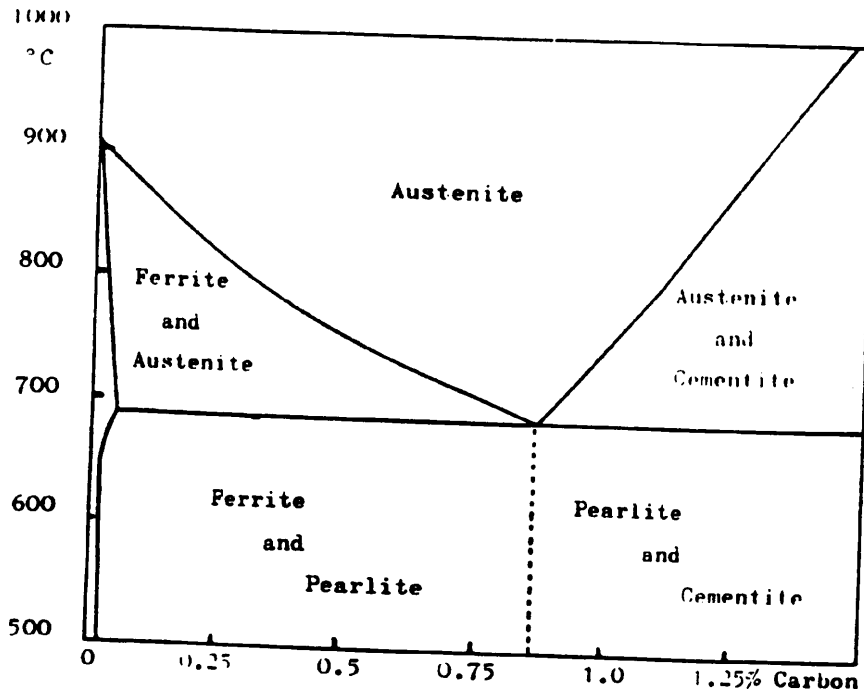
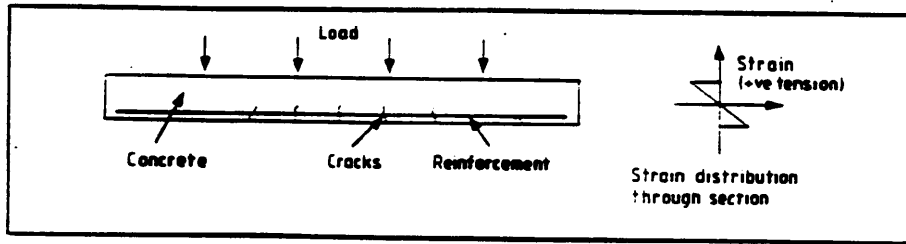


Fig.1.2- A simplified phase diagram representing change points in cooling (12).

Concrete is much stronger in compression (typical ultimate compressive strengths range between $25-60 \text{ N mm}^{-2}$) than in tension ($2-4.5 \text{ N mm}^{-2}$). Therefore steel reinforcement is used to carry the tensile stresses and concrete in the tensile zone is allowed to crack.

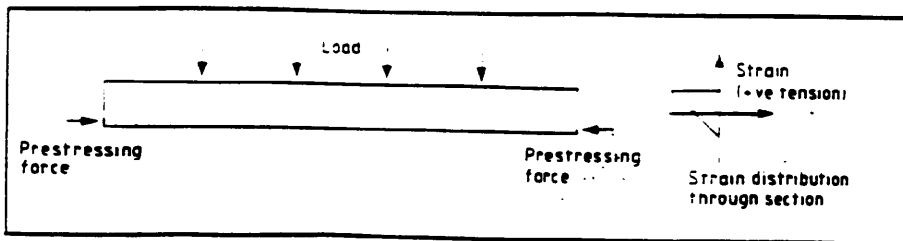
Reinforced concrete



To make more efficient use of the concrete and enable slender sections and longer spans to be built, an axial compressive force is applied which puts the entire section into compression. There are two ways of doing this:

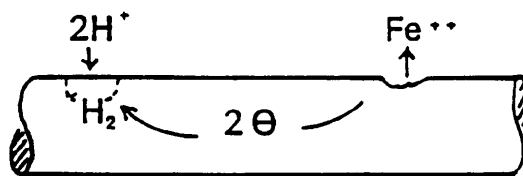
- (i) pre-tensioning – the concrete is cast around stressed steel wires which are released after the concrete has hardened;
- (ii) post-tensioning – the concrete is cast around steel ducts through which steel wires, strands or bars are passed; these are then stressed after the concrete has hardened. The ducts are subsequently grouted with a mixture of cement and water; this is both to protect the steel against corrosion and to provide a structural bond between the stressed steel and the concrete.

Prestressed concrete



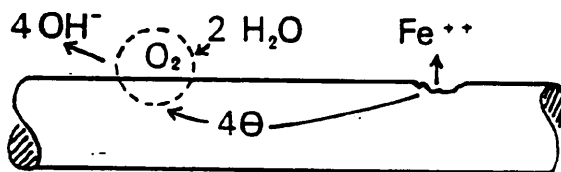
In both reinforced and prestressed concrete additional conventional reinforcement is required, for example, to resist shear stresses. In highly stressed areas, i.e. near the anchorages in post-tensioned concrete, such reinforcement is generally closely spaced.

Fig.1.3- Principles of reinforced and prestressed concrete (15).



HYDROGEN CELL

(a)



OXYGEN CELL

(b)

Fig.1.4

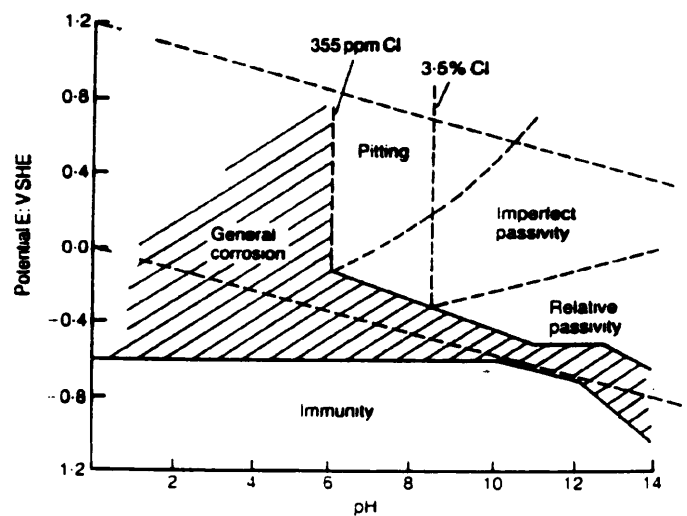


Fig.1.5- Pourbaix diagram for the effect of chloride on corrosion and passivation of iron (II).

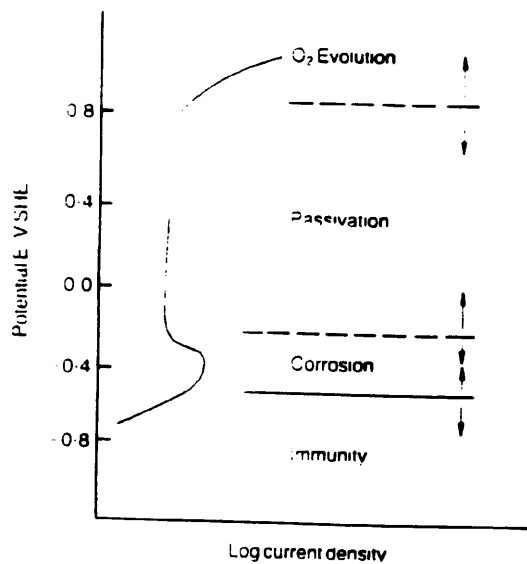


Fig.1.6- Schematic anodic polarization curve (or Tafel diagram) for steel in concrete (II).

CHAPTER 2NONDESTRUCTIVE TESTING TECHNIQUES2.1- INTRODUCTION

The purpose of this chapter is to describe the scientific principles upon which testing techniques, and especially nondestructive testing methods, are based.

The basic principle used in detecting defects not visible to the naked eye is that the defect must cause a change in the response of the interrogating signal. Furthermore, the difference in response between the defect and sound material must be large enough to be recorded on the instrumentation. Most of the nondestructive testing techniques use various waveforms as the interrogating signal. These waves are usually either electromagnetic radiations or stress waves. The principal characteristic of electromagnetic waves is that they travel freely through a vacuum. Stress waves are transmitted from one particle to another by direct contact between the particles. Stress waves are sometimes termed elastic waves because it is the elastic property of a material that controls the velocity of stress waves through it. Other methods used in nondestructive testing are magnetic, electrical, chemical, radiographic, and surface inspection. All these techniques are reviewed in this chapter, and their applications in concrete testing are given. A detailed section is given about stress wave methods and a

literature survey about their application in concrete is given too.

2.2- MAGNETIC METHODS

The main application of magnetic methods in the testing of concrete structures is in determining the position of reinforcement. Although not strictly a technique for detecting defects or deterioration, the fact is that inadequate cover is often related with corrosion-induced deterioration, which means that locating the position/depth of the reinforcing bars can be important. There are several magnetic devices available that have been designed to detect the position of reinforcement and measure the depth of cover, these devices are generally known as covermeters or pachometers.

Moore (16) evaluated the use of a rolling pachometer for nondestructive determination of the cover over the reinforcing steel on concrete bridge decks.

Brukorski and Karminski of the Institute for Building Technique in Warsaw (17), used a magnetic device, called FEMETR, made in the Institute, and were able to measure the diameter of the bar to within 10 to 15%. The covers which such devices measure are in the range of 0-75mm.

A magnetic technique was developed in the USA in the Southwest Research Institute for detecting flaws in pre-tensioned and post-tensioned steel in concrete bridges. A constant magnetic field is

applied to the beam under test by means of a large, dc-excited electromagnet and scanning along the beam with a magnetic field sensor, parallel to the direction of prestressing steel. An observed change in the field indicates a fracture or discontinuity in the steel. Difficulties in signal interpretations were reported, as signals from steel close to the surface, such as stirrups, tended to mask responses from steel deeper in the member.

Kusenberger and Birkelbach of the USA (1, 18) used the Magnetic Field Disturbance system to detect deterioration in the steel of prestressed concrete bridge members. Two general approaches to flaw signal discrimination and enhancement were investigated namely: 1) an array of magnetic field sensors to scan the structural elements of interest, and 2) electronic signal analysis to aid in the further discrimination and interpretation of flaw signals. There were some difficulties with signal recognition caused by stirrups and hardware items, such as chairs and tie wires.

Motooka and Okujima of Japan (19) derived a method of detecting the location of a steel bar within the concrete from the concrete surface by an electromagnetic impact driving method. The system is a driving coil cemented on a bakelite plate. At the centre of the bakelite plate a hole is made to insert a piezo-electric crystal receiver. When the driving coil is charged, impulsive electromagnetic flux is instantly radiated into the concrete from the coil and its flux is interlinked with the steel bar. An impulsive electromagnetic attraction force acts instantaneously

between the coil and the bar. Through this attraction force, the bar hits the concrete block and an impulsive sound wave is radiated into the concrete and caught by the receiver. They reported ability to locate bars buried in concrete at a depth of less than 15cm below a concrete surface.

This method gives satisfactory results in lightly reinforced members, such as bridge decks, but in heavily reinforced members, the effect of deeper bars cannot be eliminated, and it is practically impossible to obtain reliable results.

2.3- ELECTROCHEMICAL METHODS OR IMPEDANCE MEASUREMENTS

Corrosion of reinforcement is an electrochemical process, the electrolyte being the alkaline pore water within the concrete/mortar matrix. Electrochemical methods therefore are based on assessing the kinetics and mechanism of the anodic (metal dissolution) and cathodic (oxygen reduction) reactions.

It should be noted that existing methods cannot be directly applied to the inspection of tendons embedded in lined ducts (galvanised steel or plastic) as the latter will act as a barrier between an external electrode probe and the embedded tendon. However, if, suitable access was arranged, e.g. by drilling into the duct or providing access at time of construction, then most of the techniques could be applied. In this section most of the techniques used for evaluation of corrosion in concrete will be reviewed.

a) The Four-Electrode Method

Resistivity of concrete is one of the factors that controls the rate of corrosion of steel in concrete. As the resistivity increases, the corrosion currents decrease such that corrosion is not of practical significance in dry concrete. It is important to note that all measurements of the resistance of concrete must be made with an ac meter in order to eliminate polarization effects.

Resistivity is normally measured by the four electrode method (fig.2.1). Four contact points are placed in the concrete, equally spaced in a straight line. An alternating current is passed between the outer electrodes. The resulting potential difference between the inner electrodes is measured and the resistivity of the concrete calculated from the expression:

$$P = 6.28aE/I$$

where P=resistivity

a=electrode spacing

E=potential drop between P_1 and P_2

I=current flow between C_1 and C_2

The major disadvantage of the method is that the value of resistivity measured is dominated by the resistance of the concrete near the surface whereas it is the resistivity of the concrete at the level of the reinforcement that is the primary interest.

Moist concrete usually has a resistivity of the order of 10,000 ohm-cm whereas oven-dried concrete has a resistivity of about 100,000,000,000 ohm-cm. Vassie⁽²⁾ recommended the following values:

If the resistivity >12000 ohm-cm, corrosion is unlikely.

If the resistivity >5000 & <12000 ohm-cm, corrosion is possible.

If the resistivity <5000 ohm-cm, corrosion is almost certain.

These figures assume that the concrete contains sufficient chloride ions ^{or carbonation} to initiate the corrosion reactions. Other work (20) suggested that corrosion is unlikely to occur in concrete with a resistivity in excess of 20,000 ohm-cm and that resistivities in the range 5,000 to 10,000 ohm-cm are needed to support corrosion activity. The reasons for the different limits are not clear.

b) Corrosion Potential Measurements

When steel corrodes in concrete, a potential difference exists between the anodic half-cell areas and the cathodic half-cell areas along the reinforcing bar. The potential of the corrosion half cells can be measured by comparison with a standard reference cell, which has a known constant value, and then isopotential maps are plotted. A copper-copper sulphate cell is normally used because it is rugged, inexpensive, and reliable (9). The potential difference between the steel reinforcement and the reference cell is compared by connecting the two through a voltmeter. This is achieved by connecting one lead of the voltmeter to the reinforcing steel, and the other lead to the

reference cell, enabling electrode potentials to be measured at any location by moving the half cell over the concrete surface (fig.2.2). It is necessary to check that a good connection has been made to the reinforcement and that it is continuous. A separate connection is required wherever the steel is not continuous e.g. where expansion joints exist in a bridge. It is known that the half-cell measurements for the copper-copper sulphate cell could be interpreted as follows:

less negative than	-0.2V	-No corrosion
between	-0.2V and 0.35V	-Uncertain
more negative	-0.35V	-Corrosion is occurring

N.B. negative values because iron is more negative than copper in the electrochemical series.

If positive readings are obtained, it generally indicates that there is insufficient moisture in the concrete and the readings should not be considered valid. It is important to note that as the measured potential is the gradation of the iso-potential contours, a close spacing often indicates a rapid change from a corroding area to a passive area and provides evidence of an active cell.

It is important to recognize that half-cell measurements indicate the potential for corrosion at the time of measurement, but do not give information about the rate of corrosion. Corrosion rates of steel in bridges are primarily controlled by the resistivity of the concrete, the availability of oxygen at the steel surface and

the depth of cover. It is possible therefore to have high potential but low corrosion.

c) Linear Polarisation Resistance Method (LPRM)

The LPRM relies on the observation that the current response of a corroding electrode is approximately linear in the free corrosion potential region, i.e. within $\pm 20\text{mV}$ of E_{corr} (9).

The linear polarisation resistance method (21) is a technique for corrosion rate determination. The corroding material is polarised a few millivolts ΔE ($< 20\text{mV}$) away from its corrosion potential and the observed current response ΔI is then used to determine the polarisation resistance $R_p = \Delta E / \Delta I$, which is inversely proportional to the corrosion current density, i_{corr}

$$i_{\text{corr}} = B / (R_p A)$$

where A is the area of steel and B is the constant of proportionality which can be determined experimentally by comparison with weight-loss data, or can be calculated from the anodic and cathodic Tafel slopes (b_a , b_c):

$$B = b_a b_c / (2.3(b_a + b_c))$$

In order to obtain the estimated corrosion rate from the polarisation resistance method measurement, the area of the steel being polarised is required. Thus for application in real structures, the data can normally be obtained on special probes

embedded in the concrete. Any attempt to apply the technique directly to the steel component, reinforcing or pretension^d steel, results in an unknown area of steel being polarised. Hence the corrosion rate cannot be estimated.

d) Electrochemical Impedance Technique

Electrochemical (or ac) impedance techniques (also termed frequency response analysis), in which the response of a test electrode to a series of variable frequency impulses is monitored, have become increasingly used for corrosion studies over the past ten years following the introduction of digital instrumentation (9).

In essence the technique uses digital correlation methods to measure the variation of the cell current in response to an applied sine wave potential perturbation of a known amplitude and frequency, it then obtains the value of the complex impedance of the cell at that frequency. Since the corroding interface components behave as capacitor-resistor combinations, the impedance is frequency dependent (9). The measurement process is repeated over the required frequency range, 10kHz to 10MHz, in order to provide a full impedance spectrum. Data is normally obtained using a frequency response analyser with the data stored and subsequently analysed using a micro-computer. Analysis of data, normally in the form of Nyquist or complex plane plots of real (resistive) components vs imaginary components (capacitive) with frequency as a parameter, provides information related to the various components of the test cell equivalent circuit

(fig.2.3). This circuit, referred as a 'Randles equivalent circuit', is used to relate the observed electrical phenomena to the actual electrochemical corrosion processes (9).

Electrochemical impedance techniques have been used to study the dielectric properties of concrete (22). The technique has the same requirement as the LPRM in that the exact area of the steel is required.

e) Guard Ring Technique

As was noted above it is difficult to apply LPRM or electrochemical impedance techniques directly to large beam specimens or actual structures because of the polarization. Recent tests (22) based on previous suggestions (23, 24) have demonstrated the feasibility of the use of a guard ring technique to obtain polarisation measurements on the reinforcing steel.

The guard ring probe comprises a central probe and an outer ring electrode (fig.2.4.a). These ^{are} linked by a potentiostatic arrangement such that the electronic system operates in tandem but the actual measurement is made on the central electrode; the outer electrodes spreading the majority of the polarising signal to the rest of the reinforcement structure. The measurement is made over a small area of the steel by the central electrode (typical area 10cm^2) whilst the outer ring (typical area 1000cm^2), operated simultaneously with the central ring, polarises the reinforcement outside the test area. This converts the illdefined impedance response with no guard ring into a

recognised response (fig.2.4.b) (9). The response from the active corrosion areas in a macro-corrosion cell on reinforcement is more clearly defined and a charge transfer is observed from which a corrosion rate can be estimated.

f) Electrochemical Noise (Potential and Current) Analysis

- Electrochemical Potential Noise

All corrosion processes involve stochastic or random events, which can be observed as fluctuations in the corrosion potential (25,26). These are manifest as low frequency (<1Hz), low amplitude (<1mV), and random fluctuations. Where the corrosion is localised (the result of film breakdown events as in chloride induced pitting) then the electrochemical noise level increases. The noise is characterised by a rapid or almost instantaneous change in potential followed by an exponential recovery. This self generated noise signal can be used to monitor the corrosion processes and in the case of concrete can identify areas of pitting type corrosion (27). The data is obtained by recording the corrosion potential of the embedded steel, as measured against a surface mounted reference probe. The data is collected at regular intervals of between 1-5 sec, over a 15-80 min period. The data is then analysed by either direct statistical analysis (calculation of mean, standard deviation, trend, etc) or spectral analysis.

- Electrochemical Current Noise

Coupling current measurements, normally made between dissimilar metals via a zero resistance ammeter and used to determine the extent of galvanic corrosion, can also be made on steel reinforcement (22). Here the coupling is made between the steel and a polarisable electrode (e.g. platinum used as an oxygen electrode) or a current limited galvanostat. A mean coupling current flow and the fluctuations or current noise can then be measured. Analysis is essentially the same as for electrochemical potential noise. The technique has been applied only to laboratory test beams, but could be applied directly to reinforcing steel in concrete.

2.4- CHEMICAL METHODS

The principle of these tests applicable to concrete is to determine the depth of carbonation and chloride ion content. Both methods are used to check if the passivity of the reinforcement have been broken.

The depth of carbonation can be measured by exposing a concrete surface to a 2% solution of phenolphthalein in ethanol, phenolphthalein is a pH indicator with a colour change at about pH=10. The magenta areas represent uncarbonated concrete and the colorless areas carbonated concrete.

The chloride-ion content of concrete is usually measured in the laboratory using a wet chemical method of analysis.

2.5- RADIOGRAPHIC TECHNIQUES

Gamma-radiography has been applied to bridges for indicating the position and quantity of reinforcement in concrete and for detecting voids in post-tensioning ducts. Gamma ray sources-isotopes such as Cobalt 60, Caesium 137, and Iridium 192 are more portable ^{than} the high energy x-ray equipment. With a scintillation counter in place of a photographic film, numerical measurements of the amount of radiation transmitted can be used to determine density. A system using this technique has been developed in France for the inspection of cables in box girders, I-sections, and slab bridges. This system is known as SCORPION (fig.2.5).

These radiographic techniques are restricted in the maximum thickness of concrete structures which can be penetrated, about 0.6m with isotopes and 1.2m with linear accelerators (9).

2.6- SURFACE INSPECTION

Numerous techniques are available which rely on surface measurements of strains, stresses, crack widths, and hardness to indicate the condition of a structure.

Strains and crack widths are most commonly measured with acoustic or Demec gauges (15).

Of several techniques for relating surface hardness to strength,

the most popular is the Schmidt hammer, because it is cheap and can be used by inexpert workers.

These techniques are not accurate, accuracy ranges between (15-20%) (15), and require calibration for the concrete under test. They can be used for comparing the quality of concrete in different parts of a structure.

2.7- RADAR

Radar methods for inspection in concrete structures have been investigated by Cantorr and Keeter (28, 29), and Alongi (30). The techniques are useful for detecting gross defects in the concrete itself such as determination of voids, due to reflection from open surfaces or horizontal cracks. Embedded steel causes scatter and reflections.

The technique employed when radar is used has been the use of pulse-echo methods. A very brief pulse of electromagnetic energy (perhaps one nanosecond) is emitted from a radar transmitter. This pulse propagates out from the transmitting antenna and at any interface at which the dielectric properties of the medium through which the pulse propagates change there will be partial reflection and partial transmission of the electromagnetic energy (fig.2.6). Therefore each interface gives rise to echoes which can be picked by the same antenna. The time relationship between echoes can be related to the position of these interfaces and simple analysis of the shape of the wave forms which comprise

the echoes can lead to deductions concerning parameters such as density of the various media either side of an interface.

2.8- THERMOGRAPHY

Thermography is a technique for measuring or imaging the infra-red energy emitted from a structure. It can be a passive system in which the structure's infra-red emission is used with no normal stimulus, or it can be an active system in which the structure is initially stimulated with an active system such as some form of thermal energy and the resultant pattern of infra-red emission is then measured. The thermal image obtained can be assessed in terms of the temperature of the structure with extreme accuracy.

Use of thermography has been reported by Hillemeier (31) for location of reinforcement in concrete structures. In this technique the reinforcement is heated inductively and a thermal image of the concrete structure taken by infra-red radiation detectors/cameras. No connection is required to the embedded steel, and the technique readily locates bars up to 100mm deep. The image produced on the screen when scanning systems are used is of a bright stripe parallel to the embedded steel. Whilst it is likely that reductions in cross-sections due to corrosion or broken wires would show increased resistance and hence generate more heat under induced current, no work has been carried out to investigate this (9).

2.9- EDDY CURRENT METHODS

Investigations of eddy current methods to detect corrosion of embedded steel members in concrete has been reported by Karpov (32) in the USSR. The application was for inspection of steel ties in pre-cast panels for buildings. The technique involves constructing tomographs of the impedance with different voltages and frequencies. It is claimed that the relative magnitudes of resistive and reactive components change with different amounts of corrosion of embedded steel, including loss of initial protective metal coatings.

2.10- VIBRATION MONITORING TECHNIQUES

Vibration analysis is a technique in which some form of stimulus is applied to a structure usually in the form of either simple harmonic motion (sinusoidal motion) or in the form of an impulsive force. This stimulus is then allowed to propagate through the structure and is detected either at points remote from its application or at the point of application after the stimulus has ceased. This analysis can lead to a mathematical model of the structure which will assist in interpretation of the data. The measured data may be processed in one of two forms. The first is to use the response data and compare it with a known good pattern and hence detect the correlation between changes and defects in the structure. The second technique is based on so-called transfer function measurements in which the signal applied to the structure under test is regarded as a input to a 'black box' and the output from the 'black box' is the signal picked up

at some remote point on the structure. Techniques based on Fourier and Laplace transforms can be employed to derive parameters to describe mathematically the dynamics associated with the 'black box'. In this way a transfer function equation can be derived from the measured data and the parameters of this equation can be used to correlate with changes or defects in the structure. It is possible that a mathematical model of this structure can be constructed prior to measurement and that the mathematical model can be used to give guidance to methods of test.

In general, vibration monitoring has not been found useful for detecting corrosion deterioration in steel rods and cables, unless the damage is sufficiently severe to affect overall structural response, as opposed to local component response.

In the SHRIMP technique reported by Savage and Hewlett (33) low stress level vibrations are induced in the component, and vibrational patterns recorded as accelerometers are moved to different locations. Tests on concrete beams showed that differences in reinforcement and prestress could be detected.

2.11- STRESS WAVE METHODS

2.11.1- Introduction

With the exception of visual inspection, the use of acoustic methods is the oldest form of nondestructive testing . Striking

an object with a hammer and listening to the ringing sound is a common way of detecting the presence of internal voids, cracks or delaminations (34).

In 1929, Sokolov first suggested the use of ultrasonic waves to find defects in metal objects (35). However, it was not until the introduction of pulse-echo flaw detectors in 1942 by Firestone of US and Sproule of England (36) that significant progress was made. Since that time, ultrasonic pulse-echo testing of metals, plastics, and other homogeneous materials has developed into an efficient, reliable, and versatile nondestructive test method. The development for less ideal materials, such as concrete, has been hindered by the difficulties inherent in obtaining and interpreting a signal record from a heterogeneous material.

2.11.2- Test Methods

There are a variety of techniques that are based on using stress wave propagation for nondestructive testing. The primary distinctions between the techniques are in the methods used for generating and receiving the stress wave. Three methods that have been used for evaluation of concrete are:

- 1-The through-transmission or pulse-velocity method.
- 2-Echo methods.
- 3-The resonance method.

These methods are discussed in the following section.

2.11.3- Through-Transmission Method

In through-transmission or direct transmission method, one measures the time it takes for a stress pulse to travel from a transmitting transducer to a receiving transducer located on the opposite side of a test object. From the measured travel time and the known distance between transducers, an apparent pulse velocity is calculated. The computed pulse velocity value can be used to draw inferences about the integrity of the medium. This approach has its limitations: it requires two accessible surfaces (fig.2.7.a).

2.11.4- Echo methods

In the echo methods a stress pulse is introduced into the test medium at an accessible surface by a transmitter (crystal) or by a mechanical impact (hammer). If a transmitter is used, the method is referred to as a pulse-echo technique, if mechanical impact is used, the method is referred to as an impact-echo technique. Two arrangements for placing transducers may be used in this case: 1) semi direct transmission where transmitter and receiver are placed on adjacent concrete surfaces meeting at an angle, usually 90° (fig.2.7.b); 2) indirect (sometimes called pitch-catch or surface transmission) where transmitter and receiver are placed on the same concrete surface (fig.2.7.c).

The pulse propagates through the medium and is reflected by material defects or by interfaces between phases of different

densities or elastic moduli. These reflected waves, or echoes, are monitored by either the transmitter acting as a receiver, the method is then called pulse-echo, or by another receiving transducer coupled to the surface of the test object near the pulse source, in this case the method is called pitch-catch. The transducer output is displayed on an oscilloscope. Using the time base of the display, the travel time of the pulse can be determined. If the wave velocity in the medium is known, the round trip travel time of each echo can be used to determine the location of a defect or an interface.

2.11.5- Resonance Method

Resonance techniques are used to determine the thickness or length of a test object. Continuous waves are introduced into a test object by a transmitter or a mechanical oscillator. The frequency of these waves is systematically varied until a resonance condition is set up in a test object. Resonance occurs when the driving frequency is equal to the frequency of the fundamental mode of vibration of the test object which is monitored by a receiving transducer located close to the transmitter. When a resonance condition is achieved, there is a significant increase in the amplitude of the measured response. The fundamental mode of vibration is identified by noting the frequency (f) at which this increase occurs. If the longitudinal wave velocity (c_1) is known, the thickness of the test object (t), which equals one-half the wavelength of the propagating waves, can be calculated ($t = c_1/2f$).

2.11.6- Past Applications

The three stress wave propagation methods discussed in the last section have been used for detecting very large structural cracks in concrete structures such as dams, for integrity testing of concrete structures such as piles, for measuring the thickness of plate elements such as highway slabs, and for several other specialized applications. These applications are reviewed in the following section.

-Pavement and Bridge Decks

Resonance and echo techniques have been developed to measure the thickness of concrete pavements and to detect delaminations in bridge decks. In the early 1960's, Muenow (37) developed a technique to measure pavement thickness which was based on determining the frequency of the fundamental mode of vibration of the slab in the thickness dimension. A transmitter was used to excite resonances in the slabs.

Resonance methods have also been used to detect delaminations in concrete bridge decks. A technique developed in 1973 by researchers at Texas A&M University (38) used an oscillating steel plunger to excite the characteristic vibrations of a delaminated area. As the plunger oscillates at 60Hz, the vibrations of the bridge deck were monitored by a receiving transducer. The location and extent of delaminated areas could be determined from the relative amplitude of the received signals. The use of this technique has been limited by the fact that it

cannot be used where concrete decks have asphaltic overlays exceeding approximately 5cm.

In 1964, Bradfield and Gatfield (39) reported the development of an echo technique for measuring the thickness of concrete pavements. Using two 100kHz resonant transducers, 16cm tall, 10cm wide, and 25cm long, in a pitch catch arrangement, they were able to measure the thickness of a 30cm concrete specimen with an accuracy of 2%. The transducers were coupled to the concrete by a large plastic block which required a smooth flat concrete surface for good coupling. Difficulties were reported in obtaining reflections from the bottom of rough textured pavement surfaces. The reason of using a large diameter radiator is that it emits a sound beam, the half-angle of this beam is governed by the following equation: $\theta = \text{asin}(1.2\lambda/D)$, where λ =wavelength and D =diameter of the transducer, for the above transducers $\theta \approx 29^\circ$.

An echo system was developed by Mailer (40) to measure pavement thickness by monitoring the travel time for an ultrasonic pulse to propagate through the thickness of the concrete and return to the receiving transducer at the top surface after being reflected by the concrete pavement-subbase interface. A large transmitter was needed to introduce sufficient acoustic energy into the medium to overcome wave attenuation problems due to coarse-grained aggregates and to obtain coherent reflections from rough subbase interfaces. The transmitter was a hollow cylinder, with a 46cm outer diameter, a 15cm inner diameter, and a 200kHz resonant frequency. The receiving transducer was placed in the centre of the transmitter.

-Erosion Cavities Below Slabs and Behind Walls

In Russia (34) an acoustic resonance technique was used for finding large erosion cavities behind concrete canal walls and below reinforced concrete slabs on soil substrates. In the case studies presented, the canal walls were 18 to 28cm thick and the reinforced concrete slab was 10cm thick. The resonance technique used was an adaptation of a standard technique in the USSR for checking bonds in multilaminate plastic structures; this technique is referred to as the method of free vibration. Flexural modes of a wall or a slab were excited by the periodic impact of an electromechanical vibrator operating at a frequency of 16Hz. The response of the wall or slab was monitored by an accelerometer, and a spectral analyser was used to obtain the frequency spectrum of the received signal. The presence of a cavity was detected by monitoring the change in the amplitude of the frequencies corresponding to the thickness of the slab. When a cavity was present, there was a noticeable increase in amplitude. Cavities approximately 2m and larger were detected.

-Cracks and Corrosion of bars in concrete

Sansalone and Carino (34, 41) carried out experiments using the impact echo method to determine the depth of vertical surface opening cracks, the condition of honeycombed concrete and to locate an ungrouted metal duct. An impactor with a 3mm diameter spherical steel tip and 5.5g spring driven mass, with a broad band displacement receiver were used. It was shown that the

contact time duration of the impact device is an important variable because it determines the size of the defect which can be detected, the shorter the time the smaller the defect. Experimental results showed that it was possible to distinguish between the hollow and fully grouted duct, because the hollow duct produces high amplitude reflections while the grouted ducts cannot be detected because the thin interface is transparent to propagating waves.

Damaj (42) used pulse-echo techniques to detect cracks in wires spanning in air, water, and concrete. For application of this method, one end of the wire must be accessible and have a smooth surface for the transmitter and receiver. Using a 5MHz transducer, well damped, manufactured at the Department of Instrumentation at UMIST, he was able to get the back reflection or echo of a wire of 7mm diameter, 3m long, embedded in concrete. He found that the intensity of ultrasound falls off with increasing distance from the transducer as the energy is lost to the surrounding concrete, and the back echo is damped or attenuated.

The through-transmission method, where the velocity is measured, is used extensively as a reliable indication of the overall quality of concrete. This is because the wave velocity is reduced by the presence of porosity, which affects strength, and internal cracking, which is often associated with deterioration. A number of qualitative scales have been published to relate pulse-velocity measurements to the quality of concrete, examples are given in table 2.1. It should be noted that measurements of

pulse velocity through concrete are affected by the smoothness of the concrete surface, concrete temperature, moisture content, mix proportion, age of the concrete, and presence of the reinforcing steel. Knab et Al (43) performed a laboratory study to quantify the crack detection capabilities of ultrasonic through-transmission measurements in concrete. Pulse velocity and amplitude measurements were taken perpendicular to the crack plane (in cracked concrete) and compared with measurements parallel to the crack plane (in uncracked concrete). A sensitivity ratio was used to determine if the cracks could be detected, the numerator of this ratio was the difference between velocity or amplitude values in the cracked as compared to uncracked concrete while the denominator represented the variability of the velocity or amplitude values in both the cracked and uncracked concrete. It was shown that the sensitivity values could be used for greater crack depths which could be reliably detected.

Chung (44) reported that fire damage of concrete can be assessed approximately by the echo-method. Both the pulse velocity and the compressive strength of concrete are reduced after a fire attack, but the rate of reduction is not the same. Using the indirect or surface transmission method, a transmitter is placed on the concrete surface at a fixed point while the receiver is placed at fixed increments of distance along a straight line. The transit times measured are plotted as points on a graph showing their relation to the distance separating the transmitter and the receiver (fig.2.8). Thickness of the surface layer is

calculated from:

$$t = X/2 \sqrt{(\tan\alpha - \tan\beta)/(\tan\alpha + \tan\beta)} = X/2 \sqrt{(v_s - v_c)/(v_s + v_c)}$$

where v_s = the velocity in sound concrete

v_c = the velocity in damaged concrete

refer to fig.2.8 for other symbols.

A recent paper in the Indian Concrete Journal (45) reported that a number of tests have been carried out to examine prestressed concrete bridges. One of these tests was an ultrasonic method which was used to locate voids in cable ducts. It consists of placing a transmitter and receiver on opposite sides of a slab and measuring changes in velocity. Erroneous results are obtained if voids are small compared to concrete thickness or where cables shade each other.

-Dams

Engineers in India (46) used an impact echo method to estimate the depth and extent of large horizontal cracks that developed in Koyna dam during 1967. Very low frequency stress wave (200-600Hz) were introduced into the concrete by mechanical impact with a free falling steel hammer. This range of frequencies allowed detection of cracks on the order of 15m and larger. The energy generated by the mechanical impact was sufficient to obtain reflections from cracks located 100m away from the point. After existing cracks were grouted, the impact-echo was used to assess the degree of grout penetration. The assesment was made qualitatively by comparing the echo amplitude in signal records

obtained before grouting to those after grouting.

-Piles

Since the early 1970's, impact-echo and resonance techniques have been widely used for integrity testing of concrete piles (34). The behaviour of stress waves in slender rod-like structures, such as piles, is well known. If a pulse is generated by mechanical impact at one end of the pile, the resulting wavefront is initially spherical but quickly becomes planar as the pulse propagates down the long slender pile. Plane wave reflection occurs at the bottom surface, and the reflected wavefront travels back up to the receiving transducer. Thus, the pile acts as a waveguide. Because of the length of piles, long duration impacts can be used. As a result, signal analysis is relatively simple.

Steinbach and Vey (47) were among the first to apply impact-echo techniques to field evaluation of piles. A pulse was introduced a concrete pile at the top surface by mechanical impact and returning echoes were monitored by an accelerometer mounted on the same surface. The signal record could then be used to detect partial or complete discontinuities, such as voids, abrupt changes in cross section, very weak concrete, and soil intrusions, as well as the approximate location where such irregularities existed. In the absence of major imperfections the location of the bottom of a sound pile could be determined. However, little specific information could be obtained about the extent of defects or the relative soundness of concrete at the location of an irregularity. The success of the method is

dependent upon the damping characteristics of the surrounding soil, a high degree of damping can severely weaken returning echoes.

Work at Edinburgh University (48, 49) has involved experiments on concrete test beams and piles. The basic apparatus used was an acoustic transducer mounted at one end of the test specimen to monitor surface movement for display on the oscilloscope, an electrical circuit which is routed through a hammer and pile head to the external trigger input of the oscilloscope. It was shown that by adding sequentially a series of signals obtained by moving one transducer around on the pile head, the magnitude of Rayleigh waves would be reduced, as these differ in phase and amplitude at each reading, relative to the main echo signal. The time domain signal was analysed by using the autocorrelation function. By autocorrelating the input signal, the hammer signal in this case, with the response of the pile, it was possible to detect reflections from within the pile or the pile base. Furthermore, frequency domain analysis was used. The procedure is to obtain the time domain signals of both the hammer impact, and the response of the pile via the accelerometer, these two signals are then transformed into the frequency domain using an FFT algorithm, the frequency domain from the accelerometer is then divided by the frequency domain signal from the input hammer. This is known as the frequency response function (fig.2.9). From this graph the length of the pile or distance to a defect can be calculated from the relationship:

$$L = c_1 / (2\Delta f)$$

where L =distance to end of pile or defect

c_1 =longitudinal sonic velocity through concrete

Δf =frequency interval between resonances.

-Reactor Structures

In 1976, Sutherland and Kent (50) of Sandia Laboratories used an ultrasonic pulse-echo method to measure the thickness of concrete reactor substructures subjected to the thermal energy of a hypothetical core meltdown. Two transducers were used in the pitch-catch mode. The relative position of a concrete-gas interface subjected to a high heat flux from a plasma jet was monitored as a function of time to determine the erosion rate of the concrete substructure.

-Refractory Concrete

Clayor and Ellingson (51) used an echo method to measure the thickness of 30.5cm thick refractory concrete specimens. It was found that for frequencies below 100kHz, the use of a single transducer as both the transmitter and the receiver was impractical because of the ringing of the transmitter^{which} obscured the echo signal. Tests were also carried out using two transducers in a pitch-catch arrangement, however, the transmitting transducer generated strong Rayleigh-waves which interfered with the reception of the echo signal by the receiving transducer. To reduce R-wave interference, large diameter

(17.8cm) transducers were constructed. As the response of a transducer is an averaged phenomenon over the contact area, the sensitivity of a larger diameter transducer to localized surface disturbances (R-waves) was reduced. Furthermore, the large diameter probe had a sound beam, the half-angle in this case was about 16° .

-Surface Opening Cracks in Submerged Structures

Smith (52) demonstrated that Rayleigh waves can be used to detect surface opening cracks in submerged concrete structures, such as concrete tanks and offshore structures. Two 0.5Mhz, 25mm diameter, longitudinal-wave or P-wave transducers were used as a transmitter and receiver. When a transmitted P-wave strikes the surface of a solid at a critical angle (defined by Snell's Law), mode conversion occurs producing R-wave which propagates along the solid-liquid interface. As the R-wave propagates, mode conversion also occurs, producing a P-wave which radiates into the liquid at the same critical angle and is picked up by the receiving transducer. The distance between the transducers can be adjusted to optimize the amplitude of the received signal. If the path of the propagating R-wave is crossed by a crack, reflection occurs and no signal will be picked up by the receiving transducer. If a crack is favourably oriented (a crack at 90° to the propagating wave is the best orientation, the P-wave produced by mode conversion of the reflected R-wave will be picked up by the transmitting transducer. Analysis of the received signals obtained from a complete scan allowed the location of surface opening cracks to be determined.

-Arch Masonry Bridges

Forde and Birjandi of Edinburgh University (53, 54) used a hammer to excite a 120 years old stone masonry bridge. A low frequency signal (2Khz) was produced. The objective of the investigation was to determine voiding in the bridge. The technique has proved capable of identifying a large void at a specific location.

2.12- ACOUSTIC EMISSION

This has been applied to both steel and concrete structures to detect growth of defects, but it does require the system to be connected continuously during long periods. By use of multiple listening transducers, it is possible both to detect and locate sources of emission of acoustic signals from within the material and this is particularly useful for detecting the development of cracking. In a programme of research at University College, Swansea, Casey and Taylor (55) have used acoustic emission on wire ropes of the type used in lifting and mechanical handling equipment. They have shown that it is possible to detect fractures of individual wires in cables of length up to 30m. Leiard (56) has reported application of pulsed acoustic emission techniques to masonry although this was effectively monitoring the signal received from an external impact by using standard acoustic emission methods of analysis. He monitored the acoustic emission behaviour of a brick wall with and without defects, using 13kHz resonant transducer, and reported significant differences.

Wang et al (57) have used the AE techniques to detect and characterise concrete damage resulting from the reinforcing steel corrosion. It was concluded that although some success has been achieved with laboratory specimens, more experiments are necessary to demonstrate that the system can be effectively employed on full scale on service structures. Hartt et al (13) have reported use of acoustic emission technique to detect corrosion induced damage in reinforced concrete. Essentially the acoustic emission techniques has been used in these cases to detect cracking of the concrete under the effect of expansion of corroded embedded steel. The work was carried out on reinforced concrete specimens with a single bar, monitored on a daily basis. The techniques used included both event counting above a threshold, and signal amplitude analysis. Work by Dunn (58) suggests the accumulative distribution of amplitude may be characteristic of failure mechanisms, and the few results presented suggest a good correlation between such counts and the onset of cracking around reinforcing bars. In France, Robert and Brachet-Rolland (59) have reported ^{the} use of acoustic emission to detect fractures of individual wires in tensioned cables and active cracks in concrete. The method has been used in practice for suspension and cable-stayed bridges, but the authors indicate the need for further research on interpretation of received signals for pre-stressed concrete structures.

2.13- OTHER TECHNIQUES

Many other techniques are used for examining concrete structures.

Some of these techniques are listed next, detailed information could be found in the references given for each method.

a) Rebound and Penetration Methods: These methods are used mainly to measure hardness of concrete (60).

b) Nuclear Methods: This is based on the measurement of moisture content in-situ by neutron absorption and scattering techniques (61).

c) Detecting Cracks Using Fibre Optics: Rossi (62) proposed to use the optical fibres as detectors of disorders (cracks, damage) in the field of civil engineering. The operation of the device is based on the finding that an optical fibre embedded in a piece of concrete breaks as soon as a crack propagating in the material surrounding it reaches it, and that this break causes an almost complete disappearance of the luminous signal transmitted by the fibre.

d) Air Permeability Measurements: It is used to obtain an in-situ assessment of the resistance of concrete to carbonation and to penetration of other ions such as chloride (63, 64).

e) Visual Inspection: This is carried out to determine the type and extent of deterioration of a structure (65).

f) Concrete cores: Drilling concrete cores from concrete structures is a standard method for checking the performance and

quality of concrete. This procedure is semi-destructive and only a limited number of cores can be taken from one location. Tests carried out on cores may include strength, porosity, permeability, density, chloride depth (65).

2.14- SUMMARY

A review of the literature shows that stress wave methods have been used successfully to detect thickness of concrete slabs and to detect voids beneath them. Delaminations within bridge decks and cracks within dams have been detected.

It appears from the survey that none of the techniques currently available meets the requirements for a generally applicable method to detect deterioration in high strength steel wires and cable embedded and grouted in concrete.

Preliminary work undertaken at UMIST (9, 42) has suggested that a development programme should be investigated using ultrasound, namely, acoustic pulsing and impact-echo method. The research requires theoretical and experimental work of the behaviour of stress signals in reinforced and prestressed concrete.

Therefore, theoretical and experimental studies have been carried out as a basis for developing a non-destructive testing system to detect corrosion and cracks in high strength steel components embedded in concrete.

Table 2.1- Relation between sound velocity and quality of concrete .

Longitudinal Velocity Km/Sec	Quality of concrete
>4.6	Very Good
3.5-4.6	Good
3.0-3.5	Moderate - Questionable
2.0-3.0	Bad
<2.0	Very bad

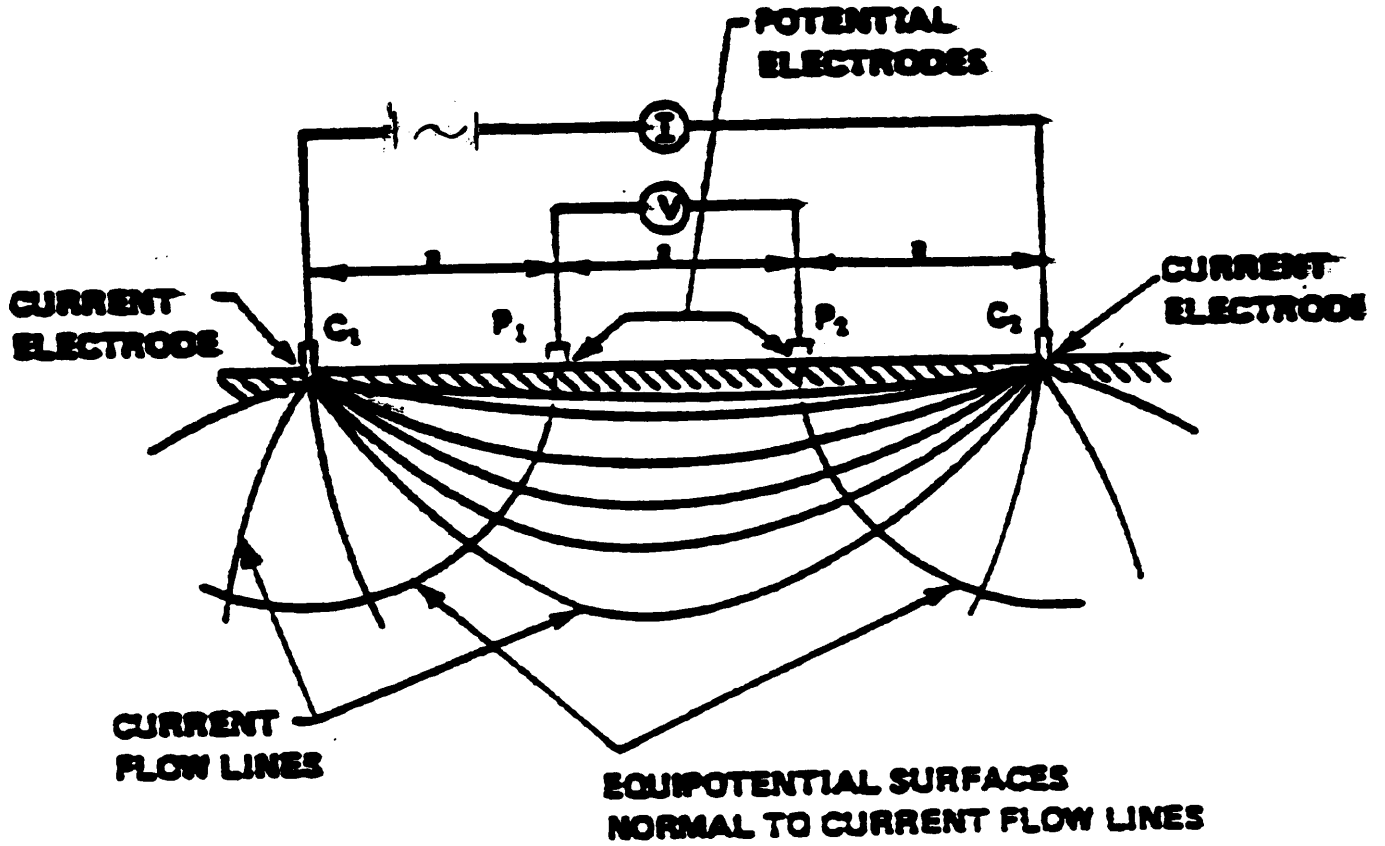


Fig.2.1- The four electrode method (9).

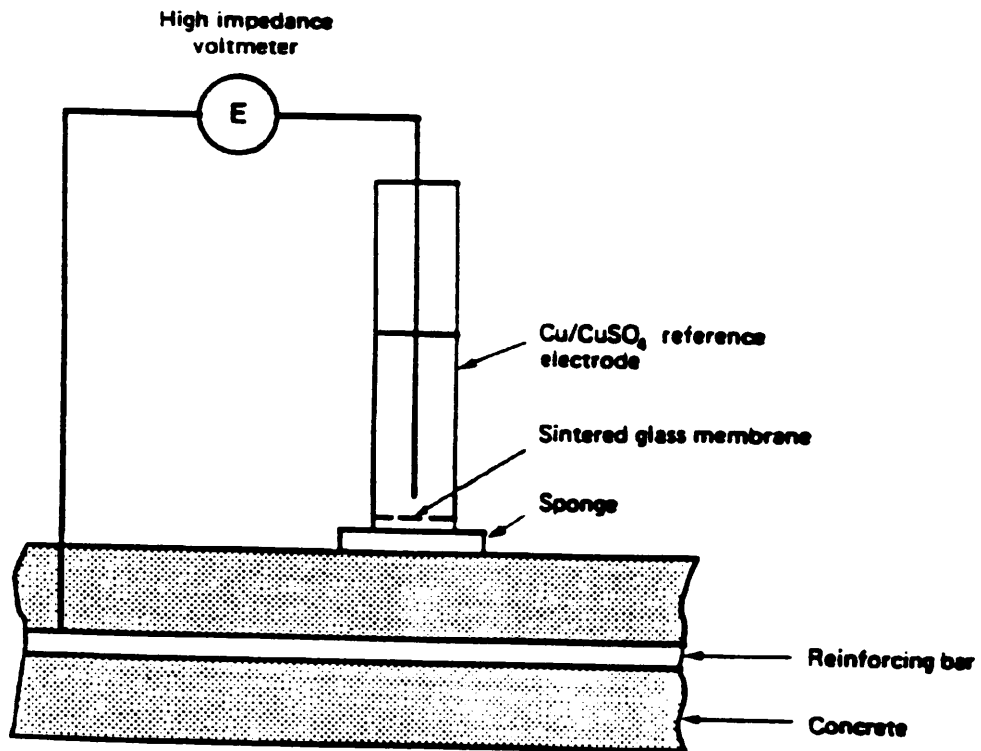
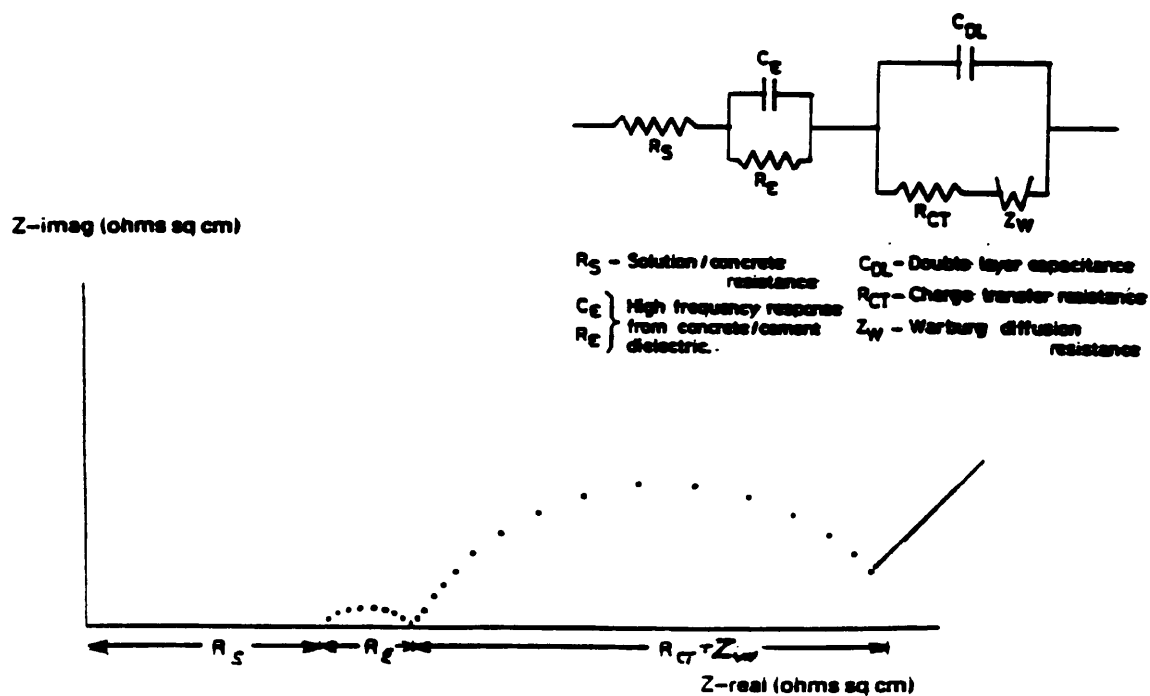
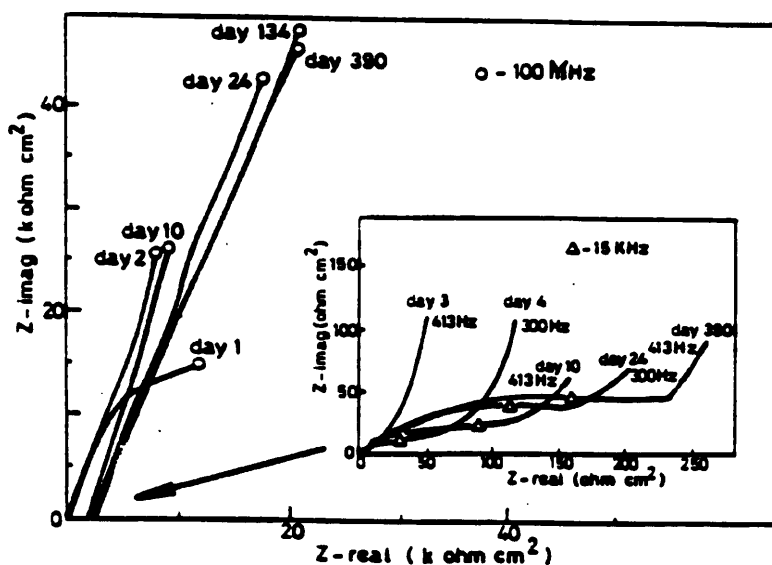


Fig.2.2- A system for measuring electrode potential of reinforcement.

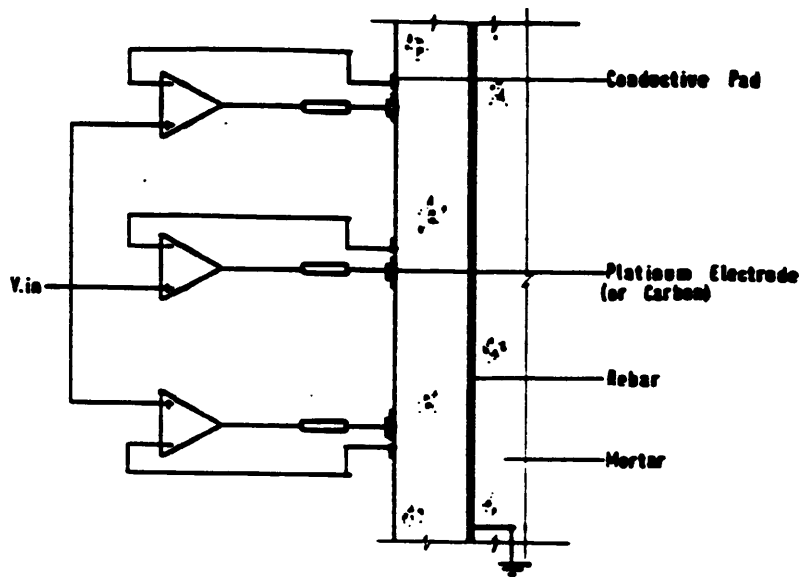


Equivalent circuit representation of steel in concrete and schematic impedance plot showing active corrosion (measurable R_{CT}) (9).

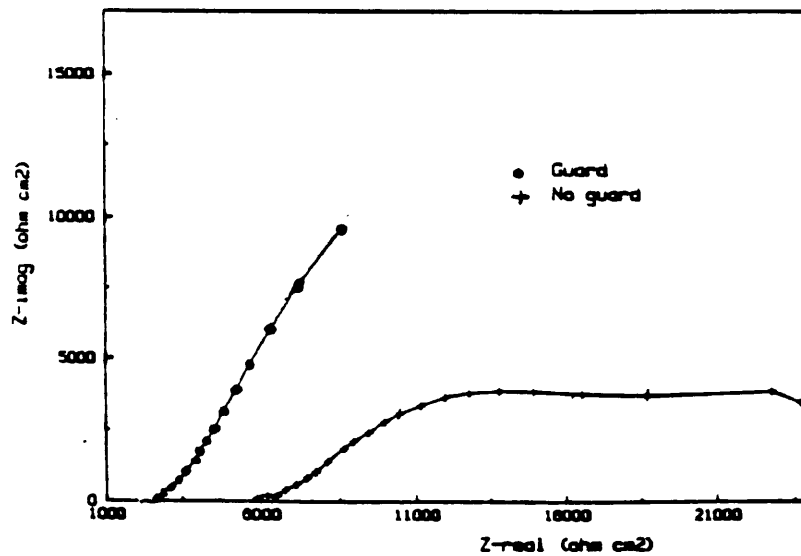


Impedance response from steel in a mortar containing chloride. No obvious corrosion. Note large diffusion effect in lower frequency range (9).

Fig.2.3



a) Guard ring arrangement.



b) Impedance measurements on reinforcement steel with and without guard ring (9).

Fig.2.4

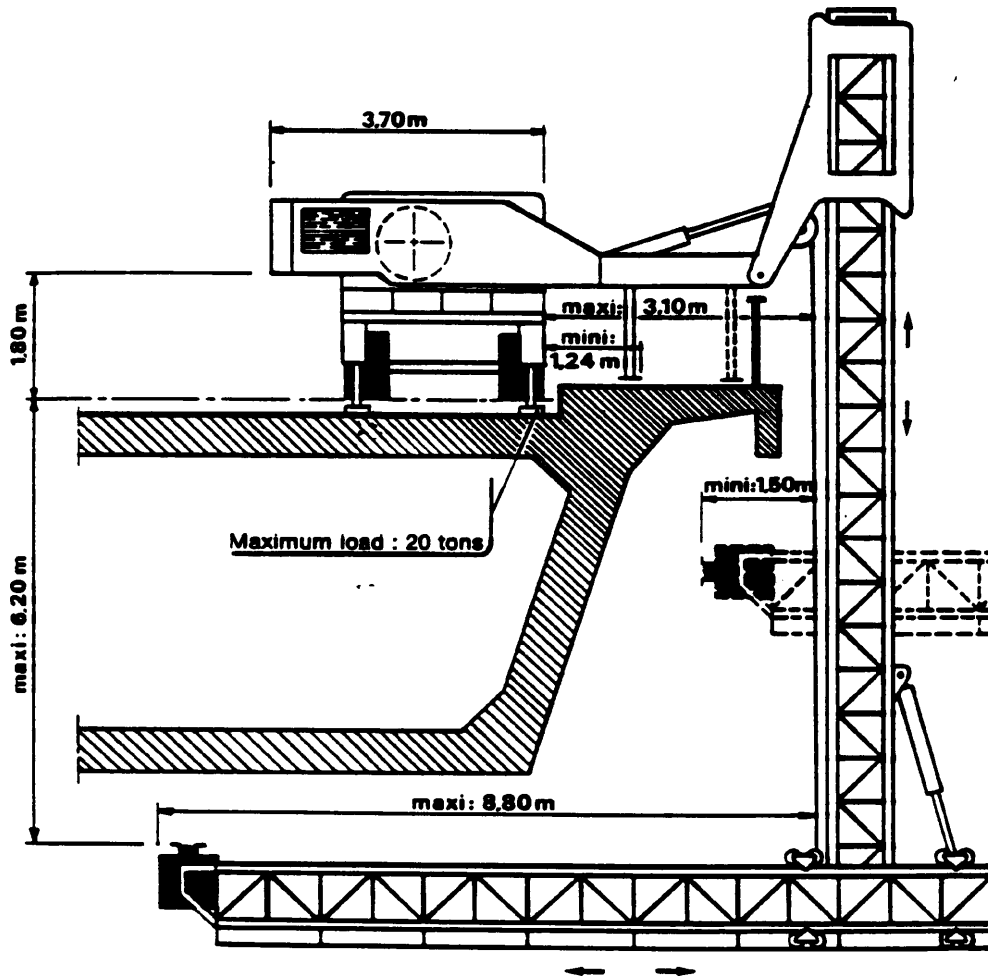


Fig.2.5- The SCORPION system (9).

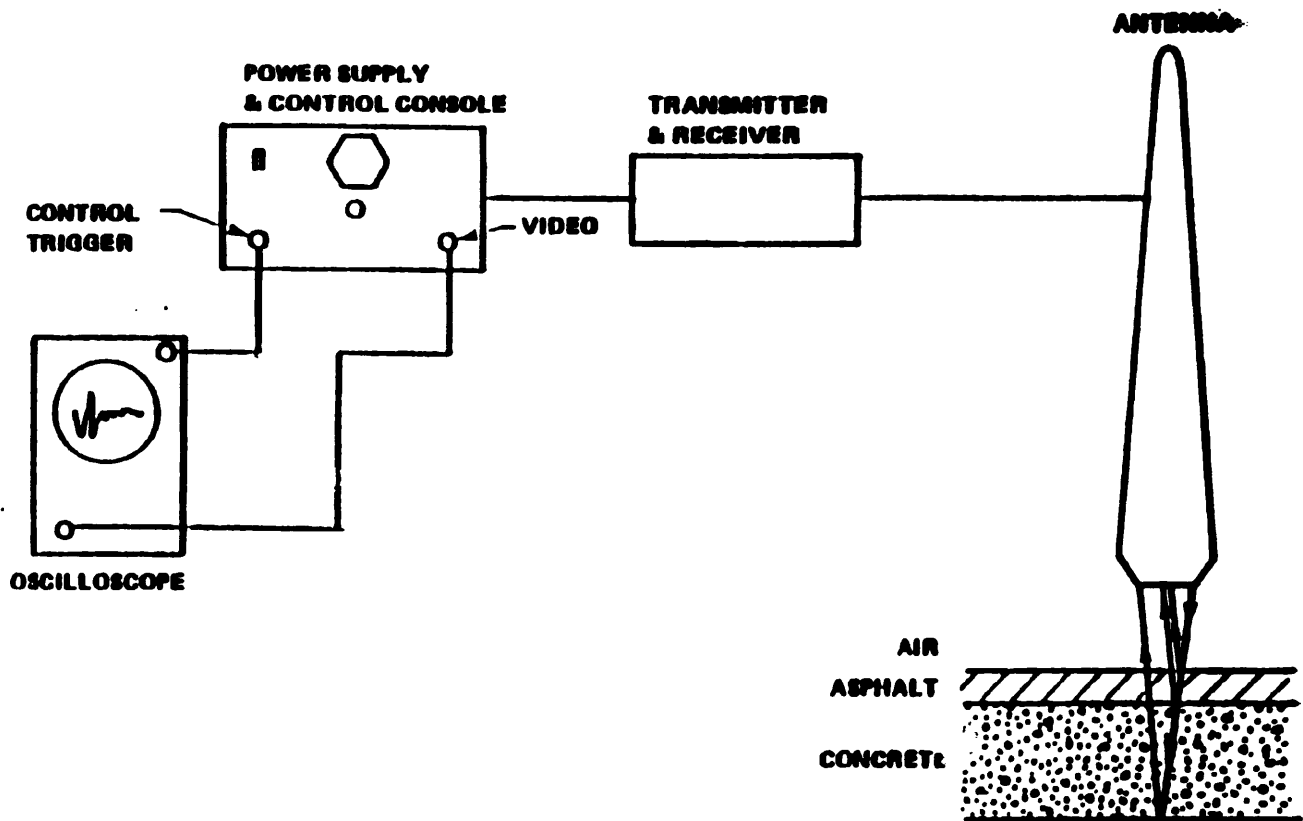


Fig.2.6- Elements of a radar system.

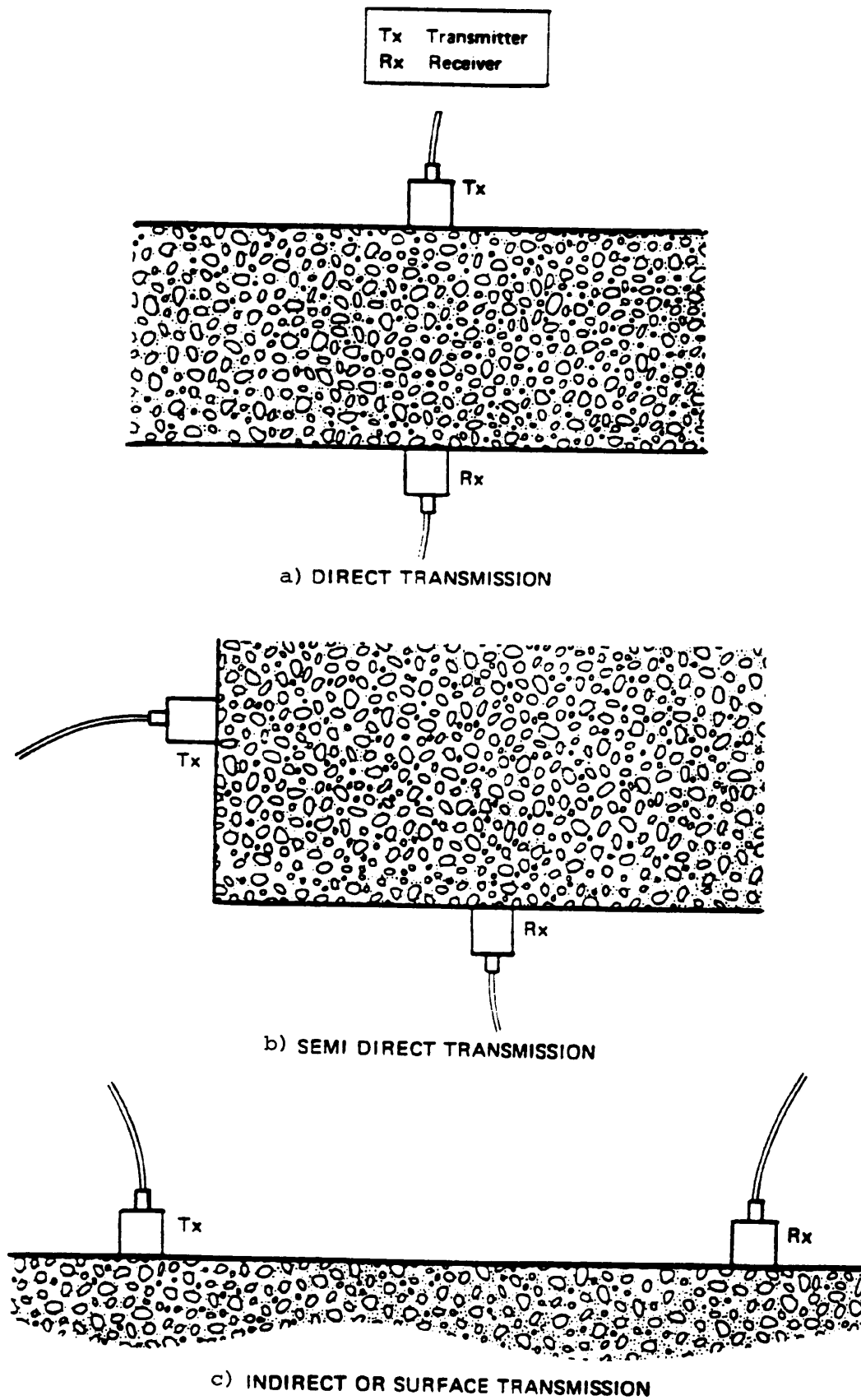


Fig.2.7

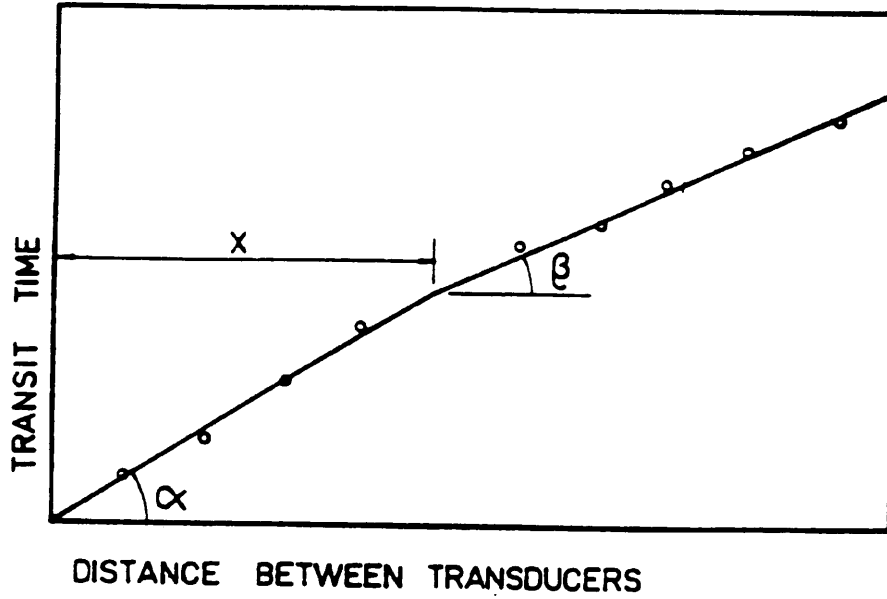
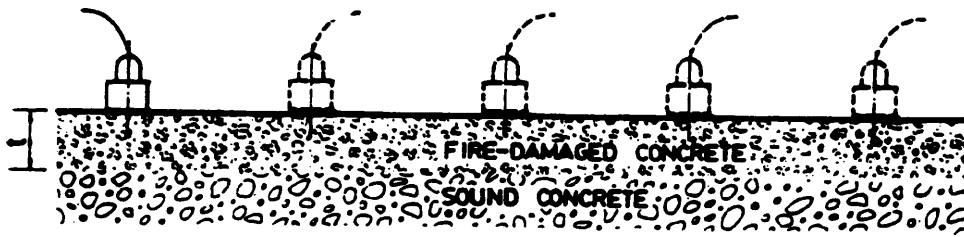


Fig.2.8- Ultrasonic measurement in fire-damaged concrete (44).

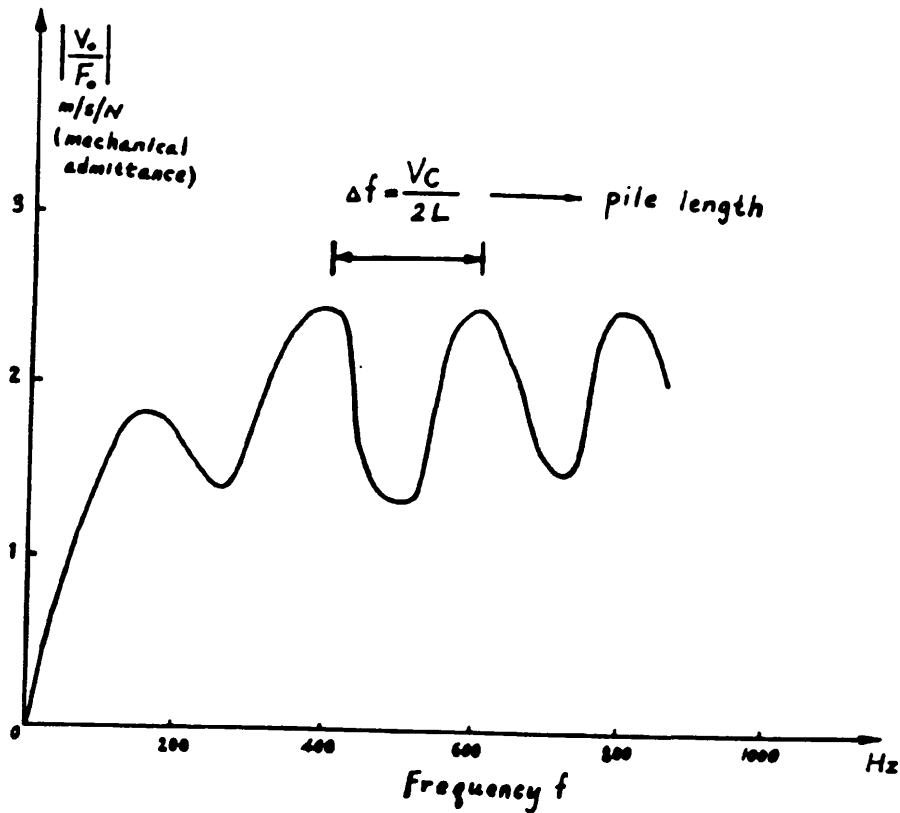


Fig.2.9- Frequency response function when a pile head is excited by a hammer (48).

CHAPTER 3

BACKGROUND TO WAVE PROPAGATION IN SOLIDS

3.1- INTRODUCTION

The purpose of this chapter is to provide background information on elastic wave propagation in solids and to study the losses due to boundaries.

3.2- BASIC PRINCIPLES OF ELASTIC WAVE PROPAGATION

3.2.1- Wave Types

There are three primary modes of stress wave propagation through isotropic, elastic media: dilatational, distortional, and Rayleigh waves.

Dilatational and distortional waves, commonly referred to as compression and shear waves, or P- and S-waves, are characterized by the direction of particle motion with respect to the direction the wavefront is propagating. In a P-wave (known as longitudinal or compressional waves), motion is parallel to the direction of propagation (see fig.3.1.a), in the S-wave, (known as shear or transverse waves) motion is perpendicular to the direction of propagation (fig.3.1.b). P-waves can propagate in all types of media, S-waves can propagate only in media with shear stiffness, i.e. solids. Where there is a solid/liquid or solid/gas

interface, Rayleigh waves (R-waves) can propagate along the interface. In an R-wave, particle motion is retrograde elliptical (fig.3.1.c). The amplitude of motion in the R-wave decreases exponentially with distance away from a free boundary (66). The shape of the P-, S-, and R- wavefronts depends upon the characteristics of the source that is used to generate the waves. There are three idealized types of wavefronts: planar, spherical, and cylindrical, e.g. when the stress waves are generated by a point source applied normal to the top surface of a plate, the resulting P-, S- wavefronts are spherical and the R-wavefront is circular.

3.2.2- Wave Velocity

The propagation of stress waves through a heterogeneous bounded solid, such as a structural concrete member, is a complex phenomenon. However, a basic understanding of the relationship between the physical properties of a material and the velocity of wave propagation can be acquired from the theory of wave propagation in infinite isotropic elastic media.

In infinite elastic solids, The P-wave velocity c_1 is a function of Young's modulus of elasticity, E , the mass density, ρ , and Poisson's ratio, μ ,

$$c_1 = \sqrt{E(1-\mu)/\rho(1+\mu)(1-2\mu)} \quad (\text{ref.67})$$

In bounded solids, such as thin plates or long rods, the P-wave velocity can vary depending on the dimensions of the solid

relative to the component wavelength (λ) of the propagating wave. For rod-like structures, such as piles, the P-wave velocity is independent of Poisson's ratio if the rod diameter is much less than the component wavelength (λ) of the propagating wave. In this case, c_1 is given by the following equation:

$$c_1 = \sqrt{E/\rho}$$

For a Poisson's ratio of 0.2, a typical value in concrete, the P-wave velocity is 5 per cent higher in an infinite solid than in a long thin rod.

The S-wave velocity, c_s , in an infinite solid is given by the following equation:

$$c_s = \sqrt{E/2\rho(1+\mu)} = \sqrt{G/\rho}$$

where G = shear modulus of elasticity.

A useful parameter is the ratio of S- to P- wave speeds:

$$c_s/c_1 = \sqrt{(1-2\mu)/2(1-\mu)}$$

For Poisson's ratio of 0.2, the ratio of the S- and P- wave velocity is 0.51.

Rayleigh waves propagate at a velocity, c_r , which can be

determined from the following approximate formula (67):

$$c_r = (0.87 + 1.12\mu) / (1 + \mu) c_s$$

For Poisson's ratio of 0.2, the R-wave velocity is 92 per cent of S-wave velocity.

P- and R- wave velocities are related by the following equation:

$$c_r = (0.87 + 1.12\mu) / (1 + \mu) \sqrt{(1 - 2\mu) / 2(1 - \mu)} c_p$$

Thus, if Poisson's ratio is known, the measured R-wave velocity can be used to estimate the P-wave velocity. For Poisson's ratio of 0.2, the R-wave velocity is 56 per cent of the P-wave velocity.

Wave velocity, c , and frequency, f , and wavelength, λ , are related by the following equation:

$$c = f\lambda$$

Stress waves generated are ^{normally} composed of a range of frequencies, therefore, they contain a number of different wavelengths.

3.3- REFLECTION AND REFRACTION

When a P- or S- wavefront is incident upon an interface between dissimilar media, 'specular' reflection occurs. The term specular reflection is used since the reflection of stress waves is similar

to the reflection of light by a mirror. Stress waves can be visualized as propagating along ray paths and the geometry of ray reflection is analogous to that of light rays. Representative ray paths are shown in fig.3.2. The path of the R-wave is denoted by an R, and the paths of variously reflected P- and S- wave rays are denoted by a P or an S. For example, the 2P- ray (or PP ray) represents a P-ray incident upon and reflected by an interface. The shape of the reflected wavefront can be determined by considering the reflection of individual rays.

At a boundary between two different media only a portion of a stress wave is reflected. The remainder of the wave penetrates into the underlying medium (wave refraction). The angle of refraction, β , is a function of the angle of incidence, θ , and the ratio of wave velocities, c_2/c_1 , in the different media, and is given by Snell's Law:

$$\sin\beta = c_2/c_1 \sin\theta$$

where c_1 = sound velocity in medium 1

c_2 = sound velocity in medium 2.

Unlike light waves, stress waves can change their mode of propagation when striking the surface of a solid at an oblique angle. The incident P-wave can be partially reflected as both P- and S- waves, depending on the angle of incidence. Since the S-waves propagate at a lower velocity than P-waves, they will reflect and refract at angles (determined using Snell's Law) that are less than the angles of reflection and refraction for P-waves.

The relative amplitudes of reflected waves depend upon the mismatch in specific acoustic impedances at an interface, The angle of incidence, the distance of an interface from the pulse source, and the attenuation along the wave path. The influence of each of these factors is considered in the following discussion.

The position of an incident plane P-wave that is reflected at an interface between two media of different densities or elastic moduli depends on the specific acoustic impedances of each medium. The specific acoustic impedance, Z , of a medium is:

$$Z = c_1 \rho$$

If we assume c_1 is approximately equal to $\sqrt{E/\rho}$ then

$$Z = \sqrt{E\rho}$$

Specific acoustic impedance values for P-waves in selected materials are given in table 3.1.

The formula for acoustic impedance is also valid for S-waves if the S-wave velocity is used to calculate it.

The amplitude of particle motion in a reflected ray, A_r , is maximum when the angle of incidence of ray is normal to the

interface and is determined from the following equation:

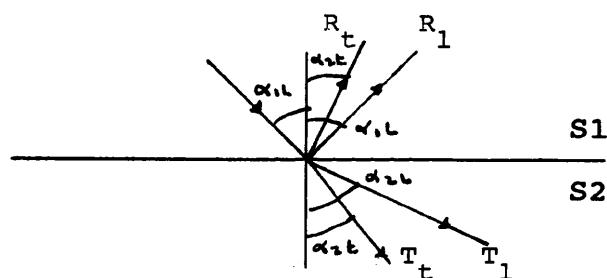
$$A_r = A_i (Z_1 - Z_2) / (Z_1 + Z_2)$$

where A_i = the amplitude of motion in the incident ray.

Z_1 and Z_2 are the acoustic impedances in media 1 and 2 respectively.

To derive the coefficients of reflection and refraction for the amplitude of a reflected and refracted wave for different boundary conditions, two mathematical models are generally used. The first is the plane wave model, the second is the spherical wave propagation model (usually used in seismology) which is more complicated to solve than the plane wave model. For the present work only the plane wave case will be considered, coefficients of reflection for spherical wave are discussed by Nickerson (68). The following equations are for the case of longitudinal wave incidence.

The equations for the case of solid-solid interface are:



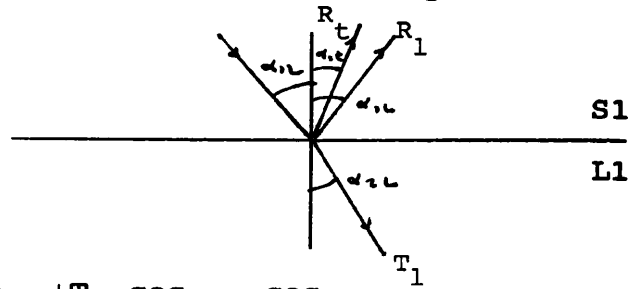
$$R_1 \cos \alpha_{1t} - R_t \sin \alpha_{1t} + T_1 \cos \alpha_{2t} + T_t \sin \alpha_{2t} = \cos \alpha_{1t}$$

$$R_1 \sin \alpha_{1t} + R_t \cos \alpha_{1t} - T_1 \sin \alpha_{2t} + T_t \cos \alpha_{2t} = -\sin \alpha_{1t}$$

$$R_1 Z_{11} \cos 2\alpha_{1t} - R_t Z_{1t} \sin 2\alpha_{1t} - T_1 Z_{21} \cos 2\alpha_{2t} - T_t Z_{2t} \sin 2\alpha_{2t} = -Z_{11} \cos 2\alpha_{1t}$$

$$R_1 Z_{1t} c_{1t} \sin 2\alpha_{1t} / c_{11} + R_t Z_{1t} \cos 2\alpha_{1t} + T_1 Z_{2t} c_{2t} \sin 2\alpha_{2t} / c_{21} - T_t Z_{2t} \cos 2\alpha_{2t} = Z_{1t} c_{1t} \sin 2\alpha_{1t} / c_{11}$$

The equations for the case of solid-liquid are:

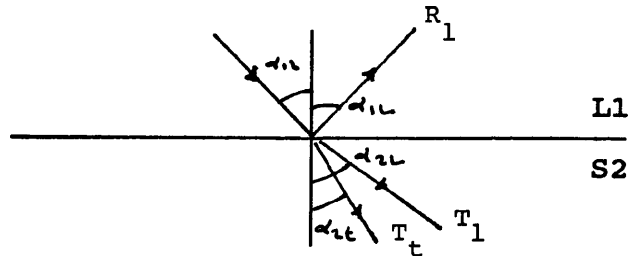


$$R_l \cos \alpha_{1l} - R_t \sin \alpha_{1t} + T_l \cos \alpha_{2l} = \cos \alpha_{1l}$$

$$R_l \sin 2\alpha_{1l}/c_{1l} + R_t \sin 2\alpha_{1t}/c_{1t} = \sin 2\alpha_{1l}/c_{1l}$$

$$R_l Z_{1l} \cos 2\alpha_{1t} - R_t Z_{1t} \sin 2\alpha_{1t} - Z_{2l} = -Z_{1l} \cos 2\alpha_{1t}$$

The equations for the case of liquid-solid are:

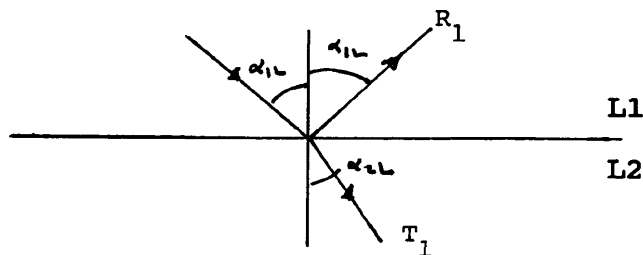


$$R_l \cos \alpha_{1l} + T_l \cos \alpha_{2l} + T_t \sin \alpha_{2t} = \cos \alpha_{1l}$$

$$T_l \sin 2\alpha_{2l}/c_{2l} - T_t \cos 2\alpha_{2t}/c_{2t} = 0$$

$$R_l Z_{1l} - T_{2l} Z_{2l} \cos 2\alpha_{2t} - T_{2t} \sin 2\alpha_{2t} = -Z_{1l}$$

The equations for the case liquid-liquid are give by:



$$R_l Z_{1l} - T_l Z_{2l} = -Z_{1l}$$

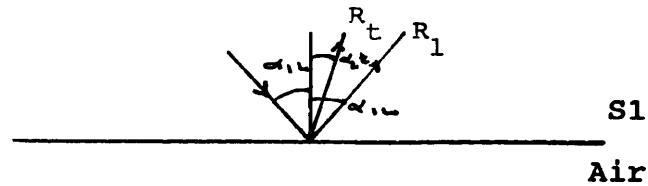
$$R_l \cos \alpha_{1l} + T_l \cos \alpha_{2l} = \cos \alpha_{1l}$$

Where R_l , R_t : the coefficients of reflection for longitudinal and transverse waves respectively

T_l , T_t : the coefficients of refraction for longitudinal and transverse waves respectively

Z_l , Z_t : the acoustic impedances for longitudinal and transverse waves respectively.

The equations for solid-vacuum interface are:



$$R_1 Z_{1l} \cos 2\alpha_{1t} - R_t Z_{1t} \sin \alpha_{1t} = -Z_{1l} \cos 2\alpha_{1t}$$

$$R_1 Z_{1l} \sin 2\alpha_{1t} / c_{1l}^2 + R_t Z_{1t} \cos 2\alpha_{1t} / c_{1t}^2 = Z_{1l} \sin 2\alpha_{1l} / c_{1l}^2$$

It should be noted that the indices used are: '1' for incident or first surface, '2' for the second material, and 'l' for P-wave (longitudinal), 't' for S-wave (transverse). In the above equations the angles are related by the following relationship (known as Snell's Law):

$$\sin \alpha_{1l} / c_{1l} = \sin \alpha_{1t} / c_{1t} = \sin \alpha_{2l} / c_{2l} = \sin \alpha_{2t} / c_{2t}$$

Computer programs were written to plot the coefficients of reflection and transmission for the cases steel/air, concrete/air, concrete/water, water/concrete, steel/water, water/steel, concrete/steel, and steel/concrete.

Fig.3.3 shows the coefficients of reflected waves against the incident angle of longitudinal wave in case of steel/air (fig.3.3.a) and concrete/air (fig.3.3.b).

Fig.3.4 shows the coefficients of reflected and transmitted waves against the angle of incidence of longitudinal wave in the case of steel/water (fig.3.4.a) and water/steel (fig.3.4.b).

Fig.3.5 shows the coefficients of reflected and transmitted waves

against the angle of incidence of longitudinal wave in the case of concrete/water (fig.3.5.a) and water/concrete (fig.3.5.b).

Fig.3.6 shows the coefficients of reflected and transmitted waves against the angle of incidence of longitudinal wave in the case of steel/concrete (fig.3.6.a) and concrete/steel (fig.3.6.b).

In the previous discussion it was assumed that reflection and refraction of wavefronts occurred at planar interfaces between two dissimilar media. This type of analysis is also applicable to flaws or discontinuities within a medium.

The ability of stress wave propagation methods to detect flaws or discontinuities (sensitivity) depends on the component frequencies or wavelengths, in the propagating wave, and on the size of the flaw or discontinuity.

A general rule is that waves will diffract or bend around the edges of discontinuities if the size of the discontinuity is of the same order or less than the component wavelengths in the propagating wave. Therefore, to detect flaws of the order of 0.1m, it is necessary to introduce into the concrete (P-wave velocity of 4000m/s) a stress pulse that contains frequencies greater than approximately 20kHz (wavelengths less than approximately 0.1m).

3.3.1- Diffraction at a Crack Tip

Where a stress pulse is incident upon a crack tip (or the sharp

edge of a discontinuity) diffracted waves are produced. Mode conversion of the incident wave also occurs at the crack tip producing a second diffracted wave (67). For example, a P-wave incident upon a crack tip produces a diffracted P-wave, and a diffracted S-wave.

3.3.2- Attenuation and Divergence

As a wave propagates through a solid the acoustic pressure, and thus the amplitude of particle motion decreases with path length due to attenuation (scattering and absorption) and divergence.

The acoustic pressure (P) and the particle amplitude (A) are connected to each other by the relation (67):

$$P = Z\omega A \text{ where } \omega \text{ is the angular frequency} = 2\pi f$$

Another important relation which relates the sound pressure and the intensity of a wave:

$$J = P^2 / 2Z$$

In a heterogeneous solid, scattering is the result of wave reflection, refraction, diffraction, and mode conversion at each interface between dissimilar media.

In ordinary concrete, the density and the elastic modulus of the coarse aggregates are higher than those of the mortar. If the wavelength of the propagating wave is less than the size of the

aggregate, this mismatch in impedances causes scattering of the incident wave as the waves undergo reflection and refraction from each mortar-aggregate interface. For higher quality concrete (higher density, and greater elastic modulus of mortar) the specific acoustic impedance of the mortar approaches that of the coarse aggregate, and scattering is reduced. Hence, in evaluation of concrete, lower frequency waves should be used i.e. the wavelength to aggregate size ratio must be increased λ/D_{agg} , to reduce the attenuation of wave energy due to scattering. However, use of lower frequency waves reduces the sensitivity of the propagating waves to small flaws. Thus, there is a limitation in the flaw size, that can be detected within concrete.

Although attenuation of wave energy in heterogeneous solids is primarily due to scattering, part of the wave energy is absorbed and turned in heat, (hysteretic damping) (69). In solids, damping is mainly caused by internal friction.

Attenuation also affects the frequency content of the pulse propagating in a heterogeneous medium, which will be discussed more in chapter 6. Pulses produced contain a range of frequencies, and in a material such as concrete, the higher frequency components of the propagating pulse will be preferentially attenuated with the path length. As a result, the frequency spectrum of the pulse is continuously shifted to lower frequencies. Thus, both the sensitivity and the acoustic pressure of a pulse decrease with path length.

For non-planar waves (e.g. spherical waves) reduction of the

acoustic pressure also occurs due to spreading of the wavefront as it propagates through the test medium (divergence) (67). For a transducer producing a spherical wavefront, divergence causes the pressure to vary as the inverse of the distance from the source (67). Both incident and reflected waves undergo attenuation and divergence, thus, the amplitude of the signal decreases with total path length. The relative losses caused by attenuation and divergence will depend upon the attenuation coefficient of both the test medium and the frequency content of the propagating wave. Chapter 6 will deal with the attenuation of sound in concrete.

3.4- TRANSDUCERS FOR TRANSMITTING AND RECEIVING WAVES IN ULTRASONICS

Sound waves are generated or received by a device called a transducer, this converts energy from one form to another. There are various types of transducers such as: electrostatic, piezoelectric (crystal), electromagnetic transducers and others. In this study only piezoelectric oscillators have been used. If external mechanical pressure is applied to a piezoelectric material, electric charges are produced on its surface, this is called the direct piezoelectric effect. The second is the inverse piezoelectric effect, which occurs when such material is placed between two electrodes, when it changes its form producing mechanical pressures, deformations, and oscillations.

A number of materials have been found to show the piezoelectric effect such as lead zirconate titanate (PZT), barium titanate

(BaTiO₃), quartz (SiO₂), lead metaniobate (PbNb₂O₆) and others. Table 3.2 gives constants of some piezoelectric materials.

In table 3.2, g_{33} is the piezoelectric pressure constant and is related to the receiving voltage and the pressure by:

$$U_e = g_{33} d P \quad (\text{ref.67})$$

where U_e is the receiving voltage, Volts

d is the thickness, in $m = \lambda/2 = c/2f$ for longitudinal transducers

P is the pressure which produces the change in thickness, N/m^2

c is the velocity of sound in the crystal

Moreover, k_{33} (table 3.2) is the electromechanical coupling coefficient factor which for a piezoelectric material is a reference for the efficiency of the conversion of electric voltage into mechanical displacement and vice versa, and is given by:

$$U_e / U_s = k_{33}^2 \quad (\text{ref.67})$$

where U_s is the transmitting voltage, Volts.

Most of the crystals used in this study were barium titanate, from table 3.2 $k_{33} = 0.45$, and the transmitted voltage was 600V, thus:

$$U_e = 121.5V$$

For example for 200kHz transducer, the thickness of the crystal would be $d = 12.75\text{mm}$, therefore the pressure which produces the change in thickness is: $P = 9.5 \times 10^6 \text{ N/m}^2$.

After this introduction to the structure of ultrasonic transducers, the sound field produced will now be defined. Consider a piston source, i.e. an acoustic source which consists of a surface moving backwards and forwards like a piston. According to Huygen's principle, each point of this surface acts as an elementary source radiating elementary wavelets into the medium in contact with it. These elementary wavelets interfere with each other, resulting in the emerging acoustic wavefront (70).

In front of^a circular radiator a complicated interference pattern is formed with pressure minima and maxima, this is called the near field, and it extends from the source to the last interference maxima and its length, N , can be expressed as:

$$N = (D^2 - \lambda^2) / 4\lambda \approx D^2 / 4\lambda, \text{ if } \lambda \ll D$$

where D is the diameter of the oscillator

λ is the wavelength in the material.

At the end of the near field is the beginning of the far field, the characteristic feature of which is that it is divergent, and the half angle θ of the beam is given by:

$$\sin\theta = 1.2\lambda / D$$

The directional sound pressure in the far-field is given by:

$$P_\theta = J_1(x) / x$$

where $x = \pi D \sin\theta / \lambda$, and $J_1(x)$ is the Bessel function of the first order, which can be approximated to the sine (71).

Fig.3.7 shows the polar diagrams for $d/\lambda=2$ and 4.

The acoustic pressure along the axis is given (67):

$$P = P_0 \sin\left(\frac{\pi}{\lambda} (\sqrt{R^2+x^2} - x)\right)$$

where P_0 is the the initial pressure

x is the axial distance from the transducer

R is the radius of the radiator.

At large distance x , this relation can be approximated to:

$$P = P_0 \frac{\pi D^2}{4\lambda} \frac{1}{x}, \text{ for } x \gg D^2/4\lambda$$

A computer program was written to plot the pressure against the distance in the far-field along the axis. Fig.3.8 illustrates the result for $f=5\text{MHz}$ and $D=20\text{mm}$.

For $\lambda/D > 1$, the angle increases to 90° , Roderick (55) showed the characteristic of an oscillator of this type. Fig.3.9 shows the far-field characteristic for this case. It consists of an almost spherical portion for longitudinal waves and a lobed section for transverse waves, which ^{is} also associated with strong surface waves radiated simultaneously by a small oscillator.

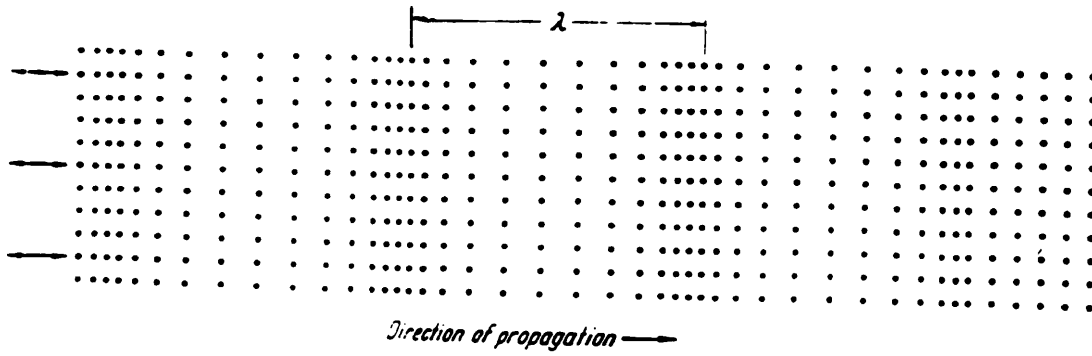
Table 3.1- Specific acoustic impedances

Material	Density Kg/m ³	P-wave velocity velocity, m/s	Specific acoustic impedance, Kg/(m ² .sec)
Air	1.205	343	0.413
Concrete*	2300	3000-4500	6.9-10.4 10^6
Granite	2750	5500-6100	15.1-16.8 10^6
Limestone	2690	2800-7000	7.50-18.8 10^6
Marble	2650	3700-6900	9.80-18.3 10^6
Quartzite	2620	5600-6100	14.7-16.0 10^6
Soils	1400-2150	200- 2000	0.28-4.30 10^6
Steel	7850	5940	46.6 10^6
Water	1000	1480	1.48 10^6

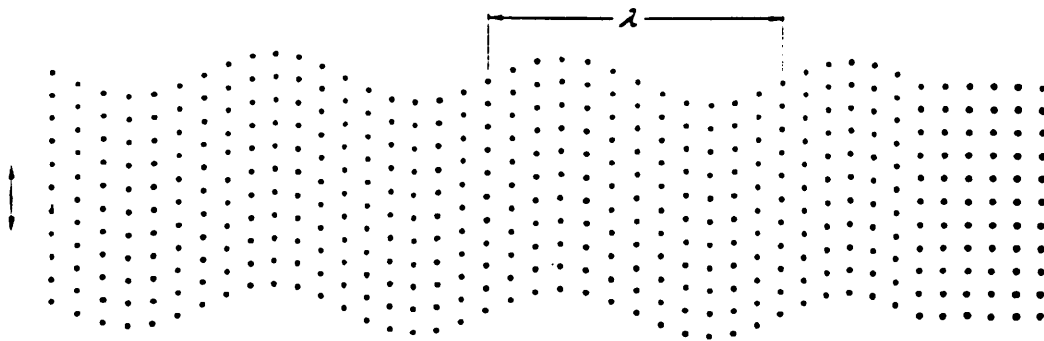
* The mass density of concrete depends on the mix proportions and the specific gravities of the mix ingredients. The given density is for an average, normal weight concrete.

Table 3.2- Constants of some piezoelectric materials (67)

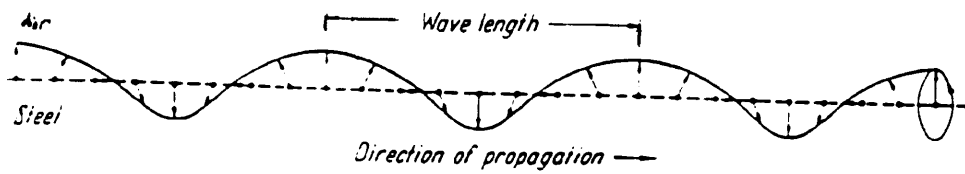
	Lead Zircontate Titanate	Barium Titanate	Quartz
Density (Kg/m ³)	7500	5400	2650
Acoustic Velocity (m/s)	4000	5100	5740
Acoustic Impedance (N.s/m ²)	30E+6	27E+6	15.2E6
k ₃₃ (Electro-mechanical Coefficient of Coupling)	0.6-0.7	0.45	0.1
g ₃₃ (Piezoelectric Pre- ssure constant), V.m/N	20-40E-3	14-21E-3	57E-3



(a) Longitudinal wave.

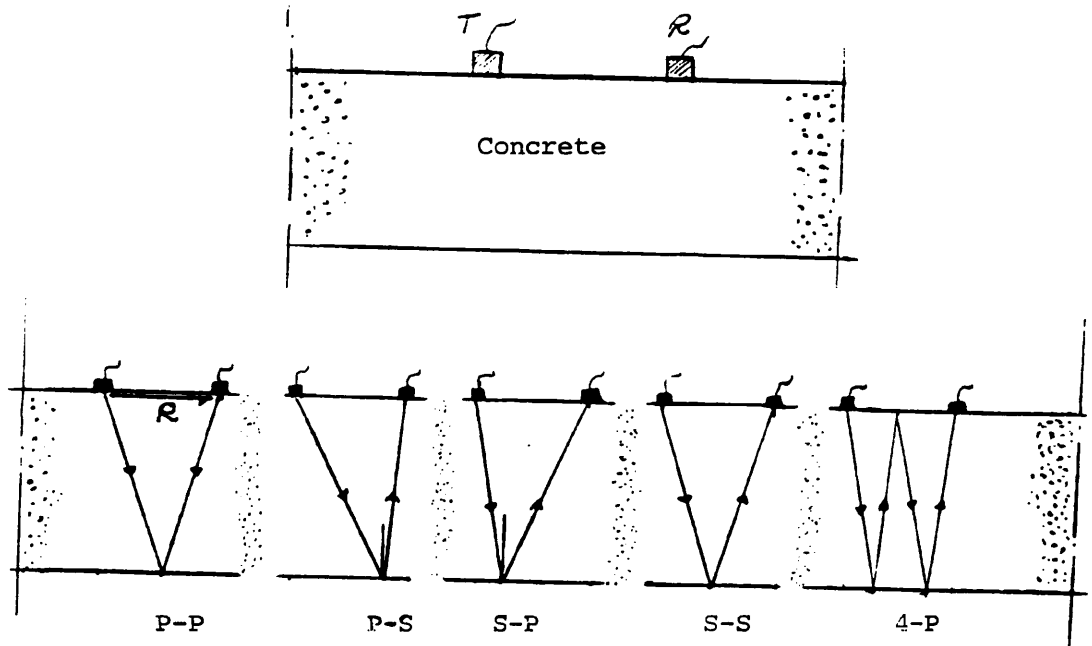


(b) Transverse wave.



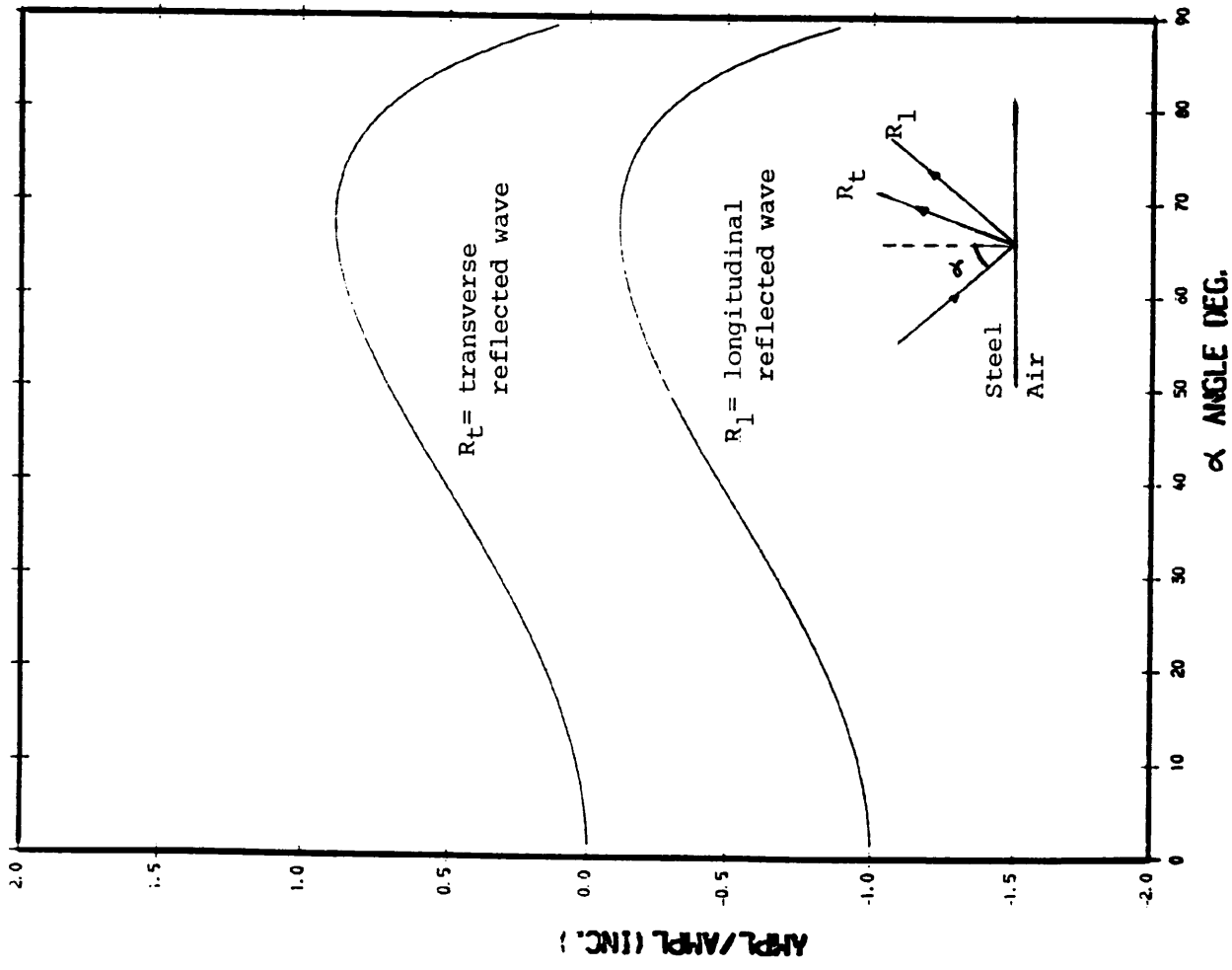
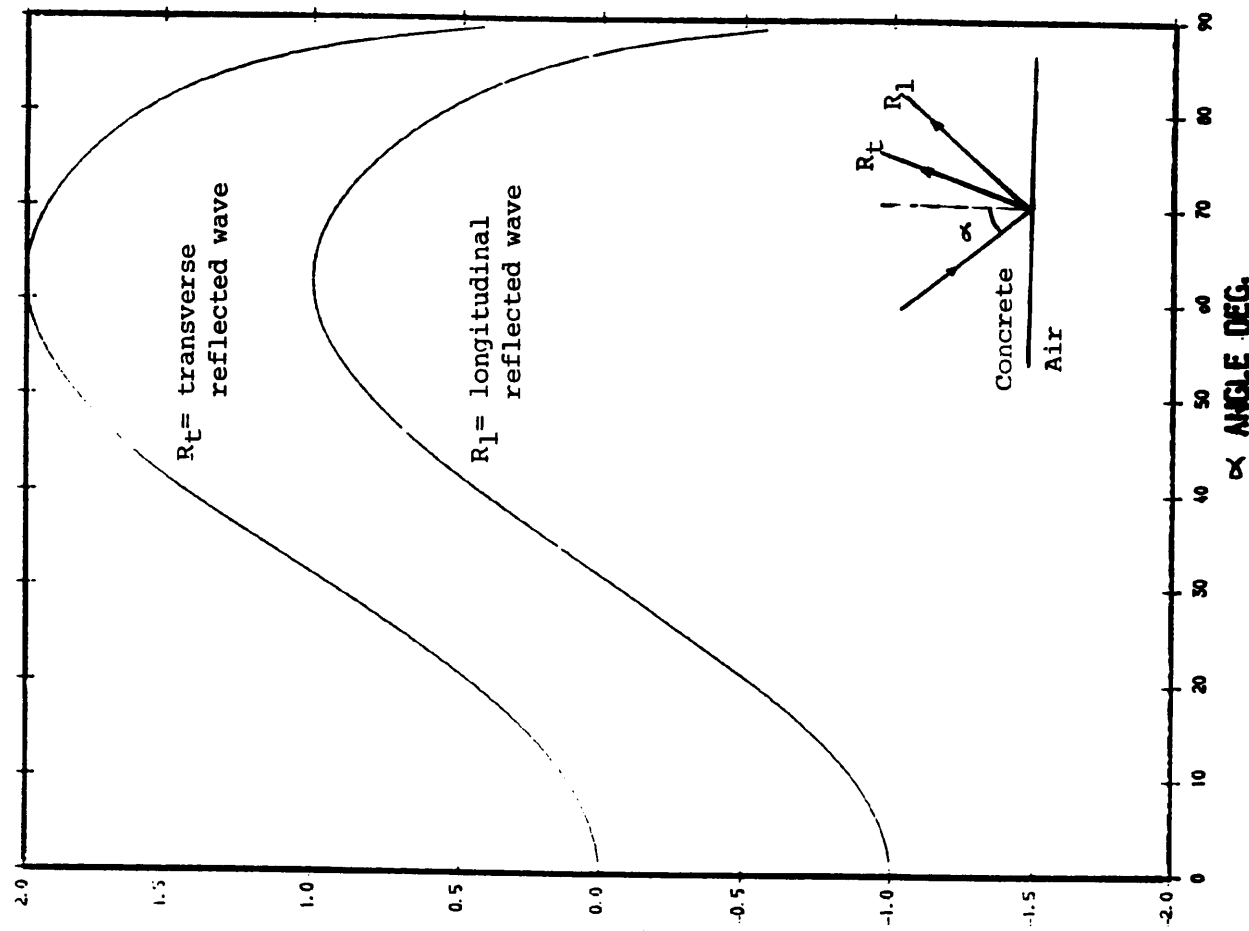
(c) Surface wave on steel. On the right, oscillation ellipse of a particle and sense of rotation

Fig.3.1- Modes of vibrations.



R= Rayleigh wave, P= Longitudinal wave, S= Shear wave.

Fig.3.2- Representative ray paths expected in concrete.



(a) (b)

Fig.3.3- Coefficients of reflection for steel/air and concrete/air.

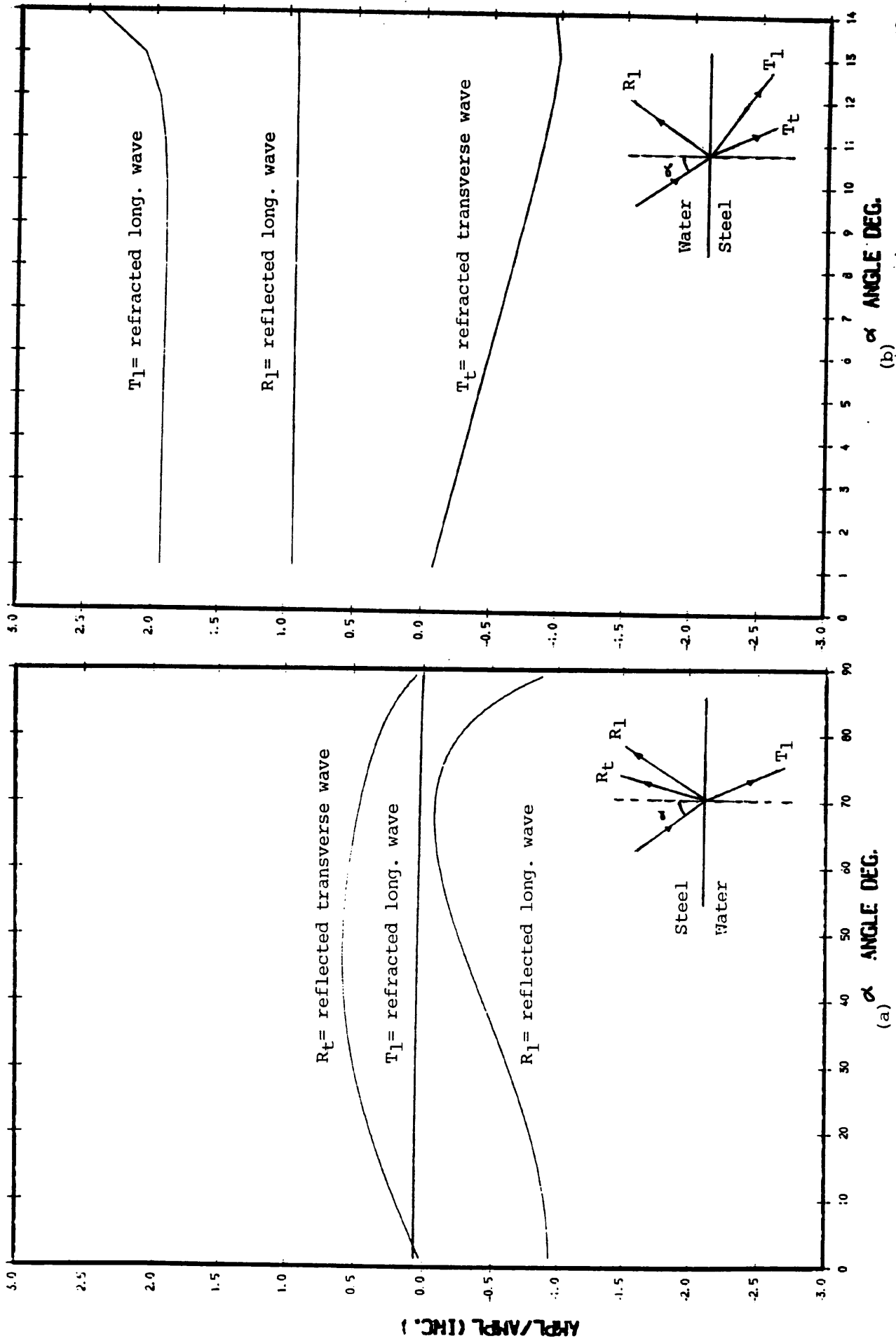


Fig. 3.4- Coefficients of reflection and refraction for steel/water and water/steel.

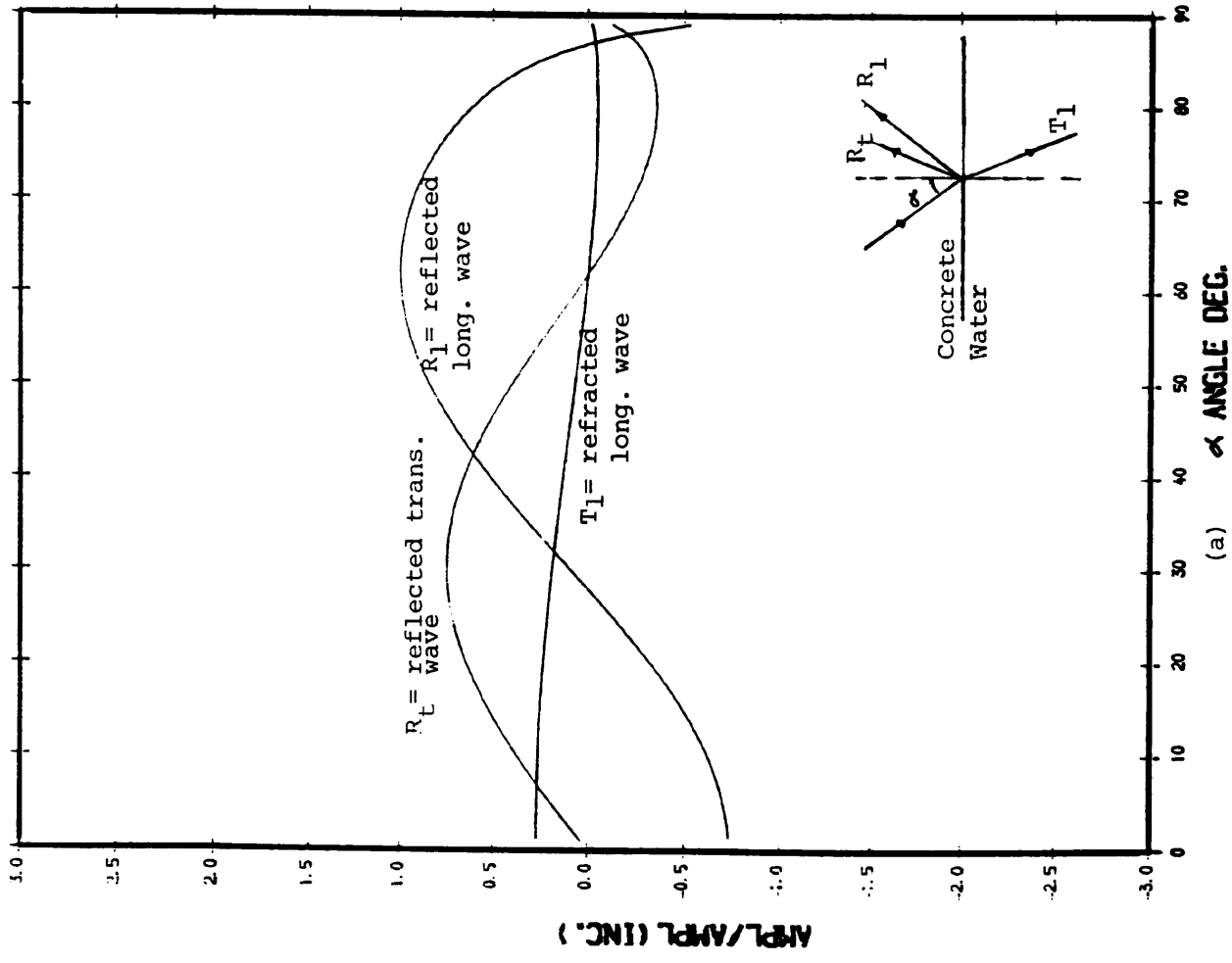
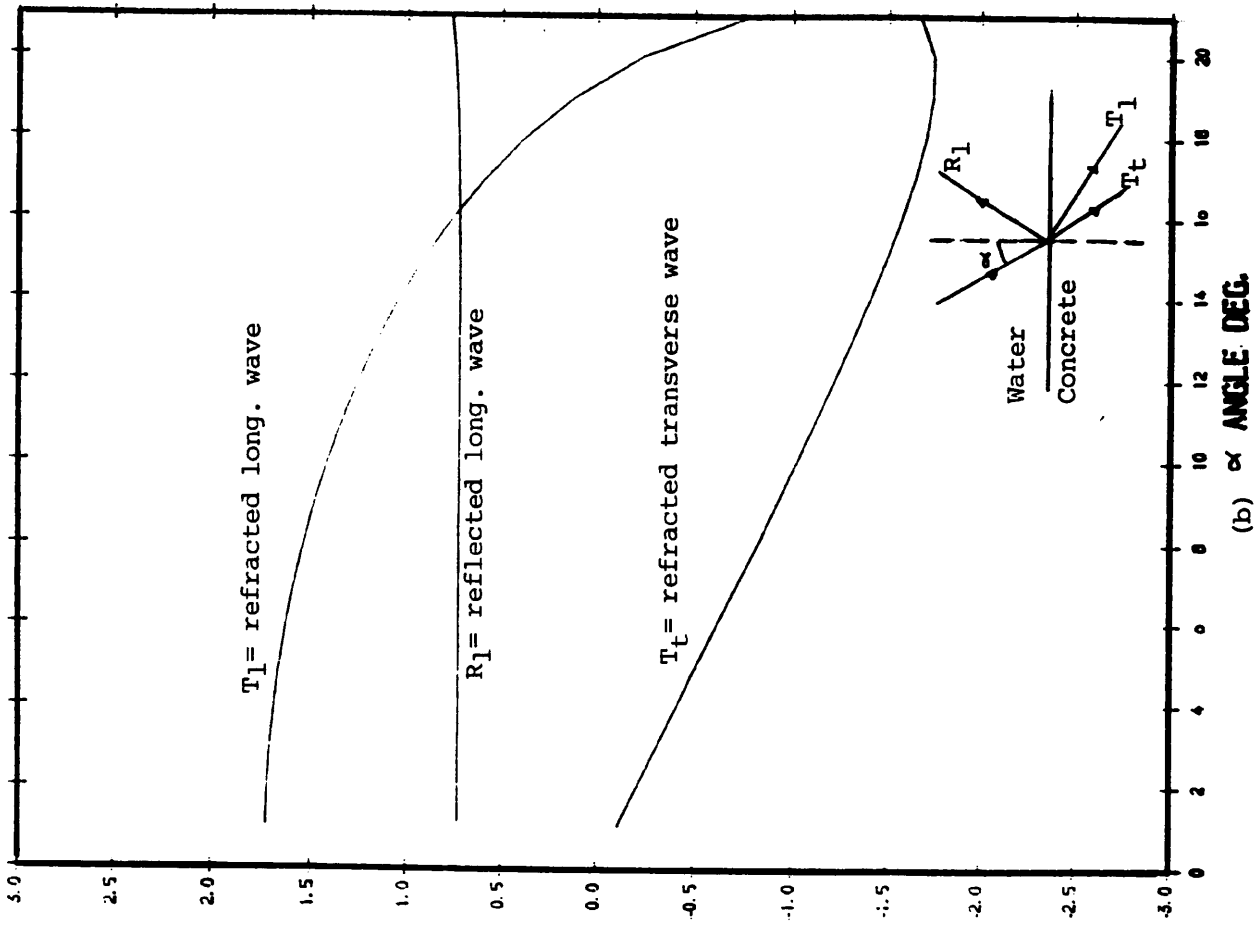


Fig.3.5- Coefficients of reflection and refraction for concrete/water and water/concrete.

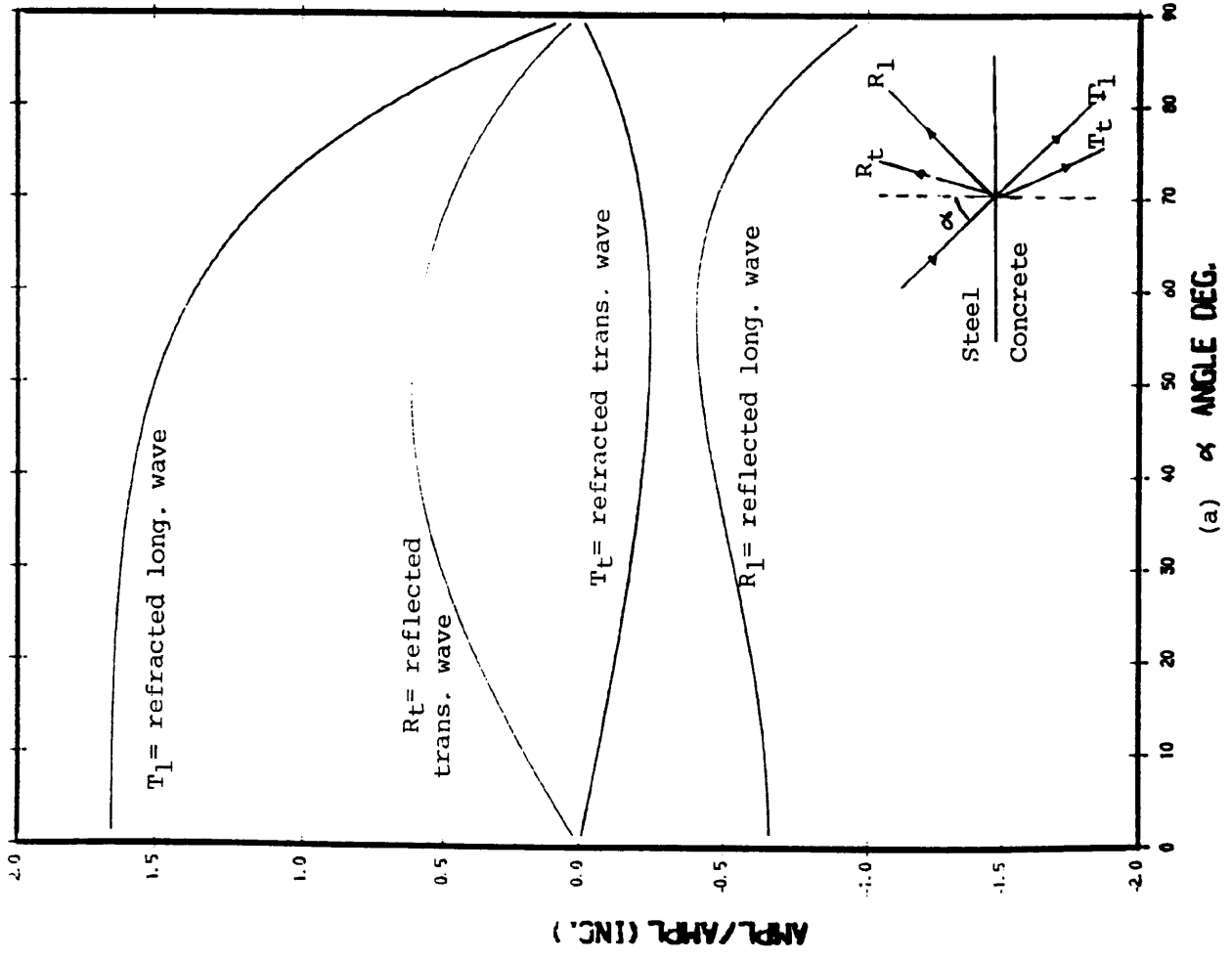
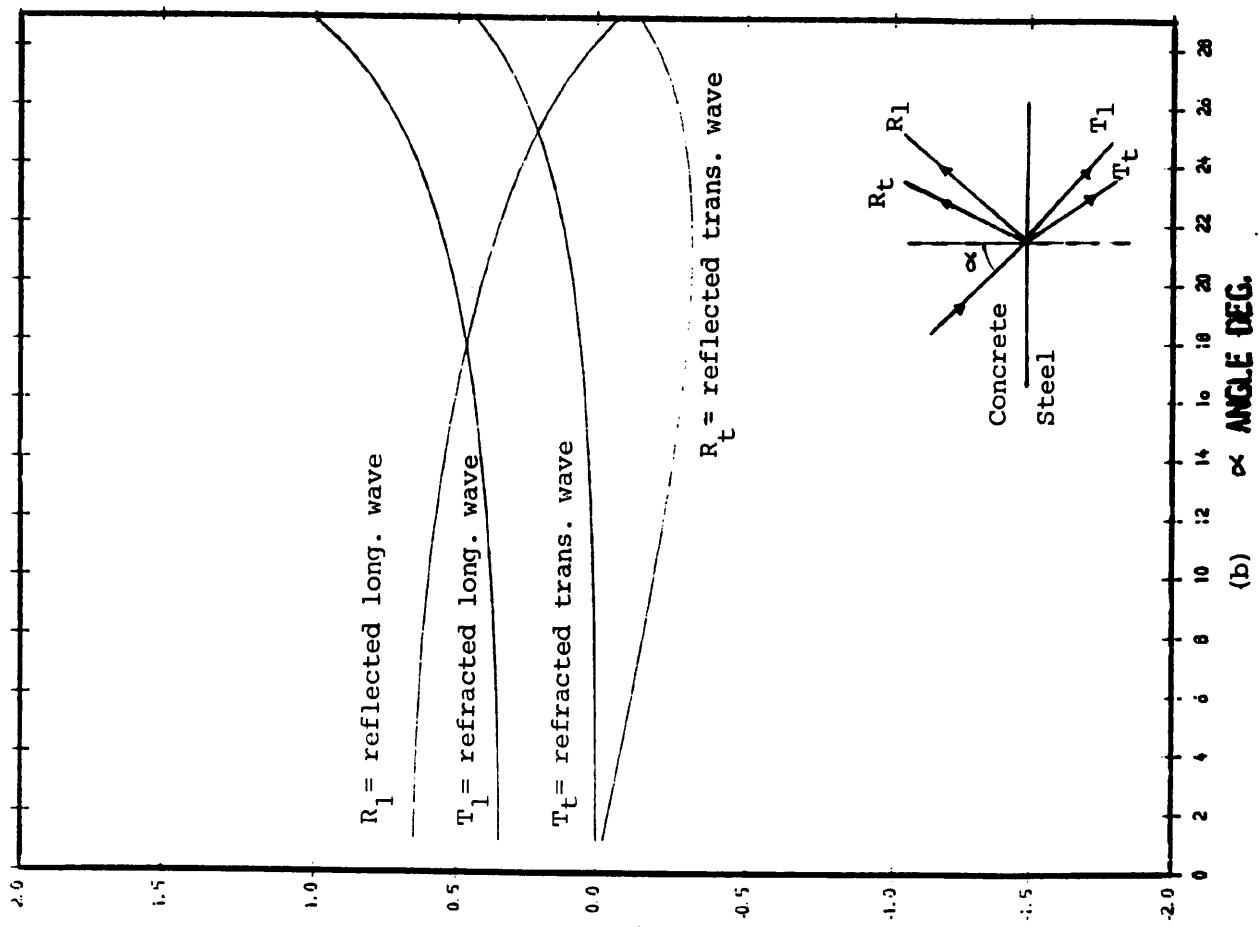


Fig.3.6- Coefficients of reflection and refraction for the steel/concrete and concrete/steel.

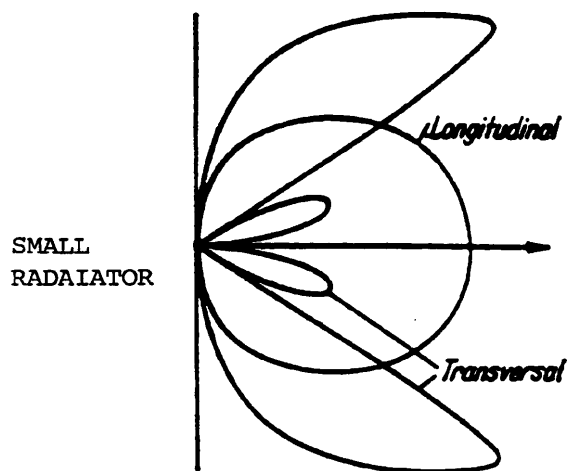


Fig.3.9- Directional characteristics of a very small radiator (large wavelength to diameter of probe ratio) in a solid material (67).

CHAPTER 4

TECHNIQUES USED FOR SIGNAL PROCESSING

4.1- INTRODUCTION

The emergence of digital signal processing as a major discipline began in the mid 1960s when high speed digital computers became widely available for serious research and development (72).

In digital signal processing, we deal with signals which operate in discrete-time, a discrete-time is a sequence of numbers.

For the purpose of this research, a package for signal processing was developed using the BASIC language on the 9000 series HEWLETT-PACKARD computer.

The analysis of the signals captured when testing the steel embedded in concrete, was divided into two parts:

- 1-Time domain analysis.
- 2-Frequency domain analysis.

The time domain analysis involves operations on a specific time record or combinations of records. If analysis is to be made on only one part of the data, rather than the full 1024 bytes, the window program option can be used which provides the means of isolating a specific segment of the record. The arithmetic operations contain a list of processing functions such as

squaring, differentiation, phase shifting, root mean square (RMS), and energy statistics, these operations need only one record of data. However, other processing requires more than one signal and is carried out on groups of signals, such as adding, subtracting, multiplying, dividing, and signal cross-correlation.

The frequency domain analysis includes the real, the imaginary, the magnitude, and the phase components of the spectrum. The window facility in the frequency domain is similar to the window facility which operates in the time domain, but in this is referred to the amplitude spectra. The inverse Fourier transform (IFFT) retransforms a frequency spectrum to its equivalent time record. The arithmetic operations perform calculations which are referenced to the amplitude components of a given spectrum. Hence the amplitude chosen may be linear, logarithmic, or a self-referenced scaling. Squaring can also be carried out to give the power spectrum, in addition to spectrum integration. Moreover, cross-correlation, subtraction, adding, dividing, and multiplication are performed on groups of signals. A filter design facility has been included too. The method computed was the brick-wall filter which is performed by removing bands of harmonics, such filter could be lowpass, band pass, or band stop filter. Subsequently after performing filtering, IFFT on the edited spectrum can be calculated. The digital filtering technique proved to be important in identifying defects in concrete. This will be discussed in detail in chapter 11.

In chapter 9, more detailed information about the package will be given. After finding that spectral analysis is needed for

development of a method using ultrasonic techniques to detect corrosion/cracks in steel embedded in concrete, it was decided in the last year of the research that a waveform analyser was needed which was bought, a description of the analyser and its operations is given in chapter 9.

In this chapter, a literature survey about the past application of signal processing in the field of non-destructive testing will be reviewed, with the mathematical approach of operations carried out in the program.

4.2- PAST APPLICATIONS OF SIGNAL PROCESSING

a- Defect Characterization

A new approach to flaw characterization was suggested by Gericke (73) in 1963. He used a broadband ultrasonic pulse and found that the spectrum (Fourier Transform of the signal) of the echo from a void is altered by the geometry of the void. Whaley and Cook (74) and Whaley and Adler (75) have adapted the spectral analysis technique to an immersed system, introduced a multitransducer system, and developed a model to measure size and orientation of circular reflectors in water (simulating planar flaws in solids) from the scattered spectral distribution. Major variations of the reflected spectrum as a function of the incident angle were observed (fig.4.1 shows one of the results). The frequency spectrum of the reflected signal was also sensitive to the size of the reflector. It was concluded that the variation of the frequency spectra with angle and reflector size can be

explained by the frequency and angular dependence of scalar wave diffraction by circular obstacles. Tittman et al (78) designed an experimental system for measurements of ultrasonic wave scattering from simulated defects in solids. Both angular and frequency dependence of the scattered energy were analysed from these simulated defects (fig.4.2). Another experimental technique was used by Adler and Lewis (79) to study broadband pulse spectra from simulated defects in titanium samples. Both longitudinal and shear wave scattered amplitude were studied. It was found that the phase spectra for scattered longitudinal waves from spherical cavities shows size dependence. Bifulco and Sachse (76, 77) studied the frequency dependence of broadband ultrasonic pulses scattered from cylindrical fluid-filled cavities in a solid, and related the frequency spectrum to the diameter of the cavities (fig.4.3).

b- Adhesive Bonds

Laminates of metal and polymer (adhesive bonds) have been studied for a number of years by utilizing ultrasonic techniques. The strength of the bond is of primary importance and so many of the investigations have been aimed at deducing this property from non-destructive ultrasonic measurements. For instance, Chang et al (80) measured transmission spectra for several single layers of various thickness and three-layer sandwiches of aluminium, adhesive, and air. Resonance behaviour was noted in the spectra. For the single layers, the spectral structure was simple, with the peaks equally spaced, but the transmission spectra of the laminates were considerably more complex.

c- Surface Roughness

Quentin et al (81) have investigated backscattering of ultrasonic waves for both one dimensionally and two dimensionally periodic surfaces i.e. rough surfaces. Scattering from perfect and flawed gratings gave the expected modulated frequency spectra. The modulation was quite uniform for the perfect grating but increased in complexity for gratings with an increasing number of imperfections.

d- Surface Breaking Cracks

The interactions of ultrasonic waves and surface-breaking cracks have been studied by a number of investigators.

Silk (82) noted that the interaction of surface waves and surface-breaking defects is wavelength dependent. When the wavelength of the ultrasound is much greater than the defect depth, little energy is reflected or delayed by the crack. Conversely, for the case of very small wavelengths the ultrasonic wave follows the surface of the crack. Reflections can occur at each corner or along the rough surface of the crack. If transit time measurements are made for surface waves passing across a defect, the time can be expected to change with the frequency of the wave. The change in transit time (relative to the transit time across an uncracked surface) is plotted versus frequency for three crack depths (fig.4.4). The depth of the surface-breaking crack can be inferred from the slope of the curve.

Fitting and Adler (83) have shown that the lateral extent (depth) and the depth of the crack may be measured from the frequency and angular dependence of interactions of ultrasonic surface waves with the crack.

e- Strength-Related properties

Ultrasonic spectral analysis techniques have been used in attempts to determine the strength of composite materials. Stone and Clarke (84) described a technique for determining the void content of carbon-fibre-reinforced plastics from ultrasonic attenuation measurements. They found a correlation between attenuation and interlaminar shear strength. They noted attenuation increased with frequency, fig.4.5 shows the attenuation against frequency at various percentage of voids contents.

Jones, Elvery, and others (69, 85, 86, 87, 88) have found a good correlation between concrete strength and ultrasonic pulse velocity, a typical correlation is illustrated in fig.4.6.

f- Detection and Characterization of Porosity

Thompson et al (89) developed an ultrasonic measurement technique which is based on ultrasonic backscatter measurements. Glass was chosen as a model sample material. The time domain windowed results were Fourier transformed into an amplitude-frequency

description, and were then deconvolved with the transducer response function. Then a comparison of a theoretical backscattered spectrum based on Born's approximate solution to the wave equation was made with the experiment results. They showed that the two results compare favourably.

g- Cracks in Concrete Piles

Forde and Chan (48, 90) carried out experiments to detect cracks in piles using an impact-echo method. The results were interpreted in the time domain and the frequency domain. They demonstrated that the reflection from a crack could be detected by the auto-correlation function otherwise would not be detected by visual inspection in the time domain. The frequency domain analysis confirmed the time domain analysis.

h- Detection of Cracks in Masonry Structures

Forde and Birjandi (53, 91) used sonic techniques to detect large voids or cracks and to measure thickness of masonry structures. Auto-correlation and cross-correlation functions were used to locate the presence of voids and cracks. Frequency domain functions and particularly cepstrum was used to determine the hidden depth of a structure such as determining the thickness of a bridge abutment.

i- Cracks and Voids in Concrete

Sansalone et al (34, 41) used an impact echo method to detect

voids in concrete. They interpreted the signal in time and frequency domains. Time domain was used to calculate the arrival of longitudinal waves, moreover in the frequency domain, the depth of reflecting interfaces was easier to determine from the dominant peaks in the frequency spectra than the time domain.

j- Detection of Flaws in Reinforced Steel

Kusenberger and Birkelbach (1, 18) used the magnetic field disturbance technique together with signal processing techniques to detect flaws in reinforcing steel in bridge members. The techniques explored were the Fast Fourier Transform, differencing, and correlation.

4.3- TIME DOMAIN FUNCTIONS

The time domain functions used in the current work are squaring, differentiation, phase shifting or delay, root mean square RMS, and energy statistics, with one record interpreted. However if two signals were studied adding and eventually averaging (if needed), subtracting, multiplying, dividing, and signal correlation can be performed.

4.3.1- Squaring

The algorithm is the point-by-point square of data in the same trace. The mathematical definition of the function is as follows:

$$M(t) = f(t)^2 \text{ for } t=1,2,\dots,n$$

where n is the number of points in the trace and $f(t)$ is the

amplitude of the signal at t.

4.3.2- Differentiation

The mathematical definition of the function is as follows:

$$f'(t) = [f(t+1) - f(t)]/dt \text{ for } t=1,2,\dots,n$$

where dt is the period or time-increment.

4.3.3- Phase Shifting or Delay

The algorithm is to add or subtract points i.e. to shift the signal to the right or to the left.

4.3.4- RMS, Energy, and Mean Calculations

The RMS is the square root of the average value of the squares of the y-values in the trace:

$$\text{RMS} = 1/n \sum_{t=1}^{t=n} f(t)^2$$

The energy calculates the sum of the squares of the y-values and multiplies by the period:

$$\text{ENGY} = t \sum_{t=1}^{t=n} f(t)^2$$

The mean is the average value of the n-points in the signal is:

$$\text{Mean} = 1/n \sum_{t=1}^{t=n} f(t)$$

4.3.5- Addition, Subtraction, and Multiplication of Two or Group of Signals

Addition is performed by point-by-point addition in two sets or more of signals, for two signals:

$$f(t) = f_1(t) + f_2(t) \text{ for } t=1,2,\dots,n$$

Eventually after carrying out addition averaging could be achieved as follows:

$$f(t) = [f_1(t) + f_2(t) + f_3(t)]/3 \text{ for } t=1,2,\dots,n$$

see next section about the reason for averaging.

Subtraction is carried out by point-by-point subtraction on two records:

$$f(t) = f_1(t) - f_2(t) \text{ for } t=1,2,\dots,n$$

Multiplication is done by point-by-point multiplication on two records:

$$f(t) = f_1(t)f_2(t) \text{ for } t=1,2,\dots,n$$

Division is applied by the division of point-by-point in two records:

$$f(t) = f_1(t)/f_2(t) \text{ for } t=1,2,\dots,n$$

4.3.6- Signal Averaging or Noise Reduction

The term 'noise' when used in connection with signal transmission and receiving systems applies to any additional source of energy which in some manner interferes with, obscures, or degrades the wanted echo. It may be, for instance, electromagnetic or thermal, and it may be random or non-random, coherent or incoherent.

During this research the averaging process was applied in the time domain only.

Two noise problems are encountered during the ultrasonic inspection of reinforced concrete. The first arises from both the amplification and measuring system. The second is when the signal is scattered by the coarse aggregate (max. diameter of aggregates used about 20mm, wavelength is equal 20mm if 200kHz transducer is used) present in concrete which obscured the echoes reflected from the steel components.

In the first case, the noise levels produced when high-gain amplifiers are used can virtually drown the wanted signal, but because such noise is random with time, and the echo is temporarily invariant, temporal signal averaging can be performed which very dramatically improves the S/N (signal-to-noise) ratio. Fig.4.7 shows how the averaging techniques improves the S/N ratio. Since the noise is random, averaging the signals in time will cause the ratio of output signal power to noise power to approach infinity, since the noise amplitudes being equally

likely to be positive or negative, approach zero on the average.

Expressed in RMS terms, this improvement is given as:

$$SN_b/SN_a = n/2 \quad (\text{ref.92})$$

where SN_b = S/N before averaging

SN_a = S/N after averaging

n = number of averages

Hence, a very weak signal having an RMS S/N of unity, or 0dB, can be improved to 40dB by taking 200 averages.

The second case, which is more important, is where the signal degradation is due to the backscatter produced by the aggregates. In quality it is termed coherent noise, since it is temporally invariant and is correlated with the output (interference from the mains is also non-random and temporally invariant given a fixed measuring point -since it is cyclical- but it is not coherent since it, in no way, correlates with the shape of the output pulse in this case). It is theoretically possible to reduce the effects of signal back-scatter by spatial averaging. Since the distribution of aggregates within the concrete is random, and the position of steel components is constant with respect to the surface, signals taken at different points in the concrete parallel to the steel should, when averaged, provide an improvement in the ratio between the echo from the steel and the echo from the aggregates. This same procedure has been used before, Newhouse and Ferguson (93) reported that to enhance the S/N ratio when testing cracks near a weld, the transducer is scanned along the weld and the echo signals are averaged during

the scan, the averaged clutter signals being random tend to cancel, whereas the signals from a crack add to produce a strong output. However, because of the transducer ringing, surface wave, and the highly heterogeneous material such as concrete, this technique had offered no improvement in the ratio between the echo from the steel and the echo from the aggregates.

4.3.7- Correlation

There are several different uses for the correlation function. Two important uses are to determine the statistical properties pertaining to the similarity of two data, and to determine the time delays between repeated events in a data set.

An example of the first use is in evaluation of the power spectral density of a process (92). In the second application, there are many examples in the fields of ultrasonics, geophysics, and radar. In all these cases, a pulse is sent out by a transducer or a hammer and a modified version of the pulse is returned some time later. Since the return signal may be computed by amplitude and phase changes as well as the addition of noise, the time of the return echo could be difficult to detect. The correlation function is used to locate the echo in the noise.

The expression for the discrete time domain correlation is:

$$y(t) = \sum_{t=1}^{t=n} f_1(t) f_2(t+T)$$

where $f_1(t)$ =first input signal, $f_2(t)$ =second input signal

n =length required, and T =offset or delay.

Auto-correlation is a special case of the cross-correlation where the signal to be correlated against is the same as the input signal. Mathematically, this means $f_2(t)=f_1(t)$. The auto-correlation function is equal to the power spectral density.

In practice the correlation function is scaled by a factor:

$$f = 1 / \sqrt{S_x S_z}$$

where

$$S_x = \sum_{t=1}^{t=n} f_1(t) f_1(t)$$

$$S_z = \sum_{t=1}^{t=n} f_2(t) f_2(t)$$

The relevant applications of auto-correlation are:

1- To detect echoes or reflections in the signal For example from a void or crack, at a time delay of T in the signal, the auto-correlation function will have a peak at T. The coefficient $y(T)$ is clearly a measure of the relative strength of the echo.

2- To detect periodic signals hidden in a random noise The reason for this is that the auto-correlation function of a periodic signal is also a periodic function with a periodic delay time of T, 2T, 3T and so on. However the interfering background noise has an auto-correlation function which tends to zero with increasing delay time, and therefore, the periodic signal can be detected.

Fig.4.8 shows an example of this technique.

Moreover, the relevant applications of cross-correlation

functions are the following:

1- Determination of signal reflection delays If a signal is transmitted between two transducers i.e. transmitter (the input pulse) and a receiver (the captured pulse), the cross-correlation function between the input pulse delayed to a position T where the return echo is expected, will peak at the time delay corresponding to the transmission time T between the input and the output.

2- Identification of transmission paths If there are several transmission paths between the transmitter and the receiver, there will be several maxima and minima peaks in the function and each peak corresponds to a transmission path. The magnitude of the peak is an identification of the relative strength of the transmission path.

Fig.4.9 shows an example of the cross-correlation technique.

4.4- FREQUENCY DOMAIN ANALYSIS

The frequency domain functions used in this research are FFT (Fast Fourier Transform) and IFFT (Inverse Fast Fourier Transform).

The calculations of addition, subtraction, multiplication, division, squaring, and energy are similar to those of the time domain, the only difference is that the y-values or the amplitude are now the magnitude of the spectra and the x-increment or

period is the sampling frequency.

4.4.1- Fast Fourier Transform and its Inverse

In recent years, digital electronics have seen a dramatic development (Lynn), and there has been a corresponding growth of interest in discrete-time Fourier techniques. It is now commonplace to use digital computers for the Fourier analysis of signals.

The discrete Fourier transform operates on a set of samples of the time-domain signal (taken at equally spaced intervals dt). It gives a set of frequency-domain coefficients (at equally spaced frequency df) (72) :

$$F(kdf) = dt \sum_{n=1}^N f(ndt) \exp(-j2\pi kdf ndt)$$

$$f(ndt) = df \sum_{k=1}^N F(kdf) \exp(+j2\pi kdf ndt)$$

where N = the number of samples
 k, n = the frequency and time domain indices
they take the values $1, 2, \dots, N$
 $f(ndt)$ = the set of discrete-time samples
 $F(kdf)$ = the set of fourier coefficients
Additionally time-record length = Ndt
frequency sampling interval = $df = 1/(Ndt)$

When the Fourier transform is performed, the output will be complex

the real part is

$$\text{Re}(F(k)) = 1/N \sum_{n=1}^N f(n) \cos(2\pi nk/N)$$

and the imaginary part is

$$\text{Im}(F(k)) = 1/N \sum_{n=1}^N f(n) \sin(2\pi nk/N)$$

Phase and magnitude are calculated from:

$$\text{Mag}(F(k)) = \sqrt{\text{Re}^2(F(k)) + \text{Im}^2(F(k))}$$

$$\text{Phas}(F(k)) = \text{Im}(F(k)) / \text{Re}(F(k))$$

Highly efficient computer algorithms for estimating the Discrete Fourier Transform (DFT) have been developed since the middle 1960's (72), these are known as Fast Fourier Transforms (FFT). By careful ordering and structuring of the required numerical computations, FFT algorithms aim to eliminate the redundancy in the DFT. Basically, this is done by dividing up, or decimating the sample sequence $f(n)$ into subsequences whose transforms are easier and quicker to compute. The process of decimation is repeated until only two-point transforms remain. In this way the overall transform may be reduced to a succession of simple weightings and additions of carefully ordered sample values. Decimation may be also performed in the frequency-domain rather than the time-domain. The development of FFT algorithms can be found in several books (72, 94, 95), and will not be covered here. It should be noted that the term FFT refers to any algorithm which reduces the number of operations to less than N^2 , most commonly the sample size is restricted to a power of two (radix 2).

Aliased spectra are normally undesirable effects caused by undersampling data. The theoretical sampling rate should be 2 times the highest frequency component in the signal. In practice, the sample rate is taken minimum 3 to 4 times the highest frequency component. For example, if we have a signal with a 100kHz component, the sample period should be a maximum of $3\mu\text{s}$, a factor of at least 3 times.

The thrust of this technique, FFT, is to characterize the frequency spectra associated with various signal types, embedded in the received signal, such as simulated flaws and embedded steel, and to determine if there are any unique spectral characteristics associated with each.

Fig.4.10 shows a time record, its FFT , and its phase.

4.5- DIGITAL FILTERS

Signals may be contaminated by interference or noise of some origin such as, for example, 50Hz mains hum (94). Interference can be removed or at least attenuated by an appropriate filtering process. An important feature of the use of filtering in this research was the elimination of frequencies outside some spectral band prior to further analysis.

The total signal that arrives at the receiver will include low-frequency components of large amplitude and relatively little information and high-frequency components, that do change according to the variations in the material composition through which they propagate and surfaces at which they are reflected, but whose energy is very often weaker than their low-frequency counterparts. For this reason, analysis of the total signal has yielded sometimes to a limited success since the frequencies of interest were completely buried in noise. What was needed was a filter which removes the lower portions of the spectra. This technique proved to be very important in identifying those parts of the signal which are affected by the presence of corrosion

and other defects present in the hardened concrete. This will be shown in chapter 11.

A brick-wall filter was therefore computed.

4.5.1- Brick-Wall Filter

The method is carried out by removing bands of harmonics from the frequency spectra i.e. the removed harmonics are replaced by zeroes. Then, the resultant spectra is Inverse Fourier Transformed (IFFT) to the time domain for the remaining harmonics. It is worth mentioning that this kind of filtering could be low-pass, band-pass, high-pass, or band-stop filter.

Fig.4.11 shows the original time record, its spectrum, the filtered spectrum, and the IFFT of the latter.

4.6- SUMMARY

The use of the methods outlined earlier in this chapter have been investigated and applied to two pre-tensioned beams and to a number of laboratory specimens (a description of specimens used in this research will be given in a later chapter).

The Fast Fourier Transform was used to characterize the frequency spectra associated with the signal of interest, and then the technique was used to characterize the spectra associated with various signal types (simulated flaws, corrosion, embedded steel,...), to determine if there are unique spectra associated

with each. It was found that when steel is present in concrete the frequency spectra of the signal contains higher harmonics than that of a signal with plain concrete. More discussion about this result will be given later.

Following the above argument, digital filters were applied to remove bands of harmonics, such as the low frequency components and keep the high frequency components; the output record from the filter was IFFT'd to time domain, and then an energy trend plot of the filtered data from scan was carried out. The application of this technique proved to be very important in identifying corroded components and flaws in concrete. This technique will be discussed in detail in chapter 11.

Differencing, multiplication, dividing, and addition were performed point-by-point of signals from different scan signals. The thrust of this technique is to enhance any flaws, and/or steel presence signals with respect to those with no steel embedded and/or artefacts.

Correlation techniques have been used, which can be regarded as a process similar to using a signal shape of interest as a template and sliding it along a scan record to determine if the template is a good match to any given region in the scan record. A good match between the template signal and a portion of the scan record indicates the possibility that the source typical of the template-type signal is present in the beam at a location corresponding to the matching location in the scan record. The thrust of this technique is to assess quantitatively the degree

of similarity between a selected signal (sometimes a signal is produced to represent the portion coming from a sound, corroded, or cracked wire embedded in concrete) and those signals taken previously and stored on a disk. Different shapes of correlator signals were used to try identify and assess the degree of strength of the reflected echo from the steel embedded in concrete. It is necessary to point out that the correlation techniques were found to be of little value since the constituents of the concrete (cement, sand, and gravel) scatter the signal and exhibit no periodicity.

Finally, after establishing that signal processing techniques can provide powerful tools for signal enhancement and recognition, it was found possible to have access to a waveform analyser, which was used in the final stage of this research. The analyser was the ANALOGIC Model 6100, a 9-bit analyser, which performs many of the functions mentioned in this chapter, in seconds, and moreover other functions not mentioned such as trend, zoom czt, and many other features. A description about the machine is given in the chapter of Experimental Details.

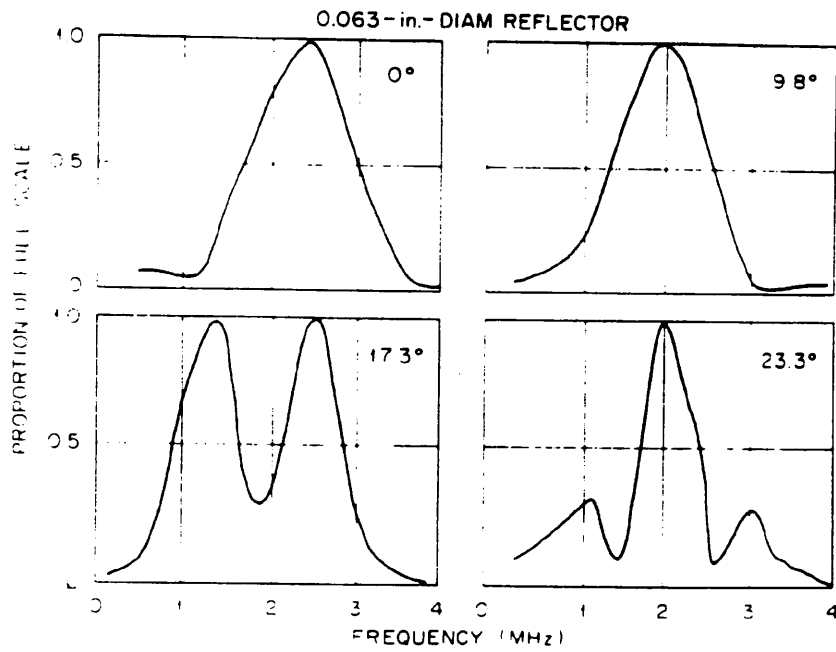
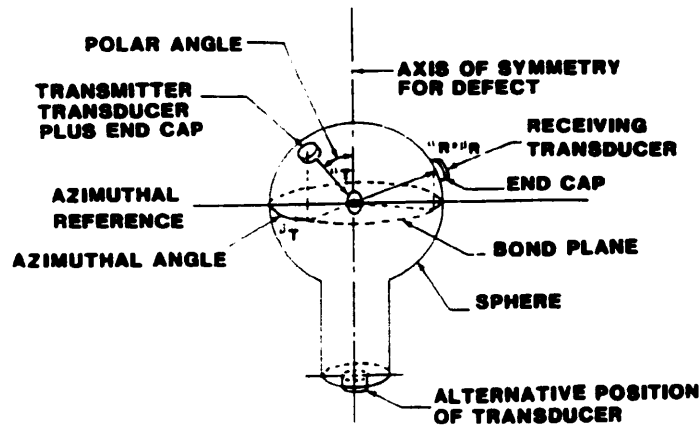
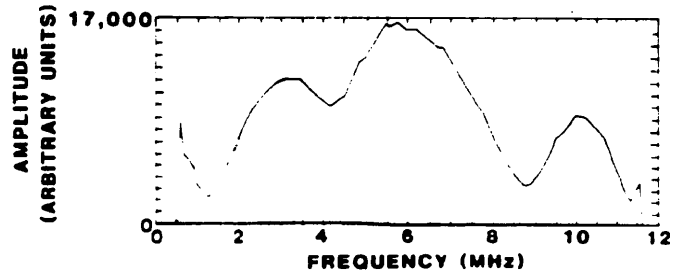
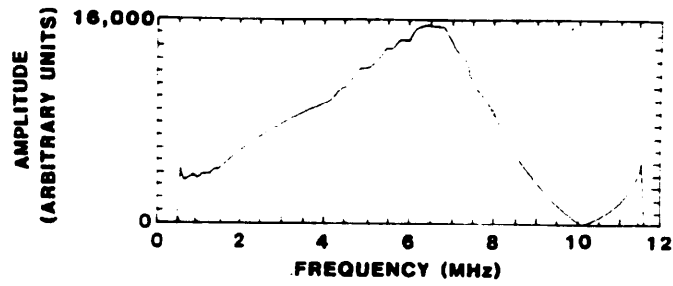


Fig.4.1- Spectra of ultrasonic waves scattered from a small reflector for different incident angles (75).

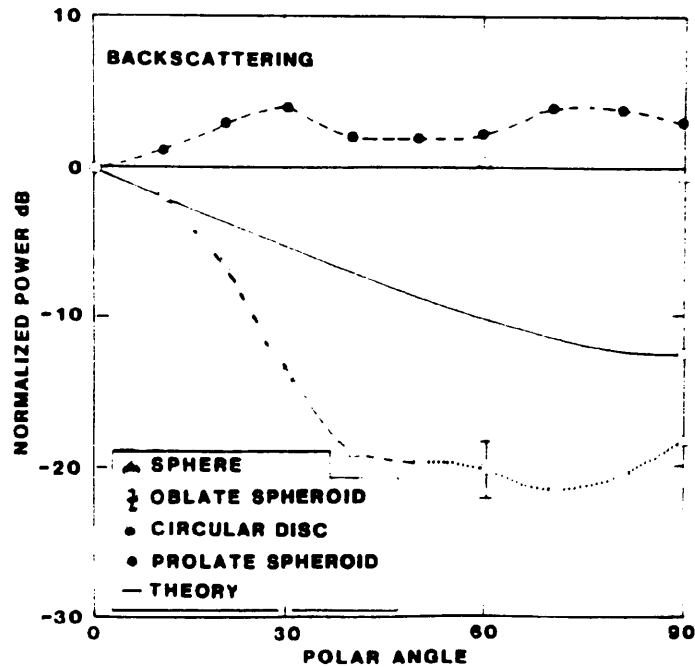
Fig.4.2



a) Measurement fixture for obtaining scattering information from voids in a solid (78).



b) Backscattered spectra from an oblate spheroid for 10° and 60° off the axis of symmetry (78).



c) Angular dependence of pulse-echo power (78).

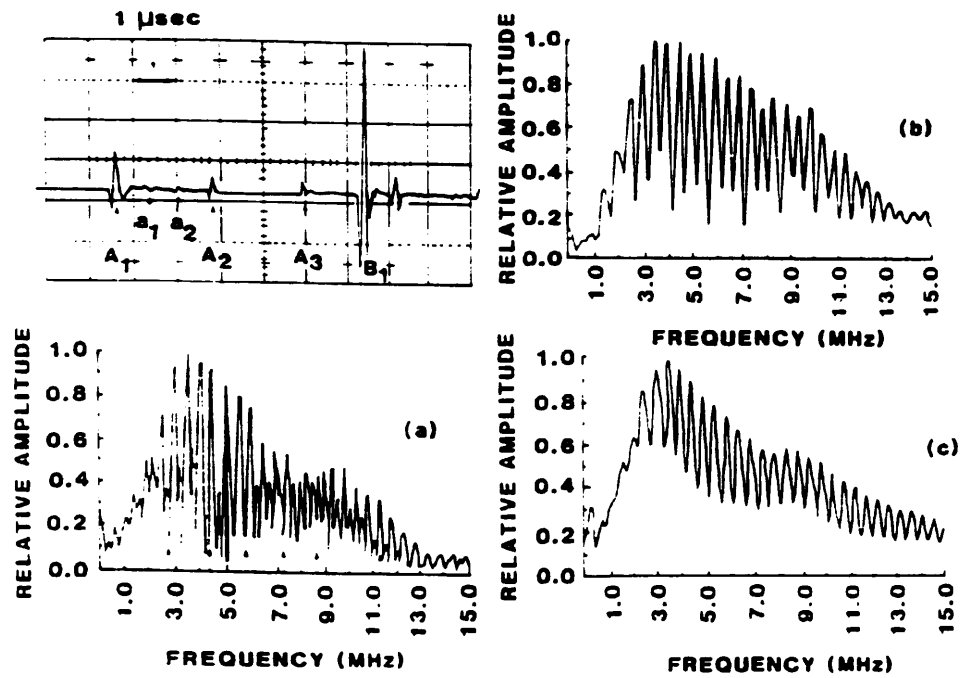


Fig.4.3- a) Amplitude-time record and power spectrum of a water-filled cavity; b) spectrum of amplitude pulses A₁, a₁, a₂, and A₂; c) spectrum of amplitude pulses A₁ and A₂ (76).

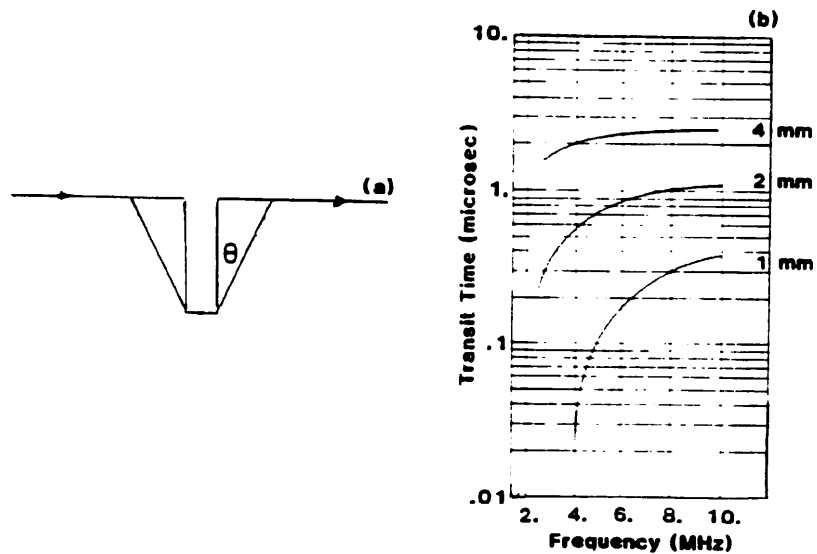


Fig.4.4- Surface wave propagation about a crack: The transit time variation with frequency for crack depths 4, 2, and 1mm (32).

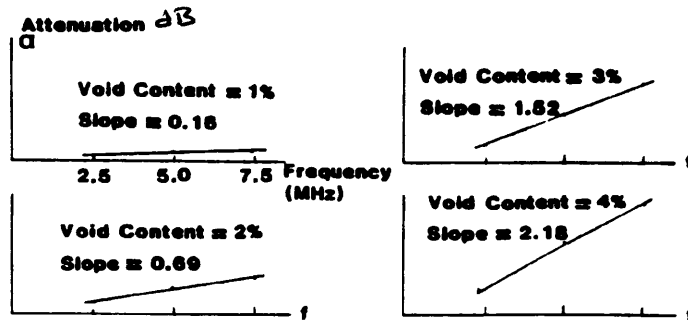


Fig.4.5- Attenuation spectra for carbon-fibre-reinforced plastics with increasing void content (84).

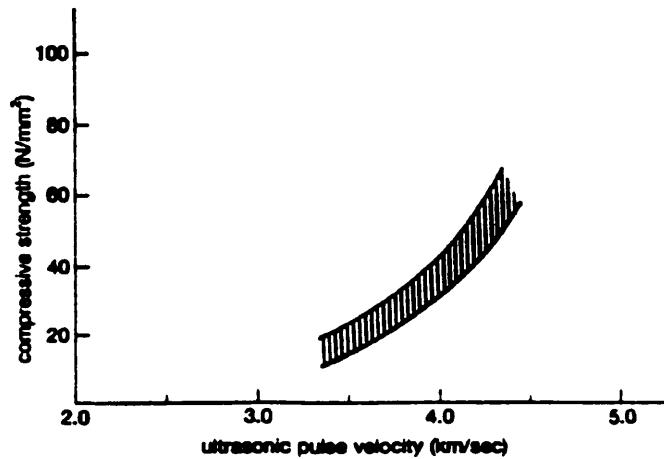


Fig.4.6- A typical correlation between compressive strength and ultrasonic pulse velocity in concrete.

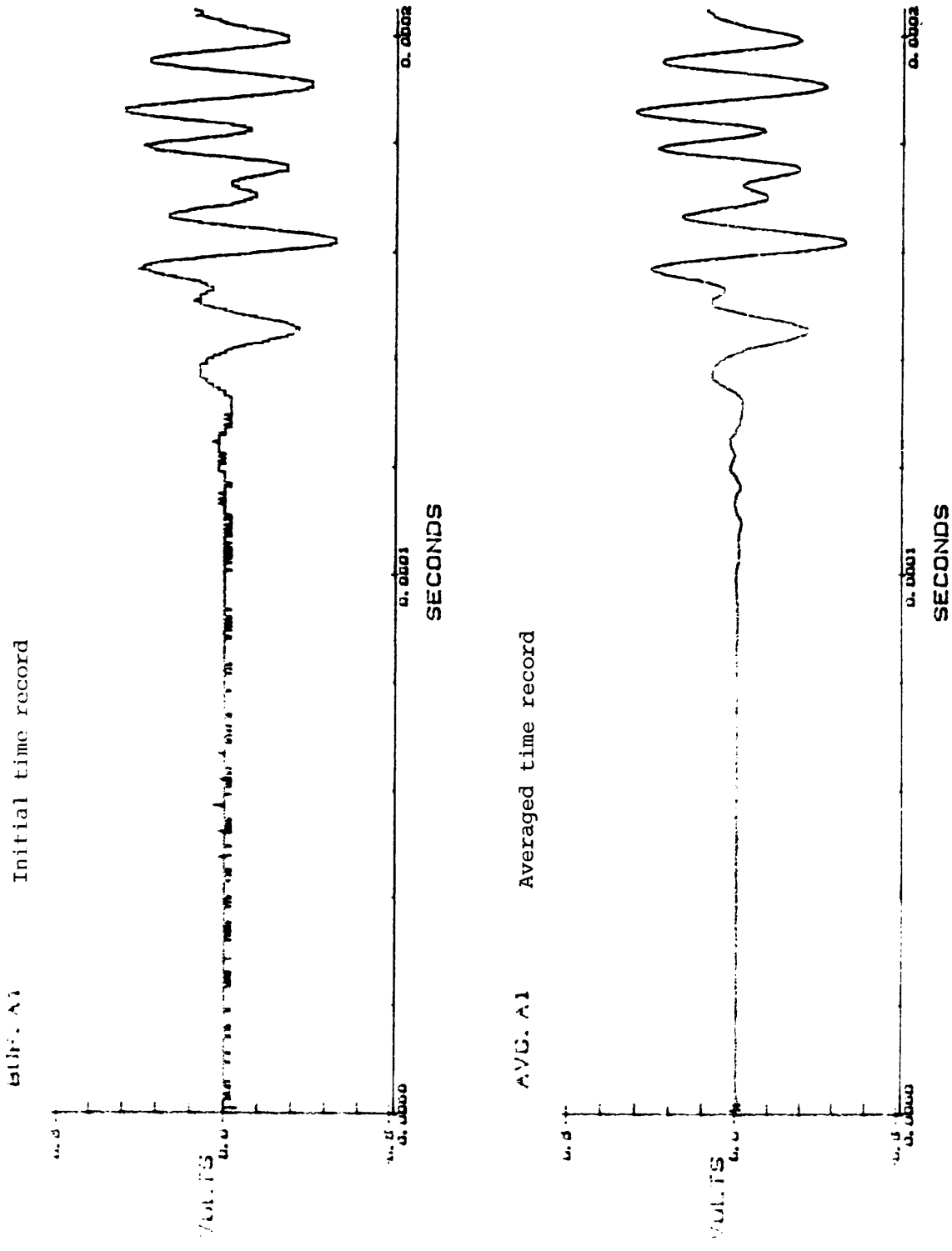
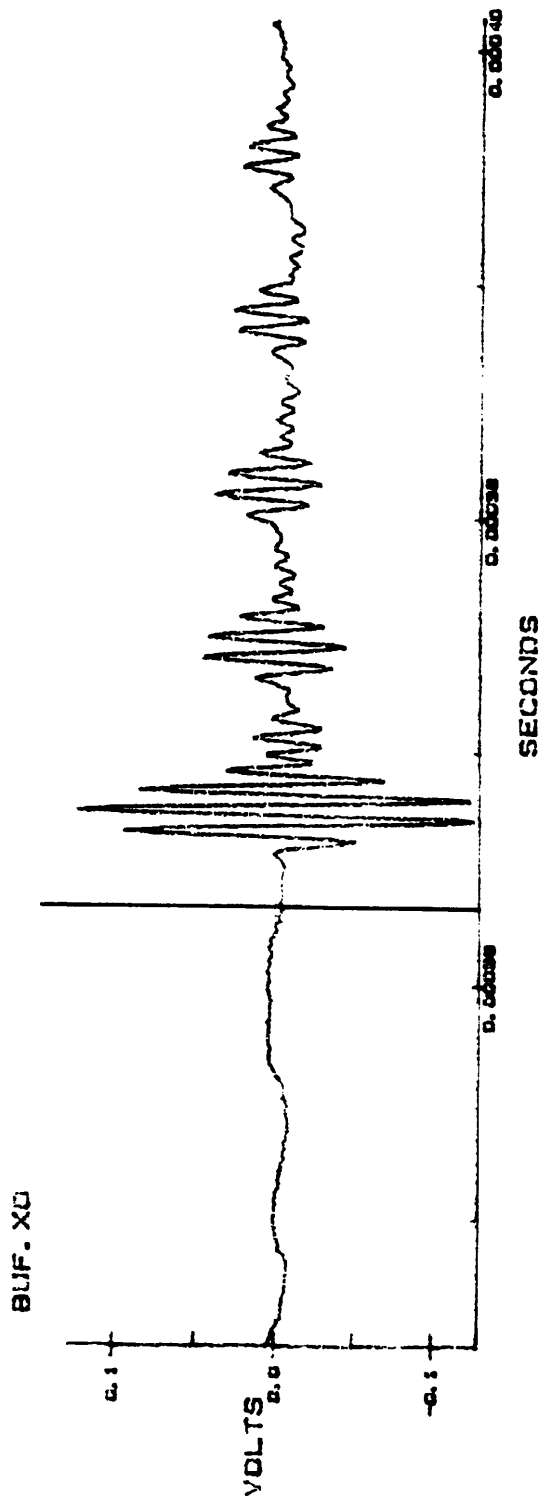


Fig.4.7- The averaging technique.



ACORXO The auto-correlation of the above signal delayed to the cursor

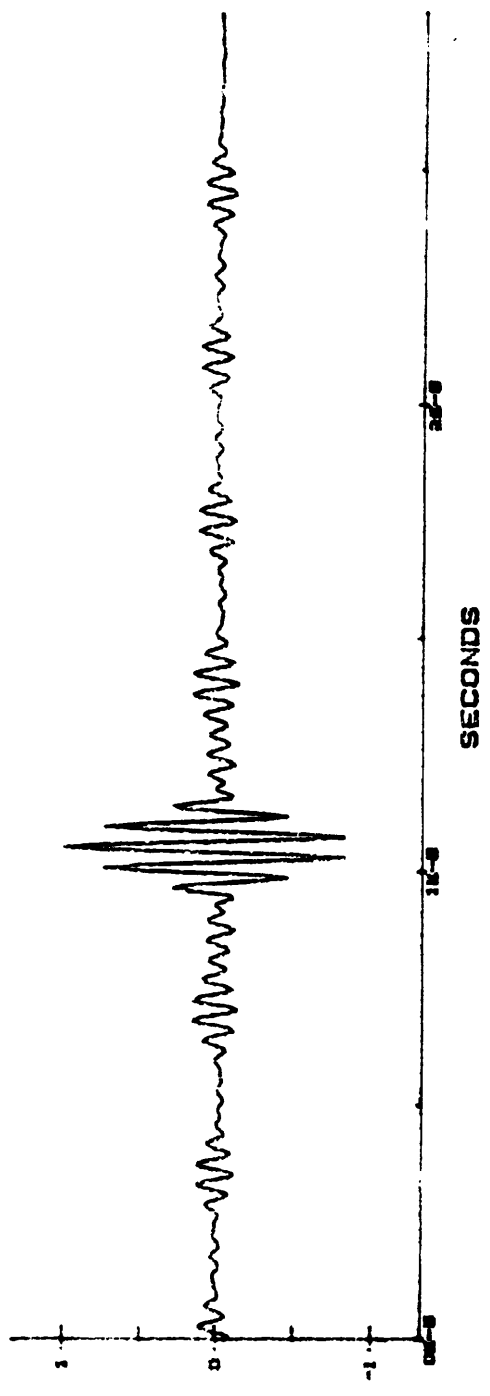


Fig.4.8- The auto-correlation technique.

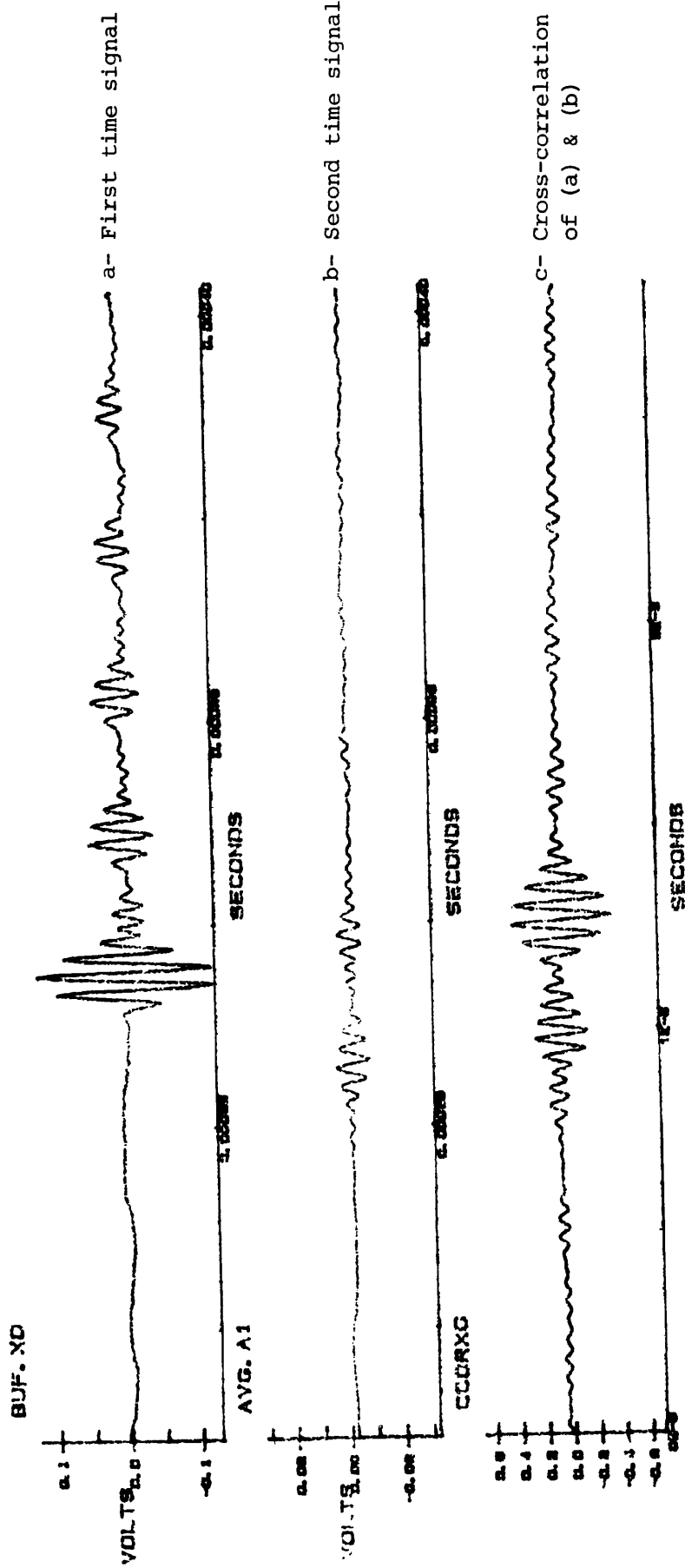


Fig.4.9- The cross-correlation technique.

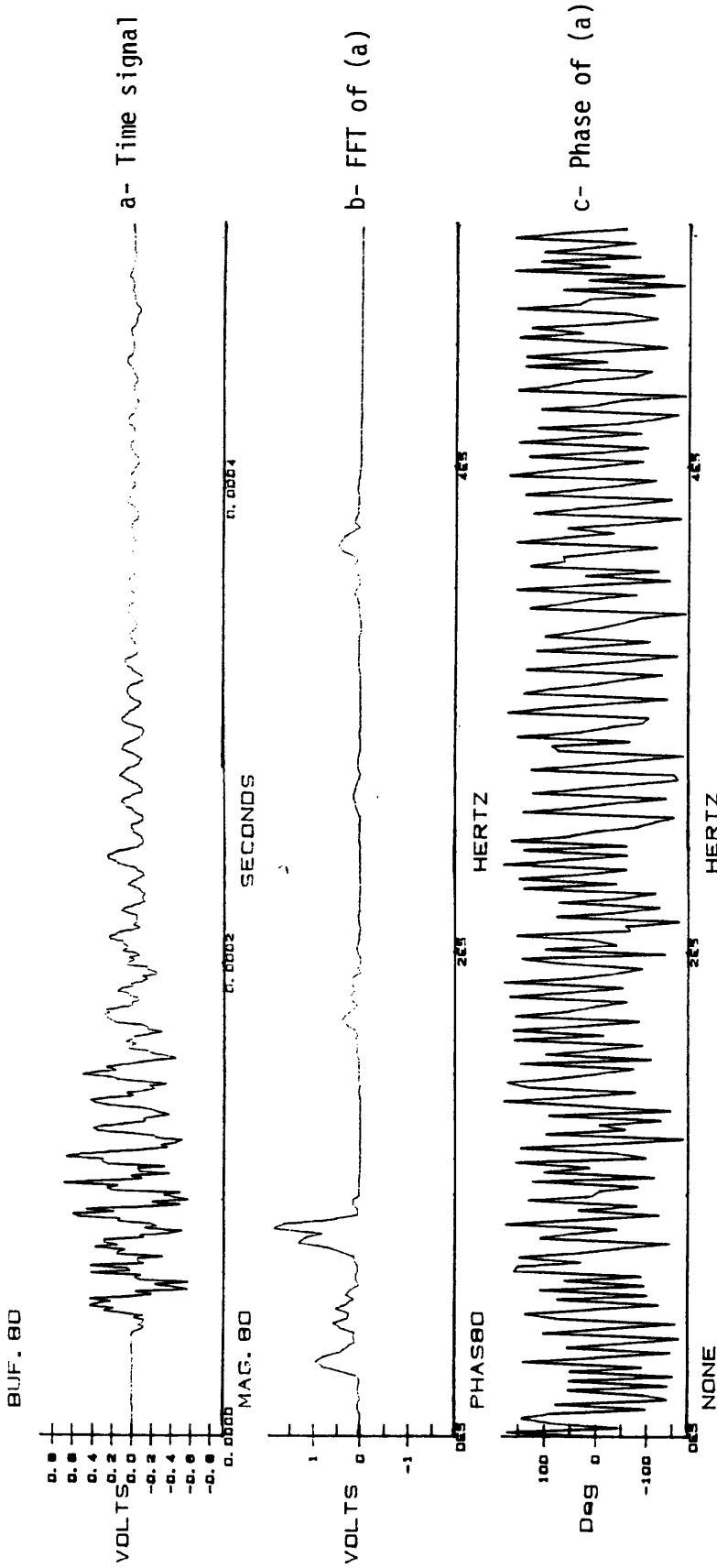


Fig.4.10- FFT and phase of a time record.

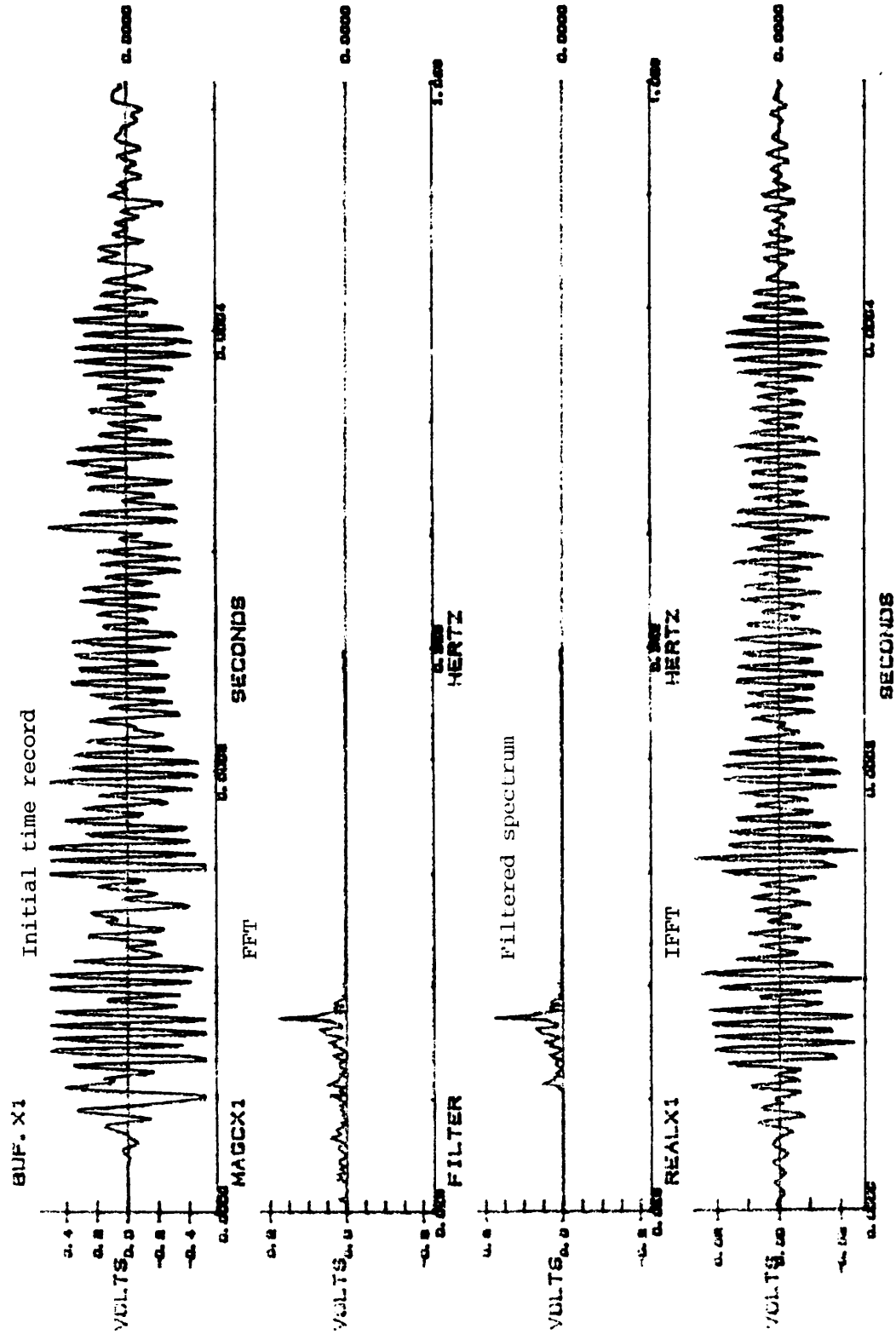


Fig.4.11- Application of a brick-wall filter.

CHAPTER 5ATTENUATION OF WAVESIN RODS5.1- INTRODUCTION

In this chapter, a discussion is presented on the phenomenon of attenuation of waves in rods depending on the surrounding medium. Zakadi and Takizawa (97) suggested that the phenomenon of decay of a vibrating system seems to be mainly due to the emission of sound waves into the surrounding medium and not to the friction in the vibrating system.

In previous work carried out by the author (42), a pulse-echo system was used in which a pulse^{was} applied to one end of a wire in air, water, and concrete.

It will be shown in the present work that the attenuation of the signal in rods embedded in concrete is so severe that the application of this method has to be restricted to short rods. Furthermore, the application of this method to testing for cracks in cables in a bridge would require access to one end of the wire which means exposure of an anchorage which is not always possible.

In this chapter, experimental results and theoretical work found in the literature will be compared.

Two equations were found in the literature (98, 99) which give the attenuation in bars. The first for a bar embedded in a solid, and the second for a bar in air.

The experimental work is divided in two parts:

1-Experiments carried out previously where a pulse-echo system was used. From these experiments, the attenuation of high frequency waves of bars in air, water, and concrete were calculated.

2-Experiments carried out during the present reasearch, where the transmission method was used for bars embedded in concrete and where low frequency transducers were used.

5.2- VARIATIONS OF ULTRASONIC PULSE VELOCITIES IN CYLINDRICAL RODS

In a thin rod, three types of wave can occur: longitudinal, torsional or transverse (fig.5.1). In transverse vibrations, the centre of gravity of the rod is vibrating (string vibrations). The propagation velocity of longitudinal rod waves is:

$$c = \sqrt{E/\rho}$$

where E= the Young's modulus

ρ = the density

c= the velocity.

The torsional wave velocity is equal to the velocity of shear

waves in the bulk medium.

Tu and Brennan (100) carried out experiments which were concerned with the variations of ultrasonic pulse velocity, using cylindrical rods spanned in air of aluminium alloy, brass, copper, and steel, using both the pulse-echo and pulse transmission methods for pulsed longitudinal and shear waves. It was found that for longitudinal waves, the measured velocity not only depends upon the elastic constants of the medium but also on the ratio between the radius (r) of the rod and the wavelength (λ). When (r/λ) is very small, the measured velocity approximates to the modulus velocity $\sqrt{E/\rho}$ where ρ is the density. For larger values of (r/λ) , the measured velocity approaches the bulk velocity $\sqrt{(1+2\mu)/\rho}$ where l and μ are the Lamé elastic constants. When (r/λ) approximates unity, the velocity drops and seems to equal the Rayleigh surface wave velocity. It was also found that the velocity dispersion effect was not observable when pulsed shear waves were used.

For a steel reinforcing bar in air, it has been shown (101) that the velocity is likely to be 5.75km/s for bars of 30mm diameter or greater, reducing linearly to 5.05km/s for bars of 6mm diameter. These values are reduced when the bars are embedded in concrete, depending upon the pulse velocity within the concrete.

Chung (102) attempted to derive an empirical formula for the effective pulse velocity in the composite material. He found that the effective pulse velocity was mathematically related to the diameter of the bar and the difference between the pulse

velocities in steel and concrete, and proposed an empirically based general relationship for longitudinal bars:

$$c_{st} = 5.9 - 10.4(5.9 - v_c)/D$$

where v_c is the velocity of longitudinal wave in concrete in km/s.

D is the diameter of bars in mm.

The validity of this formula is subject to a lower limit of D i.e. $D > 10\text{mm}$.

However, Bungey (101) carried out an experimental investigation to get the effect of bars spanned longitudinally on the velocity of sound in concrete, and compared his results with Chung (102). Fig.5.2 shows his result where the combined effects of v_c and bar diameter are illustrated. It was found that the influence of the reinforcement is greatest when v_c/v_s is smallest, as for large diameter bars in concrete having a low pulse velocity, but for diameters below 10mm the value of v_c/v_s changes rapidly with v_c and bar diameter. Bars below 6mm diameter cannot normally be detected.

It is worth mentioning that the experiments carried out by Chung and Bungey were done using the through-transmission method at 54kHz transducers where the wavelength in concrete is 75mm for 4km/s longitudinal velocity and 102mm in steel for 5.5km/s longitudinal velocity.

5.3- ATTENUATION OF WAVES IN BARS

It was established during previous work carried out by the author (42) that the signal is attenuated due to the surrounding medium for a bar embedded in concrete, or water.

During the present research, a literature survey was carried out to find any work related to the attenuation of cylindrical bars embedded in a medium.

Two papers were found. The first paper is written by Paquet(98) where he derived a theoretical formula for the attenuation of sound in a cylindrical solid embedded in a solid medium. He gives an equation as follows:

$$\alpha = (\pi/48)(\mu_c/\lambda)(c_{st}/(2\pi fr^2)), \text{ Np/m}$$

where μ_c is Lamé constant for the surrounding medium (concrete)

r is radius of the bar in m

c_{st} is velocity of sound in the cylinder in m/s

f is the frequency in Hz.

For a steel bar embedded in concrete, this equation becomes:

$$\alpha = 6.86/(fr^2), \text{ Np/m}$$

$$\alpha = 60/(fr^2), \text{ dB/m}$$

It should be noted that the above equation should be applied for low frequency waves.

The second paper was by McSkimin (99) and it deals with high frequency waves in rods spanned in air. The equation derived was:

$$\alpha = 0.00545c_{st}(1-L^2)/(2\pi fr^2), \text{ Np/m}$$

where L is the absolute value of the reflection coefficient $=A_r/A_i$ (refer to chapter 3), and depends on the angle of incidence at the interface between bar and the surrounding medium, which is in this case air.

For a steel bar this equation is

$$\alpha = 4.38(1-L^2)/(fr^2), \text{ Np/m}$$

$$\alpha = 38(1-L^2)/(fr^2), \text{ dB/m}$$

It is important to note that this equation should be restricted to high frequency and to diameter of a bar greater than the wavelength.

This equation, as it has been noted before was derived for the case of a rod in air, and will be applied for the case of a rod in water, but for the case of a bar in concrete, the experimental results will only be given for high frequency application.

It can be seen from the two equations that the attenuation is inversely proportional to the square of the radius of the bar, which means that for long, fine wires the attenuation will be so severe that it will be difficult to detect the return echo. It

should be noted that for prestressed concrete, wires are typically of 7mm diameter and less, unless bars are used where diameters range up to 40mm.

5.4- EXPERIMENTAL INVESTIGATION

Experiments were carried out using both pulse-echo and transit-time methods to evaluate the two equations mentioned earlier.

5.4.1- High Frequency Testing

These tests were carried out in the previous research (42) to check if a pulse-echo system could be applied at one end of the wire and cracks could be detected where a reflected echo occurs, see fig.5.3 for the system used.

The probes used had the following (nominal) peak frequencies:

Frequency (MHz)	Diameter (mm)
1	20
2.25	6.3
5	12

a- Materials and Methods

-In air: A 7mm diameter wire spanned in air was tested (7mm diameter wire because it is widely used in prestressing concrete) included lengths of 0.9, 1.6, 3, and 4.5m.

-In water: A 7mm diameter wire spanned in a bath of water, specially built, was tested, using lengths of 0.9, 1.6, 3, and 4.5m.

-In concrete: A series of 7mm diameter wires spanned in concrete beams (blocks of concrete were cast of 125x125xLmm, where L is the length of the beam) were tested, using lengths of 0.9, 1.6, and 3m.

b- Methods of Analysis

A pulse-echo system was used for this analysis, where a pulse was applied to one end of the wire, and the same transducer received the echo after travelling twice the length of the wire. The signal was averaged over 100 samples to reduce the noise.

Velocity and attenuation analysis were carried out. Table 5.1 shows the average velocity and attenuation of the four samples (0.9, 1.6, 3, 4.5m) in air and water, but for the concrete case the results were the averages for the two specimens (0.9, 1.6m) where the echo in the 3m specimen was hardly recognised, so this result was rejected. Fig.5.4 shows the result for 0.9m length in air, water, and concrete using 2.25MHz transducer.

Velocity measurements were carried out by dividing twice the length of the wire ($2L$) over the time between the ingoing pulse and the received echo (t):

$$c = 2L/t$$

Attenuation measurements were calculated by dividing the peak amplitude of the received echo over the peak amplitude of the input signal. But attenuation coefficients are usually given in dB/m, hence

$$\alpha = 20 \log A_r / A_i$$

where α is the attenuation in dB/m.

A_r is the amplitude of the received echo.

A_i is the amplitude of the ingoing pulse.

c- Theoretical Values

McSkimin's equation is:

$$\alpha = 38(1-L^2)/(fr^2), \text{ dB/m}$$

To calculate L, we need to find first the angle of incidence at which the rays strike the boundary. This angle equals (180° minus the angle of divergence at the beginning of the far field), therefore:

$$\theta = 90^\circ - \sin^{-1}(1.2c/fD)$$

where c is the velocity

f is the frequency

D is the diameter of the radiator

θ is the angle of incidence.

As mentioned, the above equation shall be used for two cases, wire in air and wire in water. Using the equations of chapter 3, the coefficients of reflections were calculated for these cases.

Table 5.2 shows the values of the attenuation coefficients for the frequencies mentioned earlier for a wire of 7mm diameter using the above formula.

d- Discussion

Measured values, for the air and water cases, were of the same order as the calculated values as one might reasonably expect in view of the approximate analysis used. The difference could be explained by the approximation assumed when deriving this equation. However, for a concrete bar (an important prestressing component), the attenuation coefficient is about 21dB/m. Since the minimum span in a bridge is 10m (sometimes 20m and greater span prestressed bridges are built), if the pulse-echo system is used, this means a 20m minimum path length, which in turn means 420dB loss of the input signal. In practical terms it is therefore impossible to recover the echo, unless a crack is present in the steel near the end where the transducer is positioned, where an echo could be reflected back before the signal is totally attenuated.

5.4.2- Low-Frequency Testing

The objectives were to determine the effect that different lengths of concrete have on the signal strength of ultrasound

waveforms that have been introduced through the wire reinforcement and to compare the results with Paquet's equation.

a- Materials and Methods

Concrete cylinders of 150mm diameter, all with 7mm wire reinforcement, using lengths of 0.15, 0.25, 0.5, and 1m were cast.

The transducers used in these experiments had 150kHz (nominal) peak frequency.

The transit-time method was adopted, where one transducer (transmitter) was coupled to one end of the wire and another (receiver) with the same nominal frequency coupled to the other end. Each signal collected was averaged 128 times.

b- Modes of Analysis

A Pundit pulser was used to excite the 150kHz transducer (transmitter). To achieve consistency of the measurements good acoustic coupling is essential between the transducers and the wire. To effect a good contact between the wire and the transducers, the wire ends had to be filed square and flat. A grease couplant was used to reduce the energy losses at the contact between transducer and wire. Furthermore, to assure good contact, and the same applied pressure between transducer and wire during testing, a holder was designed and used (42).

The transit time method was used (see fig.5.5), as no commercial system was found available which uses low-frequency transducers in a pulse-echo system. The problem of using the commercial low-frequency transducers is the ringing time i.e. pulse width of the input signal, for instance for the transducers used in this study the ringing time is 3msec until the input signal is fully decayed. This long duration input pulse implies that the return echo from times up to this order will be embedded in the input signal, i.e. it would be difficult to detect or extract it.

Table 5.3 shows the experimental results over the different lengths. It includes the velocity and attenuation measurements.

The velocity values were calculated from the following equation:

$$c = l/t$$

where l is the length of the wire embedded in concrete

t is the time of flight

Attenuation coefficients were calculated from the following equation:

$$\alpha = 20 \log(\text{RMS}_r / \text{RMS}_i), \text{ dB}$$

where RMS_r is the root-mean square of the received signal

RMS_i is the root-mean square of the input signal.

To calculate RMS_i of the input signal, the two transducers were immersed in water, and placed 3mm apart (water was used because

the signal suffers very low attenuation $9.31E-9$ dB/m). The signal captured using this set-up was used to calculate RMS_i .

The RMS_r was calculated after transmission through the stated length embedded in concrete.

Fig.5.6 shows some of the results.

As can be seen from table 5.3, the attenuation coefficients are not consistent or approximately equal which suggests that the attenuation coefficient is length dependent.

By using Paquet's equation, the theoretical value of attenuation for $r=0.0035\text{mm}$ and $f=134000\text{Hz}$ is 36.55dB/m .

c- Discussion

By comparing the values of attenuation measured by experiment of a bar of 0.15, 0.25, 0.5, and 1m lengths embedded in concrete (average 40.5dB/m) with the calculated value from Paquet's equation (36.55 dB/m), the result is found to be highly satisfactory and the slight inaccuracy errors could be from the assumptions used in derivation the equation.

As can be seen from table 5.3, the experimental attenuation coefficients varied with the length of the wire embedded in concrete (it is worth mentioning that the concrete mix was the same for all cylinders). It was therefore decided to investigate the theoretical effect of changes in the length of the wire

embedded in the concrete sample on attenuation of signal strength.

The assumptions made were:

-The compressive strength of concrete samples were equal, the cube strength of the mix was 40N/mm^2 at 28 days, and the pulse velocity was 4.2km/s . This condition was assumed to neglect any contribution of the concrete in the derived equation.

-The attenuation of the signal is logarithmic i.e.

$$\alpha = a + b \log x$$

where a and b are constants

x is wire length embedded in concrete

α is attenuation in dB.

Using a regression analysis package yields to:

$$\alpha = 56 + 13 \log x$$

Fig.5.7 shows the attenuation against distance.

It should be noted that this equation should only be used for low-frequency testing and for wires embedded in concrete with high compressive strength.

5.5- MECHANICAL ANALYSIS

This section is included to show the mechanical configurations of a bar in air or in concrete, and is not going to be taken into

more detail other than what it is mentioned.

a- Wire in Air

Fig.5.8 shows the mechanical configuration of a bar in air. The resonant frequency for a such configuration is:

$$f = 1/2\pi \sqrt{R/M}$$

where R= spring stiffness/meter= SE/L

M= linear mass of the wire/meter= Sρ

S= cross-section of the wire

E= modulus of elasticity of the wire

ρ= density

c= longitudinal velocity= $\sqrt{E/\rho}$

Replacing the above values in the equation yields to:

$$f = c/2\pi \sqrt{1/L}$$

For a steel wire of 1m length in air, we have f=923 Hz

b- Wire Embedded in Concrete

Fig.5.9 shows the machanical configuration of a bar embedded in concrete. In this case, the damping is due to:

- Viscous damping.
- Mass of the bar.
- Friction or vertical reaction around the wire.

In this case, it can be taken as an approximation that the resonant frequency is equal to (103):

$$W = W_0^2 - d^2$$

where $W_0 = \sqrt{R/M}$

$$d = \alpha/2M$$

R= spring stiffness/meter= SE/L

M= linear mass of the wire/meter= $S\rho$

S= cross-section of the wire

E= modulus of elasticity of the wire

ρ = density

α = attenuation per unit length, or in mechanical terms viscous damping

r= friction or vertical reaction around the wire per unit length.

An approximation could be assumed (103) that the resonant frequency is equal to the resonant frequency of a wire in air.

$$W \approx W_0^2$$

5.6- SUMMARY

This chapter has examined attenuation of different frequency signals of rods embedded in concrete.

Theoretical and experimental comparisons have been found to be satisfactory.

It was established from the experimental work that high frequency attenuation (between 1MHz and 5MHz) is around 22dB/m, and for low frequency attenuation (200kHz and 300kHz) is around 42dB/m.

As access to the ends of wires in a prestressed bridge is often not possible, the application of these methods i.e. pulse-echo and transit-time, in crack detection is restricted to laboratory beams (span <2m). Fig.5.10 shows the detection of a crack in a wire embedded in concrete (the concrete beam was 1m long, the wire diameter 7mm with a 2mm saw-cut at 640mm from one end, using a 2.25MHz pulse-echo system. The figure shows the echo from the crack and from the other end.

Further studies are therefore necessary regarding the condition of steel embedded in concrete, using a method of testing which is applied to the outside, i.e. the surface, of the concrete. The following two chapters will cover the attenuation of sound in concrete and the expected amount of energy reflected by a wire embedded in concrete.

Table 5.1- Experimental results of high frequency (7 mm dia. wire)

Medium	Frequency MHz	Velocity km/s	Attenuation dB/m
Air	1	5.36	4
Air	2.25	5.41	4.25
Air	5	5.52	4.3

Water	1	5.32	6
water	2.25	5.3	6.8
water	5	5.41	6.5

Concrete	1	5.3	21
Concrete	2.25	5.3	22
Concrete	5	5.4	22

Table 5.2- Attenuation coefficients using McSkimin's Eq. (7 mm dia. wire)

Medium	Frequency MHz	Attenuation dB/m
Air	1	2.9
Air	2.25	1.36
Air	5	0.4

Water	1	3
Water	2.25	1.37
Water	5	0.4

Table 5.3- Transmission Characteristics, Wire-to-Wire in Concrete

Wire Length, m	Velocity km/s	RMS _r V	RMS _i V ⁱ	α dB/m
0.15	6.097	0.011	0.497	-33.10
0.25	5.605	0.157	0.497	-39.85
0.5	5.176	0.0397	0.497	-43.88
1.0	4.917	0.00274	0.497	-45.16

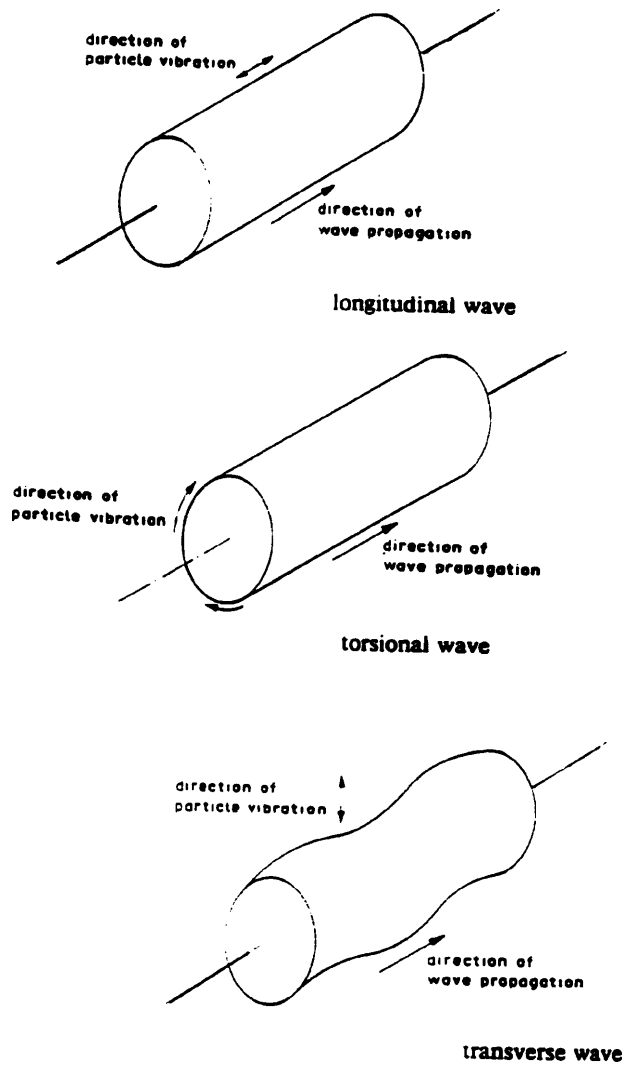


Fig.5.1- Modes of rod vibrations.

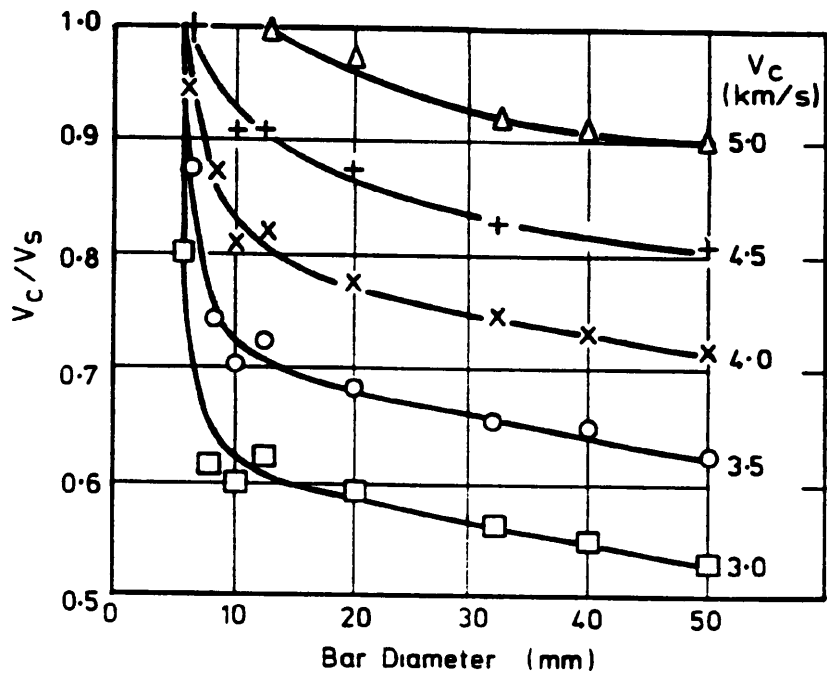


Fig.5.2- Relationship between V_c , V_s , and bar diameter for longitudinal bars in concrete (101).

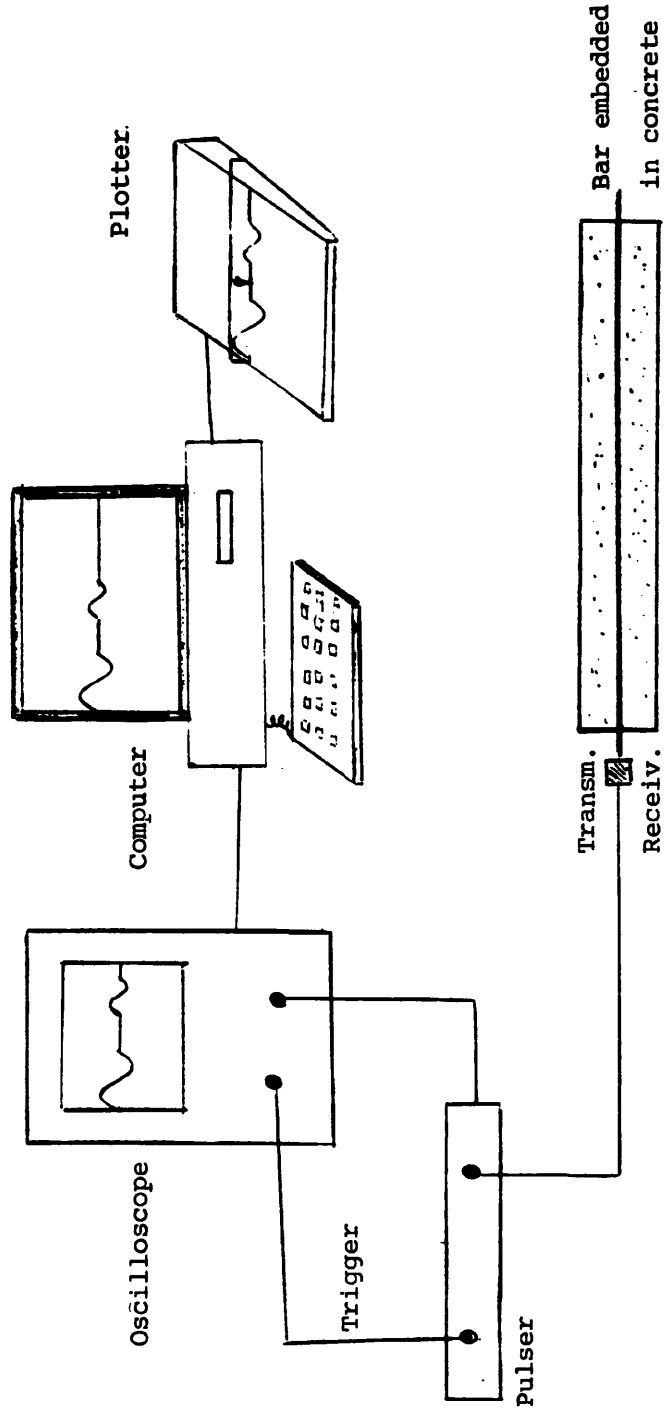


Fig.5.3- Pulse echo-system used.

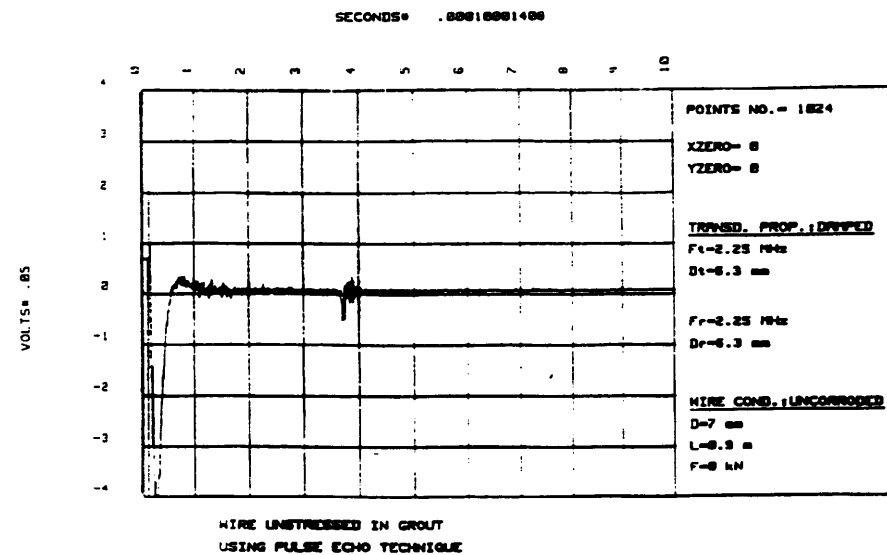
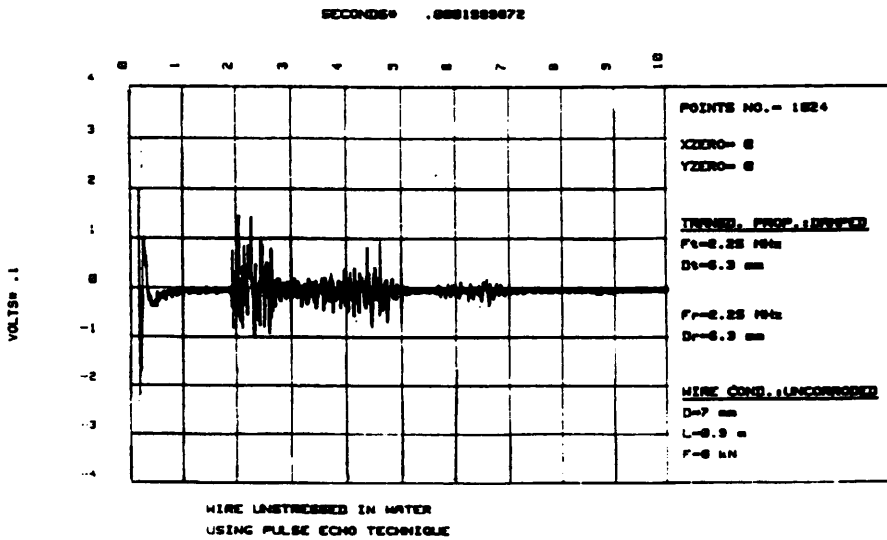
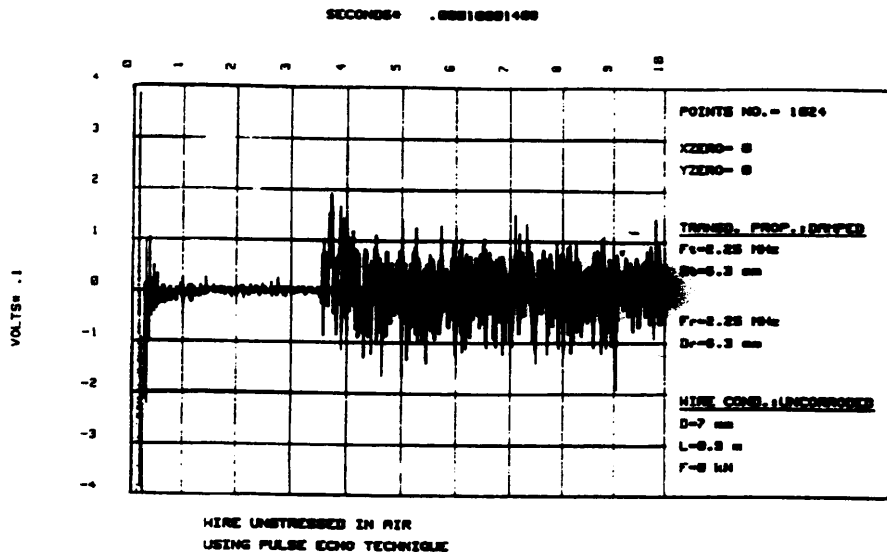


Fig.5.4- Some examples when a pulse is applied and received on the same end of a wire in air, water, and concrete.

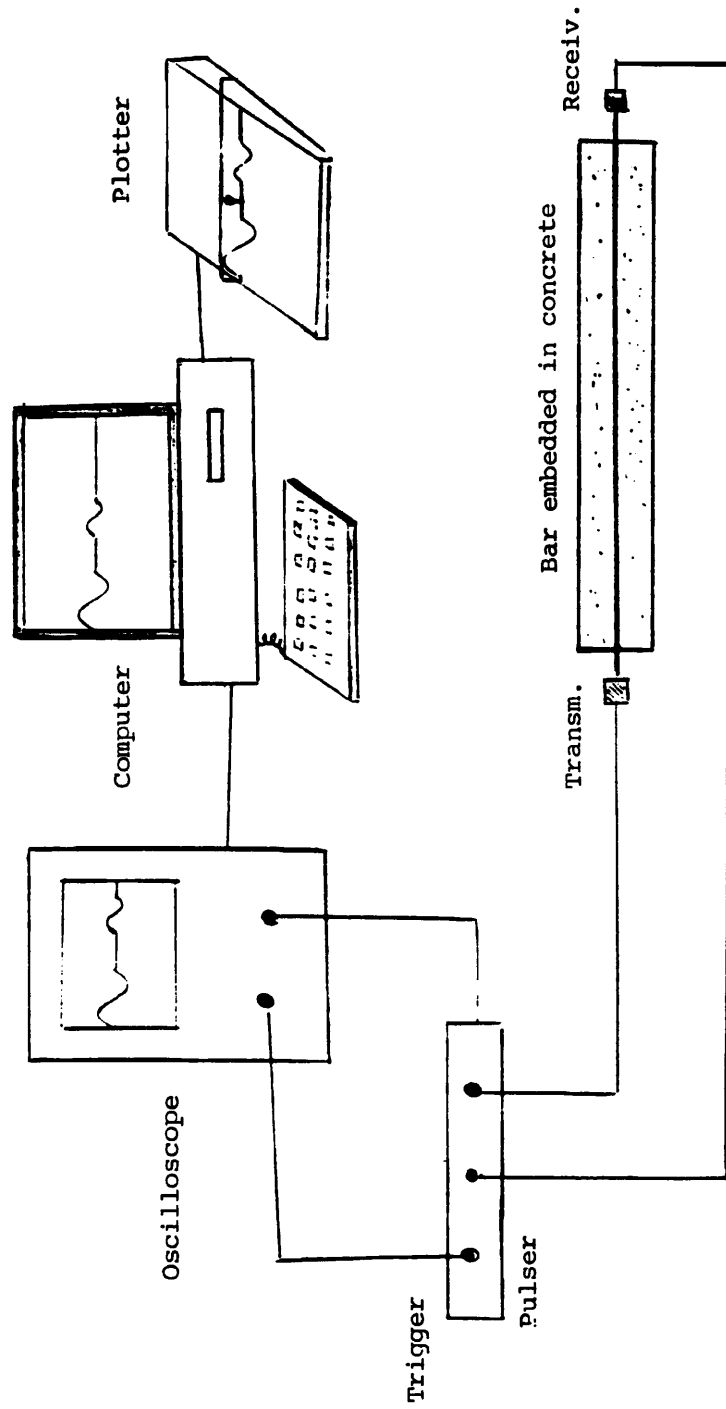


Fig.5.5- Pitch-catch system used.

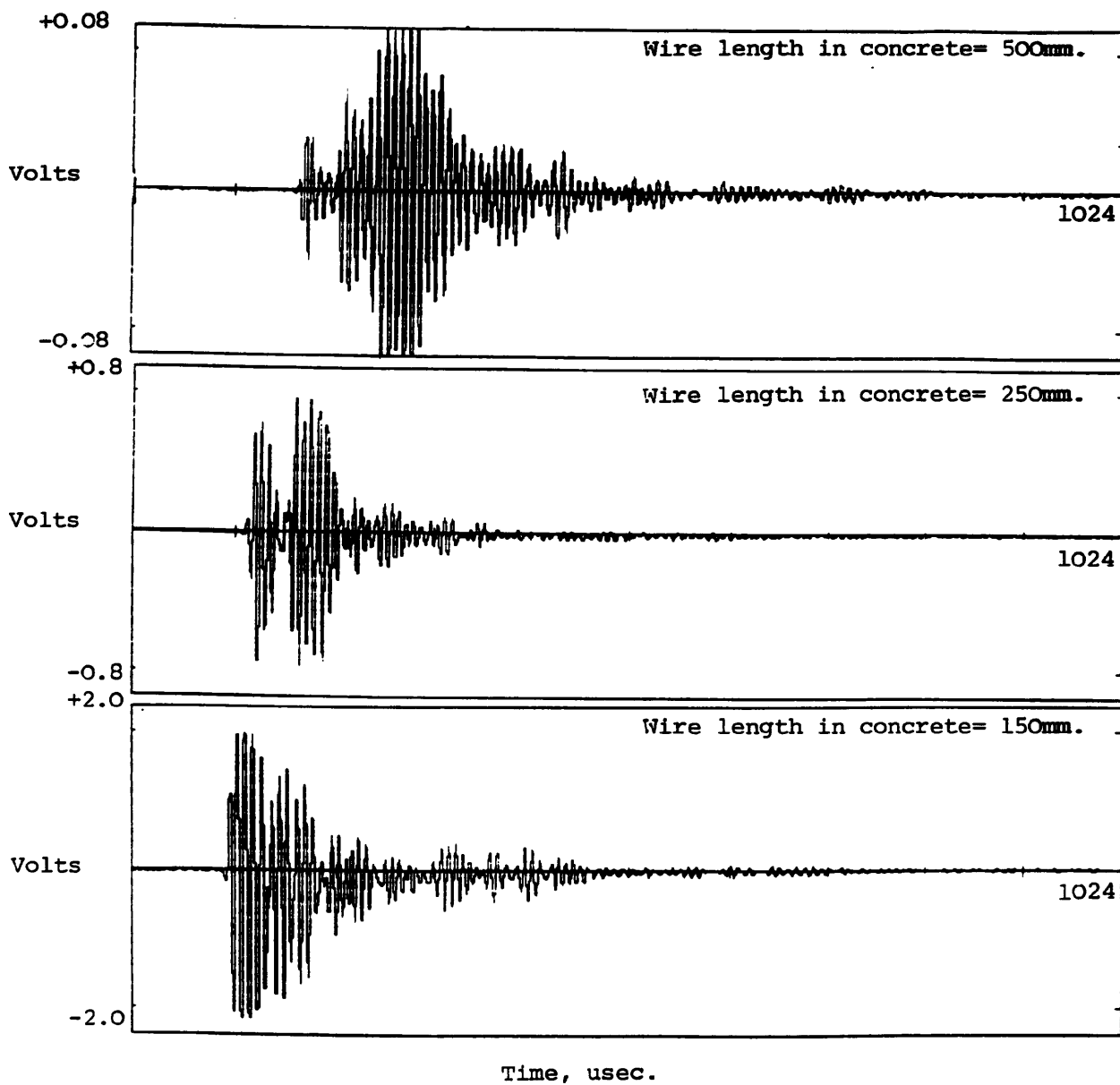


Fig.5.6- Some examples when a pulse is applied at one end and received at the other of a wire embedded in concrete.

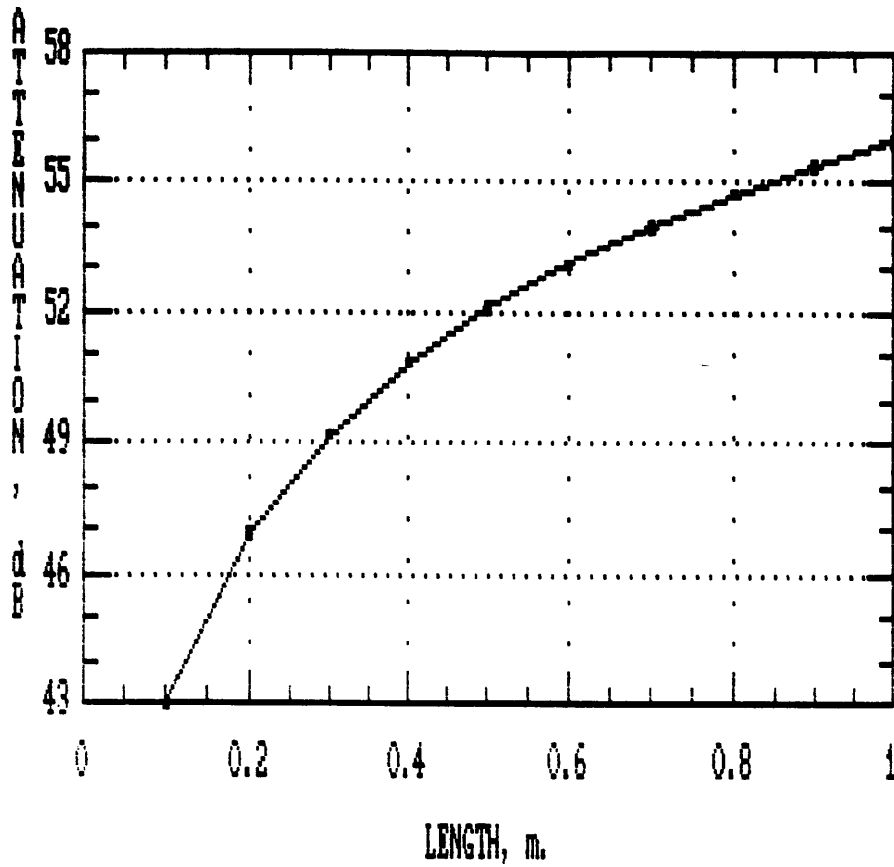


Fig.5.7- Variation of experimental attenuation coefficients with the length of the wire in concrete.

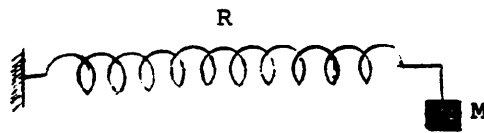


Fig.5.8- Mechanical configuration of a bar in air.

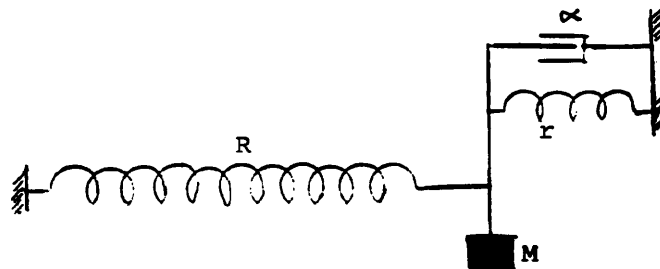


Fig.5.9- Mechanical configuration of a bar embedded in concrete.

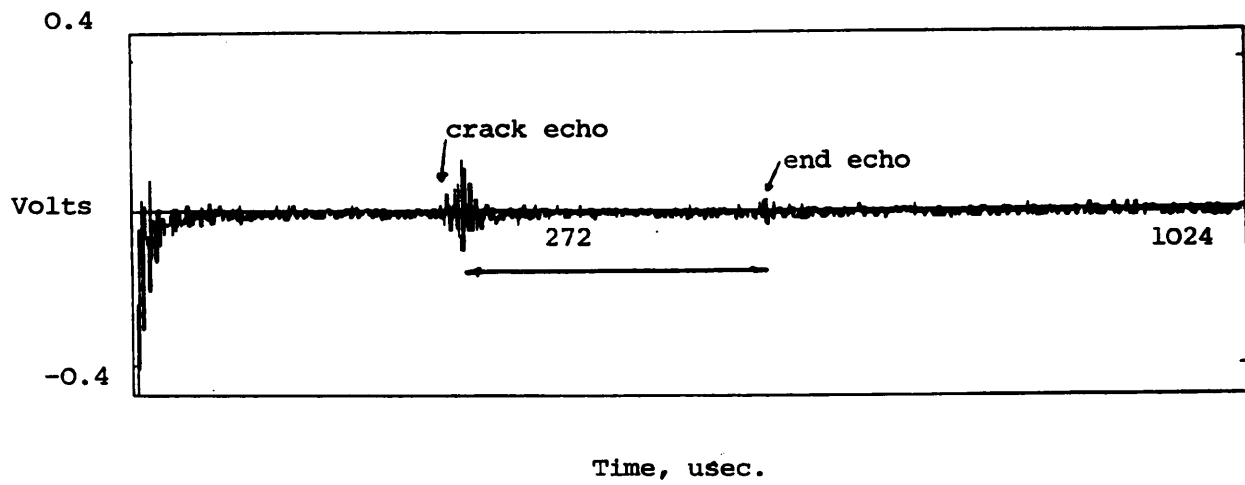


Fig.5.10- Detection of a crack in a wire embedded in concrete using pulse-echo technique.

CHAPTER 6

ATTENUATION OF SOUND IN CONCRETE

6.1- INTRODUCTION

The application of ultrasonic methods, i.e. pulse methods (pitch-catch, pulse-echo), to concrete is largely concerned with the observations of a pulse transmitted either directly through the concrete or along its surface. Hence an approximate assessment of the ratio of the amplitude of the received signal to the initial pulse is often extremely useful in interpreting measurements obtained on concrete, this ratio being referred to as the attenuation coefficient. Previous work by Facaoaru on Non-destructive testing of concrete in Romania (104) showed that the attenuation changes with the maximum size of aggregate. He plotted the attenuation against the strength of concrete, fig.6.1 shows his result. It was reported too that by measuring the attenuation, an estimation of the strength of the concrete could be evaluated. Moreover Serabian (105) showed the attenuation changes due to the age of concrete against frequency (see fig.6.2)

6.2- ATTENUATION OF ULTRASONIC WAVES IN CONCRETE

Concrete when hardened contains the following constituents: cement, fine aggregate (diameter < 0.6mm), and coarse aggregate

(diameter between 1.18mm and 20mm), and each of these have different acoustic impedances (see chapter 3 for the different coefficients).

Thus, when a signal is propagated through concrete, its strength will weaken. This results from two causes: a) scattering and b) absorption. These can both be combined by the concept of attenuation.

Total losses due to scattering and absorption may be incorporated in the linear attenuation coefficient:

$$\alpha(f) = \alpha_s(f) + \alpha_a(f)$$

where α_s includes all losses from scattering

α_a includes the losses from any mechanisms producing absorption.

In concrete the major contribution to the scattering coefficient is grain boundary scattering, and the largest absorption loss is that due to thermal conductivity.

6.2.1- Scattering

The scattering results from the fact that the concrete is not homogeneous. It contains boundaries on which the acoustic impedance changes suddenly because two materials of different density, elastic modulus, and sound velocity meet at these interfaces. Such inhomogeneities in concrete include:

-Crystallites of different structure and composition, i.e.

cement+sand+gravel.

-The compaction process in concrete, often causing anisotropy (but the effect is usually small); the pulse velocity in the direction of compaction is rarely more than a few percent below that in the directions at right angles (69).

In a material such as concrete, with very coarse grain compared with the wavelength the scatter can be argued geometrically: when a wave strikes a boundary, say mortar-gravel, at an oblique angle, the wave is split into various reflected and transmitted wave types. Thus the initial signal is constantly divided into partial waves which along their long and complex paths are slowly converted into heat (absorption, see next section).

The magnitude of the scattering loss is dependent on the relationship of ultrasonic wavelength to the dimensions and the impedance of inhomogeneities.

Table 6.1 lists the predominant scattering mechanism for a given wavelength (λ) to average grain diameter D , as well as the functional dependence of attenuation upon frequency.

Table 6.1- Mechanisms involved in the scattering of ultrasonic waves (106)

Wavelength to Grain diameter range	Mechanism	Frequency Dependence on Attenuation
>> D	Rayleigh	Vf^4 or D^3f^4
= D	Stochastic	Df^2
<< D	Diffusion	$1/D$

V = average grain volume, D = average grain diameter
 f = frequency

For scatterers much larger than the ultrasonic wavelength, the

losses are caused by specular reflections which change the direction of the ultrasound incident on the boundary. The attenuation depends on the mean free path distance between grain boundaries, so as the grain size increases relative to the wavelength the losses decrease.

As the wavelength approaches the dimensions of the discontinuities, the interactions become complex, a combination of specular reflection and diffraction, and for this range, the attenuation coefficient is proportional to the product of the grain size and the square of the frequency.

In the last case where the boundaries are much smaller than the wavelength, energy is scattered isotropically, and the amplitude of the scattered waves depends not on shape but only on the volume of the scatterer.

In this research, when testing was carried out on the surface, the maximum frequency used was 500kHz, which gives a wavelength of 8mm for 4 Km/sec longitudinal velocity, and the minimum frequency used was 45kHz, which gives a wavelength of 89mm for the same velocity. The average diameter of aggregates is about 10mm, where one can expect the scattering to be either stochastic, where $\lambda \cong D$, or Rayleigh where $\lambda \gg D$, depending on the frequency.

6.2.2- Absorption

The second cause of attenuation is absorption, which is a direct

conversion of sound energy into heat. Several processes can be responsible, which, for the case of concrete, are visco-elasticity and heat conduction.

As an ultrasound wave travels through a material the viscosity of the material tends to oppose the motion of the particles disturbed by the wave, and absorption of energy occurs. Energy lost in this manner is converted into heat. The absorption coefficient representing losses due to viscosity is given by:

$$\alpha_a(f) = A \frac{c}{c_0^2} \frac{2\pi f t^2}{1 + (2\pi f)^2 t^2} \quad (\text{ref.107})$$

where A= constant depends on the material

c, c₀ = the velocity at the frequency of interest and the velocity as the frequency of the ultrasound approaches zero, respectively.

$$t = (4/3)n/\rho_0 c_0^2$$

n = coefficient of viscosity

ρ_0 = density.

In concrete, visco-elasticity has a much less important effect on the attenuation than does heterogeneity and scattering (69).

The other factor governing absorption is heat conduction. When an ultrasonic wave passes through a medium an increase in temperature will be produced at points where the material is in compression (106). The heat will flow from the high-temperature regions into regions of lower temperature.

Thermal conductivity leads to an absorption coefficient given by (for solids) (107):

$$\alpha_a(f) = (2\pi f)^2 / (2\rho_0 c^2) [x + 2n + (K_h / C_v) (K_a - K_i) / (K_a + 2\mu)]$$

where x , n = the compressional and shear viscosities.

K_a , K_i = the adiabatic and isothermal Lamé constants.

K_h = coefficient of thermal heating.

C_v = specific heat of the material at constant volume.

This coefficient may usually be neglected as it is small compared to the losses from scattering effect due to grain diameter.

6.2.3- Summary

From the above, the attenuation is then divided into absorption coefficient and scatter coefficient, thus:

$$\alpha = \alpha_a + \alpha_s$$

We will assume that for concrete, for the absorption coefficient we have:

$$\alpha_a = C_1 f$$

where C_1 is a constant unaffected by grain size and anisotropy.

and for the scatter coefficient, depending on the ratio of grain size to wavelength there are three possibilities (see table 6.1):

$$\alpha_s = C_2 f^4 \text{ or}$$

$$C_2 f^2 \text{ or}$$

$$C_2/D, \text{ where } C_2 \text{ is a constant dependent on grain size.}$$

Thus, the attenuation coefficient (there are three possibilities) will be:

$$\alpha = C_1 f + C_2 f^4 \text{ or}$$

$$C_1 f + C_2 f^2 \text{ or} \quad (6.1)$$

$$C_1 f + C_2/D$$

6.3- EXPERIMENTAL ATTENUATION ANALYSIS

Two groups of experiments were performed:

a-The first group was carried out on a number of concrete mixes and sample lengths in order to quantify the effects of signal scattering and attenuation at different frequency levels.

b-The second group was carried out on blocks of the same mix with with different lengths in order to establish a relationship between attenuation and frequency for high strength concrete.

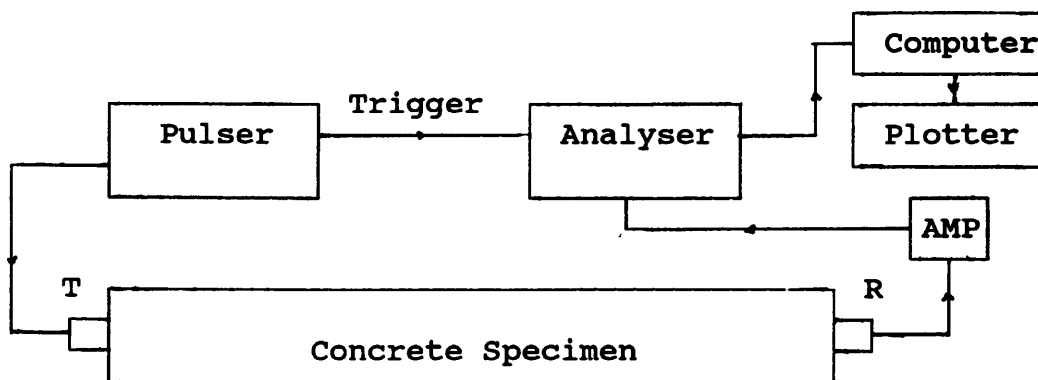


Fig.6.3

6.3.1- Group One Experiments

Fig.6.3 shows the configuration used in these experiments. Two wide-band transducers with a nominal centre frequency of 500kHz were coupled to either end of a solid concrete cylinder using a medium grade grease. One transducer was excited to resonance by a 600V spike and the other, acting as receiver, was connected directly to the input of a digital storage oscilloscope.

After the time records were acquired, they were transferred to computer and subsequently analysed using the package on the Hewlett-Packard computer.

The specimens were cylinders of 50mm in diameter and ranged in length from 200mm to 500mm, in 100mm increments.

Three mixes were investigated for this experimentation, mix 1 contained no aggregate just sand and cement only, mix 2 was composed of aggregates of diameter less than 10mm, mix 3 contained aggregates with a diameter less than 20mm. The designed strength for the mixes with aggregates was 30N/mm², see table 8.1 for the proportions used in these specimens.

a- Analysis

Table 6.2 contains information relating to the first 512 μ s of the received signal. In the time domain, this information includes the propagation velocity which is the compressional wave velocity. In the frequency domain, the signal strength at three

various frequency bands has been calculated, using absolute voltage amplitude from linear spectra. The frequencies are 120kHz, 40kHz, and 10kHz. The attenuation coefficient given in this table was calculated from

$$\alpha = 20 \log A_{rf} / A_{if}, \text{ dB}$$

where A_{rf} is the amplitude at a frequency of the received signal
 A_{if} is the amplitude at the same frequency of the input signal (this was calculated from the signal which was recorded when the two transducers are 3mm apart and immersed in water)

In order that these experiments provided reliable attenuation loss statistics, the effects of divergence loss were minimised by the appropriate choice of sample dimensions. Unlike attenuation loss, divergence loss is related to the beam-spread function of the transducer/medium combination, and is given by:

$$P_a = P_o J_1(\pi D \sin \theta / \lambda) / (\pi D \sin \theta / \lambda)$$

where θ is the angle with the acoustic axis

P_o is the pressure at the axis

J_1 is the Bessel function of the first order

D is the diameter of the probe

λ is the wavelength

Generally speaking, the signal strength declines not only with length of sample, but also with increase in frequency. Moreover, the weakest signals are also, shown to be associated with the samples containing the largest mean aggregate size, mix 3.

b- Discussion

For mix 1, where the wavelength for $f=120\text{kHz}$ ($\approx 40\text{mm}$) is much greater than the average grain diameter ($<0.6\text{mm}$), the scattering is due to Rayleigh type where $\lambda \gg D$, and thus affects the higher frequency components more severely. Hence mix one, which contained only sand and cement, with particles less than 0.6mm in diameter, gave rise to the most severe attenuation in relation to frequency.

From eq.6.1 we have

$$\alpha = C_1 f + C_2 f^4$$

For mix 2 and 3, where the wavelength for $f=120\text{kHz}$ ($\approx 30\text{mm}$) is of the same order of size as the average grain diameter, the scattering is stochastic, sometimes called phase scattering. This is less severe than Rayleigh scattering, being proportional to f^2 . However, for the longer wavelengths, this aggregate would also be a source of Rayleigh scattering. The absolute attenuation figures should ^{be} higher for mix 2 and 3 than mix 1, because they are a source of Rayleigh and stochastic scattering.

From eq.6.1, we have

$$\alpha = C_1 f + C_2 f^2$$

By using the regression analysis package, we derive the

following equation, taking into account the absorption coefficient:

$$\alpha = 0.0508f + 0.1f^2, \quad f \text{ in kHz and } \alpha \text{ in dB/m.}$$

Fig.6.4 shows the attenuation against the frequency using this equation.

It should be emphasized that the last equation should only be used in a concrete of strength around 30N/mm^2 , and where the input wavelength of the signal is roughly equal to the mean aggregate size.

From table 6.1, it can be seen, that as the frequency increases, the attenuation does not increase rapidly as expected in each mix. It was decided, therefore, to investigate the matter. It was found that when the cylinders were cut (they were cast in 1 metre length and cut later) to the required lengths, the cut had produced damage to the ends (especially to the weak specimens, cement+sand) i.e. there were cracks at the ^{cut} face, which meant that additional scattering occurred at the face. It was decided, therefore, to carry out another set of experiments with high strength concrete and cast in blocks, and not to accept the results of the last experiments as accurate (they could be used as a rough approximation for attenuation for such mixes).

6.3.2- Group Two Experiments

Fig.6.3 shows the configuration used in these experiments. Two

wide band transducers with a nominal centre frequency of 700kHz were coupled to either end of a solid concrete block using a medium grade grease.

One transducer was excited to a resonance by a 600V spike and the other, acting as a receiver, was connected directly to the input of a digital oscilloscope.

After the data was acquired, it was transferred to, and subsequently analysed on, the computer.

The specimens were blocks of $150 \times 150 \times 150 \text{mm}^3$, $150 \times 150 \times 455 \text{mm}^3$, and $150 \times 150 \times 997 \text{mm}^3$.

The mix investigated has an average cube compressive strength after 28 days of 45N/mm^2 , see table 8.1 for composition proportions.

a- Analysis

These experiments were carried out to try to establish a relationship between frequency and attenuation for high strength concrete.

After capturing the signal it was transformed to the frequency domain by Fourier analysis. Then the signal strength at 10kHz, 40kHz, and 120kHz was calculated. The method of calculation is similar to that mentioned earlier for group one. Table 6.3 represents the average attenuation loss coefficients at those

frequencies over the three specimens under investigation.

b- Discussion

From table 6.3, it can be seen that the higher frequency components are highly attenuated compared with the lower frequency components. In this study the maximum frequency which was possible to detect in concrete was 700kHz, however, frequencies above 700kHz would be expected to suffer severe attenuation in concrete, and rarely used.

Between frequencies 700kHz and 300kHz, stochastic scattering occurs where $\lambda \approx D$, and for frequencies lower than 300kHz, diffusion scattering occurs.

If we assume the attenuation coefficient will take the following form:

$$\alpha = C_1 f + C_2 f^2$$

By regression analysis, the derived equation is:

$$\alpha = 0.1844f + 0.001f^2 \text{ (dB/m)}$$

where f in kHz.

This equation should be used for high strengths concrete and for frequencies up to 700kHz.

Fig.6.5 shows the attenuation against frequency.

6.4- SUMMARY

These groups of experiments were performed on a number of concrete mixes and sample lengths in order to quantify the effects of signal scattering and attenuation at different frequency levels.

The general conclusion which could be drawn from this study is that as the frequency increases, the attenuation increases rapidly. These results have important implications for any final interrogation system, i.e. pitch-catch or pulse-echo. Furthermore, it shows how to differentiate between signal attenuation through absorption, and signal attenuation through scatter. Rayleigh scattering results in a general weakening of the signal through thermal conversion, but phase and diffusion scattering, whilst less severe, give rise to coherent noise at the receiver transducer because each scattering interface produces an echo which is embedded with ^{the} echo produced by any internal object, say steel wire or strand. It therefore follows that if a method should be found to obviate the effects of coherent signal noise, which does affect the shorter wavelengths much more than the long ones, the use of signal processing techniques to try to extract the echo from the subject of investigation if high frequency system could be a choice. If such a system is used, the digital filtering technique should be applied to filter out the unwanted part of the signal. Consider an ultrasonic pulse containing frequencies up to several hundred kHz travelling through concrete containing inclusions such as small voids and steel cables. The high frequency components are

attenuated more severely due to the heterogeneous nature of the concrete, as has been demonstrated in this chapter, leaving the low-frequency to be dominant. This is undesirable, because it is mainly the higher frequencies which contain information regarding the internal composition of the structure and condition of the embedded components. Therefore it will be important to filter out the unwanted signal, for example to remove the lower portions of the frequency domain spectrum. This argument will be discussed in detail in chapter 11.

Finally, in order that these experiments provide reliable attenuation loss statistics, the effects of divergence loss which was neglected in this study, should be taken into account when considering the signal-to-noise characteristics of a system, and the total signal loss, α_t in dB, is given by:

$$\alpha_t = \alpha_s + \alpha_a + \alpha_f$$

where α_s = scatter coefficient

α_a = absorption coefficient

α_f = this attenuation is a function of sound frequency, probe to specimen contact, type of probe, dimensions of specimen, divergence loss (beam spread).

α_t = total attenuation coefficient.

Table 6.2- Attenuation Analysis Results for Group One

	Length	Velocity	Attenuation at Frequency dB		
	mm	m/sec	120kHz	40kHz	10kHz
mix1	200	3636.3	-8	-6	-6
mix1	300	3571.4	-16	-11	-14
mix1	400	3478.8	-24	-23	-23
mix1	500	3496.5	-43	-41	-40
mix2	200	4545.5	-6	-5	-5
mix2	300	4225.4	-13	-12	-18
mix2	400	3669.7	-31	-31	-34
mix2	500	3311.3	-44	-43	-42
mix3	200	4651.2	-10	-12	-13
mix3	300	3947.4	-21	-30	-31
mix3	400	3333.3	-40	-43	-44
mix3	500	3472.2	-50	-52	-55

Table 6.3- Attenuation Coefficients for Group Two

Frequency kHz	Average Attenuation coefficients, dB/m
10	-35
40	-50
75	-65
120	-70
200	-90
700	-200

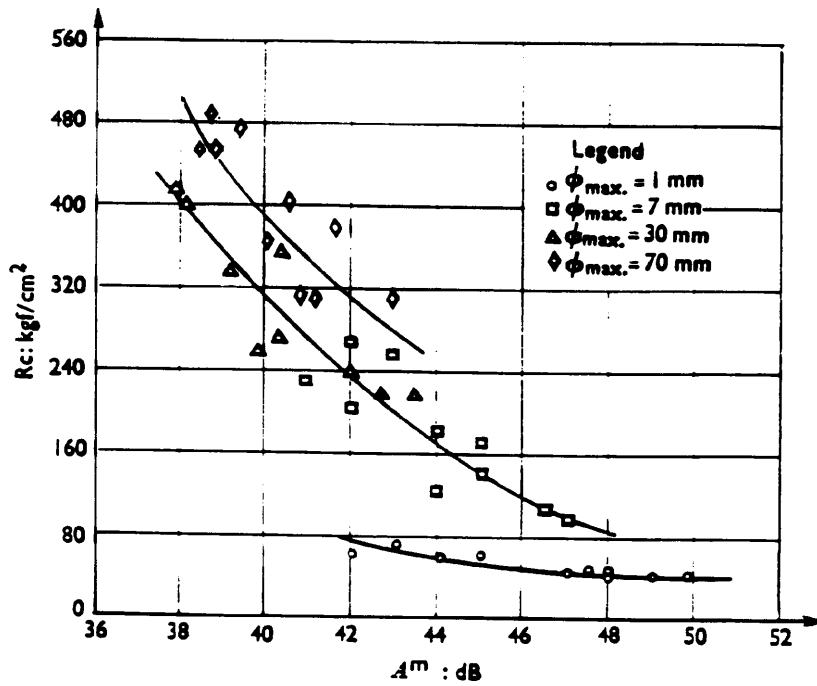


Fig.6.1- Influence of maximum size of aggregate on the correlation between attenuation and strength (104).

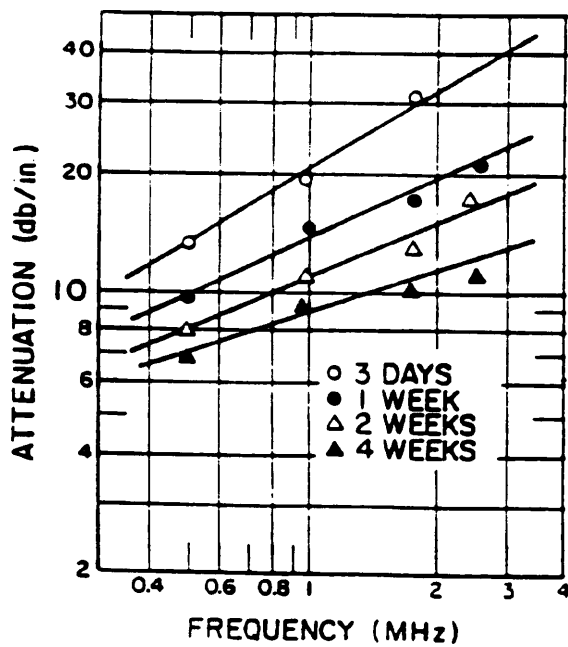


Fig.6.2- Attenuation monitoring of concrete with a water to cement ratio of 0.5 (105).

(X 100)

ESTIMATED LOSSES FOR MIX 2 & 3.

170

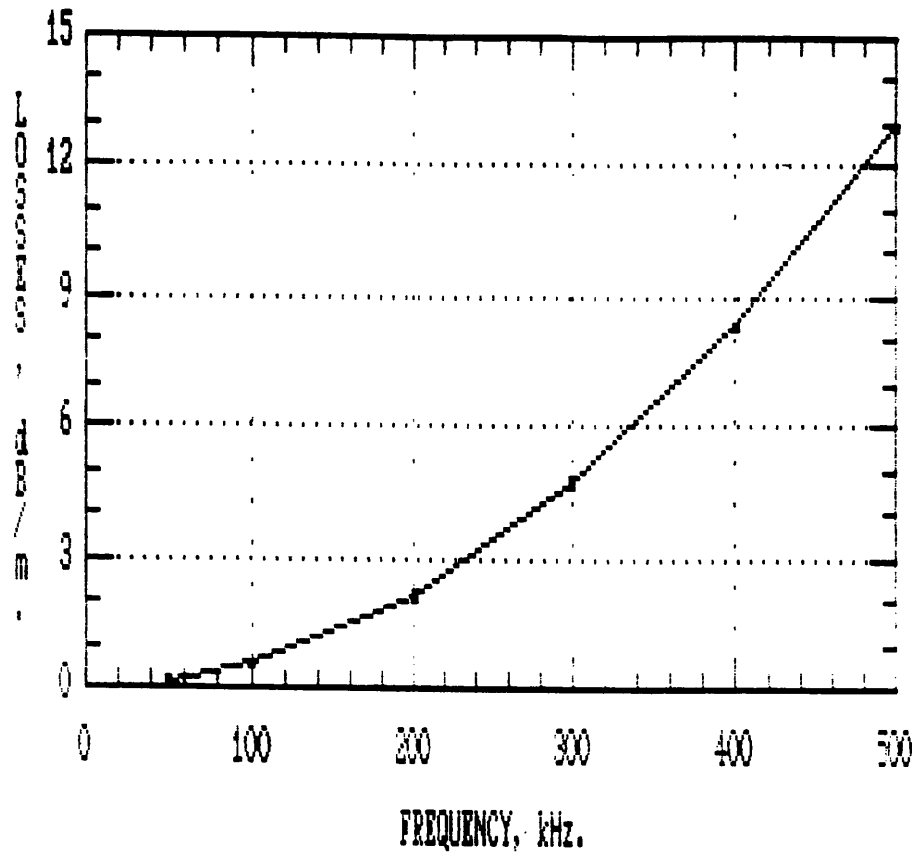


Fig.6.4

ESTIMATED LOSSES IN CASE OF HIGH STRENGTH CONCRETE

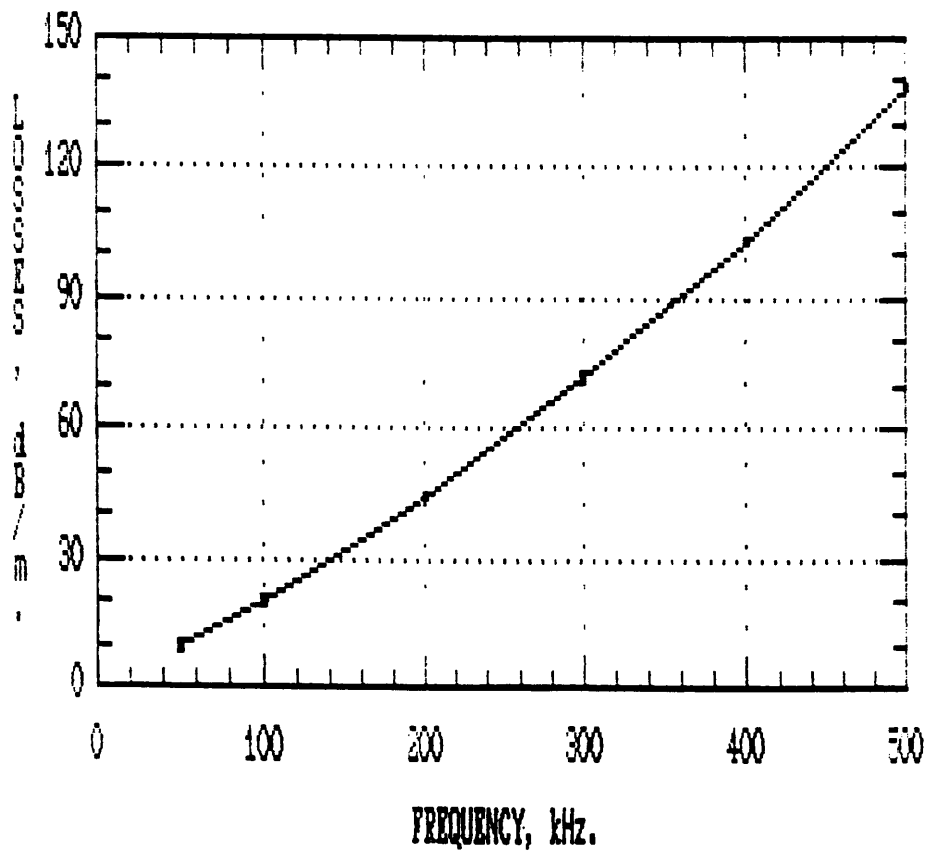


Fig.6.5

CHAPTER 7ACOUSTIC SCATTERING BY CYLINDRICAL
BARS EMBEDDED IN CONCRETE7.1- INTRODUCTION

The scattering of a wave by an obstacle in its path is a topic of particular interest in the study of wave propagation in optics, acoustics, and electromagnetics.

In chapter 5, it was established that attenuation associated with the propagation of a wave travelling along the length of a steel bar encased in concrete was too severe to allow the application of the pulse echo method in this instance. For this reason the approach that was adopted involved the mounting of transducers on the surface of the concrete directly above the steel components in an area where defects in the reinforcing were suspected to be. It is necessary, therefore, to derive a theoretical approach to calculate the expected strength of the reflected echoes from a sound bar, and a corroded one embedded in concrete, and compare the result with the strength of the back-wall echo.

For a bar embedded in concrete, no published theory has been identified. It is therefore intended in this chapter to describe the behaviour of solid cylindrical reflectors embedded in concrete with the help of simple geometrical derivations, without having to use extensive calculations, in order to give an

approximate picture of the dependence of the echo amplitude on the diameter of the bar, the distance from the probe, the frequency of this probe, and the roughness of the corroded surface of the bar. The waves were assumed to be plane during the derivation.

Attempts were made to cross-correlate the captured signal from a sound wire embedded in concrete with that derived theoretically.

7.2- SIGNAL LOSSES

An ultrasound beam introduced into a medium will lose energy with distance as a result of beam divergence (known as divergence loss), and as a result of attenuation loss which encompasses the phenomena of scatter and absorption. When the wave encounters an acoustic interface, the pressure reflected will depend upon the ratio of acoustic impedances and the angle of incidence.

A transducer of diameter D , and resonance f with a wavelength $\lambda = c/f$ in a given medium will radiate with a half angle θ given by:

$$\theta = \sin^{-1}(1.2\lambda/D), \text{ rad.}$$

This radiation pattern is applicable only in the far field, or Fraunhofer region. The length of the near field, or Fresnel region is given by $D^2/4\lambda$.

The pressure at any given point in the far-field is dependent

upon the angle that point subtends to the acoustical axis, θ , and the distance, x . The polar-pressure relationship (off-axis pressure) is expressed as; see page 87 for symbols:

$$P_{\theta} = P_0 J_1(\pi D \sin \theta / \lambda) / (\pi D \sin \theta / \lambda)$$

where J_1 is a Bessel function of the first order, θ is expressed in radians, and P_0 is the pressure at $\theta=0$.

The distance-pressure (pressure on-axis) relationship is governed by the expression:

$$P_x = P_0 \sin(\pi / \lambda [\sqrt{D^2/4 + x^2} - x])$$

This equation can be approximated by:

$$P_x = P_0 \pi D^2 / 4 \lambda \cdot 1/x, \text{ for } x \gg D^2 / 4 \lambda$$

This effectively is the equation which describes the divergence loss.

An ultrasonic wave travelling through a medium of acoustic impedance Z_1 and normally incident on a medium of acoustic impedance Z_2 , will be partially reflected. The proportion of the signal reflected is given by:

$$P_{r1} = P_0 (Z_1 - Z_2) / (Z_1 + Z_2)$$

The above equation is applicable only to compressional waves at

normal incidence. At other angles, mode conversion occurs to shear components reflected and refracted at the boundary. At angles other than normal incidence, the reflected coefficients should be calculated using the equations given in chapter 3.

In addition to the signal losses, given so far, there are attenuation losses, due to scattering and absorption, to consider. It is usual to express the attenuation loss as:

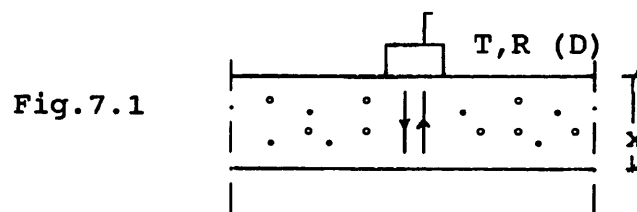
$$P_{\alpha} = P_0 \exp(-\alpha x)$$

where α = the coefficient of attenuation, derived in chapter 6.

x = distance travelled by the signal in the material.

7.3- ESTIMATED SIGNAL ATTENUATION FROM A BACK-WALL ECHO

Fig.7.1 shows the configuration used to develop a model to estimate the signal losses with regard to a pulsed acoustic system used on concrete.



In this configuration or model, a pulse-echo system will be used i.e. one transducer is used to transmit and receive.

This model is going to be used to calculate signal losses in four different configurations; four transducers were used: 200, 300, 400, and 500kHz. The echo strength in each case was calculated

at depths (x) of 60 to 420mm in 20mm intervals. In all cases the transducer diameter (D) was fixed at 30mm.

For a back-wall echo, the attenuation suffered will be of the form (and taking into account that one radiator is acting as a transmitter and receiver in the same time): (see page 87 for symbols)

a- Due to distance-pressure

$$P_x = P_o \pi D^2 / 4\lambda \ 1/2x$$

b- Due to the interface material/air

$$P_r = P_x R$$

where R is the coefficient of reflection, in this case concrete-air at normal incidence=1.

c- Due to scattering and absorption

$$P_\alpha = P_r \exp(-2\alpha x)$$

where α is the coefficient of attenuation, calculated from the equation derived in chapter 6 for high strength concrete.

Then, total attenuation for this case will become:

$$P_t/P_o = R \pi D^2 / 4\lambda \ 1/2x \ exp(-2\alpha x) \quad (7.1)$$

fig.7.2 shows the variation of attenuation against distance for the frequencies mentioned earlier.

7.4- ESTIMATED SIGNAL ATTENUATION FOR A SOUND CYLINDRICAL BAR EMBEDDED IN CONCRETE

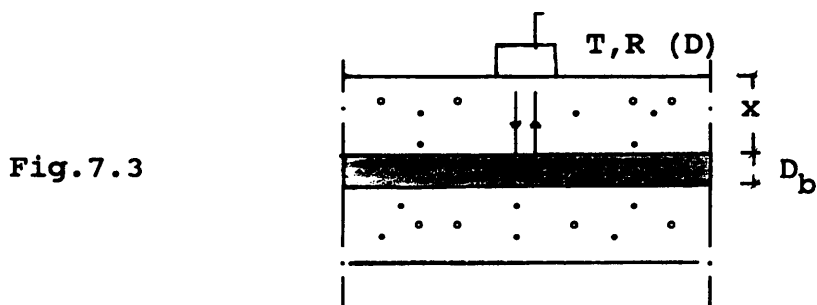


Fig.7.3 shows the set-up used in this model to estimate the signal reflected from a bar encased in concrete.

As mentioned before, a pulse-echo system will be used.

The model is used to calculate reflected signal including losses in four different configurations: four transducers were used 200, 300, 400, and 500kHz. The strength of the reflected echo from the bar embedded at depths (x) 60 to 420mm, 20mm intervals, was calculated for each case. In all cases the transducer diameter (D) was fixed at 30mm, and the diameter of the bar, D_b , at 10mm and 20mm.

For a sound bar embedded in concrete, the returned signal will be the product of:

a- Due distance-pressure

$$P_x = P_o \pi D^2 / 4\lambda \ 1/2x$$

b- To calculate the amount of energy reflected from a bar embedded in concrete an equation based on geometric optics which uses light rays which can be drawn as straight lines was used.

If a plane wave strikes the curved interface between two materials (concrete and steel), e.g. on a cylindrical surface only the ray incident at right angles can pass through or be reflected with no angular change. The lateral rays are refracted or reflected at an angle, which is greater the further they are from the axial ray, dispersion occurs, viz. the acoustic pressure decreases, as in the case of the similar optical phenomena produced by dispersing convex lens.

Krautkammer (67) gave the resultant acoustic pressure for a dispersing lens which has a sound velocity c_2 embedded in a medium where the sound velocity is (c_1):

$$P_r = P_x R \sqrt{f_c / (f_c + x)}$$

where $R =$ coefficient of reflection for concrete/steel at normal incidence $= (\rho_1 c_1 - \rho_2 c_2) / (\rho_1 c_1 + \rho_2 c_2) = -0.617$.

$$f_c = |D_b / (2(1 - c_2/c_1))|.$$

c- Due to scattering and absorption

$$P_a = P_r \exp(-2\alpha x)$$

Hence the total signal losses equation will be of the form:

$$P_t/P_o = R \pi D^2 / 4\lambda \cdot 1/2x \sqrt{f_c / (f_c + x)} \exp(-2\alpha x) \quad (7.2)$$

Figs.7.4, 7.5, and 7.6 show the variation of attenuation against

depth of bar in concrete, diameter of the bar, and diameter of the probe for a range of frequencies respectively.

7.5- ESTIMATED SIGNAL LOSSES FOR A CORRODED BAR EMBEDDED IN CONCRETE

When corrosion occurs in steel components embedded in concrete, pitting and spalling occur which lead to the surface being rough, and this roughness affects the reflection and scattering characteristics of a wave. For example, the reflection characteristics of a wave over such a surface are different from the characteristics over a smooth surface. A wave incident on a rough surface is not only reflected in a specular direction but is also scattered in all directions. For example, in biological media, rough interfaces between different organs and tissues affect propagation and scattering characteristics of a wave (108).

In rough surface scattering, it is important to recognize that the roughness of a surface should be considered relative to the wavelength and the direction of wave propagation and scattering.

Consider a wave incident on a rough surface as shown in fig.7.7. If the surface is completely smooth, two rays are specularly reflected, the reflected rays are in phase, and the reflection angle is equal to the incident angle, θ_i . If the surface becomes rough, the two rays are no longer in phase, and the phase difference $\Delta\theta$ is given by:

$$\Delta\theta = 2kh \cos\theta_i, \text{ where } k=2\pi/\lambda$$

If this phase difference is negligible compared to 2π , then the surface may be regarded as smooth (108). If the phase difference is significant, then the specular reflection is reduced due to interference and a part of the wave is scattered in all directions. Rayleigh used a criterion that a surface may be considered rough or smooth depending on whether the phase difference is greater or smaller than $\pi/2$. In term of h , the Rayleigh criterion is:

$h < \text{or} > \lambda / (8 \cos \theta_i)$, where h is the standard deviation of the rough surface.

Suppose that a wave is radiated from a transmitter and is incident on a surface, if the surface is smooth, the reflected wave is identical to the transmitted wave originated at the image point except for the reflection coefficient. However, if the surface is slightly rough, this reflected wave gets attenuated slightly due to scattering and the power corresponding to this decrease of the reflected power is scattered in all directions. This reflected power is sometimes called the specular (coherent) component, and the scattered power is called the diffuse (incoherent) component. If the surface becomes very rough, the specular (coherent) component almost disappears (108), and the diffuse (incoherent) component dominates.

There are two general approaches to rough surface scattering problems: the perturbation technique, and the Kirchhoff approximation. The perturbation technique applies to a surface

which is slightly rough and whose surface slope is generally smaller than unity. The Kirchhoff approximation technique is applicable to a surface whose radius of curvature is much greater than the wavelength.

It is not intended in this study to give detailed mathematical analysis of these two approaches (detailed analysis could be found in 108, 109, 110, and many others).

For the case of a corroded bar in concrete, the Kirchhoff approximation will be used. Beckmann and Spizzichino have shown that, within the Kirchhoff approximation, the scattering may be divided into coherent and incoherent parts. Both parts contain an exponential dependence on the root mean square amplitude of the roughness, h . It has been shown (110) that the coherent scattering dominates at low frequency, up to $kh=0.5$. Therefore, by using the low frequency approximation and backscattering geometry, it can be shown that all scattering from the surface is coherent, in this case:

$$I_{\text{total}}/I_{\text{sound}} = \exp(-(\cos\theta_i + \sin\theta_i)^2 k^2 h^2) = \exp(-4k^2 h^2)$$

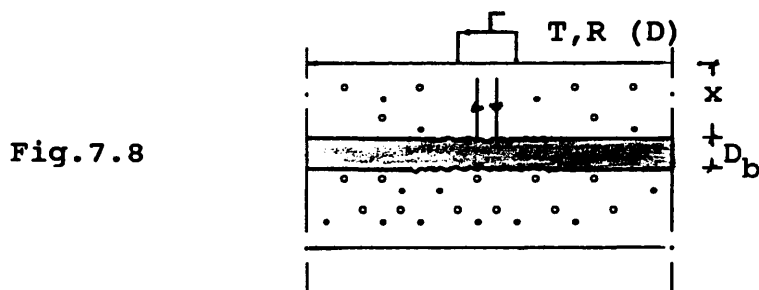
since $(\cos\theta_i + \sin\theta_i)^2 = 4$ for backscattering and normal incidence (bear in mind that a pulse-echo system is used). In this equation I_{sound} is the intensity scattered from a smooth surfaced bar of the same size as the rough surface, and h is the root-mean square roughness.

The low-frequency approximation is valid for:

$$4k^2h^2 \leq 1 \text{ where } k=2\pi/\lambda$$

Since the intensity is proportional to the square of the sound pressure, one obtains:

$$P_{\text{total}}/P_{\text{sound}} = \sqrt{\exp(-4k^2h^2)}$$



Then the total losses equation for a corroded bar at depth (x) from the surface, and (h) roughness is:

$$P_{\text{tot}}/P_0 = R \pi D^2 / 4\lambda \cdot 1/2x \exp(-2\alpha x) \sqrt{f_c / (f_c + x)} \sqrt{\exp(-4k^2h^2)} \quad (7.3)$$

The model is used to calculate signal losses in four different configurations: 200, 300, 400, and 500kHz. The strength of the reflected echo from the corroded bar at depths (x) 60 to 420mm, in 20mm intervals, was calculated. In all cases the transducer diameter was fixed at 30mm, and the diameter of the bar at 10mm. The rms of the height of roughness was taken equal to 1 and 1.6mm.

To check the validation of low-frequency approximation assumed,

we have:

$$f=500\text{kHz}, \lambda=8\text{mm}, \quad h \leq 0.7\text{mm}$$

$$f=400\text{kHz}, \lambda=10\text{mm}, \quad h \leq 0.8\text{mm}$$

$$f=300\text{kHz}, \lambda=13.33\text{mm}, \quad h \leq 1.1\text{mm}$$

$$f=200\text{kHz}, \lambda=20\text{mm}, \quad h \leq 1.6\text{mm}$$

The two chosen values for h are 1 and 1.6mm which are around the above values.

Figs.7.9 and 7.10 show the variation of attenuation against distance of the bar in concrete from surface for the frequencies mentioned earlier, for $h=1$ and 1.6mm respectively.

Fig.7.11 shows the variation of attenuation against frequency (100kHz-500kHz) for a sound bar and a corroded bar (the amplitude of the pitted surface was taken equal to 1.6mm) embedded in concrete.

7.6- DISCUSSION

In the last three sections, equations 7.1, 7.2, and 7.3 were derived to estimate the signal returned from a back-wall echo, sound bar, and from a corroded bar embedded in concrete when transducers are mounted on the surface of the concrete. These equations were used to give an approximate picture of the variation of the losses and pressure against depth, diameter of bar, roughness of the corroded bar, and the frequency of the transducer.

From the theoretical study carried out so far in this chapter, it was established that:

-The echoes reflected from a sound bar and a corroded bar similar in dimensions to the sound bar embedded in concrete at the same position are frequency dependent, i.e. the attenuation for a particular frequency is different for each case, i.e. the attenuation for a corroded bar is greater than that for a sound bar, and the difference is frequency dependent (see fig.7.11).

-As the height of the roughness of the corroded bar encased in concrete increases, the losses increase compared to the smooth bar, due to scattering (see figs.7.9, 7.10, and 7.11).

-As the frequency increases, in general, the attenuation of the received signal increases. This is due to attenuation from scattering and absorption suffered by the signal when it passes in concrete, discussed in chapter 6 (see figs.7.2, 7.4, 7.9)

-As the bar is more deep in concrete, the signal losses strength, due to greater path length hence more attenuation (see fig.7.9).

-As the diameter of the bar embedded in concrete increases, the reflected echo will be stronger (see fig.7.5).

-As the probe diameter increases, the reflected echo strength from a bar increases (see fig.7.6).

7.7- COMPARISON WITH EXPERIMENTS

In the theoretical part of this chapter, a model using pulse-echo system was assumed to estimate the strength of the reflected signal from a bar embedded in concrete. As no commercially available system at present exists for low-frequency pulse-echo testing of reinforced concrete, it was therefore decided to use a pitch-catch system for a bar spanned in a water tank, where the transducers are close enough (1cm) to be considered as pulse-echo. The set-up was two transducers of 125kHz resonant frequency and 25mm diameter, distant 1cm, mounted on a water tank, the water depth was 280mm, the bar was spanned at 100mm from the top. A range of diameters was used to check the validity of the model. The diameters were: 3, 5, 12, 25, 32mm bars. It is worth mentioning that the attenuation loss due to absorption and scattering, i.e. the coefficient α , was neglected (this coefficient is very small in water). A range of diameters was used to check the validity of the model. The diameters were: 3, 5, 12, 25, 32mm bars.

Fig.7.12 shows the results. The solid line shows the result of the model, and the dashed line shows the result of the experiment.

It can be seen from fig.7.12 that the model and the experiment compare favourably, for example, for the 32mm bar the reflected signal will be attenuated by 20.8 dB using the model and by 22.7 dB from the experiment, the difference is 2 dB, which cannot be better. However for the 3mm bar, the loss is 30.8 from the model

and 38.4 from the experiment, gives an 8 dB difference which is still small. The reason that the model gives good result for the 32mm diameter bar is that the diameter of the bar is more than twice the wavelength (in this case was 12mm) because the equation used to calculate the signal reflected from the bar was derived from geometrical optics and this equation should be used where the wavelength is very small compared with the dimensions of the bar, however where this is not applicable i.e. the wavelength is no longer small compared to the bar diameter, the results are more or less rough approximations.

Therefore the general conclusion from this comparison is that the model gives satisfactory results when compared with experiments to predict the strength of the reflected echo from a bar embedded in a medium, be it water or concrete.

7.8- SUMMARY

In this chapter, a theoretical approach and a model analysis have been given for the estimation of signal strength expected from a back-wall, sound bar, and corroded bar embedded in concrete when the transducers are mounted at the surface.

Water experiments were used to check the validity of the model. The comparison showed good agreement with the experiments.

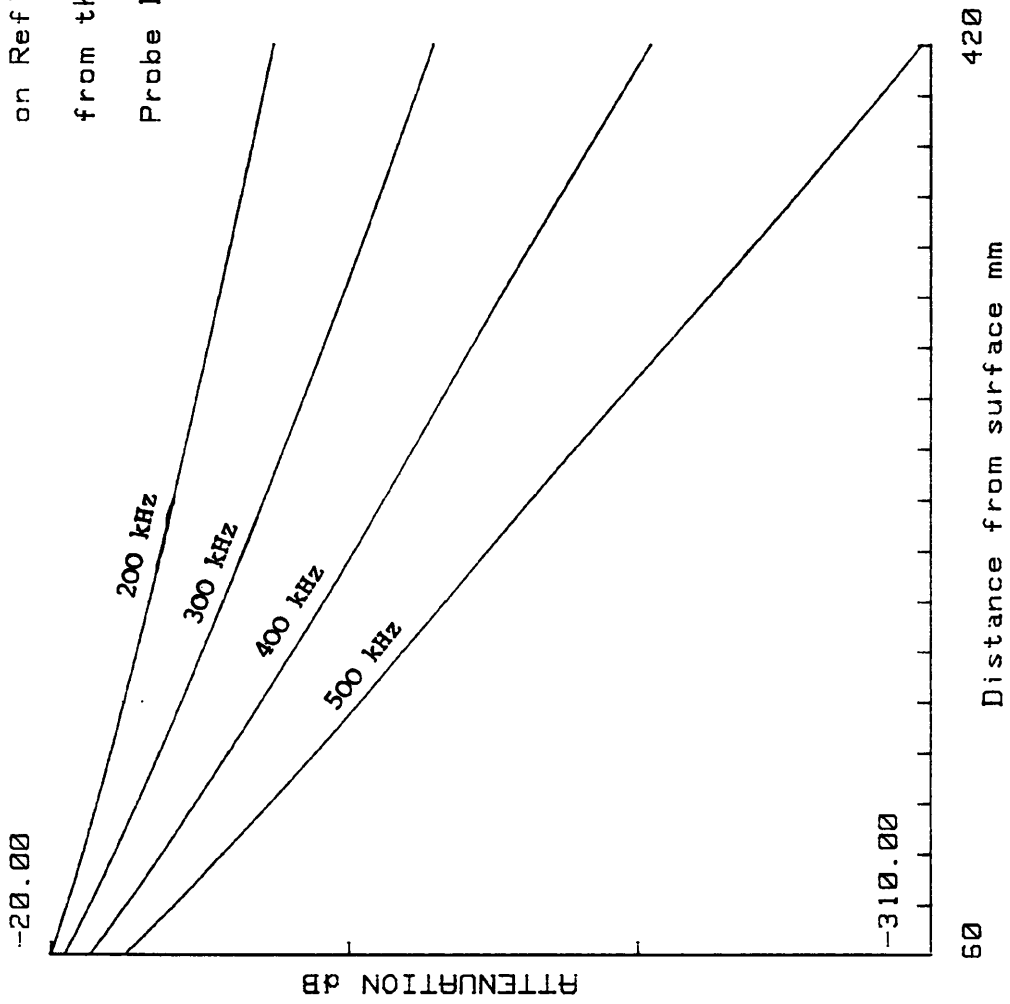
The general conclusion that could be drawn from this study in this chapter that the reflected signals from a sound bar and a corroded one are frequency dependent which means that if a 200kHz

transducer is used the strength of the received signal from a sound bar at that frequency will be different and higher from that of a corroded bar with the same dimensions. It was established too that as the transducer diameter increases, the strength of the received signal will increase for the same set-up, Furthermore, as the diameter of the bar increases, the strength of the received echo will increase. Another point which was established is that as the frequency increases, the signal strength reflected from a bar, sound or corroded, decreases dramatically. And the most important point was that the attenuation for corroded bar was greater than that for a sound bar, but the difference depends on frequency i.e. if we can identify the signal in different frequency bands it should be possible to tell whether the bar is corroded, e.g. see fig.7.11 for sound and corroded bar, the ratio of attenuation at 400kHz to that at 100kHz equal to 1.256.

Following the above argument, i.e. that it is possible to identify sound steel components from corroded steel components embedded in concrete by comparing their frequency spectra, a filter should be applied on the signal to remove bands of frequencies and leave the parts where it is easier to recognize the corroded components.

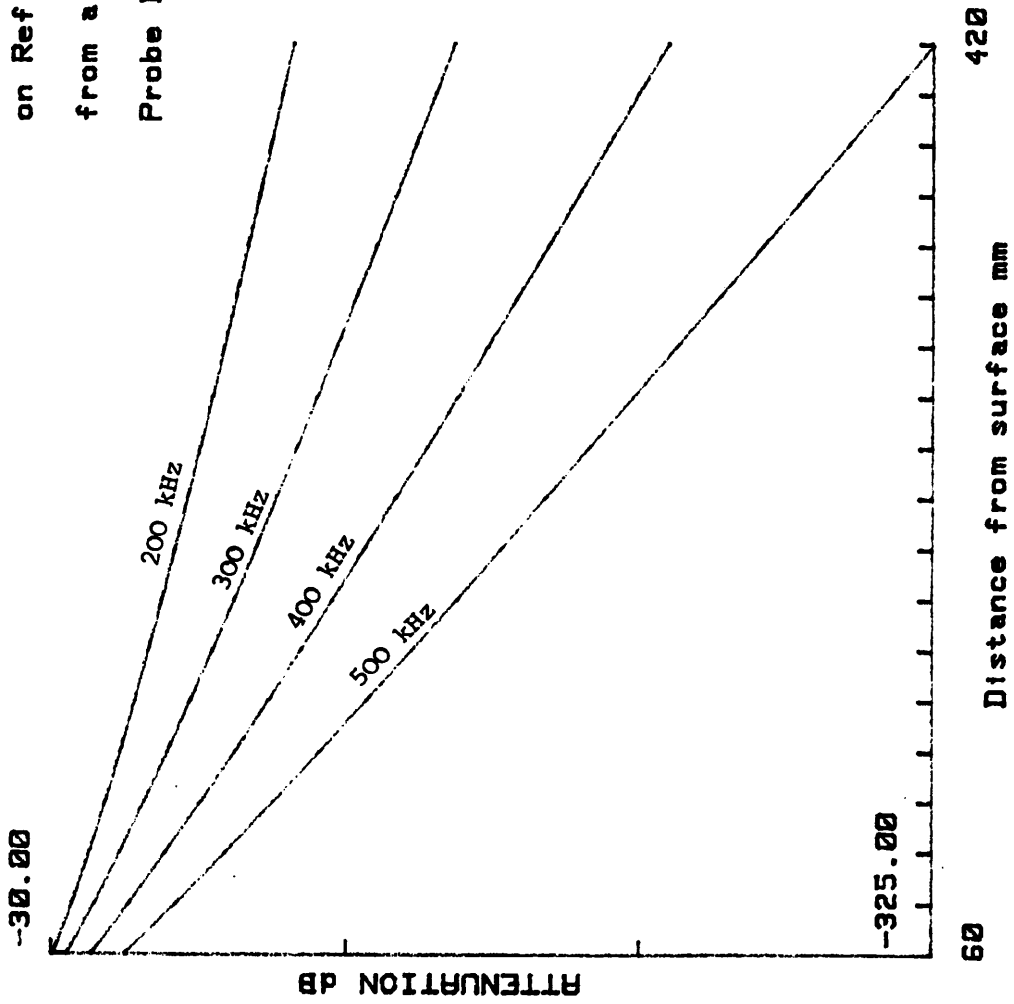
Model Analysis: Effect of Depth
on Reflected Signal strength
from the Base of a Conc. Beam
Probe Diam=30mm

Fig.7.2



Model Analysis: Effect of Depth
on Reflected Signal strength
from a Sound Bar in Conc.
Probe Diam=30mm, Bar Diam=10mm

Fig.7.4



Model Analysis: Effect of the Dia. of the Bar on the Reflected Signal Strength from a Sound Bar in Conc. for a Range of

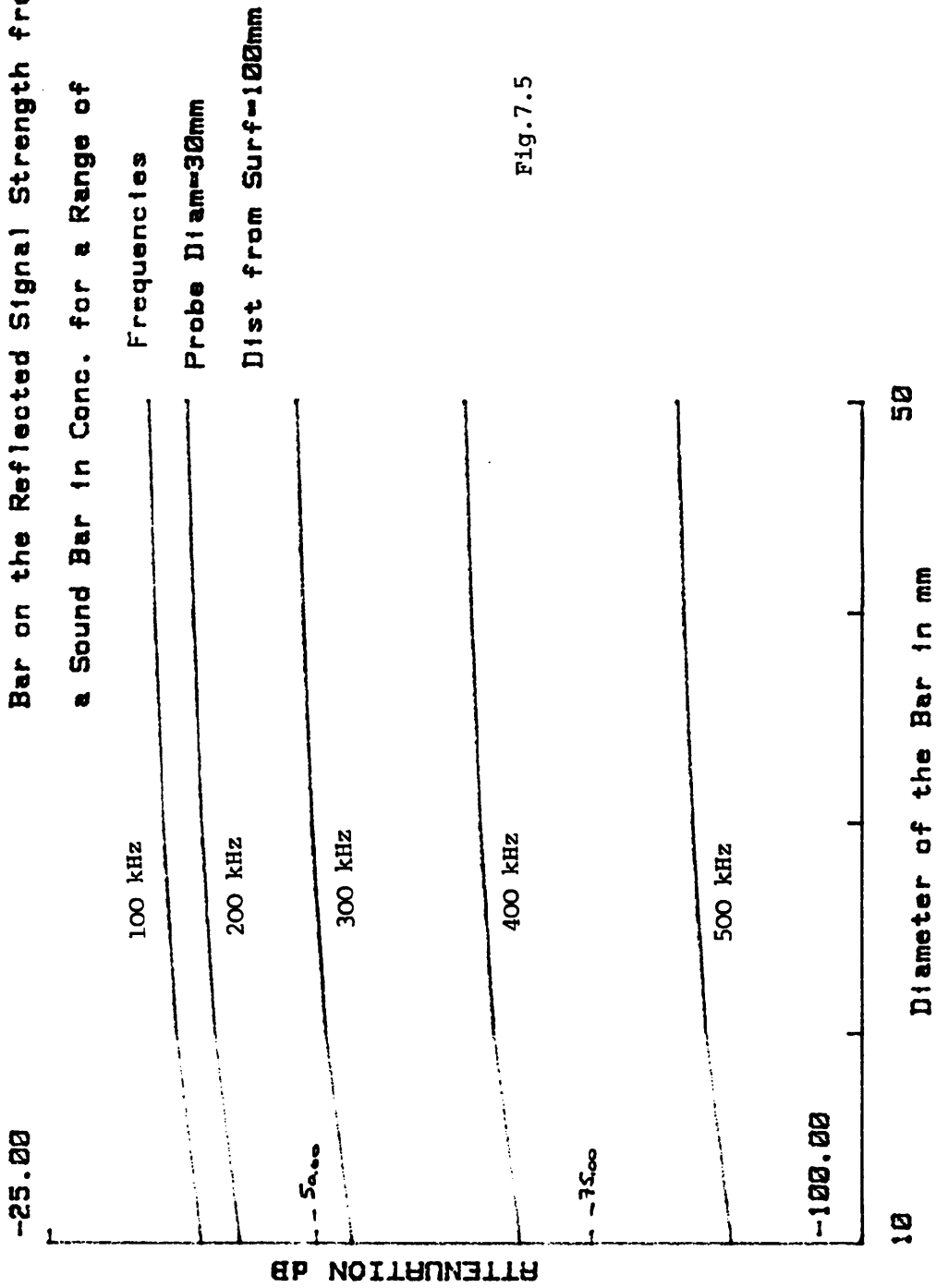


Fig.7.5

Model Analysis: Effect of the Dia. of the Probe on the Reflected Signal Strength from a Sound Bar in Conc. for a Range of Frequencies
 Bar Diam=10mm
 Dist from Surf=100mm

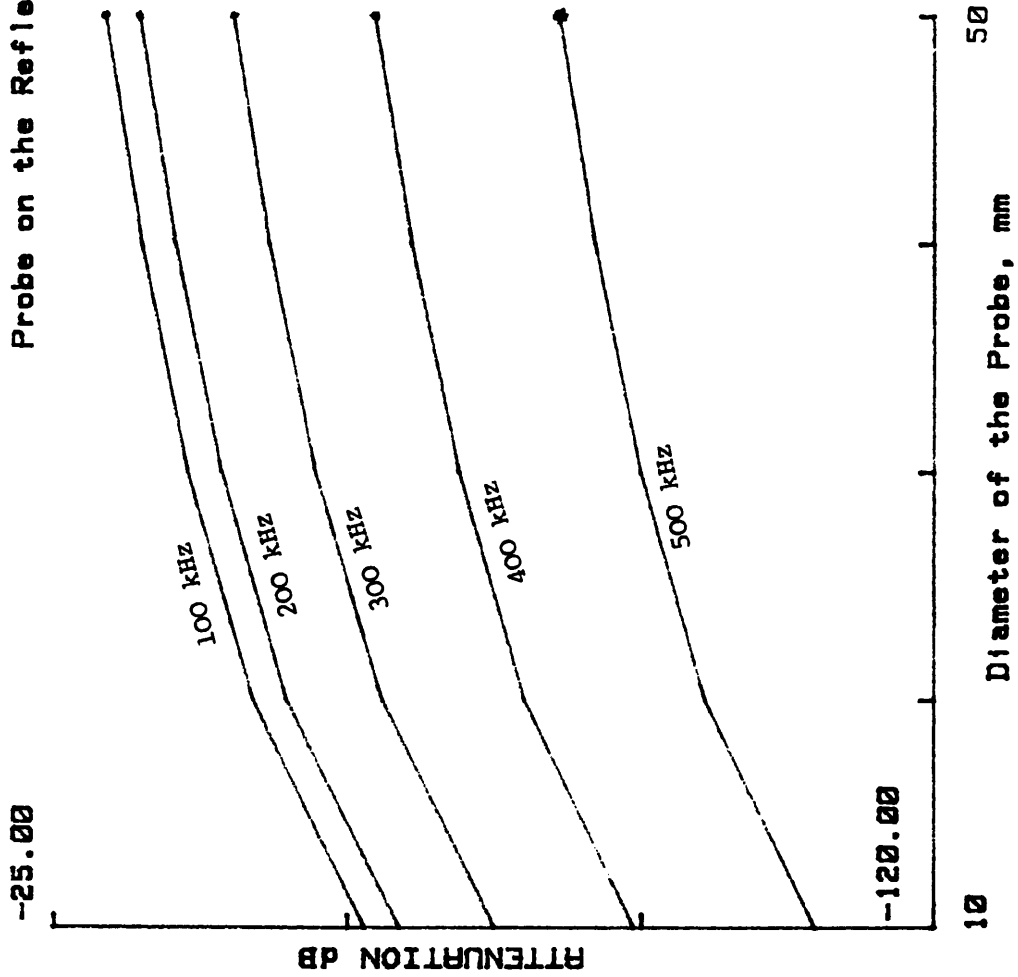


Fig.7.6

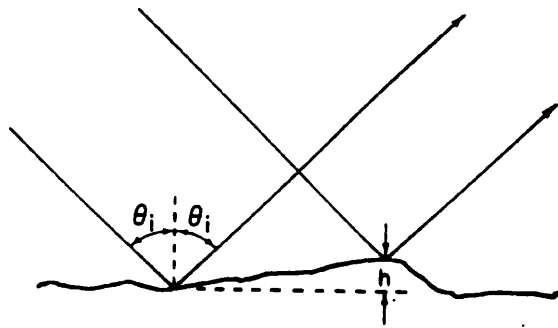
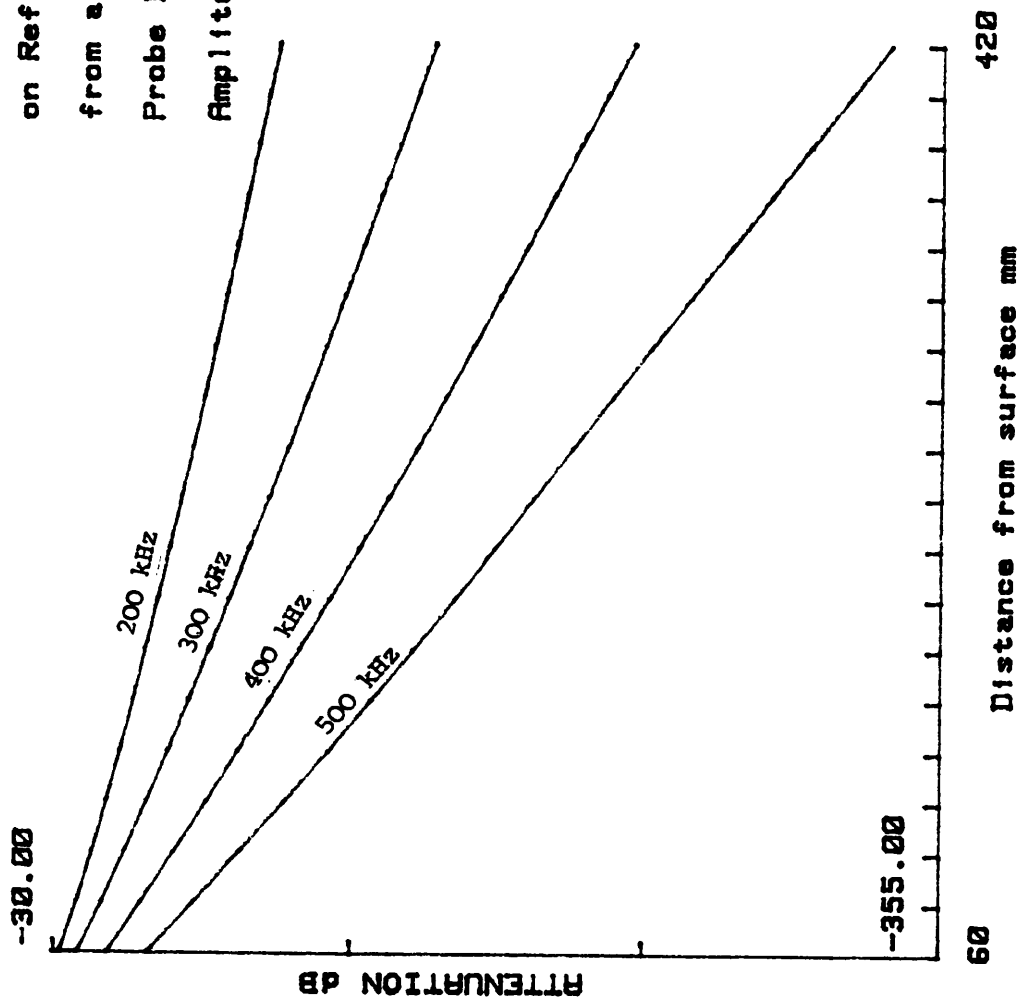


Fig.7.7- Incident wave on a rough surface.

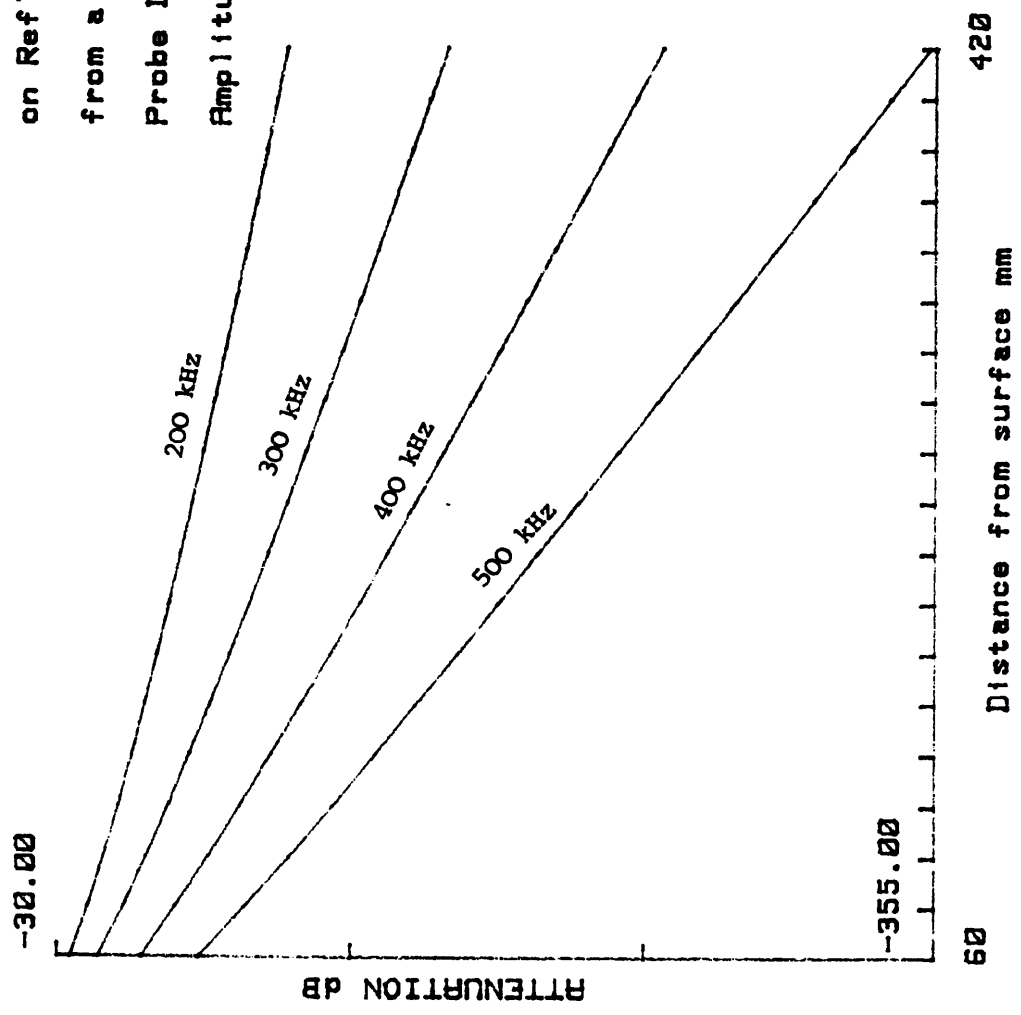
Model Analysis: Effect of Depth
on Reflected Signal strength
from a Corr. Bar in Conc.
Probe Diam=30mm, Bar Diam=10mm
Amplitude of Pitted Surf=1.0mm

Fig.7.9



Model Analysis: Effect of Depth
on Reflected Signal strength
from a Corr. Bar in Conc.
Probe Diam=30mm, Bar Diam=10mm
Amplitude of Pitted Surf=1.6mm

Fig.7.10



Model Analysis: Effect of Frequency on

the Reflected Signal strength

from a Sound & Corr. Bar

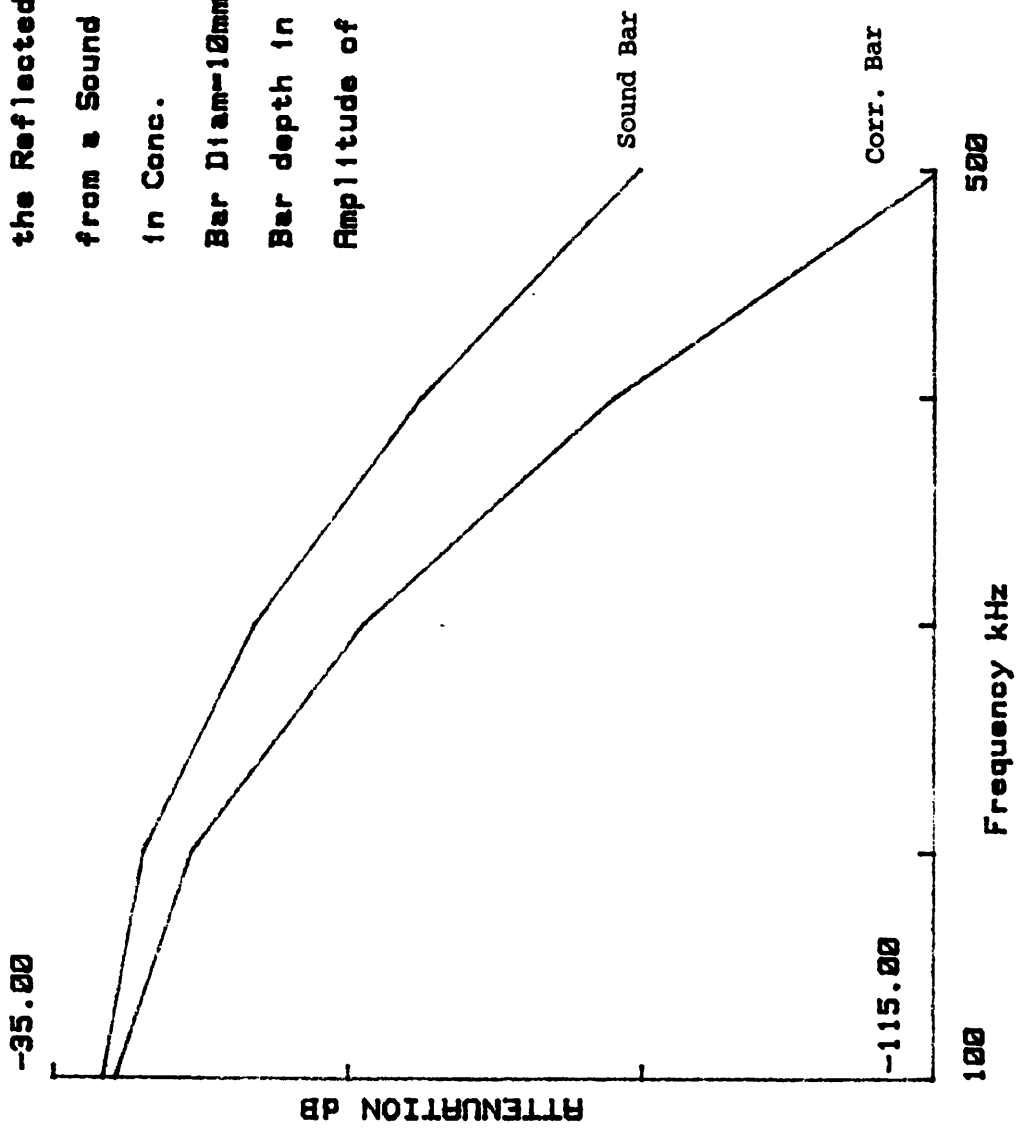
in Conc.

Bar Diam=10mm, Probe Diam=30mm

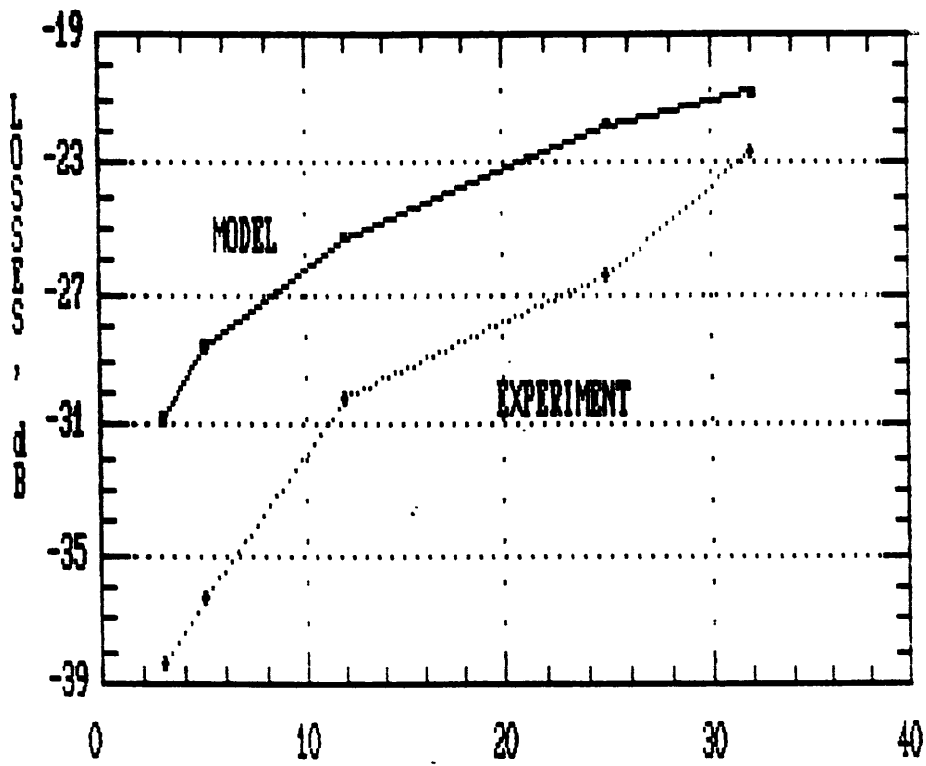
Bar depth in Conc=100mm

Amplitude of Pitted Surf=1.6mm

Fig.7.11



COMPARISON OF THE MODEL WITH EXPERIMENT
FOR A BAR SPANNED IN WATER



DIAMETER, mm.
BAR DEPTH=100mm, PROBE FREQ=125kHz, PROBE DIAMETER=25mm.

Fig. 7.12

CHAPTER 8COMPUTER MODEL USING RAY ACOUSTICS8.1- INTRODUCTION

Over the past twenty years there has been a revolution in both the range and the availability of computers, both in research and industry. This change has enabled the construction of models of the phenomena upon which NDT techniques are based (115).

The development of computer models for the study of these phenomena has to a large extent been achieved by the application of methods which received their development in other fields of study such as geophysics and seismology, where both acoustic and elastic waves and their interaction with structures were investigated (116).

What is computer modelling? Computer modelling provides representations of systems, in a mathematical form, which should respond in such a way as to provide the variation of parameters, in response to change which is observed in the corresponding physical system (115).

In this chapter a current review of computer-based numerical modelling is given and the model developed, which predicts the variations in detected echo amplitude as the probes (used in a pitch-catch mode) scan over a water tank or a concrete beam containing steel components with and without defects. The model

allows the building in of an attenuation coefficient (the ratio of the current energy of the received signal to its initial value) dependent on the material through which the rays pass, and this was used to compare the results with the experiments.

8.2- REVIEW OF SOME OF THE METHODS USED IN COMPUTER MODELLING OF ULTRASONIC WAVES IN SOLIDS

Bond (115) reviewed this matter particularly in relation to problems involving pulsed elastic wave systems for ultrasonic wave propagation and scattering. He described three main methods of modelling, namely, usage of finite-difference methods to solve equations of motion described by differential equations, the application of finite element methods in NDT, and the use of ray tracing which is a widely used form of analysis and has been applied in the present study. In addition Bond gave a review of other methods such as mass-particle models and transducer wavefields.

Vary (117) used computer synthesis to simulate thin couplant and bond-layer effects associated with broad-band ultrasonic transducers. It was shown that these thin layers in the acoustic path can produce distortions in ultrasonic signals and that these distortions become apparent and serious in the frequency regime.

In a recent book 'Mathematical Modelling in NDT', edited by Blackmore and Georgiou (116), several papers can be found about mathematical models and how to validate a model. The following is a summary of some of the papers given in this book.

Coffey in this book illustrates the features of a system model of an ultrasonic examination which should contain a quantitative description of the probe, the radiated pulse and beam, the scanning of the probe, the component's geometry, the attenuation of the material, scattering off the defect and reception of the signals. The aim of such a model is to predict the amplitude and pulse shape of signals detected in a scan over the component.

In the same book, Firth explains the role of mathematical modelling in validation i.e. the model must be checked, verified, and should be appropriate to the geometry, the flaw, and the probe being used.

Bond et al applied the finite-difference modelling to the scattering phenomena. Willis on the other hand, reviewed the approaches used in scattering from rough surfaces i.e. perturbation and Kirchoff's approximation methods. Chapman describes a model of ultrasonic NDT which predicts the variations in detected echo amplitude as a probe or probes scan over a metal component containing a single smooth planar crack, his model simulates the geometry of the component, the scanning pattern of the probes, the transmitted probe beam, the scattering of the transmitted probe beam by the defect, and the detection of the scattered ultrasound by the receiving probe. Finally Silk et al modelled an ultrasonic transducer in order to understand transducer operation and properties and secondly to provide a means of optimising transducer design to a particular inspection task.

8.3- APPLICATION OF THE RAY THEORY

A program was written during a previous study (42) by the author to show the path of rays in a wire embedded in an infinite solid body (in this case concrete), when a transducer is applied at one end as a transmitter and as a receiver at the other. Following this, a second program was written to evaluate the response of such a model when a pulse is transmitted and received using the transit-time technique (42). The severe attenuation of the signal for wires embedded in concrete precluded practical use of this arrangement over lengths up to 3m.

In the present research, the approach that was adopted in testing for broken or corroded wires or strands embedded in concrete, involved the mounting of transducers on the surface of the concrete directly above the steel components using the pitch-catch method. It was therefore decided to model this system using the ray method.

A computer program was written using Fortran to predict the amplitude of the received signal for the mentioned configuration using the transit-time method. Furthermore, the program was written to cover cases of a bar embedded in concrete or immersed in water. For these cases the modifications were the coefficients of reflections, the velocities, and the attenuation coefficient. The model was developed on the main frame at the University of Manchester.

In this model, an attempt was made to represent in one package or program most of the variables present. The model contains a quantitative description of:

1- The probe: The crystal of the probe was assumed to be circular, as all the transducers used in the experiments had circular piezoelements. The diameter and the frequency of the probe were included as input data i.e. they can be changed each run. The transmitter and the receiver probes were assumed to have the same properties i.e. diameter and frequency.

2- The radiated pulse: The input signal was assumed to be a sine of four cycles with constant amplitude or exponentially decayed, although this could be changed easily. In real life, the shape of the input signal is usually unknown especially if low-frequency undamped transducers are used (similar to many of the transducers used in this study) and having a long decay duration (about 400 μ sec). It was therefore difficult to compute the shape of this pulse and the sine wave was used as a basic component which could if necessary be combined by Fourier analysis to give other input waveforms.

3- The distance between transmitter and receiver on the surface of the material tested was included as input data.

4- The component's geometry: The model operated using a beam of rectangular cross-section. The dimensions of the cross-section could be input or fixed for each run.

5- The position of the transducer relative to the centre of the cross-section: The centres of the transmitter and the receiver were assumed to have equal edge distances i.e. the standard case used in the experiment.

6- Bar dimension and its position: The model is built for one bar running parallel and in line with the transmitter and the receiver. The position and the diameter are input by the user (the position of the bar from the top surface). It should be noted that the model is for bars of circular cross-section and does not directly represent the geometry of strands.

7- Corroded or cracked bar: After the user input the position, the program asked if the bar was sound, corroded, or cracked. The position of the cracked or the corroded part was assumed to be in the middle between the transmitter and the receiver. If it was corroded the input data in this case was the height of the roughness of the corroded bar (this was tackled as described in chapter 7). However, if it was cracked the bar was assumed to be fully cracked i.e. no continuity, and the input data in this case was the width of this discontinuity or crack.

8- The attenuation in the material: The attenuation due to scattering and absorption suffered by a signal when passing through concrete was included as a coefficient. This coefficient was derived from experimental results and it is frequency dependent (it was described in chapter 6).

9- The velocities and densities: The velocities of longitudinal

and shear waves for steel, concrete, or water (longitudinal wave only) could be changed easily as these were included as input data. Moreover to calculate the coefficients of reflections (see chapter 3) the equations require the densities of the two media i.e. concrete/steel or water/steel, which are included as variables.

10- Sensitivity (y-axis) of the received signal: This could be changed easily depending on the strength of the amplitude of the received signal.

11- Output of the program: The program could be used to scan over a beam 'model' where sound, cracked and corroded bar was present. The output of the program was the amplitude and pulse shape of the received signal i.e. time-domain signal. Moreover, a plot of the cross-section of the beam showing the transmitter and bar position was given.

The assumptions made during the building of the computer model were:

1- Ultrasonic probe: No piezoelectric properties or crystal dimensions are included.

2- It was assumed that the probe does not transmit Rayleigh or transverse waves although this is not true for low-frequency small radiators. This was established from experiments for these kind of transducers.

3- The component's surface geometry was assumed to be smooth, although this is not the case for concrete.

4- No losses due to electrical coupling to the flaw detector or oscilloscope (long cables from receiver to oscilloscope may in practice to attenuate the signal).

5- The medium, in this case concrete which is heterogeneous, where the signal is propagating was assumed to be homogeneous i.e. no scattering due to aggregates or porous (voids) medium. As mentioned earlier this attenuation effect due to scattering and absorption was included as a coefficient.

6- It was assumed that a perfect bond was present between the surface of the sound bar and the surrounding concrete. However when a corroded bar was present, the contribution of this defect was included as a coefficient loss, although this was not the case as scattering occurs. Moreover when a cracked bar was present it was assumed that the bar was fully cracked.

7- Mode-conversion was not modelled, only the coefficient of reflection of longitudinal wave was considered (when a longitudinal wave is incident on an interface concrete/steel longitudinal and transverse waves are reflected in addition to refracted longitudinal and transverse waves). Only longitudinal waves are traced which are important to our case and arrive earlier than shear waves. Shear and Rayleigh (surface) waves were not considered.

8- The coupling between transducer-concrete surface was assumed to be perfect i.e. no distortions by couplant thickness caused by acoustic impedance effects.

8.4- RAY ACOUSTICS

As an alternative to the considerations of the equations of motion, waves can be considered in terms of wavefronts and rays. In this case, rules similar to those for geometrical optics are followed.

The reflection of plane compressional waves at the free surface of a homogeneous and isotropic material is the simplest problem. Assume that the free boundary of such a medium is a plane, then for an incident longitudinal wave, in general, a reflected longitudinal and shear waves are generated. This conversion of energy between various wave types by interfaces, defects, and other targets is called mode-conversion. However when a longitudinal wave is incident at an interface between two solid media, longitudinal and shear waves will be produced in both. For this system four boundary conditions should be satisfied and these are the requirements for the continuity of two components of both displacement and stress across the interface i.e. normal and shearing stresses, and displacements in the x- and y- directions (refer to chapter 3 for the equations involved which enable the calculations of the resulting wavefield amplitudes for the two cases i.e. free boundary and interface between two solids).

8.5- GOVERNING EQUATIONS

A series of configurations, each involving the transmission of a signal and receiving it using the transit time method or pitch-catch technique, was modelled in order to predict the variations in detected echo amplitude for the following cases: a) water, b) concrete beam, c) water containing steel bar, d) reinforced concrete beam, e) corroded reinforcement in concrete beam, f) cracked reinforcement in concrete beam.

The output composite waveform is synthesized by array addition of corresponding time-domain elements, and the result is exhibited graphically, this will be explained in the next section.

In this section, simple forms of the equations involved in the system are given.

When a wave travels through a medium the sound pressure will decrease due to:

a- Polar-Pressure relationship:

It is taken in the model as:

$$P_{\theta}/P_0 = \sin(\pi D \sin \theta / \lambda) / (\pi D \sin \theta / \lambda) \quad (8.1)$$

where

θ is the angle with the vertical axis

D is the diameter of the probe, λ is the wavelength

P_0 is the initial pressure, and P_{θ} is the directional pressure.

b- Distance-Pressure relationship

It is expressed in the program as:

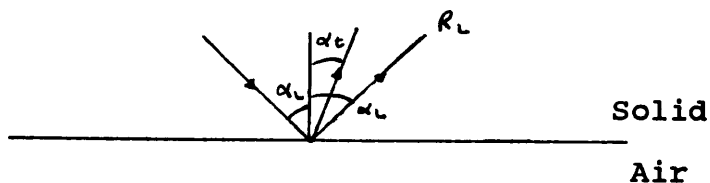
$$P_x = \sin[\pi/\lambda (\sqrt{D^2/4+x^2} - x)] \quad (8.2)$$

where x is the distance from transducer to the point where the pressure is calculated.

c- Coefficients of Reflection:

As it was mentioned the longitudinal waves are only traced although it is assumed that mode-conversion occurs (concrete medium case).

For the concrete-air interface the coefficient of reflection is (67):



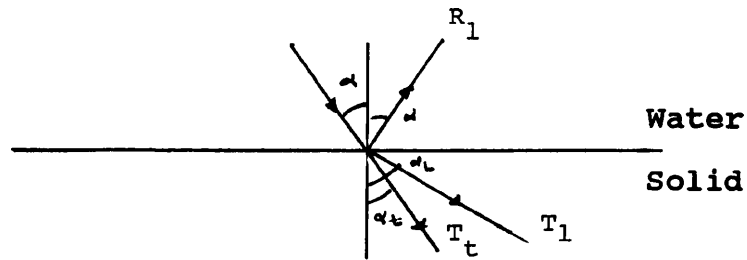
$$R_1 = \frac{(c_t/c_1)^2 \sin 2\alpha_1 \sin 2\alpha_t - \cos^2 2\alpha_t}{(c_t/c_1)^2 \sin 2\alpha_1 \sin 2\alpha_t + \cos^2 2\alpha_t}$$

Where c_1 and c_t are velocities of longitudinal and shear waves respectively

α_1 and α_t are longitudinal and shear angles after reflection respectively and are related by: $c_1/c_t = \sin \alpha_1 / \sin \alpha_t$

For the case water-air interface total reflection was assumed i.e. $R_1=1$.

For the case of water-solid, in this case water-steel interface, no reflected shear wave occurs because water does not support shear forces, the equations used were (67):



$$R_1 = 1/N [(c_t/c_1)^2 \sin 2\alpha_1 \sin 2\alpha_t + \cos^2 2\alpha_t - Z_w \cos \alpha_1 / (Z_s \cos \alpha)]$$

$$T_1 = 1/N [2 \cos 2\alpha_t]$$

$$T_t = 1/N [-2(c_t/c_1)^2 \sin 2\alpha_t]$$

where $N = (c_t/c_1)^2 \sin 2\alpha_1 \sin 2\alpha_t + \cos^2 2\alpha_t + Z_w \cos \alpha_1 / (Z_s \cos \alpha)$

and where

$Z_w = \rho_w c$ and $Z_s = \rho_s c_1$ are the acoustic impedances in

water and steel respectively, where ρ_w and ρ_s are the densities of water and steel respectively,

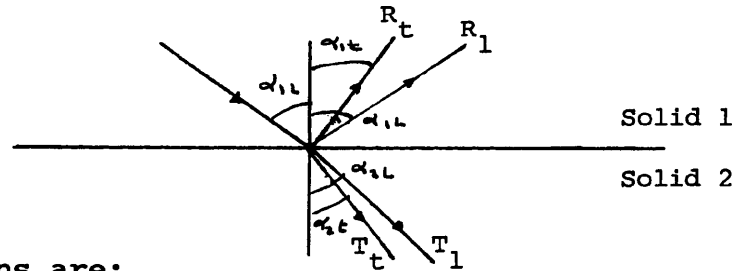
c_1 and c_t are the longitudinal and shear velocities in steel respectively, and c is the longitudinal velocity in water,

α_1 and α_t are the angles of longitudinal and shear waves in

steel respectively, and α is the longitudinal angle in

water, and related by $c_1 / \sin \alpha_1 = c_t / \sin \alpha_t = c / \sin \alpha$.

For the case of concrete/steel interface four equations should be solved to get this coefficient (a routine was written to solve the equations in the computer program).



The four equations are:

$$R_l \cos \alpha_{1l} - R_t \sin \alpha_{1t} + T_l \cos \alpha_{2l} + T_t \sin \alpha_{2t} = \cos \alpha_{1l}$$

$$R_l \sin \alpha_{1l} + R_t \cos \alpha_{1t} - T_l \sin \alpha_{2l} + T_t \cos \alpha_{2t} = -\sin \alpha_{1l}$$

$$R_l Z_{1l} \cos 2\alpha_{1t} - R_t Z_{1t} \sin 2\alpha_{1t} - T_l Z_{2l} \cos 2\alpha_{2l} - T_t Z_{2t} \sin 2\alpha_{2t} = -Z_{1l} \cos 2\alpha_{1l}$$

$$R_l Z_{1t} c_{1t} \sin 2\alpha_{1l} / c_{1l} + R_t Z_{1t} \cos 2\alpha_{1t} + T_l Z_{2t} c_{2t} \sin 2\alpha_{2l} / c_{2l} - T_t Z_{2t} \cos 2\alpha_{2t} = Z_{1t} c_{1t} \sin 2\alpha_{1l} / c_{1l}$$

Indices 1 and 2 refer to media 1 and 2 respectively, for example if a longitudinal wave is passing through concrete and later strikes a steel boundary in this case indice 1 will refer to concrete and 2 to steel.

Where R_l and R_t are the coefficient of reflections for longitudinal and shear waves respectively

T_l and T_t are the coefficient of refraction for longitudinal and shear waves respectively

$Z_l = \rho c_l$ is the acoustic impedance of longitudinal wave

$Z_t = \rho c_t$ is the acoustic impedance of shear wave

The reflected and refracted angles are related by:

$$c_{1l} / \sin \alpha_{1l} = c_{2l} / \sin \alpha_{2l} = c_{1t} / \sin \alpha_{1t} = c_{2t} / \sin \alpha_{2t}$$

d- Loss due to Corrosion

As mentioned the loss of reflected signal due to corrosion was taken as a coefficient applied to that part of the ray group incident on the bar. It was assumed that the surface of the bar had a roughness height h and the signal is scattered due to this roughness. The following equation was given and discussed in chapter 7:

$$P_c = \sqrt{\exp(-4k^2 h^2)} \quad \text{where } k=2\pi/\lambda \quad (8.3)$$

e- Attenuation Coefficient

For the concrete model, the attenuation coefficient which includes the losses from absorption and scattering was assumed to be (equation derived from experiments and included in chapter 6):

$$\alpha = 0.1844f + 0.001f^2 \quad (\text{dB/m}), \quad f \text{ is the frequency in kHz} \quad (8.4)$$

For the case of the water model the attenuation was not considered i.e. negligible which is approximately the case in practice.

8.6- APPROACH

The parameters examined using the model were as follows:

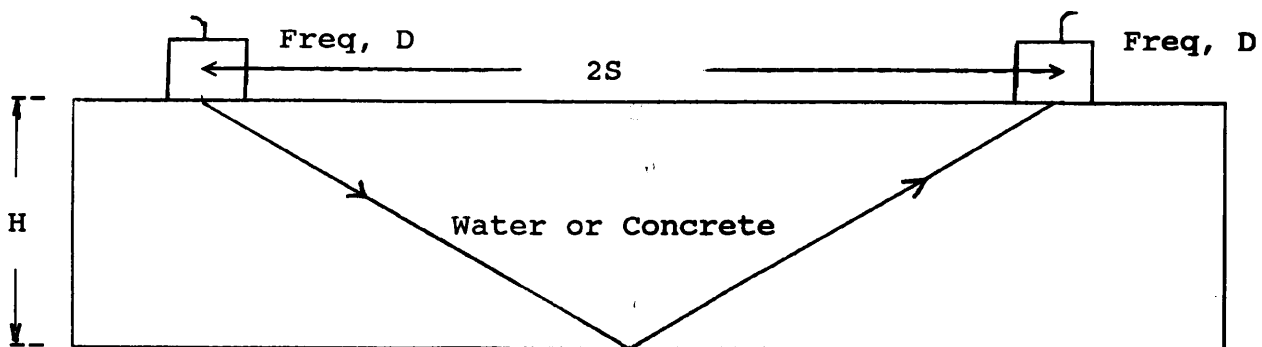
1- Transducer frequency and the spacing between radiator and receiver.

2-Bar size, depth, and condition i.e. sound, corroded or cracked.

In the following, it will be shown how the echo amplitude is derived from the back-wall and the bar.

8.6.1- Estimation of the Amplitude of the Back-Wall Echo

The transducers-specimen configuration illustrated in fig.8.1 is taken as a model for the case of no reinforcement.



2S= Spacing between the centres of the transmitter and the receiver
 H= Depth of the specimen
 Freq, D= the frequency and the diameter of the probes respectively

Fig.8.1

In this case the echo will be similar to a flat backwall of a test object. In this case the sound is reflected straight back at an angle equal to the incidence (if we take a centre ray to represent the path length, see fig.8.1) and the radiator acting as receiver measures the sound pressure obviously at distance L, and therefore can be written as:

$$P/P_0 = R P_{\theta} P_L \exp(-\alpha L)$$

where R is the coefficient of reflection of longitudinal wave for water/air or concrete/air

θ is the angle of incidence on the interface = $\tan^{-1}(S/H)$

L is the path length = $2(\sqrt{H^2+S^2})$

α is the attenuation coefficient

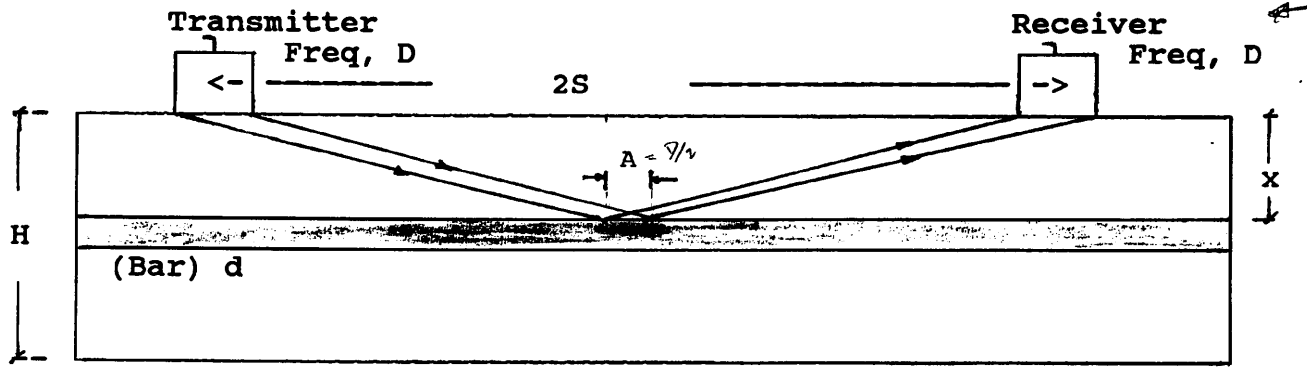
P_0 is the initial pressure

P_L is the axial pressure

P_θ is the pressure losses due to divergence

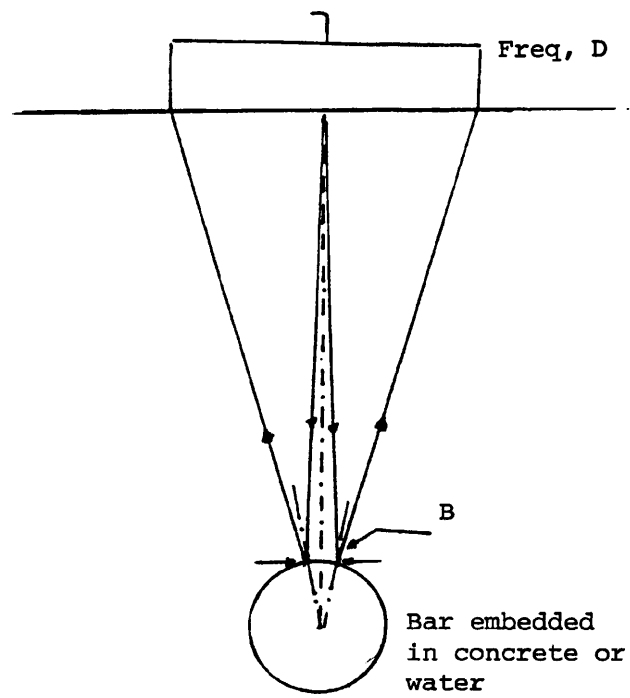
8.6.2- Estimation of the Amplitude of the Bar Echo

In this case it is not possible to derive directly the echo amplitude reflected from the bar embedded in a material, in this case water or concrete, because the bar cross-section is much smaller than that of the sound beam (in contrast to a back-wall echo). The problem is to find the area which contributes to the strength of the echo reflected when a cone of rays strikes the surface of the bar. We believe that this area is an ellipse which will be demonstrated next, and the minor and major distances will be found.



x= the depth of the bar in the specimen, d= the diameter of the bar

(a)



(b)

Fig.8.2

We will take two sections. The first is a section through the bar (fig.8.2.a), where we assume two rays, each one gets to the receiver at one of its edges, form a straight line, and this line will be the major distance and will be equal to $A = D/2$ when reflected from the surface of the bar. Now if we take the second section which is perpendicular to the bar and through the cross-section (fig.8.2.b), we are looking to the two rays which are reflected to the edges of the receiver, and hence the minor distance which is denoted by B (fig.8.2.b) could be derived, and this was calculated by numerical analysis in the program which is dependent on the the depth of the bar, the bar diameter, the transducer diameter.

Therefore the area of the ellipse , the reflected area, can be written as:

$$A_r = \pi AB/4$$

The pressure measured by the receiver will be:

$P/P_0 = R P_\theta P_L P_C \exp(-\alpha L) A_r/A_t$ for $A_r/A_t < 1$, i.e. not bigger than a back-wall echo.

where R is the coefficient of reflection of longitudinal wave for water/steel or concrete/steel

θ is the angle of incidence on the interface = $\tan^{-1}(S/x)$

L is the path length = $2(\sqrt{x^2+S^2})$, α is the attenuation coefficient

P_0 is the initial pressure, P_L is the axial pressure

P_θ is the pressure losses due to divergence

P_C is the pressure losses due to corrosion if present

A_r is the area of the ellipse, and A_t is the area of the transducer

It should be noted that the refracted signal at the interface concrete/bar when the longitudinal wave was incident on the bar was neglected because it was found to be very small.

8.6.3- The Construction of the Time Signal

The input waveform was assumed to be a sine wave of 4 cycles normalized to 1 and is used as a source signal.

From the two sections above, we have two signals one coming from the bar and the other from the base. For each the predicted amplitude is multiplied by the starting signal to give the waveform expected.

The signal from the bar precedes the echo from the base by a time difference depending on the path length. The composite signal therefore is formed by plotting a time-domain amplitude (time viz amplitude) for the two waveforms each displaced by a delay time.

8.7- RESULTS

The results presented are restricted to a few experiments which were carried out on the same geometry of specimens used in the experimental work to illustrate the effect of the frequency on the condition of the bar of different diameters. As mentioned the difference between the model and the experiments will be carried out by comparing the attenuation coefficients calculated from the two outputs. It will be shown that good agreement

exists between the model and the experiments carried out.

8.7.1- Material with No Embedded/ Immersed Steel Bars

The two media modelled were: concrete and water. The output of the program in general will be shown, and then comparison with experimental results will be examined.

a- Water Model

As mentioned earlier, the attenuation due to absorption which is frequency dependent was neglected, and it was assumed that total reflection at the boundary (water/air) occurred. The losses are therefore very small, and are mainly due to divergence.

The configurations used in the experimental work were:

Frequencies used: 125 kHz with 25mm diameter transducers.

Transducer spacings: 10, 50, 100, 200mm.

Water depth: 280mm.

The same configuration were used in the model. Fig.8.3 shows the output of the program for a transducer spacing of 50mm and frequency 125kHz.

To compare the two results i.e. the model and the experiments, a plot (fig.8.4) of the attenuation against transducer spacings was derived ^{at} the frequency used. The result shows the output of the program to underpredict experimental results but the model shows

the correct trend.

b- Concrete Beam Model

In this case, attenuation due to scattering and absorption which are frequency dependent was included using the equation (8.4). In addition the losses due to reflection at the boundary concrete/air were taken into account. In this section it will be shown that the attenuation of the signal increases with frequency, and spacing between transmitter and receiver.

The configurations used in the model were:

Frequencies used: 150, 300, 500 kHz, all with 25 mm diam. transducer
spacing: 10, 50, 100, 200mm.

Concrete depth: 150mm.

The configurations used in the experiments were:

Frequencies used: 150 kHz with 25mm diameter transducer.

spacing: 10, 50, 100, 200mm.

Concrete depth: 150mm.

Fig.8.5 shows the output of the ray tracing model program for transducer spacing of 50mm and frequency 150kHz.

Again to compare the two results i.e. the model and the experiments, a plot of the attenuation against transducer spacings will be used for the different frequencies used is shown

at fig.8.6. Part of the reason for differences could be due to the assumed attenuation coefficient (due to scattering and absorption), and due to the interference of Rayleigh wave neglected in the model but present in the experiments, however the result is not far from the experimental result with the approximation assumed. Moreover, fig.8.7 shows the attenuation of the reflected signal from the base for different frequencies. It can be seen that as the frequency increases the attenuation increases, and increases further with transducer spacing.

8.7.2- Beam with Reinforcement

The configurations modelled were:

- Sound bar immersed in water.
- Sound bar embedded in concrete.
- Corroded bar embedded in concrete.
- Cracked bar embedded in concrete.

However because the scattering due to aggregates and the Rayleigh (surface) wave were not modelled, the comparison with experiment has not been carried out because it was not possible to separate out the echo reflected from the bar which was convolved with the Rayleigh wave and with reflections from aggregates (because of the difference of acoustic impedances at the interface aggregates/mortar). For this reason additional signal processing techniques were developed for the experimental research, however the model is still a great benefit for the present study because it will illustrate how the expected strength of the part of the

signal reflected from a bar embedded in concrete changes with frequency and surface condition i.e. corrosion.

a- Sound Bar Immersed in Water

The configurations used in the experimental work were: ,

Frequencies used: 125 kHz with 25mm diameter transducer.

Transducer spacings: 10, 50, 100mm.

Water depth: 280mm.

Bar diameter: 3, 5, 12, 25, 32mm.

Bar depth: 100, 200mm.

The same configurations were used in the experiments.

Fig.8.8.a shows the model output for 10mm transducer spacing with 125kHz frequency with a bar of 5mm diameter and 100mm deep in water and fig.8.8.b shows the output of 12mm diameter bar with the other variables fixed as fig.8.8.a. It can be seen very clearly that the echo strength from the bar increases with bar diameter.

Fig.8.9.a to 8.9.d show the attenuation against spacing of transducers, from the experiments and the model for the bars used. It can be seen that agreement between experiment and model is reasonable for close spacing, but diverges with increased spacing for all bar sizes. This is probably due to simplifying assumptions in the model about pressure distribution of the beam or effect of reflected area.

Fig.8.10 shows the attenuation against diameter of the bar. This result again shows the output of the program to over predict experimental results but the model shows the correct trends.

Fig.8.11 shows predicted effects of the model against bar depth for two bar depths.

The general conclusions are:

- 1- As the bar size increases, the echo reflected is stronger.
- 2- As the spacing between transducers increases, the echo reflected is weaker.
- 3- As the bar is placed deeper in water, the echo reflected becomes weaker.

b- Sound Bar Embedded in Concrete

As mentioned before results will be restricted to the computer model.

The configurations used in the model were:

Frequencies used: 150, 300, 500 kHz, with 25mm diam. transducers.

spacing: 10, 50, 100, 200mm.

Concrete depth: 150mm.

Bar diameter: 3, 5, 12, 25, 32mm.

Bar depth: 70, 90mm.

Fig.8.12.a shows the model output for 100mm transducers spacing

with 150kHz frequency with a bar of 5mm diameter and 70mm deep in concrete, Fig.8.12.b shows the output with the same variables but with 300kHz frequency, and fig.8.12.c with 500kHz frequency. It can be seen very clearly that the echo strength from the bar and from the base decrease with frequency significantly.

Fig.8.13 shows the variation of the attenuation against the spacings of the transducers for the different frequencies used.

Fig.8.14 shows the attenuation against spacing of the transducers for the different bars used for 150 (fig.8.14.a) and 300kHz (fig.8.14.b).

Fig.8.15 shows the variation of the attenuation against the diameter of the bar embedded in concrete for the different frequencies used.

Fig.8.16 shows the variation of the attenuation against the frequency for the different bar sizes used.

Fig.8.17 shows the attenuation against bar diameter for the depths of the bar in concrete i.e. 70 and 90mm.

As it can be seen from the results as the frequency increases the strength of the signal decreases significantly (figs.8.12 and 8.13). Moreover if the spacing between transmitter and receiver increases the received signal loses strength to a greater extent at higher frequencies (figs.8.14 and 8.15). Furthermore if the bar depth in concrete increases the echo from bar is weaker

(fig.8.17). However, if the bar diameter increases the echo strength from the bar increases (figs.8.15 and 8.16).

c- Corroded Bar Embedded in Concrete

In this case two factors affect the results: the roughness height and the frequency used.

The configurations used in the model were:

Frequencies used: 150, 300, 500 kHz with diam. 25mm transducers.

spacing: 10, 50, 100, 200.

Concrete depth: 150mm.

Bar diameter: 3, 5, 12, 25, 32mm.

Bar depth: 70mm.

Roughness height: 1, 1.6mm.

Fig.8.18 shows the model output for a sound bar and a corroded bar of 1mm roughness height of 12mm diameter bar and 70mm depth in concrete with 150kHz transducers spaced ^{at} 50mm.

Fig.8.19 shows the attenuation against bar diameter for sound and corroded bar of 1mm roughness height for the frequencies used.

Fig.8.20 shows the attenuation against frequency for sound, corroded bars of roughness height of 1 and 1.6 respectively.

By studying the results above one can deduce the following

conclusions:

1- When the roughness height increases the signal reflected from the bar loses strength due to scattering to a greater extent for higher frequencies (fig.8.19).

2- As the frequency increases the reflected signal from the bar becomes difficult to detect due to scattering and absorption factor (fig.8.12) and due to the scattering produced by the roughness of the bar surface which is frequency dependent as was shown previously (fig.8.20). Therefore the spectrum of the reflected signal from a sound bar will be different from that a corroded bar as the latter is frequency dependent.

The important point deduced is that the attenuation for a corroded bar is greater than that for a sound bar but the difference depends on frequency, therefore if the signal could be identified in different frequency bands it should be possible to tell whether the bar is corroded, e.g. see fig.8.20 for sound and corroded bars, if we take the ratio of attenuation at 350kHz to that at 150kHz for the bar of 1.6mm surface roughness we get that this ratio is about 1.7.

d- Cracked Bar Embedded in Concrete

As mentioned the bar was modelled to be fully cracked i.e. not continuous. The factor which affects the result is the width of the crack. The crack is assumed to be in the mid distance between the transmitter and the receiver. The reflected area

which was taken before as an ellipse will now be the area of the ellipse minus the cracked area.

Fig 8.21 shows the output of the model for a sound bar and a bar with 5mm, and 10mm crack width.

The conclusion deduced is that as the crack width increases the signal reflected from the bar reduces because the reflected area gets smaller.

It should be mentioned that in the presence of a sharp crack or edge, diffraction may occur which is not taken into account in the present model, although any diffracted signal would be expected to be small.

8.8- CONCLUSIONS

Computer synthesis has been used to simulate the effect of the frequency range used in the experiment on the signals received from reinforcement embedded in concrete. It was shown that the signals received from sound and corroded bars are frequency dependent which represents a major factor when an ultrasonic system is derived for detecting such faults.

Selected examples were given to illustrate the effect of a corroded and a cracked bar on the received signal. The results support the following conclusions:

1- As the frequency increases the strength of the received signal

decreases, in general. This was supported by experiments.

2- As the diameter of the bar embedded in concrete increases the echo reflected increases.

3- As the depth of the bar increases in concrete the signal expected will be weaker.

4- As the spacing between the receiver and transmitter increases the echo reflected from the reinforcement gets weaker.

5- As the roughness height of the corroded bar increases the signal compared to a sound bar decreases significantly, i.e. the attenuation from a corroded bar is greater than that for a sound bar.

6- It was shown that the signal from a corroded bar is frequency dependent.

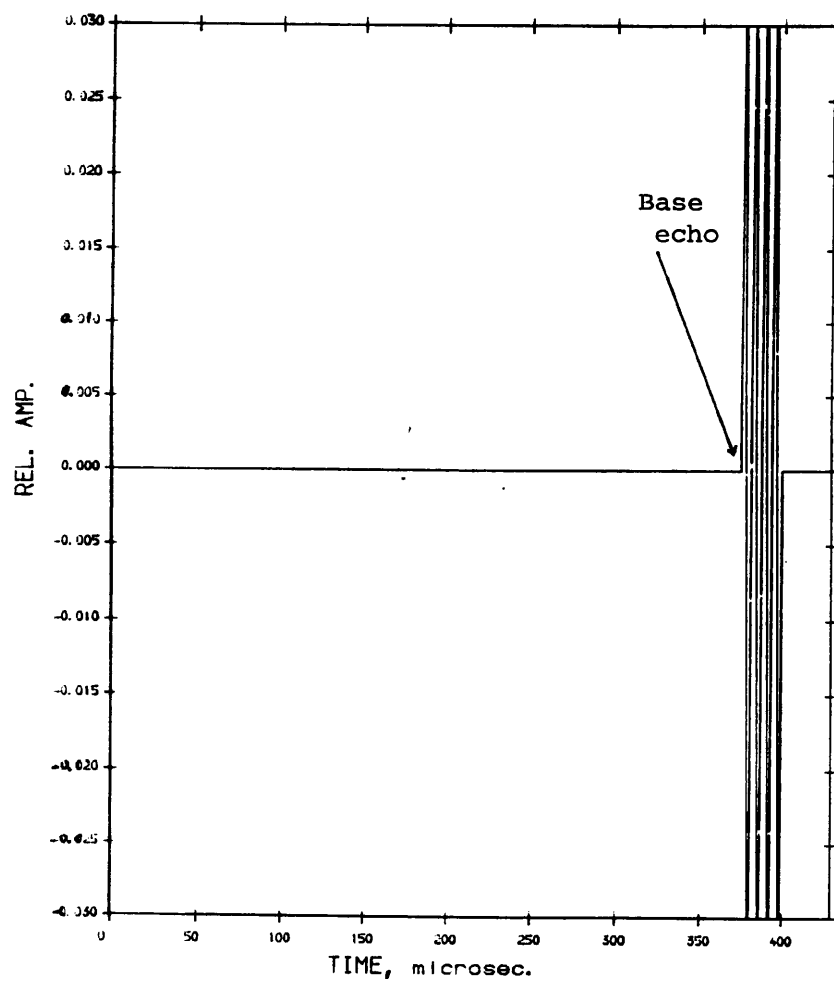
7- The signal from a fully cracked bar embedded in concrete is weaker from a signal reflected from a sound bar.

8- The model gave reasonable agreement when the loss coefficients from the experiment and the model were compared.

Therefore it should be possible to identify sound components from corroded components embedded in concrete by comparing their frequency spectra, if a filter could be applied on the signal to remove bands of frequencies and leave the parts where it is

easier to recognize the corroded components. Therefore it was decided at a later stage to use digital filtering techniques where it was possible to identify embedded corroded components in concrete.

The use of computer-simulated experimentation has clarified questions concerning the attenuation of signals due to scattering and absorption in concrete, corroded and cracked bars used in the reinforcement of concrete. Additional work is needed to model the input signal to have similar shape as the signal from the transducer used in the experiment, to model the concrete as a medium with aggregates and cement, and to include other variables neglected in this model such as surface and shear waves. This should enable better comparison between experiment and the model where it would be possible to compare the time-domain signals directly without the need to calculate the loss coefficients.

WATER MODEL.

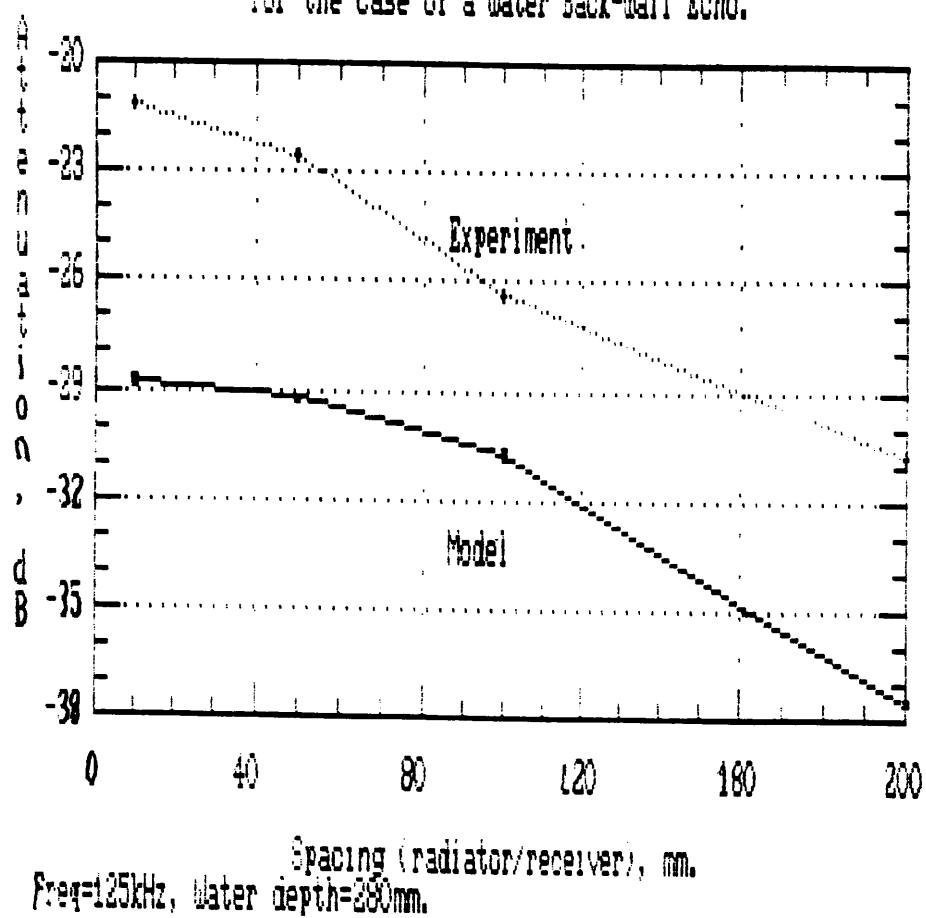
DIM. : Height= 280.00 mm
Width= 300.00 mm

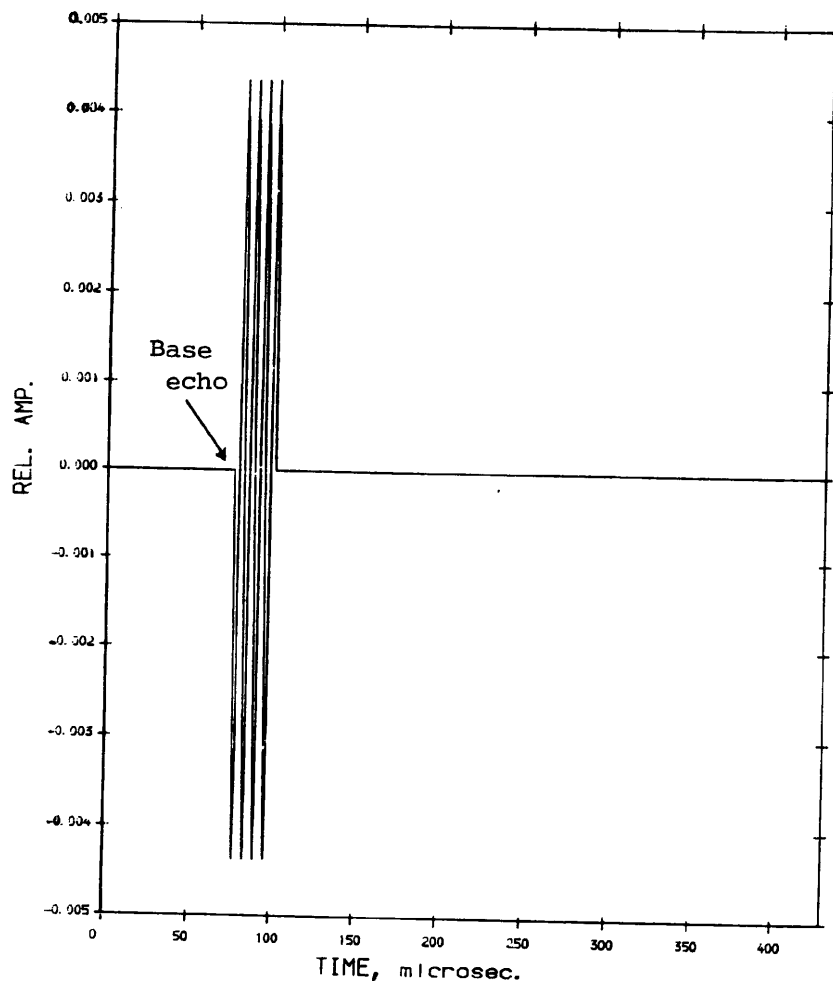
TRANSD. PROP. : F= 125.00 kHz
DIA= 25.00 mm
SPACED= 50.00 mm

Fig.8.3

Fig.8.4

Comparison between Model and Experiment
for the case of a Water Back-Wall Echo.





CONCRETE MODEL.

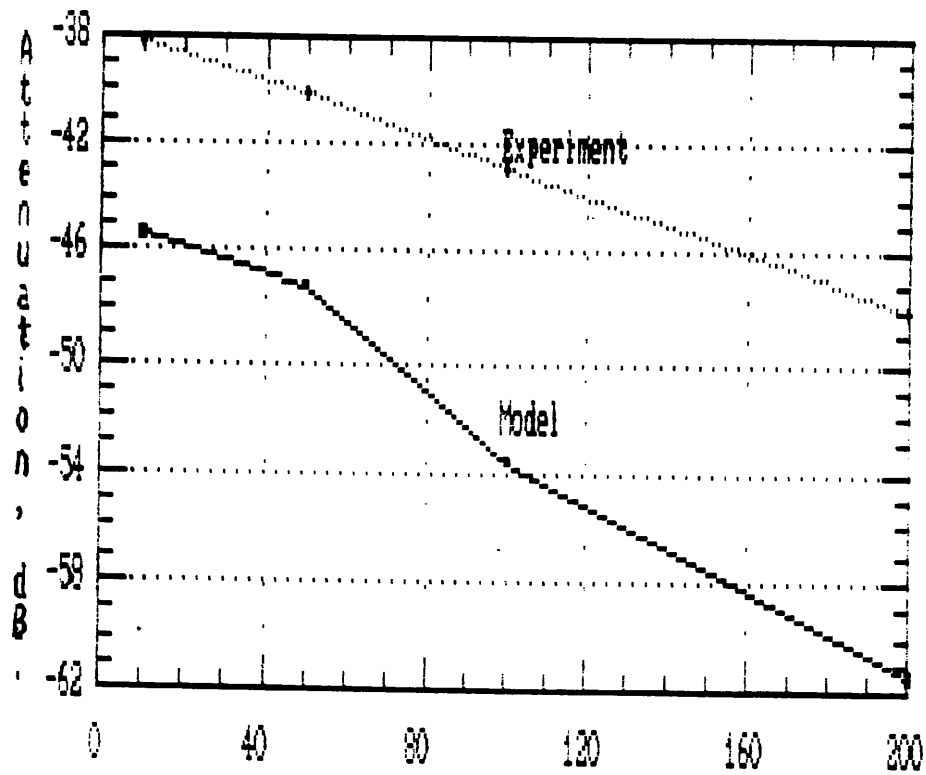
DIM. : Height= 150.00 mm
Width= 150.00 mm

TRANSD. PROP. : F= 150.00 kHz
DIA= 25.00 mm
SPACED= 50.00 mm

Fig.8.5

Fig.8.6

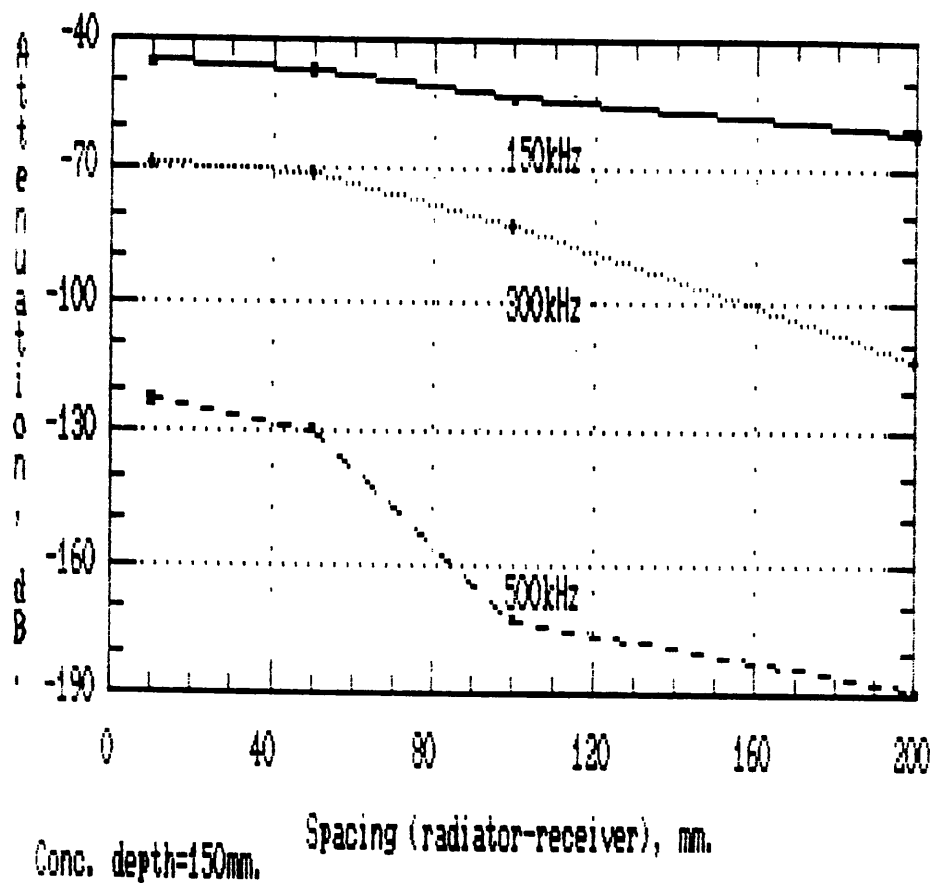
Comparison between Model and Experiment
for the case of Conc. Back-Wall Echo.

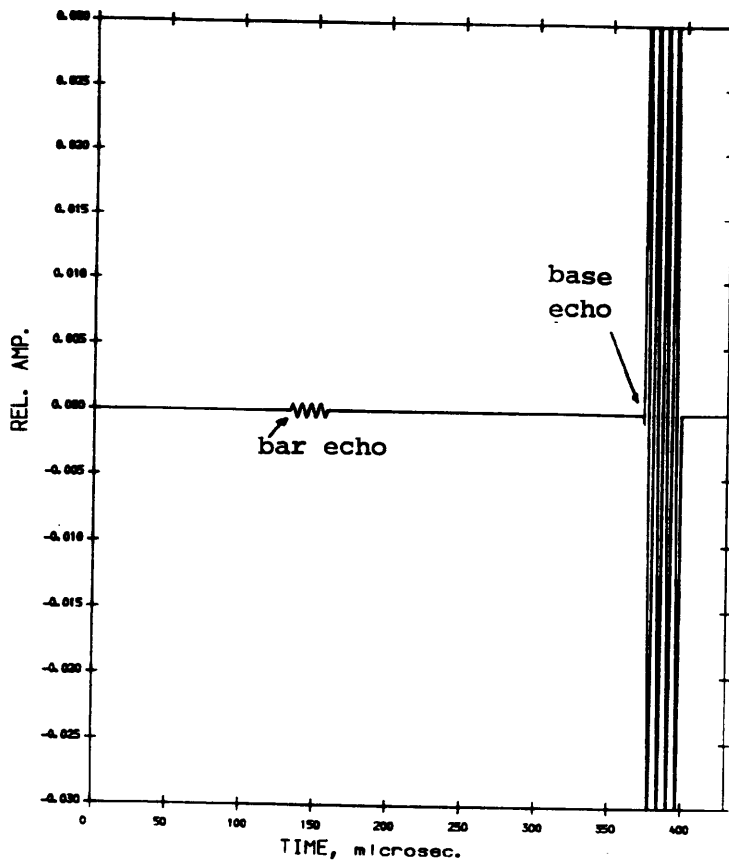


Spacing (radiator-receiver), mm.
Freq=150kHz, Conc. depth=150mm.

Fig.8.7

Model Analysis: Case of a Conc. Back-
Wall Echo.





(a)

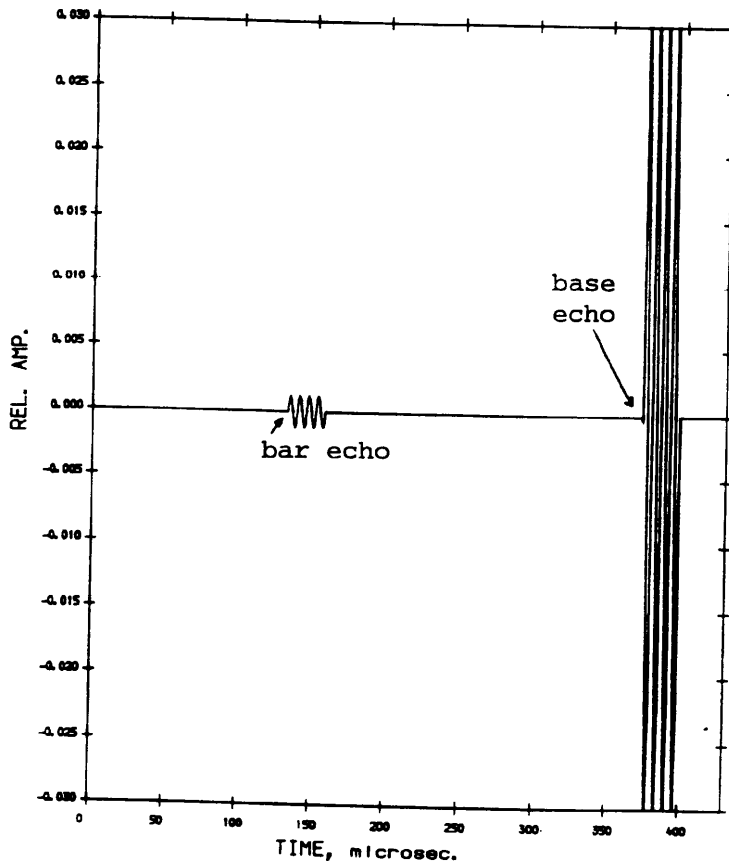
WATER MODEL, WIRE THROUGH.

DIM. : Height= 280.00 mm
Width= 300.00 mm

TRANSD. PROP. : F= 125.00 kHz
DIA= 25.00 mm
SPACED= 10.00 mm

BAR PROP. : DIA= 5.00 mm
NO CRACKS PRESENT.
BAR POS. FROM TOP= 100.00 mm

Fig.8.8



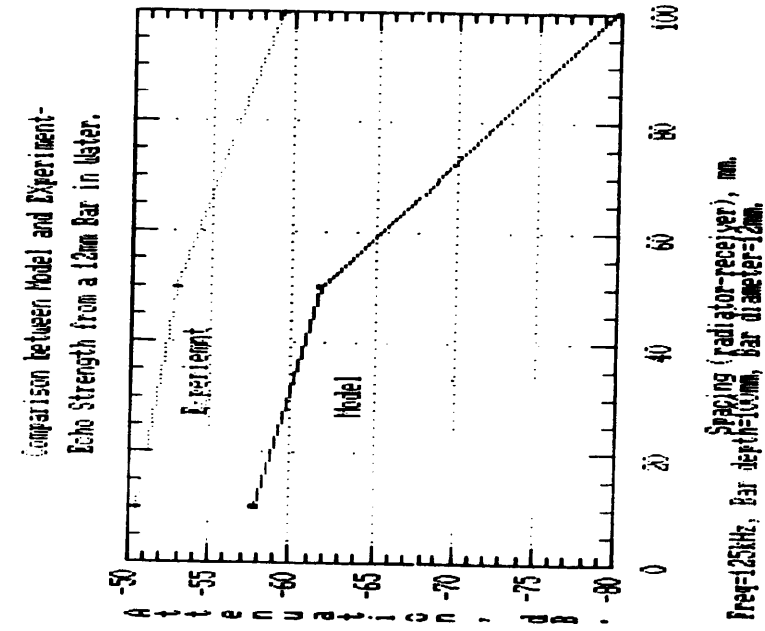
(b)

WATER MODEL, WIRE THROUGH.

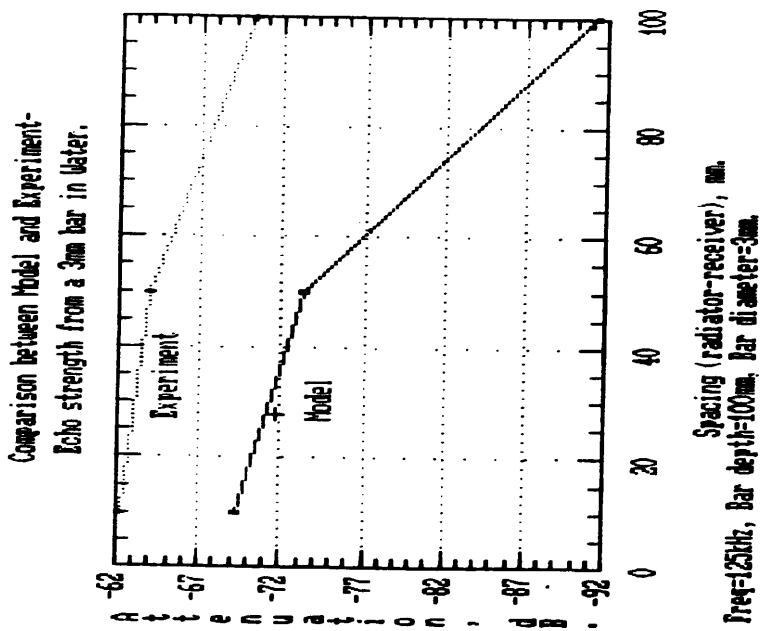
DIM. : Height= 280.00 mm
Width= 300.00 mm

TRANSD. PROP. : F= 125.00 kHz
DIA= 25.00 mm
SPACED= 10.00 mm

BAR PROP. : DIA= 12.00
NO CRACKS PRESENT.
BAR POS. FROM TOP= 100.00 mm



(a)



(b)

Fig. 8.9

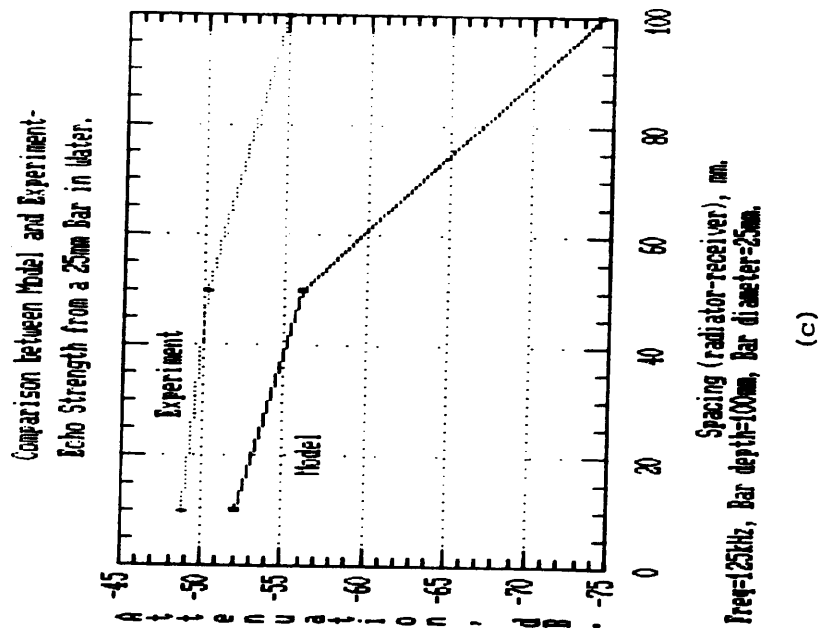
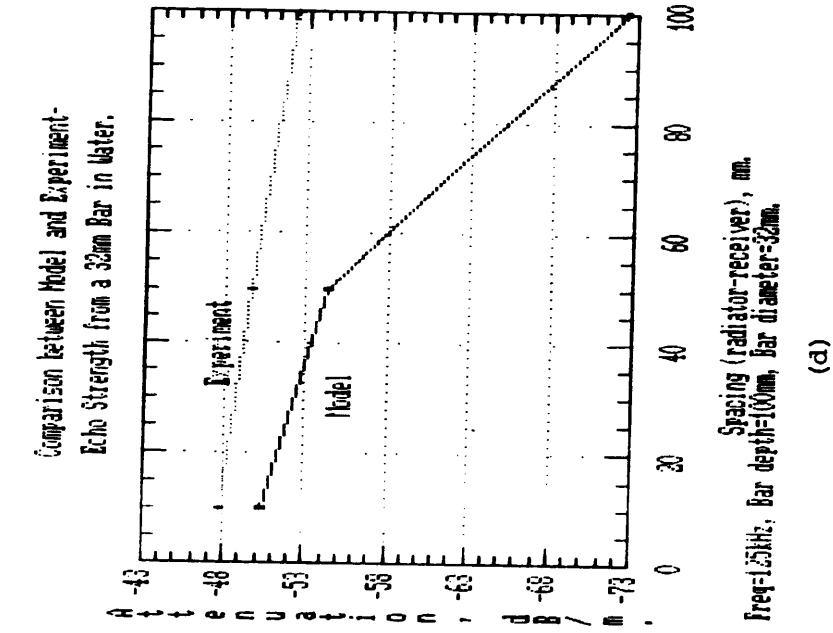
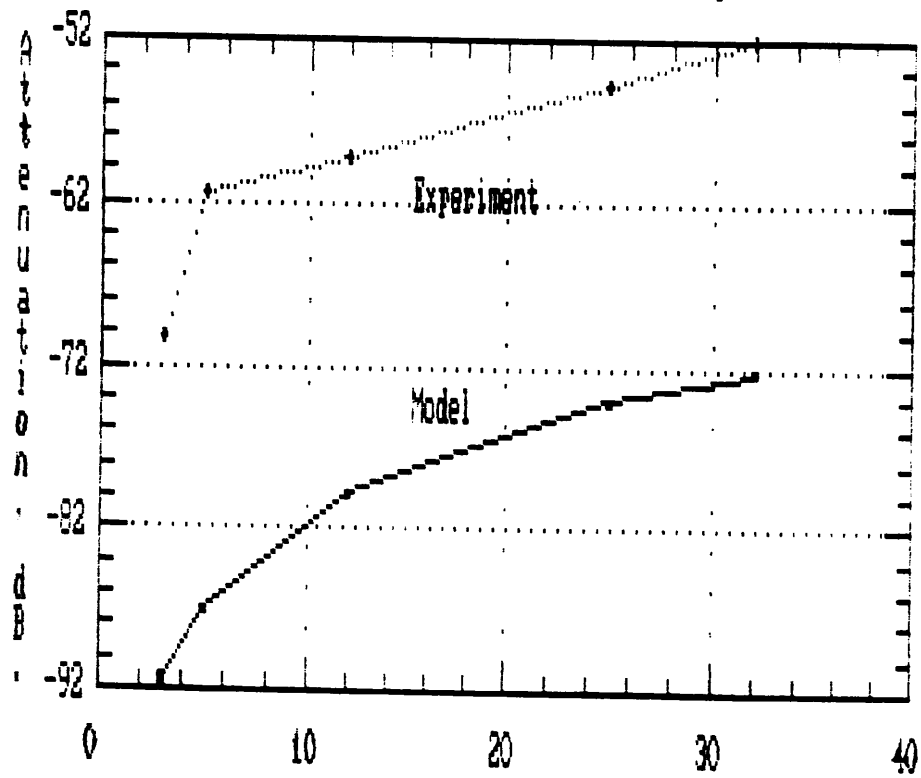


Fig. 8.9

Fig.8.10

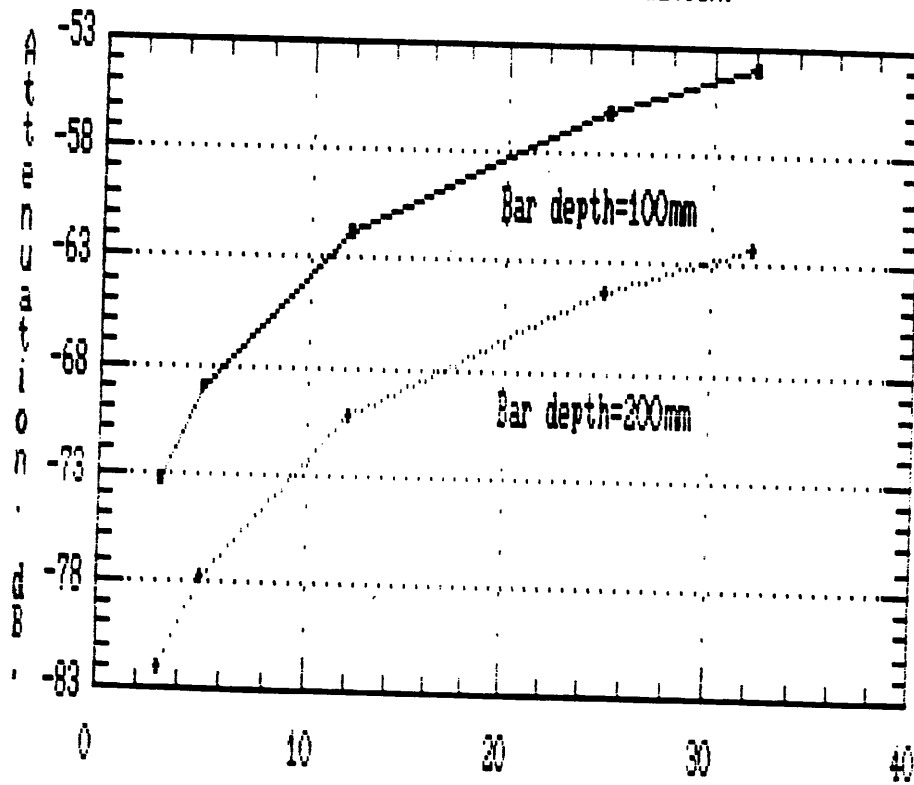
Comparison between Model and Experiment-
for Different Bar sizes at 100mm Depth.



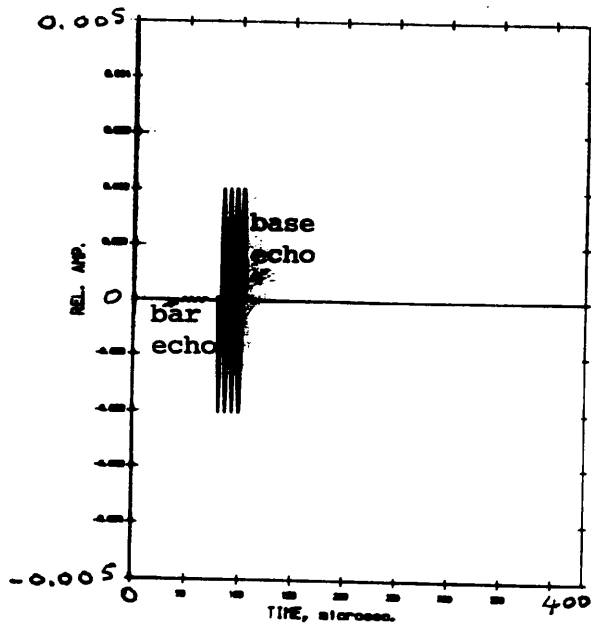
Diameter of the Bar, mm.
Freq=125kHz, Bar depth in Water=100mm, Transducers spacing=100mm.

Fig.8.11

Model Analysis: The effect of the Bar
Depth in Water on the Attenuation.



Bar Diameter, mm.
Freq=125kHz, Transd. spacing=50mm.

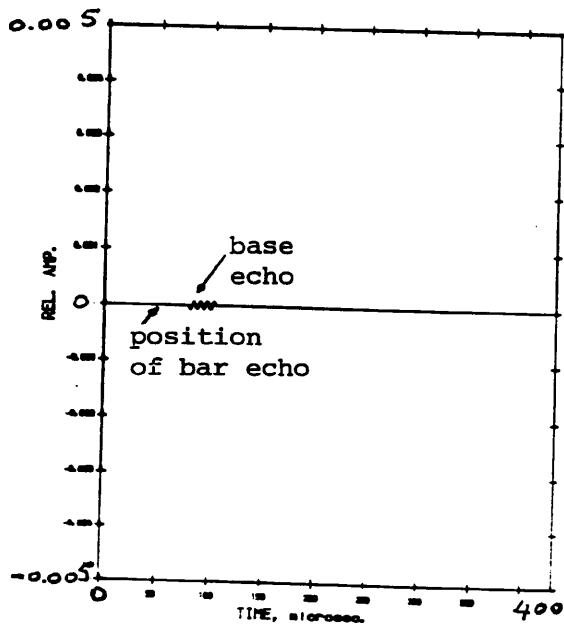


CONCRETE MODEL, WIRE THROUGH
DIL. Height= 150.00 mm
Width= 150.00 mm

TRANSD. PROP. F= 150.00 MHz
DIA= 25.00 mm
SPACED= 100.00 mm

BAR PROP. DIA= 5.00 mm
NO CRACKS PRESENT.
BAR POS. FROM TOP= 70.00 mm

(a)

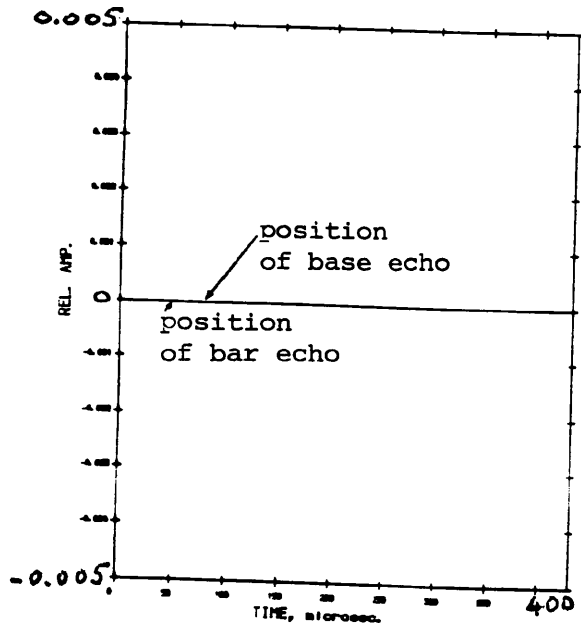


CONCRETE MODEL, WIRE THROUGH
DIL. Height= 150.00 mm
Width= 150.00 mm

TRANSD. PROP. F= 300.00 MHz
DIA= 25.00 mm
SPACED= 100.00 mm

BAR PROP. DIA= 5.00 mm
NO CRACKS PRESENT.
BAR POS. FROM TOP= 70.00 mm

(b)



CONCRETE MODEL, WIRE THROUGH
DIL. Height= 150.00 mm
Width= 150.00 mm

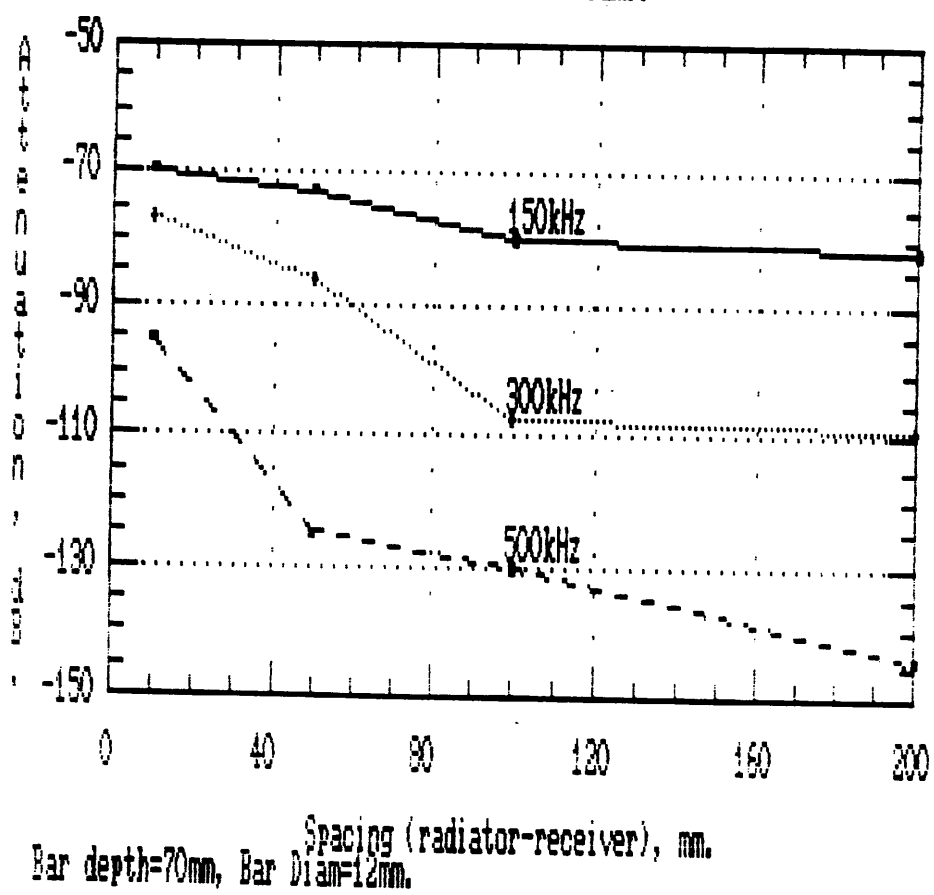
TRANSD. PROP. F= 500.00 MHz
DIA= 25.00 mm
SPACED= 100.00 mm

BAR PROP. DIA= 5.00 mm
NO CRACKS PRESENT.
BAR POS. FROM TOP= 70.00 mm

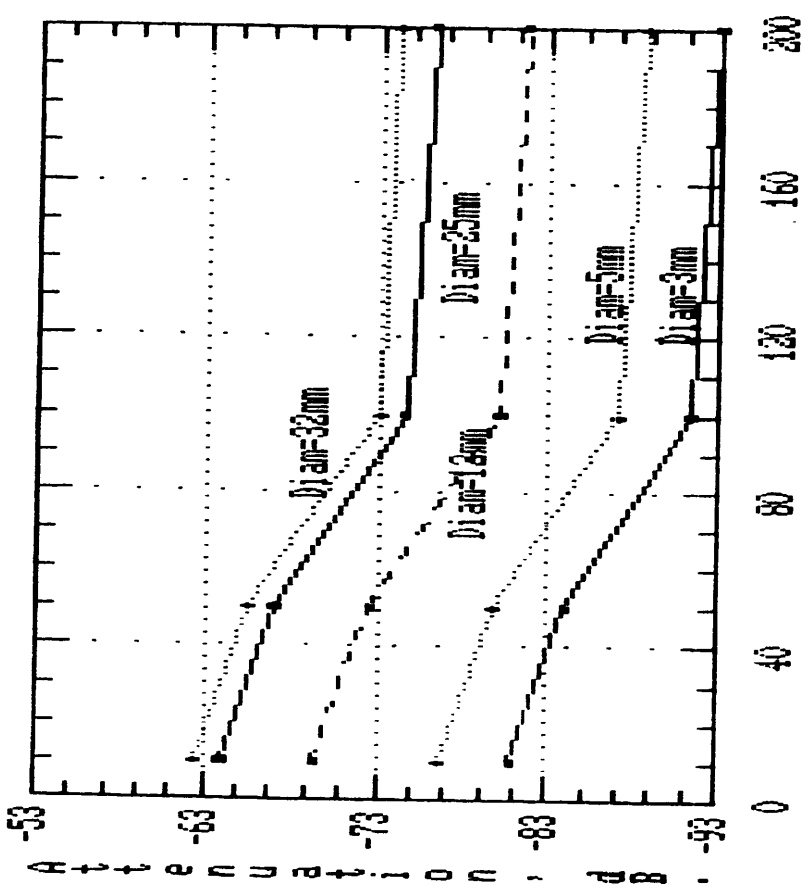
Fig.8.12

Fig.8.13

Model Analysis: Case of Bar embedded in
 Conc. of 12mm Diam.



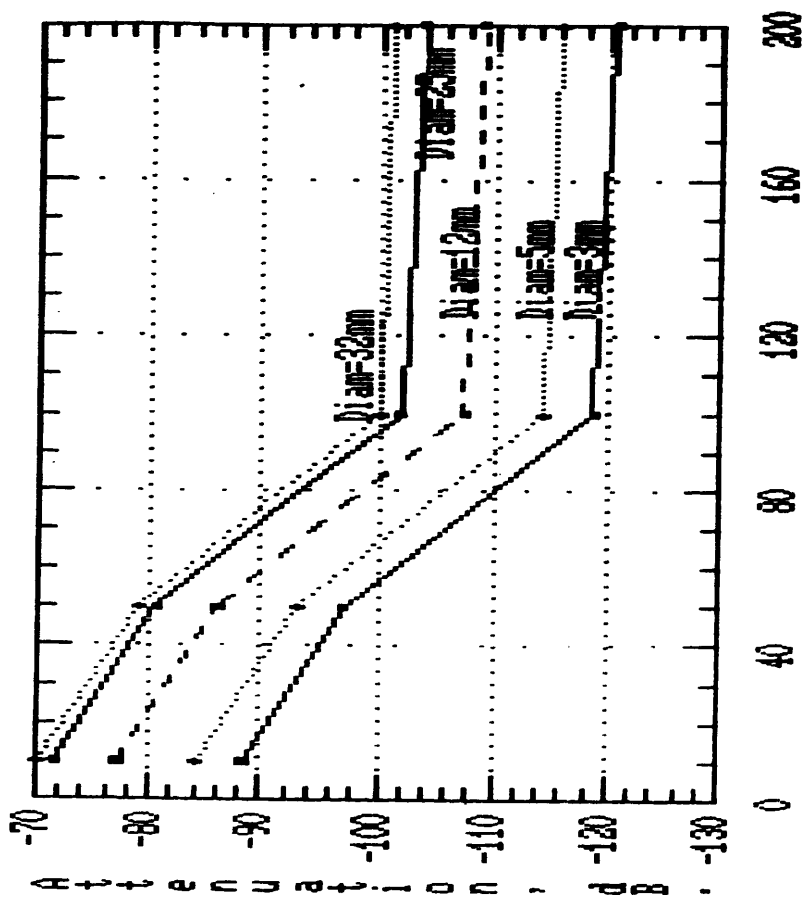
Model Analysis: The variation of transducer spacing for different bar diameter.



Spacing (radiator-receiver), mm. Freq=150kHz, Bar depth=70mm.

(a)

Model Analysis: The variation of transducer spacing for different bar diameter.



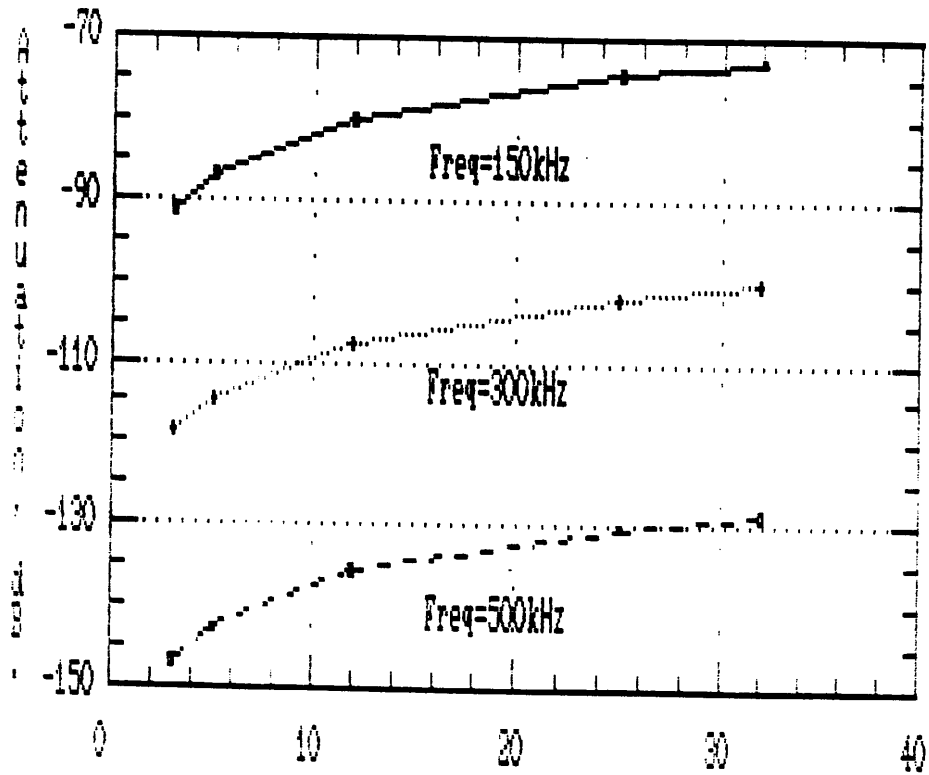
Spacing (radiator-receiver), mm. Freq=300kHz, Bar depth=70mm.

(b)

Fig. 8.14

Fig.8.15

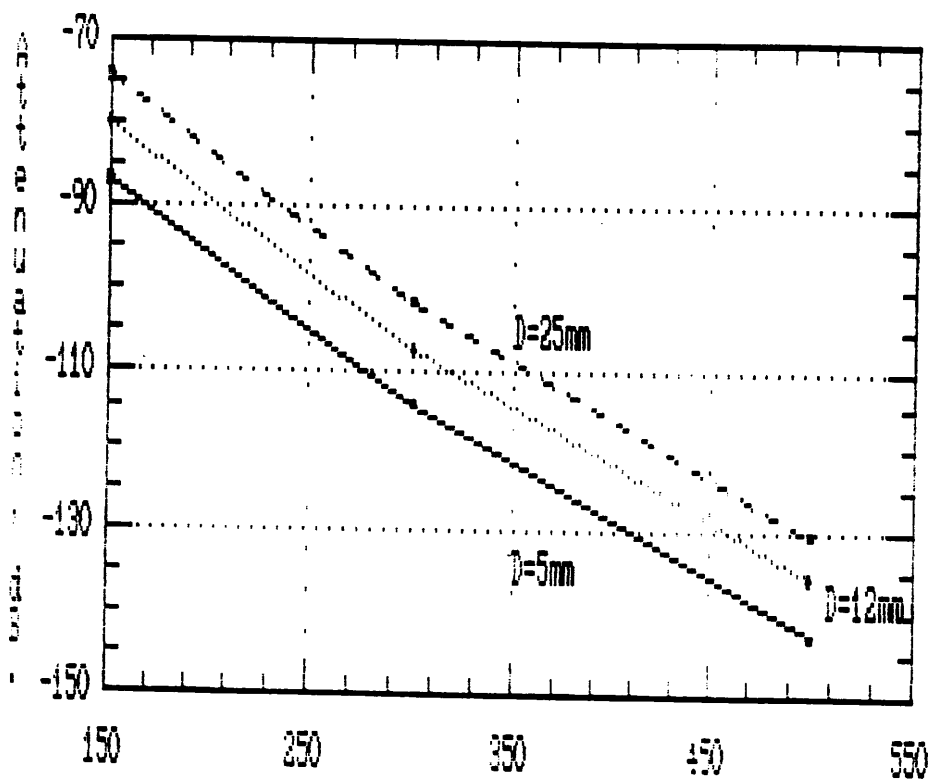
Model Analysis: The variation of attenuation against bar diameter for different frequencies.



Bar Diameter, mm.
Bar Depth=100mm, Transd. spacing=100mm.

Fig.8.16

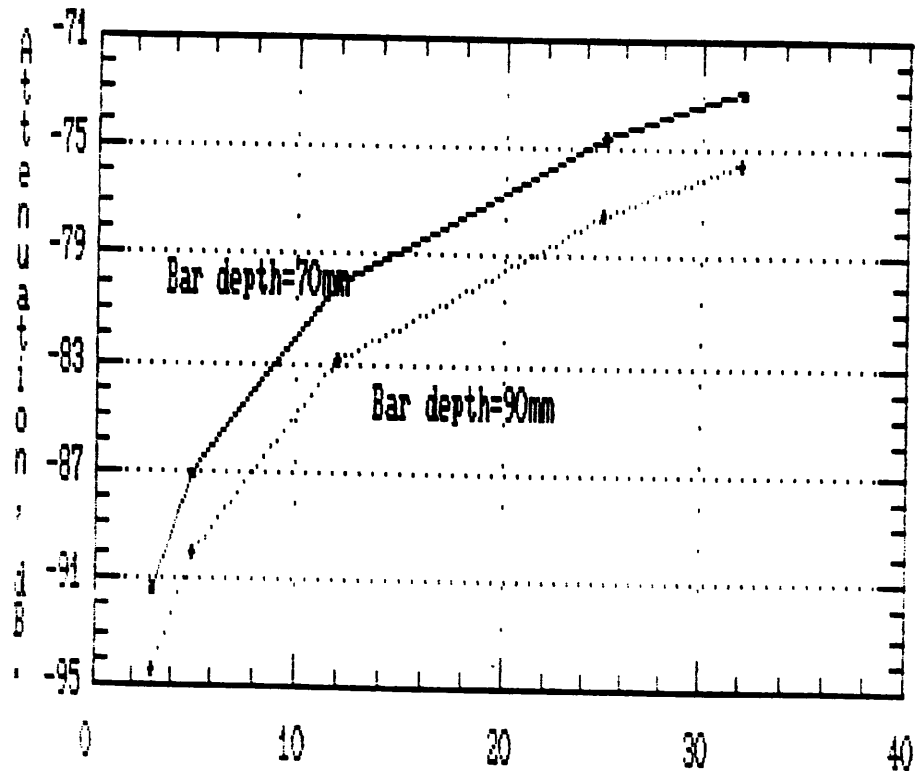
Model Analysis: The variation of attenuation against frequency for different bar diameter.



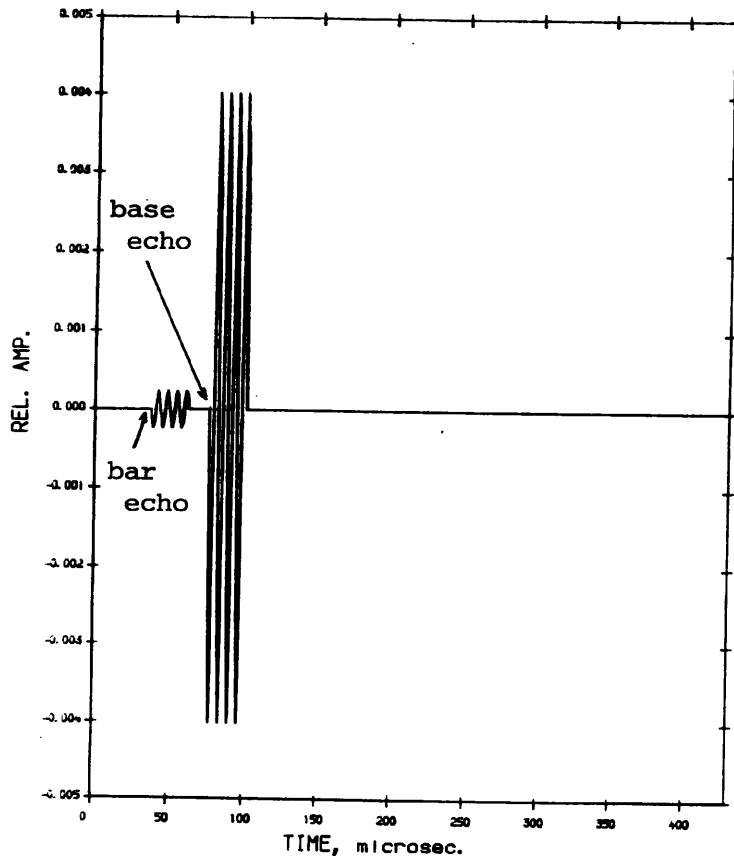
Frequency, kHz.
Transd. spacing=100mm, Bar depth=70mm.

Fig.8.17

Model Analysis: The Effect of Bar Depth
in Conc..



Bar Diameter, mm.
Freq=150kHz, Transd. spacing=100mm.



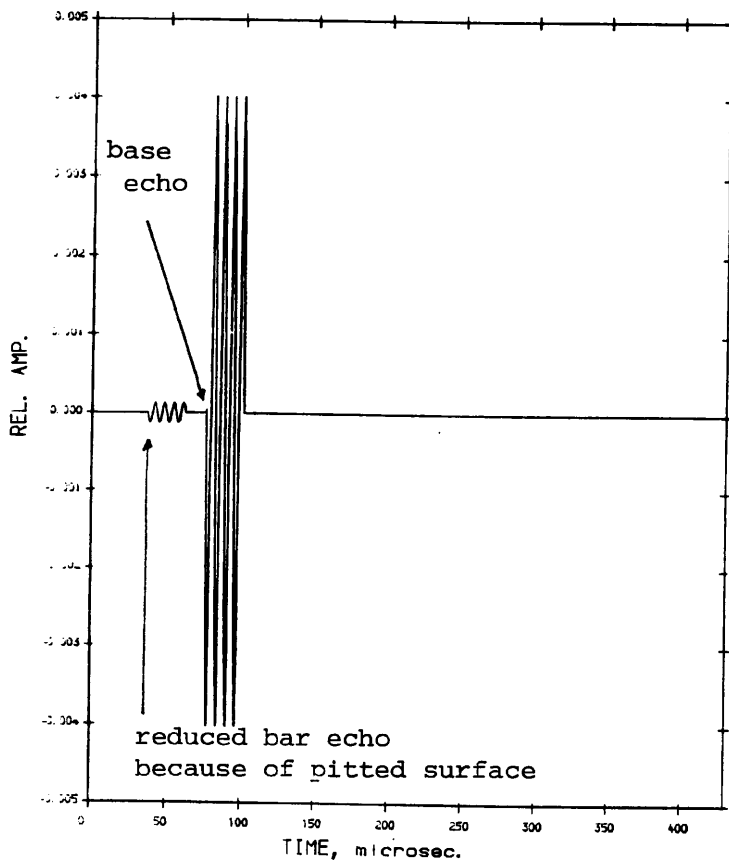
CONCRETE MODEL, WIRE THROUGH.

DIM. : Height= 150.00 mm
Width= 150.00 mm

TRANSD. PROP. : F= 150.00 kHz
DIA= 25.00 mm
SPACED= 50.00 mm

BAR PROP. : DIA= 12.00 mm
NO CRACKS PRESENT.
BAR POS. FROM TOP= 70.00 mm

Fig.8.18



CONCRETE MODEL, WIRE THROUGH.

DIM. : Height= 150.00 mm
Width= 150.00 mm

TRANSD. PROP. : F= 150.00 kHz
DIA= 25.00 mm
SPACED= 50.00 mm

BAR PROP. : DIA= 12.00 mm
CORROSION PRESENT.
BAR POS. FROM TOP= 70.00 mm

ROUGHNESS= 1.60 mm

Fig.8.19

Model Analysis: Comparison between Sound
and Pitted Bar in Conc. for Diff. Freqs.

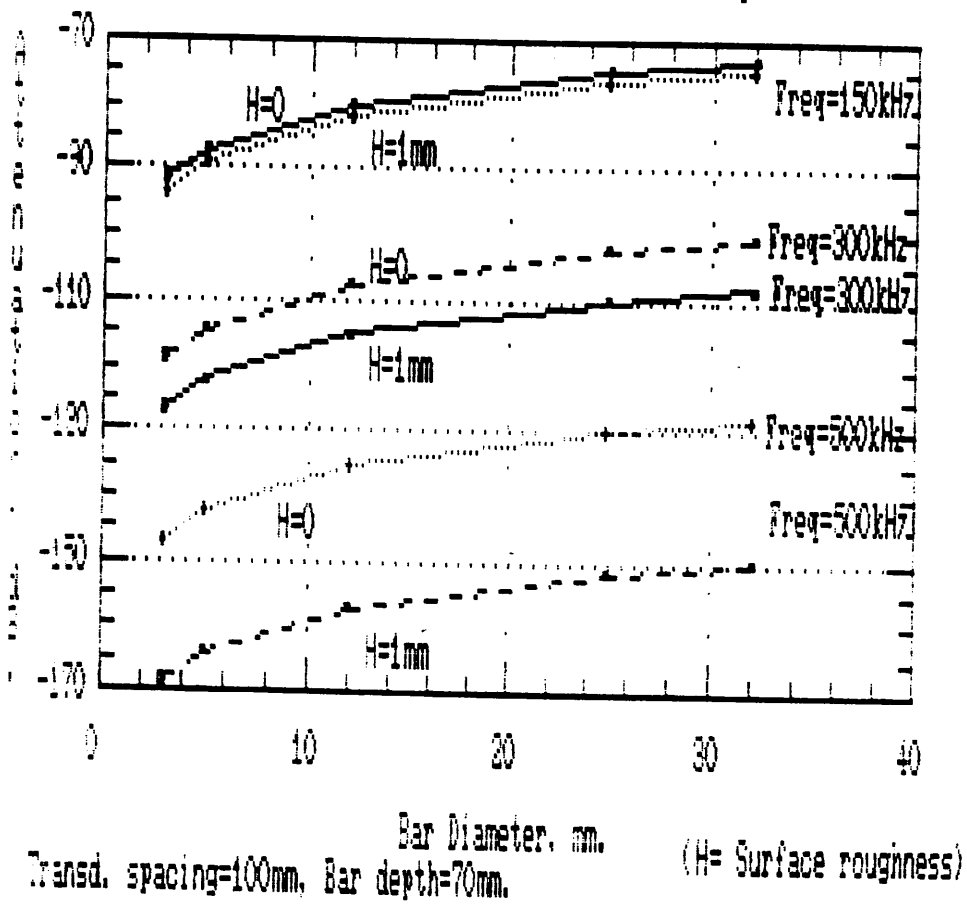
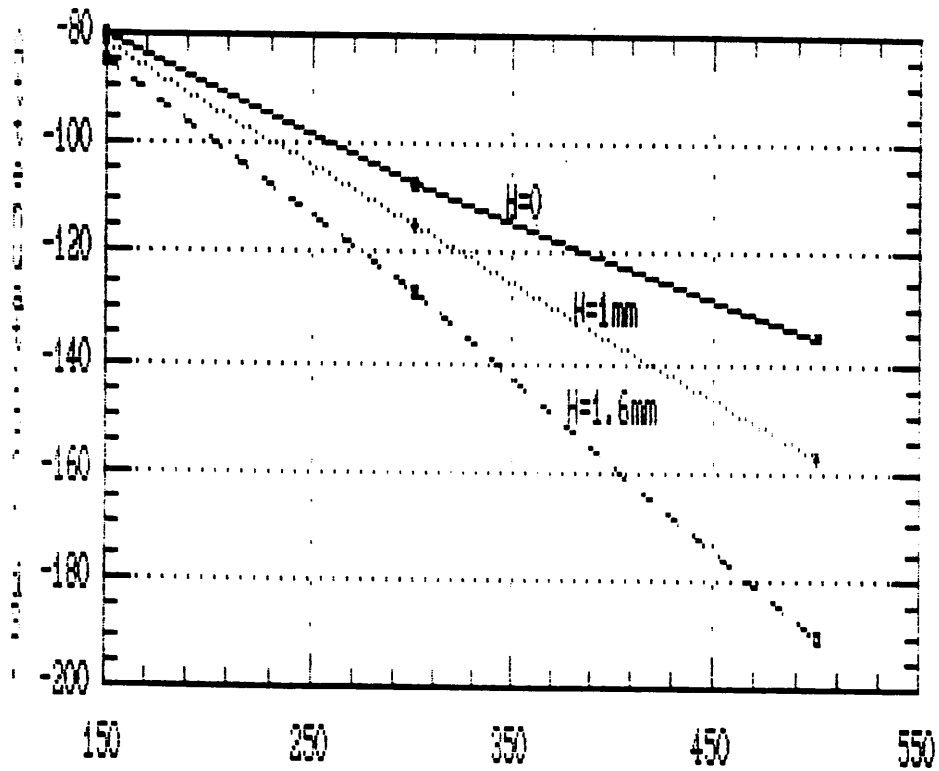


Fig.8.20

Model Analysis: Effect of surface
roughness on the frequency.



Frequency, kHz.
Transd. spacing=100mm, Bar depth=70mm, Bar dian=70mm. (H= Surface roughness)

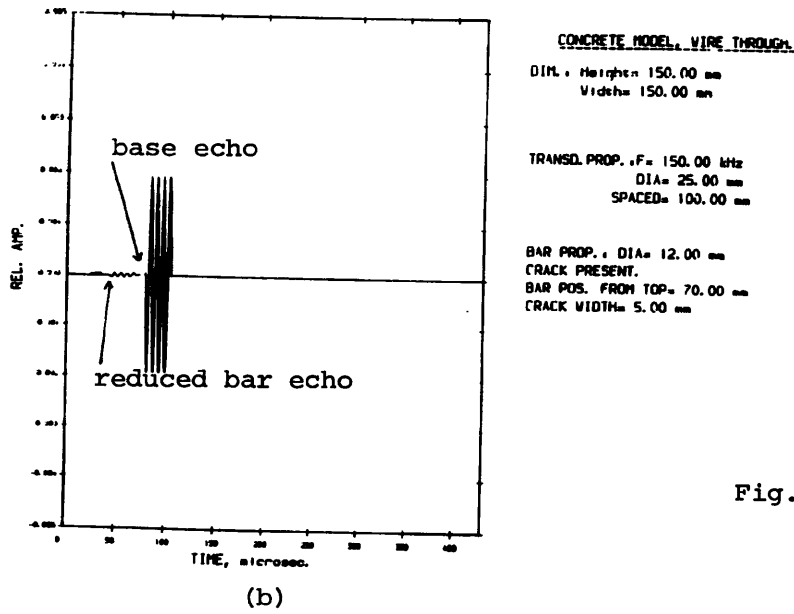
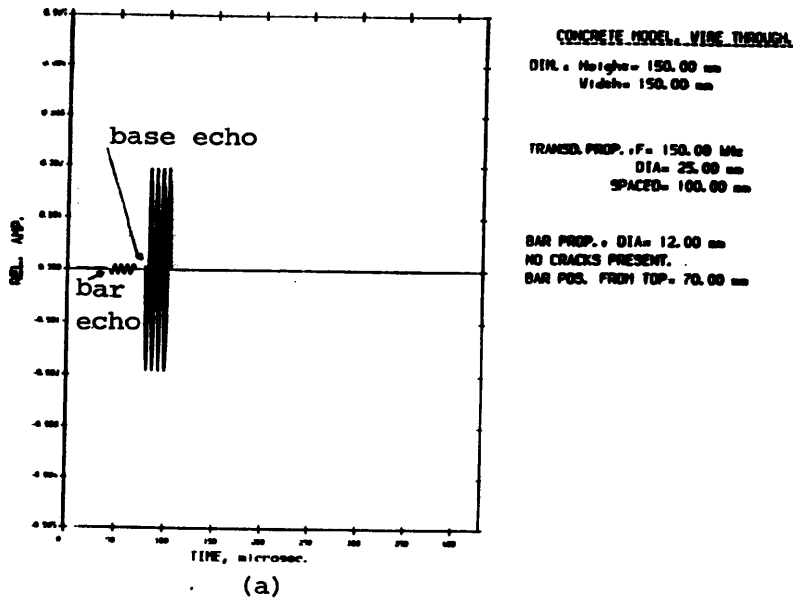
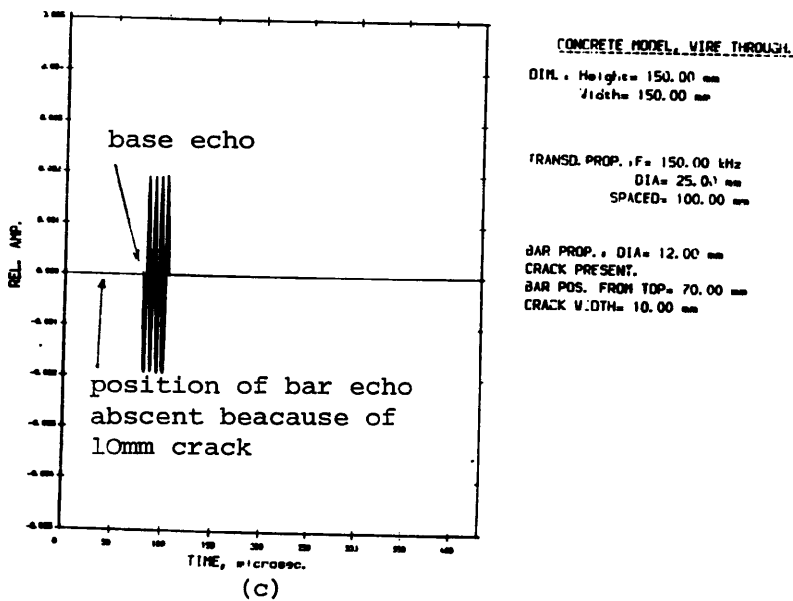


Fig.8.21



CHAPTER 9

EXPERIMENTAL DETAILS

9.1- INTRODUCTION

In this chapter, information about materials and specimens is given. Moreover, descriptions about instruments used and computer programs written for signal processing are included.

9.2- MATERIALS

a- Aggregates

Two kinds of natural coarse aggregates were used; crushed and uncrushed.

The maximum nominal size for the crushed gravel was 20mm. The relative density of the gravel was 2600 Kg/m^3 . The percentage of moisture content was assumed as 0%.

The other coarse aggregate used was uncrushed with a maximum nominal size of 15mm diameter. The relative density of the gravel was 2660 Kg/m^3 . The percentage of the moisture content was assumed again as 0%.

The fine aggregate used for all mixes was river sand with a specific gravity of 2600 Kg/m^3 . The percentage of moisture content of the sand was always determined before its addition to

the mix, and an adjustment was made in the weights of the free water and the fine aggregate going into the mix.

b- Cement

The cements used in the batches of the concrete mixes were Rapid Hardening Portland Cement and Ordinary Portland Cement.

The Rapid Hardening Portland Cement was chosen because of its increased use in the construction industry these days. It is very similar in composition to the Ordinary Portland Cement. As its name implies, it develops strength more rapidly and is sometimes called high early strength cement. This kind of cement is used where a rapid strength development is required i.e. when formwork is to be removed early for re-use, or where sufficient strength for further construction is wanted as quickly as practicable. It is characterised by a higher fineness and C_3S content than O.P.C. The requirements of soundness and chemical composition are the same as for the Ordinary Portland Cement.

The Ordinary Portland Cement is by far the most common cement in use. It is suitable for use in general concrete construction when there is no exposure to sulphate in the soil or in ground water. Over the years there have been some changes in the characteristics of the O.P.C. with respect to the fineness and the C_3S content. As a consequence O.P.C. concretes tend to have a higher 28 days strength.

c- Water

It is widely known that there is an influence of both the quality and the quantity of the water in the mix on the strength of the resulting concrete. The quality of the water is covered in many specifications by a clause stating that this should be fit for drinking. The water used for mixing and curing on this research came straight from the public supply tap, so no problem related to dissolved solids was observed.

d- Wires and Strands

High tensile steel is the most common material used for prestressing wires to provide the tensile forces in prestressed concrete. High-tensile steel can be produced by a number of different approaches (see chapter 1). The wires and strands used in the experiments were British made. The steel was of the 0.7-0.8% carbon type. The bars used were 40 and 30mm in diameter, the wires were 7mm in diameter, and the strands were 7-wires each of 5mm diameter.

9.3- TEST SPECIMENS

a- Cubes

The cube specimens were cast in steel moulds, generally 150mm cube. A set of 6 cubes was cast for each one of the mixes. These cubes were used mainly to get the ultrasonic velocity and the cubic characteristic strength of the mix.

b- Cylinders

The standard cylinders are 150mm diameter by 300mm long. A set of 2 cylinders was cast for some of the mixes. These were used again to get the ultrasonic velocity and the characteristic strength.

c- Prisms or Beams

The dimensions of the prisms cast in all the experiments were 150x150x1000mm³. Different reinforcements were used in prisms to try to observe the effect of the diameter on the signal. In some reinforced blocks, chloride was added to the mix in a proportion of 0.1% of the weight of the cement used. In order to let the chloride react with the steel components which leads to corrosion, these blocks were tested one year after establishing the presence of corrosion. Other set of prisms were reinforced with continuous strands or in selected cases cut strands. Ducted blocks were cast too, these included cases with an empty duct, a grouted duct with no strand, and a grouted duct with strand. It should^{be} noted that when steel components are present they were positioned in the middle of the section of the prism.

In summary, the following blocks were cast:

Case (specimen)	Reinforcement	Number of Specimens
1-Concrete Only	-	2
2-Concrete+Bar	One 30mm Bar	1

Case (specimen)	Reinforcement	Number of Specimens
3-Concrete+Bar	One 40mm Bar	1
4-Concrete+Strand	One 7x5mm Strand	2
5-Concrete+Cut Strand in the middle	One 7x5mm Strand	2
6-Concrete+Strand+Chloride	One 7x5mm Strand	2
7-Concrete+Empty Duct	-	1
8-Concrete+Grouted Duct	-	1
9-Concrete+Grouted Duct with Strand	One 7x5mm Strand	1
10-As 9 but Cut in Strand Midway	One 7x5mm Strand	1
11-Mortar(Cement+Sand)	-	1
12-Mortar+Strand	One 7x5mm Strand	1
13-As 12 with Chloride Added	One 7x5mm Strand	1
14-As 12 with Cut in Strand Midway	One 7x5mm Strand	1

d- Slabs

Two slabs of 150x800x800mm³ were cast. One of them was cast with very high strength concrete, and the other was of the same mix but was not compacted well, and a 200mm diameter disk of 10mm in thickness of polystyrene was inserted in the middle of the slab (when concrete is compacted, the void amount is reduced hence the density is higher and strength is increased). These two specimens were used to try to establish the influence of low strength concrete and the presence of voids on the signal.

e- Cracked Bridge Beam

This beam is a T-beam of 9000mm in length with a flange width of

495mm. The beam is pretensioned along its length by ten (7x5mm) strands, each tensioned to 115kN (see fig.9.1). This beam was cracked in the mid span due to handling and was stored outside for over one year.

The potential mapping technique (see chapter 2) was carried out to try to establish if any corrosion was occurring in the bridge beam. Potential mapping (half-cell mapping) requires that a suitable reference electrode be placed on the concrete surface and the potential difference between the reference electrode and the embedded steel measured via a digital voltmeter (dvm), this requires an electrical connection be made to the embedded steel. By obtaining potential readings at a number of locations, the corrosion hazard for the bridge can then be assessed.

In the test on the bridge beam, a standard calomel electrode (SCE) was used. Normally in field investigations either copper/copper sulfate (Cu/CuSO_4) or silver/silver chloride (Ag/AgCl) reference electrodes would be used. In all cases the measured potential to any reference electrode can be related to the other by simple conversion factors. The potentials in the bridge range from +71 to -75 mV(SCE) i.e. from approximately zero to -150 mV Cu/CuSO_4 . These potentials are indicative of passive conditions occurring throughout the bridge beam.

f- Large Scale Test Beam

The beam was fabricated within the department using an existing steel mould 5000mm long, 150mm wide and 300mm deep. Special end

plates were fabricated with openings to guide the prestressing tendons. Plates 9.1 and 9.2 show the beam during construction.

The tendons used were supplied by the British Ropes Bridon Wire division and were 15.7mm Super Prestressing strand, relaxation class 2 to BS 5896/3:1980. The strand end grips were supplied by CCL systems as was the stressing jack and pump system.

The beam was cast with different defects such as voids, cuts, and chloride around some strands. Fig.9.2 shows the details of internal reinforcement, defect locations, and prestressing forces in each strand.

Concrete for the beam was designed to have a characteristic strength of 40N/mm^2 . The concrete had a slump of 75mm (see table 9.1 for mix proportions).

After ten months, the potential mapping technique was carried out to check if corrosion was taking place in the contaminated areas where salt had been added. The potentials ranged from 100mV to -100mV Cu/CuSO_4 where no salt was present, and from -250mV to -300mV Cu/CuSO_4 where it was present, indicating that corrosion was taking place.

9.4- MIXING

The object of mixing is to coat the surface of all aggregate particles with cement paste, and to blend all the ingredients of concrete into a uniform mass. The mixer consists essentially of a

circular pan rotating about its axis, with two sets of paddles rotating about a vertical axis not coincident with the axis of the pan. They are particularly efficient with stiff and cohesive mixes, and in order to have a sufficient interchange of materials between different parts of the chamber, a minimum mixing time of 4 minutes was given until a uniform concrete was produced.

9.5- TYPE OF MIXES

In this study, four different concrete mixes were used. The basic characteristics are shown in table 9.1.

9.6- COMPACTION

The process of compacting the concrete consists essentially of the elimination of entrapped air. The oldest method is by ramming the surface of concrete to remove the air and force the particles into a closer configuration. The modern method is the use of a vibration process to compact the test specimens. A vibrating table was used in this study. It provided a reliable means of compaction.

9.7- CURING

Curing consists of controlling the temperature and the moisture movement from and into the concrete i.e. the hydration of the cement. After casting the specimens they were stored undisturbed for 3 days at a temperature 18-22°C. At the end of this period, some of the moulds were stripped and were further cured in water

at 19-21°C until the age of testing.

9.8- WORKABILITY

It is very important that the consistency of the mix be such that the concrete can be transported, placed and finished sufficiently easily and without segregation. A concrete satisfying these conditions is said to be workable. The desired workability in any case would depend on the means of compaction available. In this work the slump test was used as a physical measurement to provide information about the workability of the different concrete mixes.

9.9- TECHNIQUES USED IN TESTING

Three techniques were investigated in this study.

a- The Impact Technique

Fig.9.3.c illustrates the impulse-excitation technique. This technique is often used at frequencies lower than 30kHz ($\lambda=134\text{mm}$). A hammer or mechanical-type impactor is used to excite the wave in the concrete. The thickness may be determined from the time delay of the echo if the sound velocity in the material is known.

In this research a hammer with 3mm steel tip was used to excite the concrete and a 50kHz resonant frequency transducer was used to receive the signal. Fig.9.4 shows a signal received on a

concrete surface with strand present and its spectrum.

The problem with this technique is that the wavelength $>100\text{mm}$ is much greater than the diameter of steel wires, strands or bars (max. diameter 40mm) which means no reflection will occur from steel components embedded in concrete which are under investigation. Furthermore, the presence of Rayleigh waves which was as expected high, interfaces with the reception of the desired echoes from steel components and back-wall.

This technique could only be used for large and deep structures such as dams and where voids are expected to be large in comparison to the wavelength.

This method was studied fully with different diameter tips and impact forces. Only the thickness of the specimen was measured, no information about the steel components was detected. Therefore, this technique of inspection was discarded in this study.

b- Pulse-Echo Technique

In this technique, fig.9.3.a a short burst of ultrasound wave is sent into the material, and is reflected as echoes from cracks, voids, or boundaries. The return echo is then amplified and displayed on a CRO, showing the amplitude of the signal and the time of travel. If the velocity in the material is known, then the thickness could be calculated. As has been mentioned, no commercially available system presently exists for low-frequency

pulse-echo testing of concrete, it was therefore decided to build our own pulse-echo system. The problem encountered in low-frequency pulse-echo systems is mainly due to the ringing of the transducer when excited especially low frequency transducers. To overcome this problem three transducers of 400kHz resonant frequencies were specially built in DIAS at UMIST with heavy damping, and a 500kHz resonant frequency transducer was hired from Steinkamp, UK Branch, which was designed as a pulse-echo transducer. Two of the three transducers built in DIAS were tungsten-loaded epoxy backed, and the third was epoxy-putty backed.

Two pulsers were built for the purpose of exciting low-frequency transducers to be used in a pulse-echo system. The two pulsers were built with the help of CAPCIS.

The first pulser was a low-voltage pulser, 15V spike, with a rise time of 40nsec, with excitation period of 350nsec and variable pulse repetition frequency of 10, 15, and 100 Hz, and with built-in amplifier of 40dB gain. The circuit is shown in fig.9.5.

The second pulser was a high-voltage pulser, 450V spike, with a rise time of 20nsec, with excitation period of 100nsec and pulse repetition frequency of 100 Hz, and with built-in amplifier of 40dB gain.

The purpose of manufacturing the high-voltage pulser which gives a high energy output of the transducer is because of the losses expected in concrete.

b.1- Output Characterization of the transducers in air

In this series of experiments, the transducers were connected to the pulsers and their responses to the drive pulse were recorded and analysed. Note that these responses are not echoes, but the ringing of the transducers produced immediately after the drive pulse is received. In these tests, the transducers were free-standing in air.

Fig.9.6 represents the output of 500kHz transducer with its associated frequency spectrum. The input pulse width can be seen to extend to about 100 μ s, which is unacceptable for our purposes (we require a dead zone of approx. 30 μ s or less to detect a reflection from strand at 60mm deep in concrete).

The ringing of the tungsten-loaded epoxy transducer extends to around 40 μ s, which is a considerable improvement on the above. Fig.9.7 shows the output and its frequency spectrum. The epoxy-putty backed transducer, whose output is given in fig.9.8, is less damped than the tungsten backed but is still better than the 500kHz probe. It gave a ringing time of about 60 μ s.

The above experiments were carried out using the low-voltage pulser. However, when the high-voltage pulser was used, the ringing times for the transducers were increased.

b.2- Output Characterization in concrete

The low-voltage pulser and the 400kHz transducers were used to try to receive the echo from the base of a concrete cube of $150 \times 150 \times 150 \text{mm}^3$. The expected echo would be received at $75 \mu\text{s}$. But no echo was received. Therefore, smaller dimension cubes were used $100 \times 100 \times 100 \text{mm}^3$, but no echoes were received either.

When the high voltage pulser was used with the specially built transducers, the ringing time as mentioned before was too long to be able to detect the reflected echo i.e. any echo would be embedded in the input pulse.

It is worth mentioning that the more the transducer is backed or damped, the more its sensitivity is decreased, which means if the reflected intensity is small, and the transducer is not sensitive enough or very well damped, the echo will not be detected, which could happen when using these transducers which are well damped.

b.3- Discussion

In terms of ringing characteristics, the tungsten-loaded epoxy backed transducer gave shorter pulse-width. However, because it is well damped, the reflected echo from concrete is very weak and is not detected. Amplification does not improve the situation because no echo is identified at the transducer crystal and the signal amplified will be the input pulse itself with the noise present. Moreover, if a transducer with air backing is used, the ringing time is too long and the reflected echo will be embedded

in the input pulse and will not be recognised. It should be noted that the expected signal will be weak due to scattering and absorption. After this study, it was decided not to continue to investigate the method of pulse-echo (using one transducer to transmit and receive the signal) further.

c- Laser-Generation Acoustic Waveforms

The experiments using this method were carried out in the Department of Instrumentation and Analytical Science with the help of Dr Dewhurst.

The use of pulsed lasers to generate high-frequency acoustic pulses in both solid and liquid is well known. In solids, the method has been applied to non-destructive testing and elastic constant measurements (111, 112, 113). The experimental arrangement used is shown in fig.9.9.a. A Q-switched Nd:YAG laser was operated in a multimode configuration to give energies up to 40 mJ with a typical half width duration of 27 nsec. The unfocused beam diameter, measured using a photodiode array was 3.5mm full width-half-height. The average optical power density produced by the laser on the surface of a concrete block was 13MW/cm² which was insufficient to cause significant changes to the concrete surface condition. However by using plano-convex lenses to focus the laser beam, the incident power density on the surface could be increased well beyond plasma formation. In all the experimental trials a lens was used to get more power focussed by the laser at the surface of the concrete.

A concrete block $150 \times 150 \times 150 \text{mm}^3$ was used with the sides well polished. Acoustic waves generated in the interaction zone travelled through the sample and were detected on the same side (to mimic the pulse-echo method). The waveforms arriving at this side were detected by an ultrasonic transducer of 500 KHz resonant frequency and well damped. The received signal was then displayed, via an amplifier on an oscilloscope. The trace was triggered from the laser pulse via a beam splitter and photodiode. The transducer was placed axial with the laser beam, and was therefore at the epicentre with respect to the acoustic source.

When a laser-generated waveform hits the concrete, both longitudinal (P-) and shear (S-) waves may be propagated, further, a variety of surface waves may be present at the boundaries of the solid.

c.1- Discussion

A number of trials were conducted using a pulsed laser-generated signal directed at a concrete surface in order to assess the suitability of this method with regard to the non-destructive testing of steel components embedded in concrete. Fig.9.9.b shows a received signal from a concrete block.

The reason for trying this method is primarily to eliminate the effect of the ringing of the transmitter. The pulse generated by a laser can be approximated by a delta-function which is difficult to achieve when a low frequency piezoelectric

transducer is excited i.e. ringing time is long.

In practice, however, the most important consideration with pulse generation was not the ringing time of the transmitter alone but the combined phenomena of scattering and dispersion which tended to lengthen a short duration input pulse to not more than 500 μ s when using the laser technique using a concrete cube 150x150x150mm³ and which made difficult to detect the echo reflected from the base. Moreover, the signal generated, as it is mentioned above, produces a strong Rayleigh wave which when present could mask the weak echo from the steel embedded in concrete.

Because of this, the advantages gained by using a short response time transducer as a receiver with laser-generated pulse as a transmitter are overshadowed by the above mentioned factors.

d- Transit-Time or Pitch-Catch Method

Amongst others, Sokolov (114) suggested use of this method to detect defects in metal objects.

Defects or boundaries act as obstacles in the path of ultrasonic waves, and they may allow the waves to pass partially and the other to be reflected such as wire embedded in concrete and they may act as an impenetrable barrier such as voids.

By placing an ultrasonic transmitter at the surface, a signal can be received by a second probe placed at a distance from the

transmitter (see fig.9.3.b). Usually the intensity of the echo received is monitored so that if a defect is in the path of the signal, this will cause a drop in the intensity of the received signal from the back-wall, or a complete lack of it and the echo received in this case will be reflected from the defect.

In this study, along with the monitoring of the amplitude of the signal received, the signal was fourier transformed i.e. phase and frequency spectra, cross-correlated with other signals, filtered (low-pass or band-pass filters applied), and subjected to other signal processing techniques. However the application of digital filtering technique proved to be the most useful technique in finding corroded components and flaws in hardened concrete. This will be discussed in detail in chapter 11.

This technique was used throughout this research by applying two transducers or more i.e. one transducer emitting and up to four transducers receiving mounted like a cross on the surface of the concrete.

9.10- FREQUENCIES USED IN THIS RESEARCH

All the transducers used were compression wave transducers. But in general, a small transducer will radiate compression, shear, and Rayleigh waves.

For a small radiator the particle displacement for compression waves spread outward from the source and decay as $1/x$ in the bulk and as $1/x^2$ at the surface. The relative amplitude is greatest

directly below the source and smallest at the surface. Shear waves behave similarly to compression waves with regard to spreading loss but not with respect to the angular dependence. The Rayleigh wave is concentrated near the surface. The vertical component of the Rayleigh wave displacement is largest below the surface, whereas the horizontal component is largest at the surface. This wave decays as \sqrt{x} as it propagates from the source.

For a small probe with radius, a , such that $a \ll \lambda$ (no sound beam), the total energy radiated (W_m) is divided among the compression, shear, and Rayleigh waves as follows (51):

$w_c = 0.069 W_m$ (compression wave energy)

$w_s = 0.257 W_m$ (shear wave energy)

$w_r = 0.674 W_m$ (Rayleigh wave energy)

However, piezoelectric disks not only expand in the direction normal to the disk surface but also exhibit significant radial motion (51), which contributes to Rayleigh wave generation.

The frequencies used for the pitch-catch technique are as follows:

Resonant Frequency, kHz	Diameter mm	Number of Transducers	Manufacturer
45	25	2	Steinkamp
54	50	4	Pundit
125	25	2	Pundit
150	25	6	Pundit
170	20	7	AE Consultants

Resonant Frequency, kHz	Diameter mm	Number of Transducers	Manufacturer
200	20	2	Steinkamp
250	40	2	Steinkamp
350(rolling)	20	2	Pundit
400	30	3	DIAS
500	30	2	Steinkamp
500	40	1	Steinkamp
1000	20	1	Panametrics

9.11- PULSERS

Five pulsers were used. Two were made at UMIST and were described earlier. One of the last three is a waveform acquisition and arbitrary generator board (WAAG). It is a plug-in board and with its accompanying software, the IBM compatible PC could serve as a dual channel scope and an arbitrary waveform generator. This board was used only as a pulse generator or pulser (two scopes were available to acquire the waveform). One technique tried to reduce ringing time was when a transducer is bipolar-excited, i.e. negative shock then sudden change to positive, to see whether the transducer could be stopped from ringing for a long time after excitation, but in our case with low frequency transducers this could not be achieved. By using this board, any arbitrary waveform can be produced by defining the period and then drawing the waveform on the screen. In this way, a complex waveform is generated with frequency, amplitude, and shape completely determined. This waveform was then used to excite the transducer. The max. output is $\pm 5V$ peak. The board was used to

excite the transducers with different shape waveforms, but because of its low-voltage output $\pm 5V$ i.e. very low output energy from transducer which means that the signal is attenuated quickly in concrete because of scattering and absorption, it was considered to be unsuitable for the purpose of this research.

The other two were mainly used: one of them was supplied by Pundit and the other by Steinkamp. The Pundit unit is designed to excite crystals between 10kHz to 500kHz. The pulses in the pundit are generated at a repetition frequency of 10Hz. The pulse voltage could be 500V or 1kV. It has a 5 digit liquid crystal display. On the other hand, the pulser from Steinkamp has 600V pulse voltage, with pulse repetition frequency of 1Hz. It has a 5 digit liquid crystal display with 18mm height figures. The pulsers both have a measuring range from 0.1 to 999.9 μs .

9.12- SCOPES USED

Two digital storage oscilloscopes were used. With the help of the output unit of the oscilloscope through a microcomputer, the signals were stored on a floppy disc or hard disc and then plotted using a plotter.

a- 2220 Tektronix: Digital Storage Oscilloscope

The 2220 is a digital storage oscilloscope which also provides the analog capability of a conventional non-storage instrument. In the digital storage mode, the instrument is capable of sampling up to 20MS/sec and has an equivalent time sampling

bandwidth of 60MHz. Up to 4K record acquisitions are displayed in 1K record segments or the 4K record can be compressed to 1K for on screen viewing. It has an 8x10cm rectangular CRT, two input channels with sensitivity of 2mV/cm to 5V/cm, and time base between 50nsec/div to 5sec/div. The 2220 was supplied with a GPIB interface to transmit and receive waveform data. Most front-panel settings can be queried and many functions can be controlled over the interface.

b- 5602 Solarton Enertec: Fully Digital Oscilloscope

This instrument has a high sampling rate, 40MHz simultaneous on both channels, which allows storage of fast single or repetitive phenomena. The 5602 analyses the input signal continuously, checks the compatibility within the selected sampling rate, and warns the user of any sub-sampling. The memory depth of the 5602 is 1K/channel, and it could be chainable to 8K.

The two channels displayed on the screen can be saved in four different memories. This capability can be used for: - comparison of input signals with a stored reference. - comparison with a pattern. - later exploitation elsewhere.

Up to 4 traces can be displayed on the screen. It offers the user a wide range of pre-processing and post-processing functions: averaging up to 256 measurements, smoothing, summing, signal multiplication, curve expansion, and many other functions. Cursors are used to obtain the desired voltage, time, frequency or rise time values rapidly, and display these values on the

screen. It has two input channels with sensitivity of 10mV/div to 5V/div, and sweep rate from 20sec/div to 50nsec/div. The user can obtain hard copy record of screen display on analog or digital XY plotters (HPLG compatible). It can be used as a digitizer for slow or fast signals for an associated computer which stores the result data obtained for later processing.

9.13- AMPLIFIER

A four channel amplifier was constructed in CAPCIS, UMIST since a suitable supplier could not readily be found. The amplifier is based upon a classical three op-amp instrumentation design, configured in differential mode (a low noise op-amp, the op-37, has been used). The frequency response is flat from DC to 1.25MHz, with a -3dB point at 1.5MHz. Each channel can be independently configured regarding gain to either 40dB (x100) or 50dB (x400).

9.14- DATA STORAGE AND COMPUTER PROGRAM FOR SIGNAL PROCESSING

A microcomputer system manufactured by Hewlett-Packard (HP) was used. It is formed of HP9816 monitor, HP9121 disc drive, and HP7475A plotter.

A signal processing package using this system was written.

Early experiments on this study indicated that the signals returning to the receiving transducer(s) were buried in noise arising from scatter and Rayleigh waves so that simple time

domain analysis would be insufficient to achieve the desired objectives. Frequency domain analysis involving fourier transformation of the time record led to the identification of the steel component in a concrete structure. The transducers used in these experiments were placed in a pitch-catch configuration. It was therefore decided to write a signal processing software system which can handle up to 4-channels (4 data records, 4K each) simultaneously, table 9.2 illustrates the operational logic of the program.

At the command level or main menu the 'scope' option allows the user to read the two channels of the Tektronix 2220 or the Solartron 5602 digital storage oscilloscopes, which includes automatic sensitivity and timebase detection. Comments are included as an input during the experiment. The data are then stored on a floppy disc as real text values.

After acquiring the data, the user will be given the option to return to the main menu or command level.

The acquired data could be 512 bytes, 1024 bytes, 2048 bytes, or 4096 bytes. The user could perform any operation in the time domain, or frequency domain using any data record length up to 4096. But if analysis is to be made on only part of the data, rather than the full record length, the 'window' option provides the means of isolating a specific segment of the record. This is carried out by using two cursors on the screen and moving them to the positions required.

After windowing the data, the user can return to the main menu, and begin processing the data. He has two options: time domain analysis, or frequency domain analysis.

In the time domain analysis, there are many major options, involving operations on a specific time record or combinations of records. On a single time record, the user has the option of squaring, differentiation, multiplication by a constant, phase shifting (delay the signal or advance it), rms and energy statistics. On the other hand, when two or more signals are to be processed, the options are wave addition, subtraction, multiplication, division, cross-correlation.

In the frequency domain analysis, the FFT routine was used to transform the signal from the time domain to the frequency domain because it is quick to perform (a 1K time record takes about 15 sec to be transformed). The program can hold up to four spectra simultaneously, and these include the real, the imaginary, the magnitude, and the phase components. It may be argued that it is only necessary to hold the real and imaginary components since the other two can be derived from these if necessary. However, the computer used has more than enough memory to accommodate the magnitude and phase, therefore the speed of the processing is considerably enhanced. The 'FFT' option is simple to use and its internal logic ensures that the spectra calculated are consistent regardless of the windowing performed in the time domain. For example for a time record of 1024 values, the FFT will calculate 512 harmonics, according to Nyquist principles, if windowing has been carried out in the time domain (record < 1024), the program

performs zero-padding on the null-values (values number should be power of 2). The inverse FFT, or IFFT retransforms a frequency record to its equivalent time record. A filter design facility was included which is carried out by removing bands of harmonics, called brick-wall filter, subsequently calculating the IFFT on the edited spectrum. The filter facility was included as this proved to be important in identifying corrosion and flaws present in concrete as it is going to be shown in chapter 11. The arithmetic operations in this menu are similar to their equivalents in the time domain and comprise: squaring, element multiplication, rms and energy statistics on a single record, adding, subtracting, multiplying, dividing, and cross-correlating on a group of records.

The final option in the main menu is the display mode. A wide variety of graphical displays either on screen or on paper (plotter) can be generated. There are four basic screen modes which may be selected.

1- Mode 1: full screen, single plot. In this mode the program can display a time record (single trace), a frequency spectrum (phase or amplitude), or a cross-correlation plot.

2- Mode 2: split screen, two plots. In this mode the screen is divided into two sections, any one of which can contain either a time signal trace or a frequency spectrum, or any two records.

3- Mode 3: split screen, three plots. In this mode the screen is divided into three parts, any three data records can be plotted.

4- Mode 4: split screen, four plot. In this mode the screen is divided into four quadrants, any of which can contain any 4 data records.

The mathematical functions of the operations programmed in this software are described in chapter 4.

Although the waveform analyser was superseded by the software, its development has been extremely valuable in identifying and confirming those parts of the signal which contain useful information. Table 9.2 shows the operational logic of the package.

9.15- THE ANALOGIC WAVEFORM ANALYSER, MODEL 6100

The waveform analyser is shown in fig.9.10. Analogic manufacture a range of A to D converters to suit various applications, and most are housed within the body of the processor unit. The A/D chosen project was the 6100. The model 6100 is a dual channel, 8-12 bits user selectable, 20MHz (sample speed) if one channel is used, and 10MHz if two channels are used. It has range selection to $\pm 0.125V$ if one channel is used and $\pm 0.5V$ if two channels are used. The device can store 64K bytes of signal data on one channel, or 32K bytes per channel if both are used.

The model 6100 has very comprehensive capabilities of operations. There are more than 50 waveform analysis, manipulation, and signal processing functions, including forward and inverse FFT's,

chirp-Z transforms, convolutions and correlations. The scalar operations include period, frequency, cycle, rise time, delay, pulse width, rms, mean, area, energy, max, min, and many other operations. Record operations include addition, subtraction, division, zoom zct, FFT including spectrum magnitude plus phase for real or complex inputs, cross-correlation, auto-correlation, differentiation, integration, and N times averaging, etc.

The analyser can also be pre-programmed to step automatically through a sequence of operations once the analysis procedure has been established. The analyser has on-board software to produce hard-copy, high quality plots to a plotter (HP7475 was used), and it can also be interfaced to any IBM compatible or HP computer (to act as a controller and data store) using its existing IEEE interface. A subroutine was therefore added to the software (under the 'scope' option) described earlier to control the analyser and store data on floppy disc.

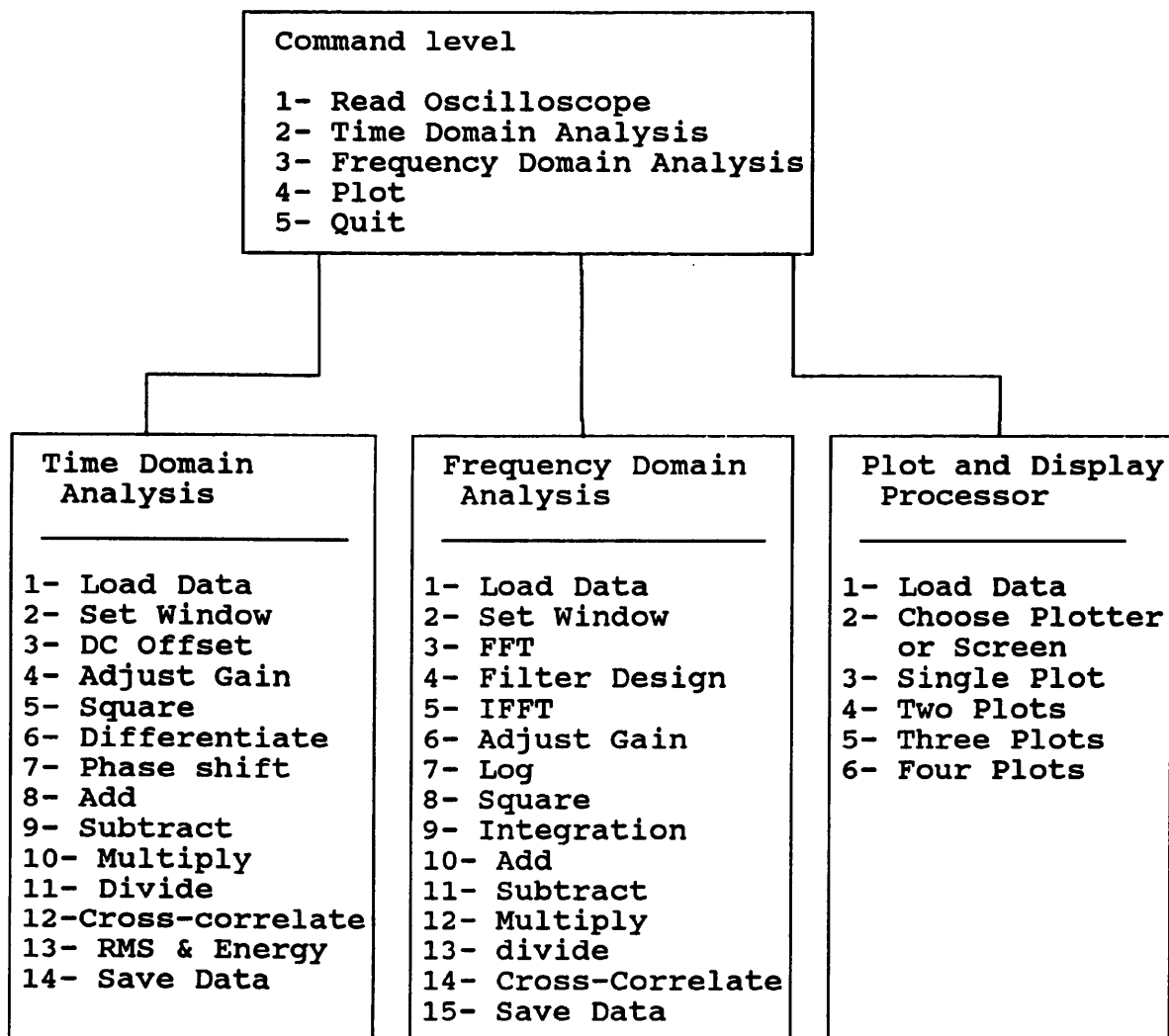
9.16- SUMMARY

In this chapter, descriptions of materials, specimens, instrumentations, computer programs, and techniques used in testing have been given. It was shown that the method adopted for concrete testing in this research is the pitch-catch technique together with signal processing techniques specially the application of digital filtering technique, this will be discussed in chapter 11.

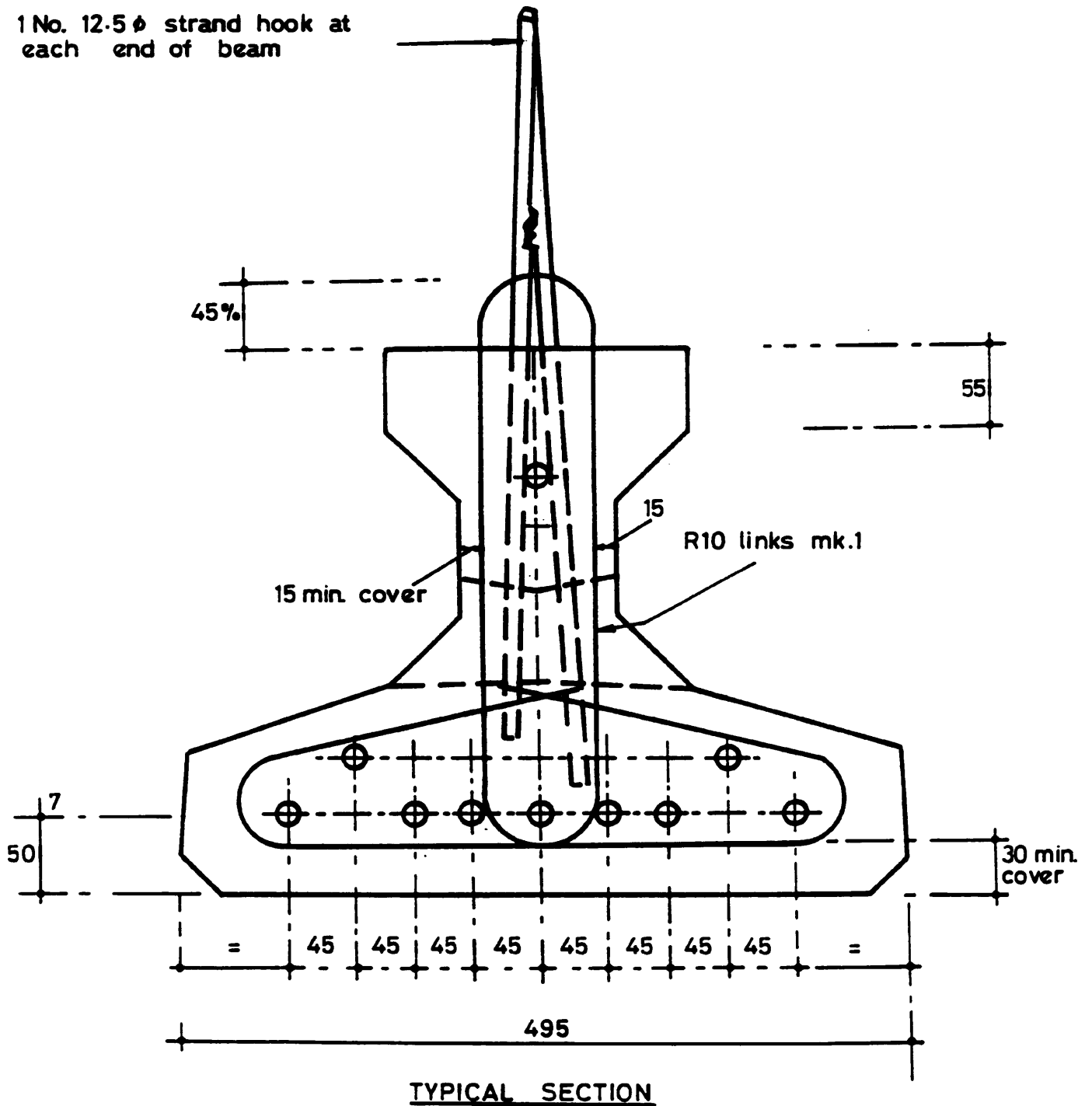
Table 9.1- Concrete Mixes Characteristics

Type of cement	Max. Aggr. mm	W/C	A/C	Design Density Kg/m ³	Average Strength N/mm ²	Slump mm
RHPC	20	0.55	4.55	2400	40	75
OPC	20	0.65	5.56	2400	30	65
OPC	15	0.595	4.96	2400	30	75
OPC	Fine	2	5.77	2400	-	-

Table 9.2- Operational logic of the signal processing program written on the Hewlett-Packard computer



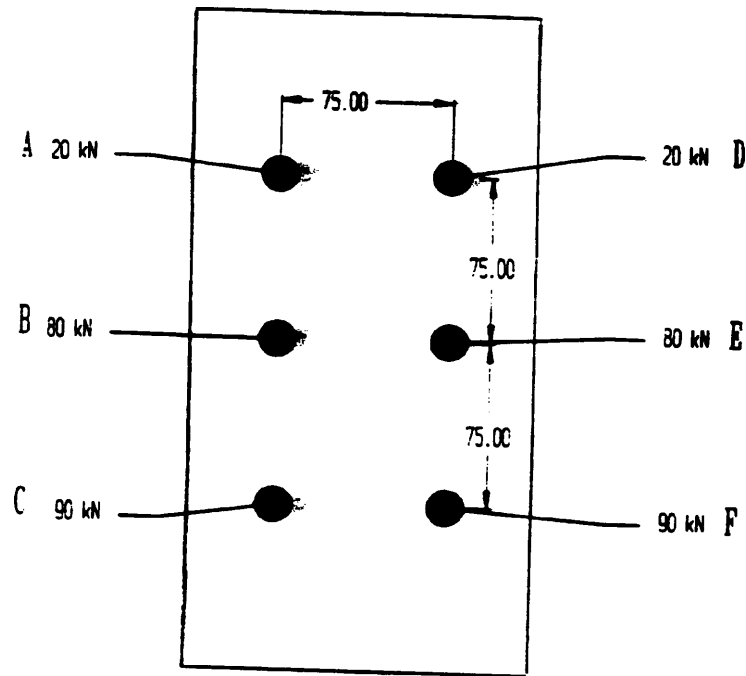
1 No. 12.5 ϕ strand hook at each end of beam



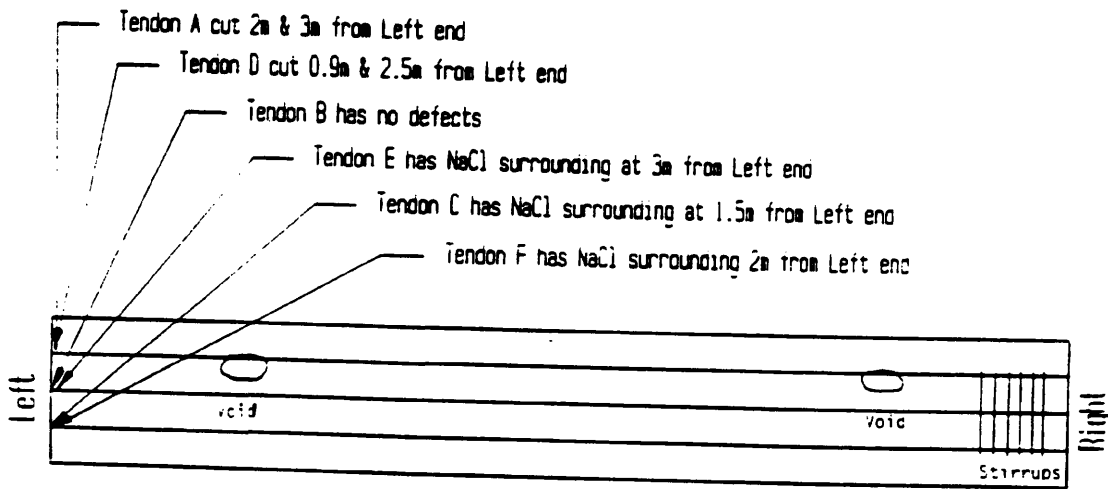
Overall length 8.79m

Overall weight 2.19t

Fig. 9.1- Cross-section of the bridge beam.



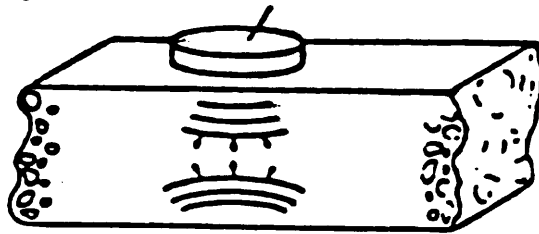
a) Section showing stresses in each Tendon



b) Elevation of beam showing Defect Positions

Fig.9.2-- Large scale test beam, showing details of internal reinforcement and defect locations.

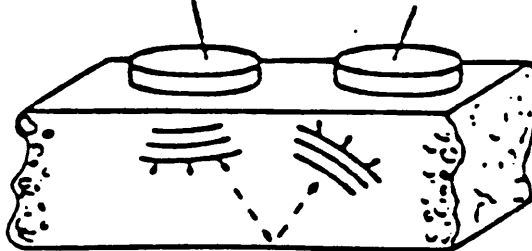
Transmitter and Receiver



a

Pulse-Echo

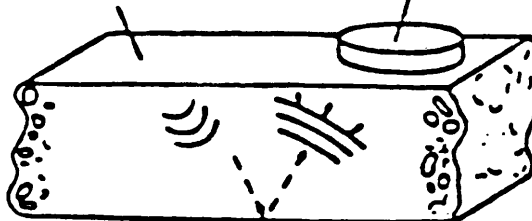
Transmitter **Receiver**



b

Pitch-Catch

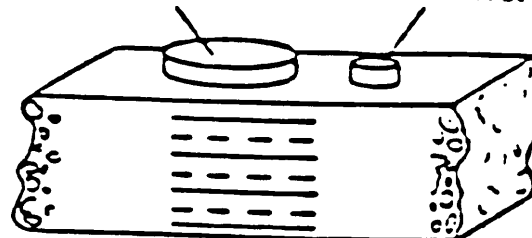
Impactor Source **Receiver**



c

Impulse - Excitation

Transmitter **Receiver**



d

Resonance

Fig.9.3

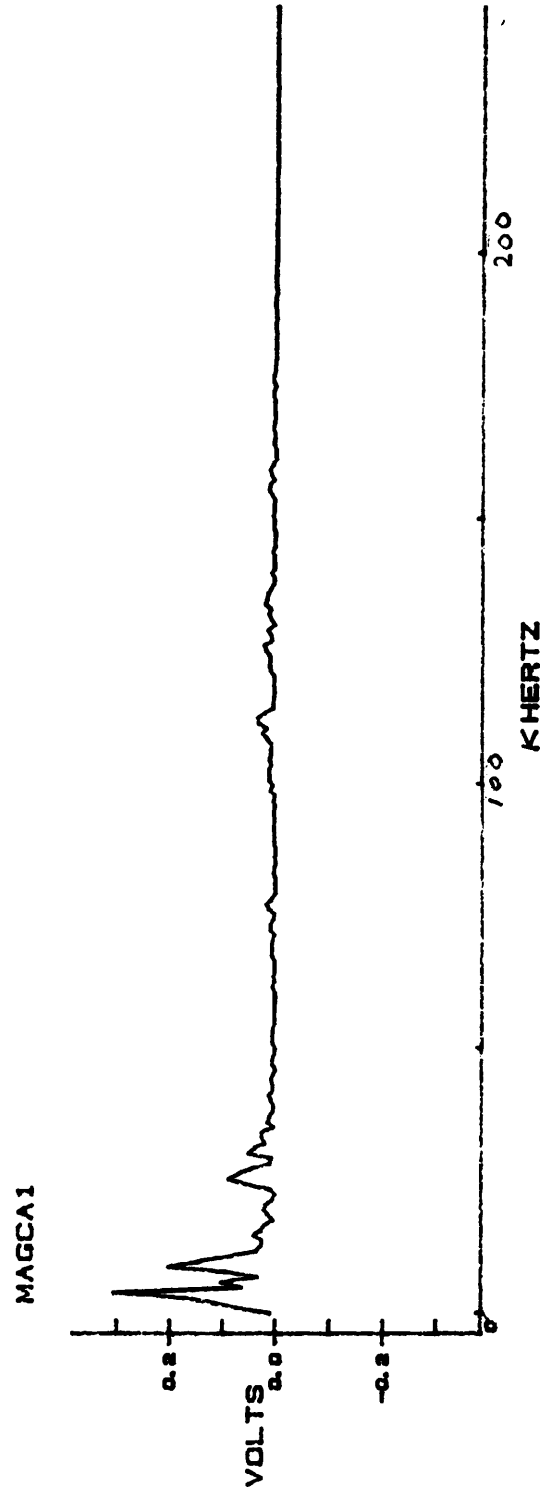
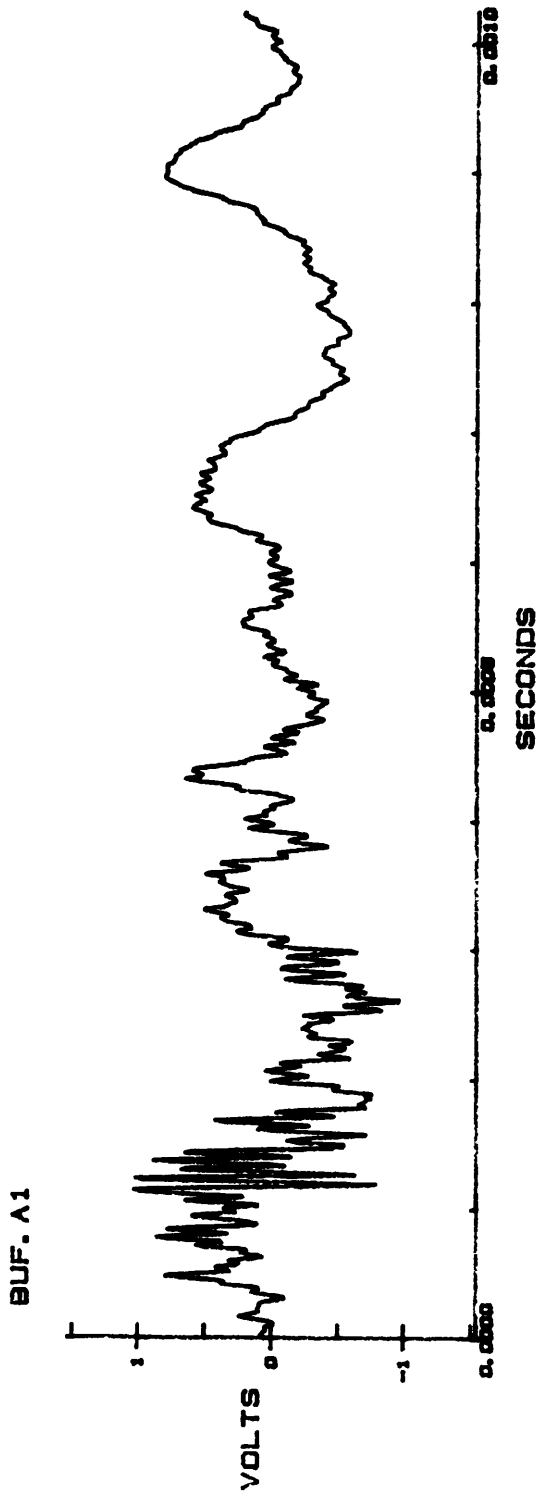


Fig.9.4- A time signal received when impulse-excitation is used on concrete and its spectrum.

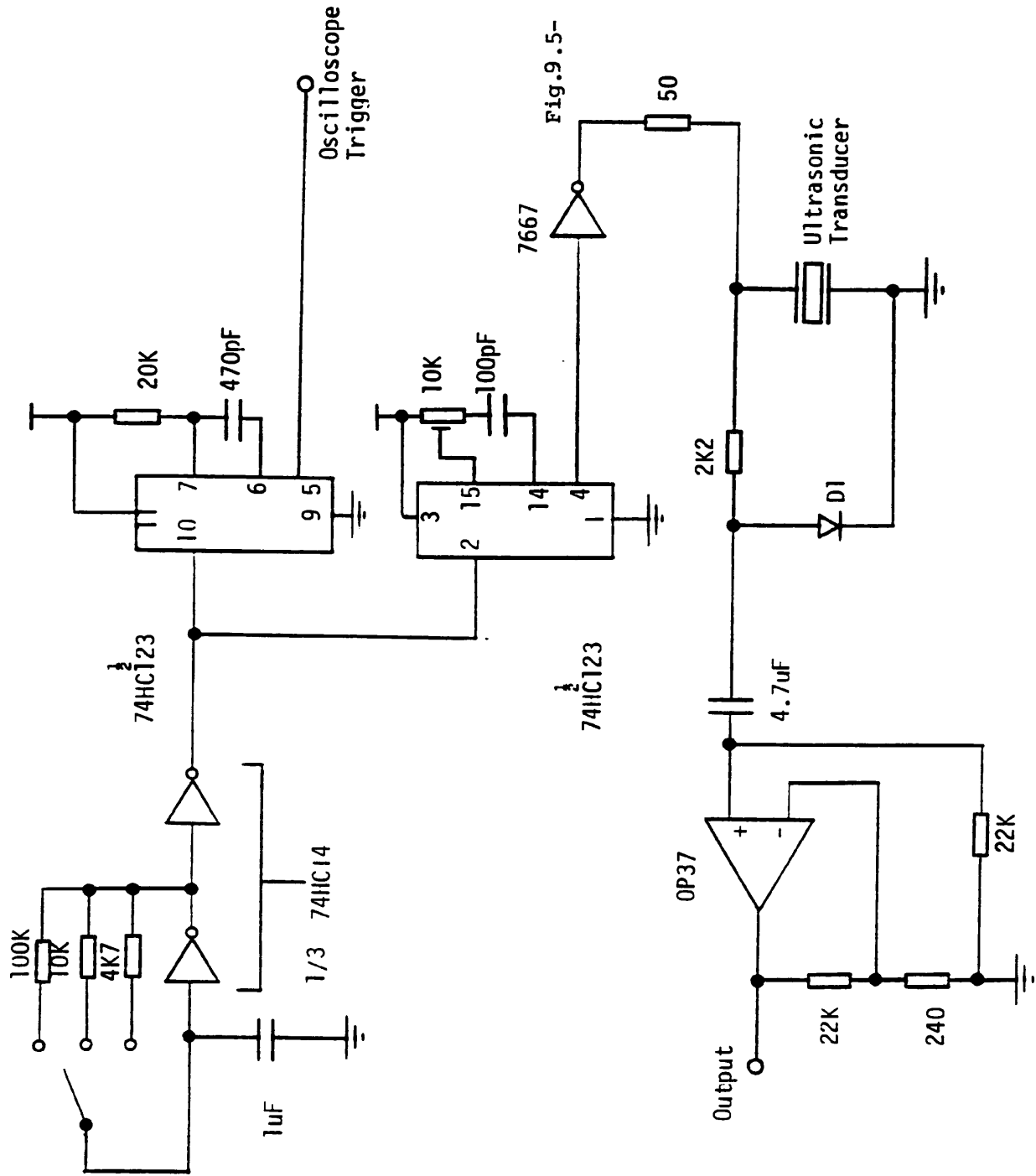


Fig.9.5- Pulse-Echo System Circuit Diagram
Note: For purposes of clarity, decoupling capacitors and power supply connections have been omitted.

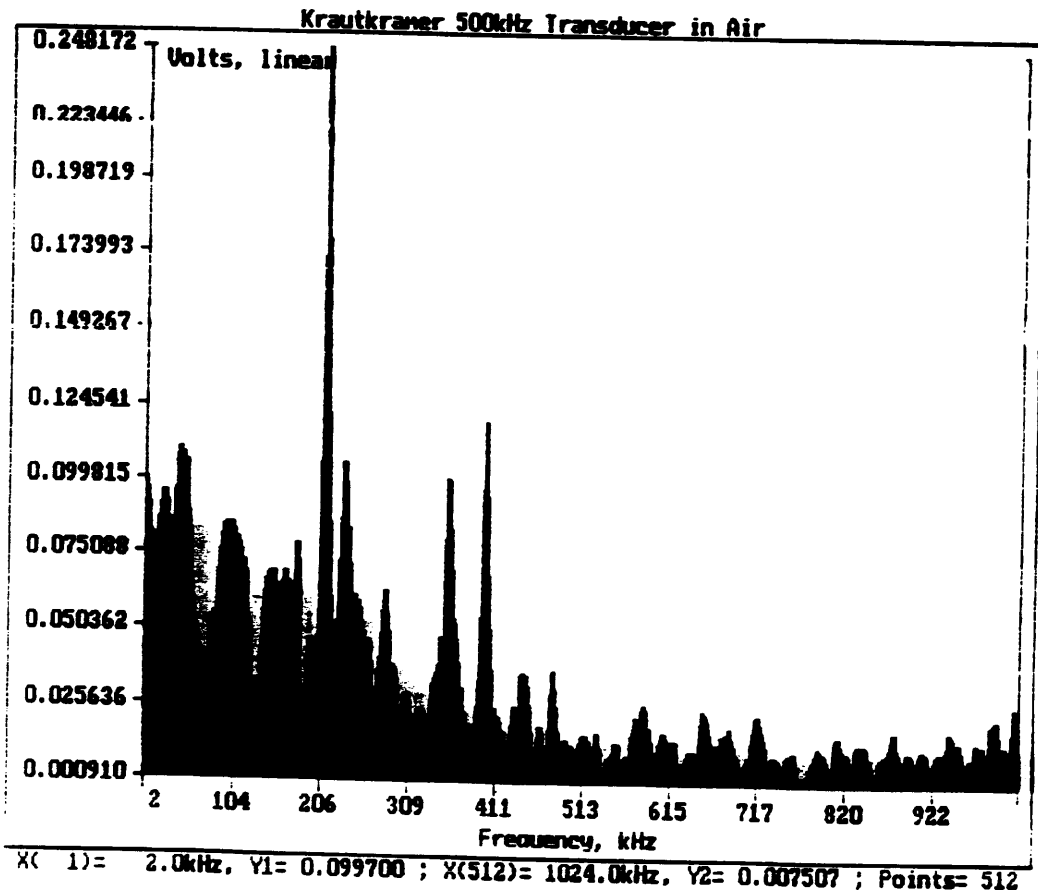
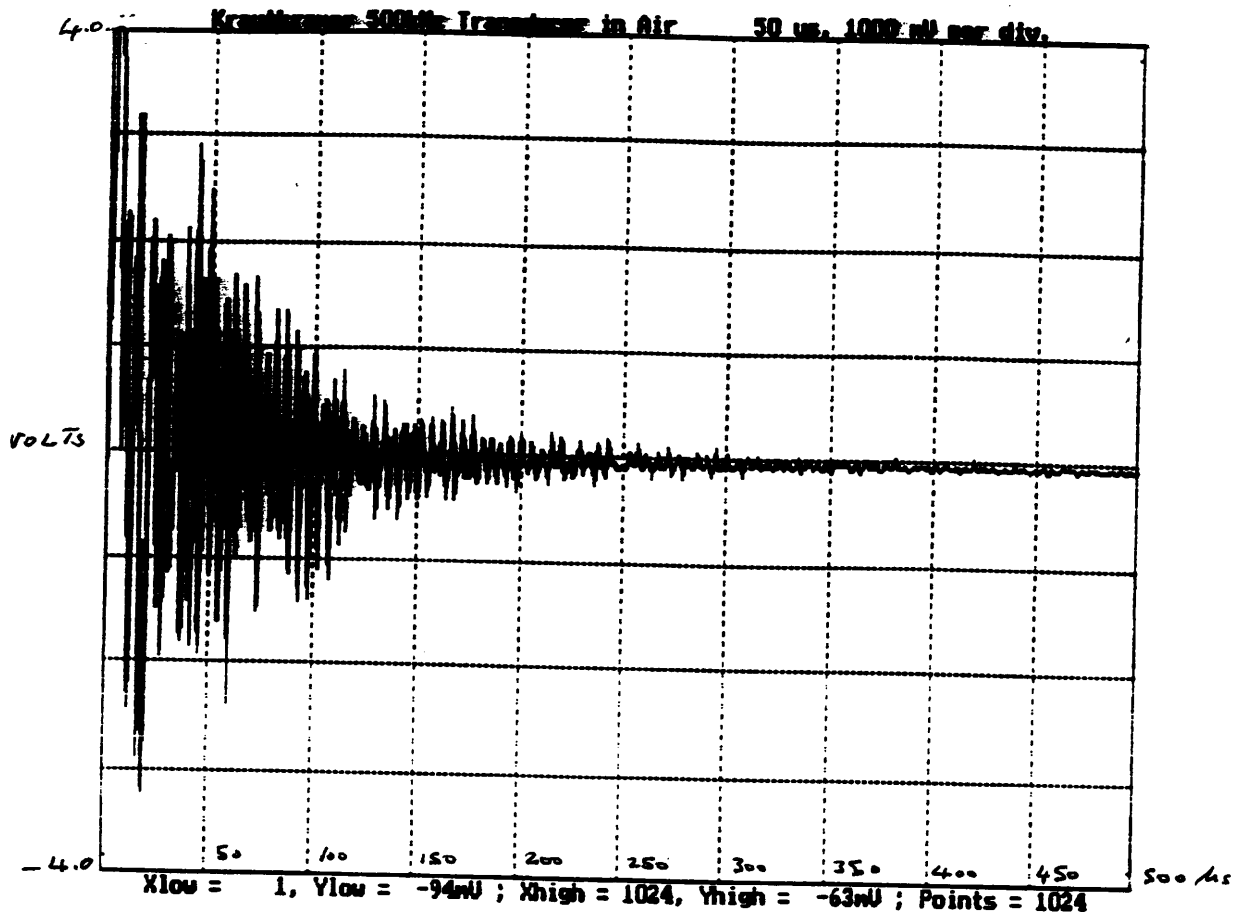


Fig.9.6

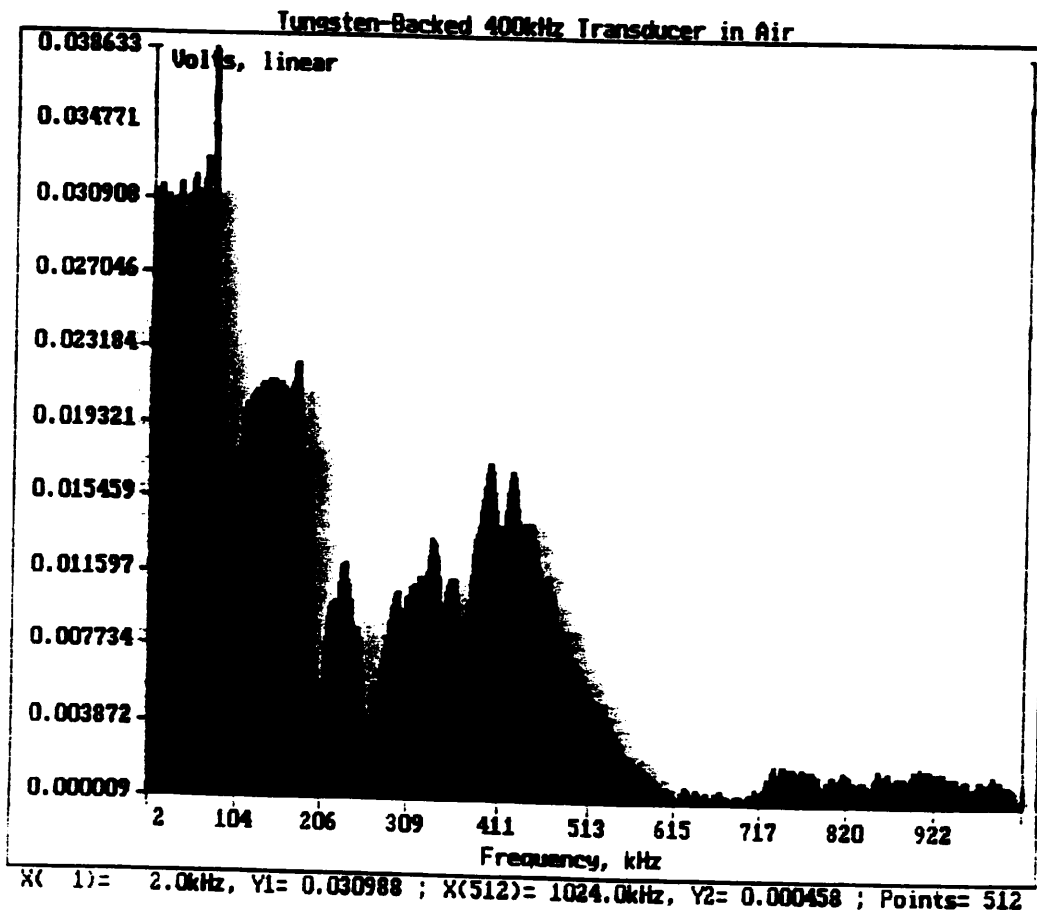
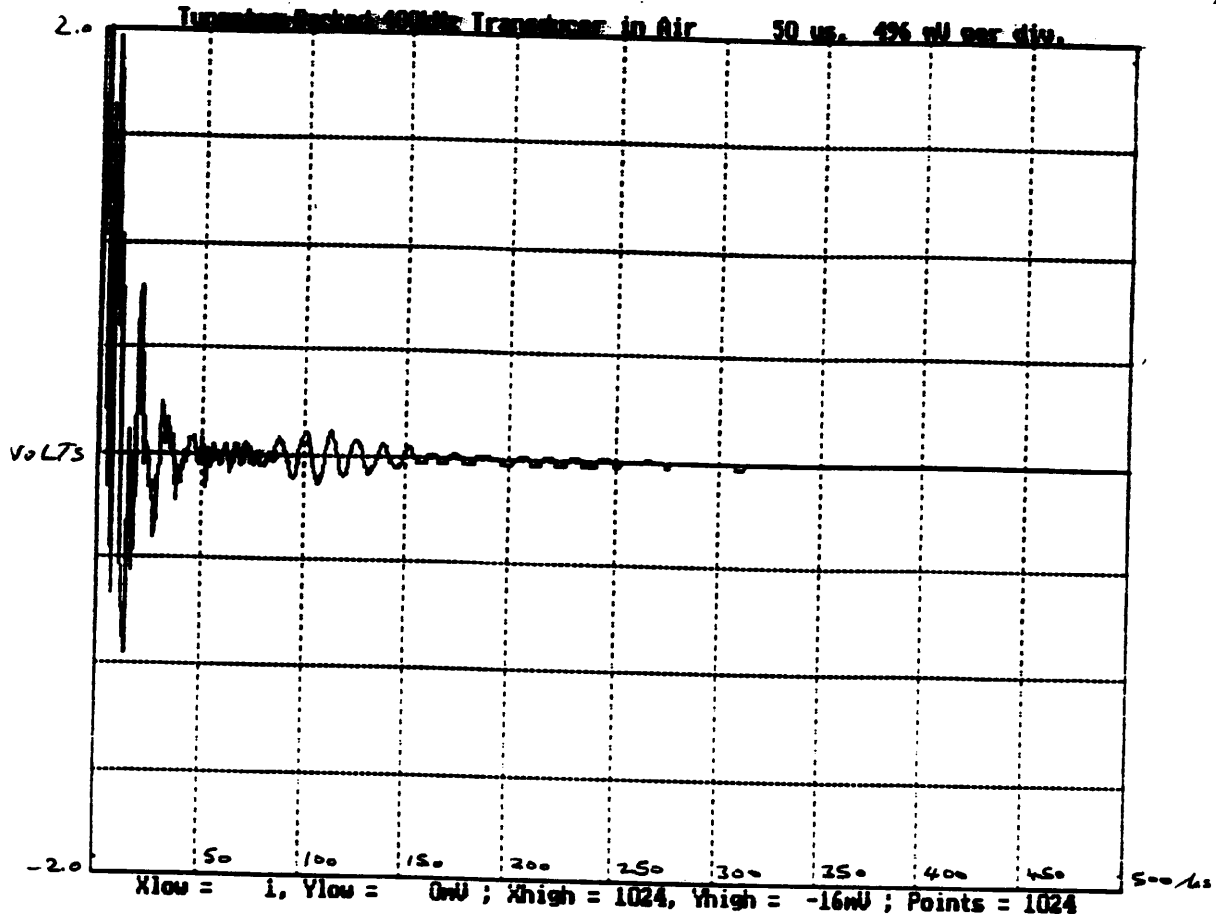


Fig.9.7

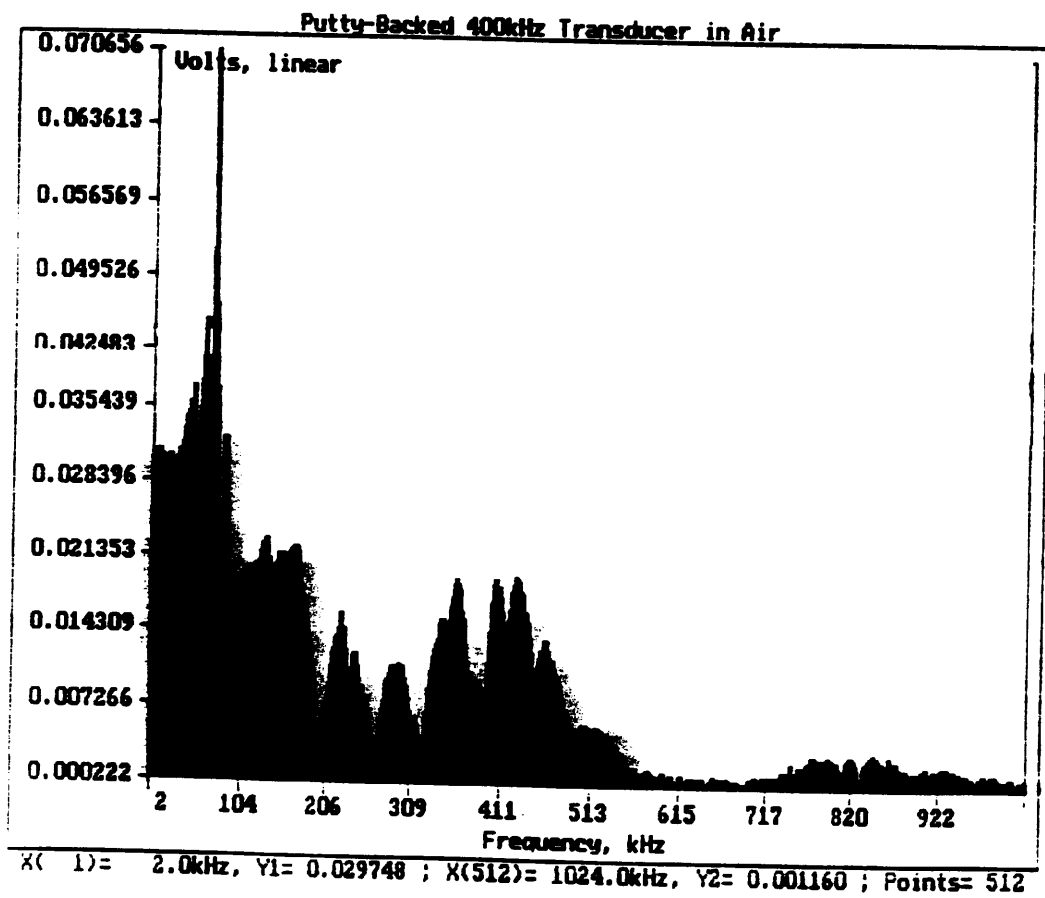
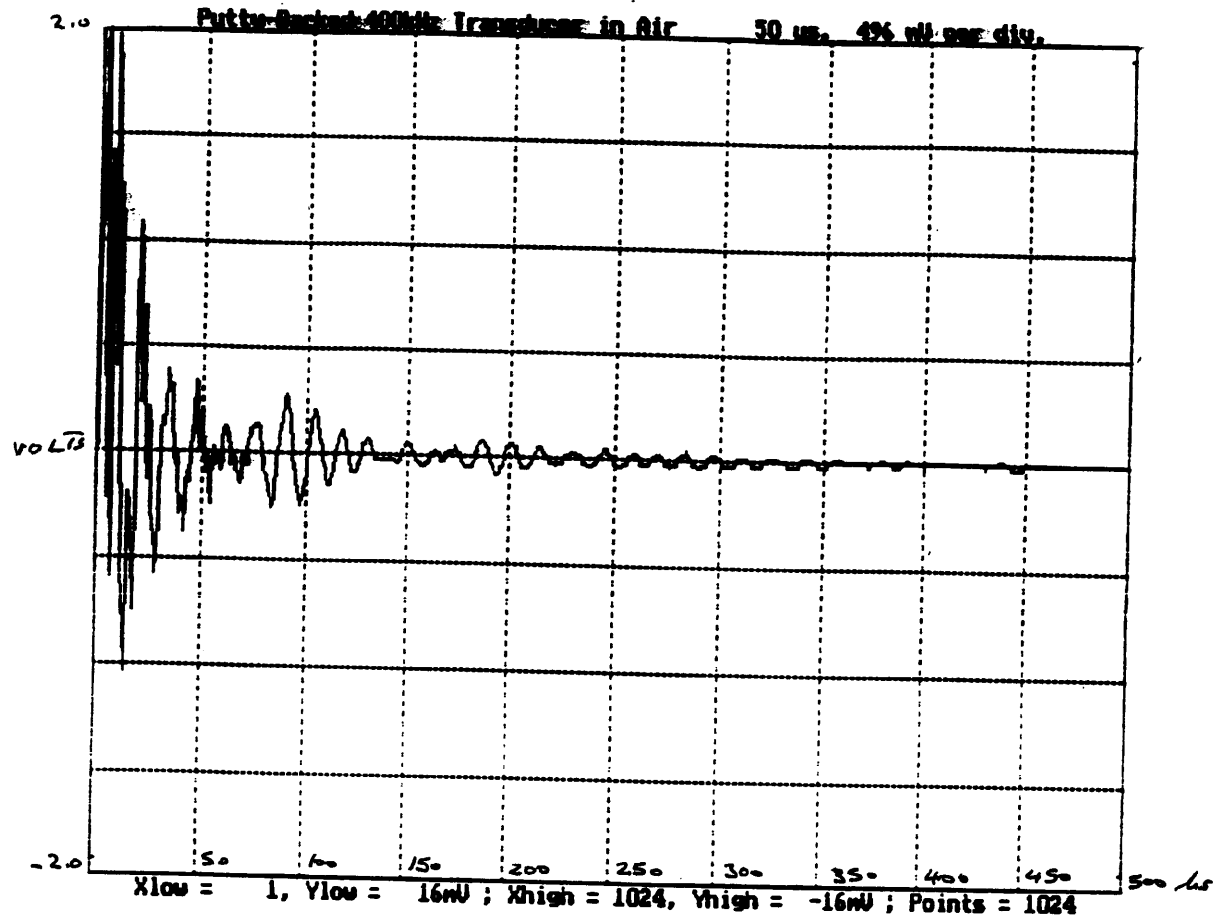
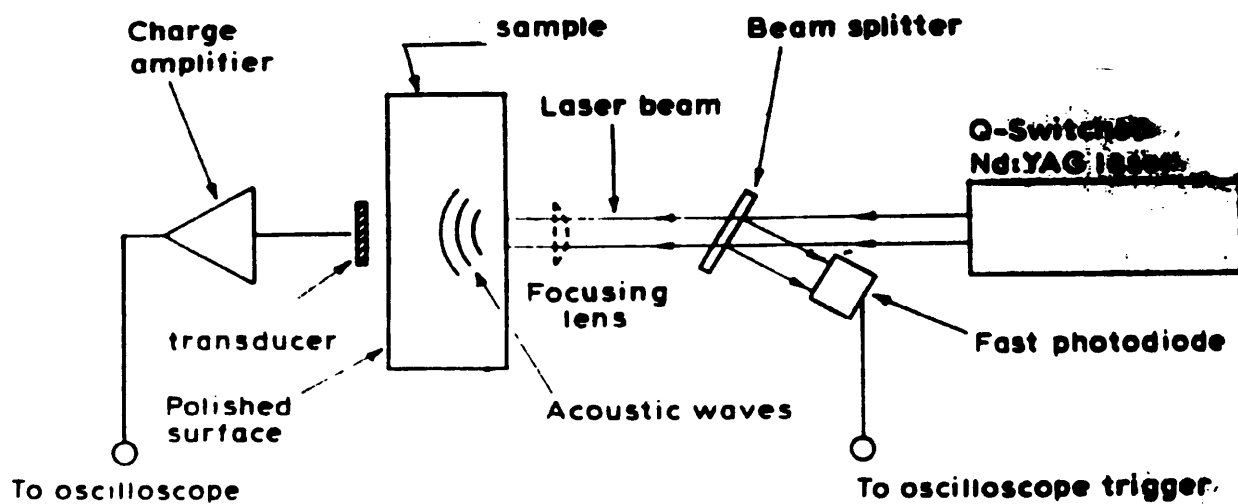
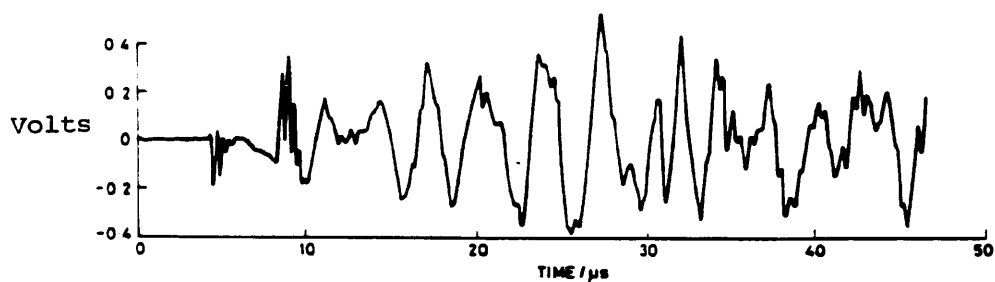


Fig.9.8



a) Experimental arrangement for laser-generated acoustic waveform.



b) Received signal from laser generated signal.

Fig.9.9

With Fast Access To All Processing, Analysis and Programming Functions

Read current parameters instantly on:

- Independent, dual timebases
- User-selectable trigger conditions for each timebase
- Offset and scales of displayed traces
- Signal-processing operation parameters

Display up to 4 traces (separately or overlaid)

- Expand or compress displayed waveforms
- From 0.005 to 512 times on Y axis
- From 0.25 to 64 times on X axis

Position display marks to:

- Automatically identify waveform features
 - calculated to 5 decimal places
- Locate baseline on each trace
- Set cursor at independent start and interval settings
- Place crosshair via 3 modes (Center, Origin, Trigger)
- Set grid (graticule) X and Y sensitivities independently

Soft control fields speed parameter entry

- On-screen labels for soft controls guide you effortlessly through setups
- Initiated setups allow immediate "turn-on" operation
- Appropriate setup choices displayed automatically for each plug-in module and option
- Coarse and fine increment control helps you zero in to right value

Set up the display with maximum flexibility and call up powerful programming, HELP, I/O functions

- Assign any data record to be displayed at any trace
- Display any combination of live, processed and stored waveforms
- Select offsets and scales independently for any waveform
- Use conditions, branching and looping statements and subroutines to fully automate test functions
- Simultaneously capture the trends of multiple scalar measurements—limited only by memory-point storage
- Access multilevel HELP screens—with one key
- Configure IEEE 488 commands, RS232C ports, plotter controls—from the front panel
- Receive and transmit all commands, data to and from external controllers, computers—under program control

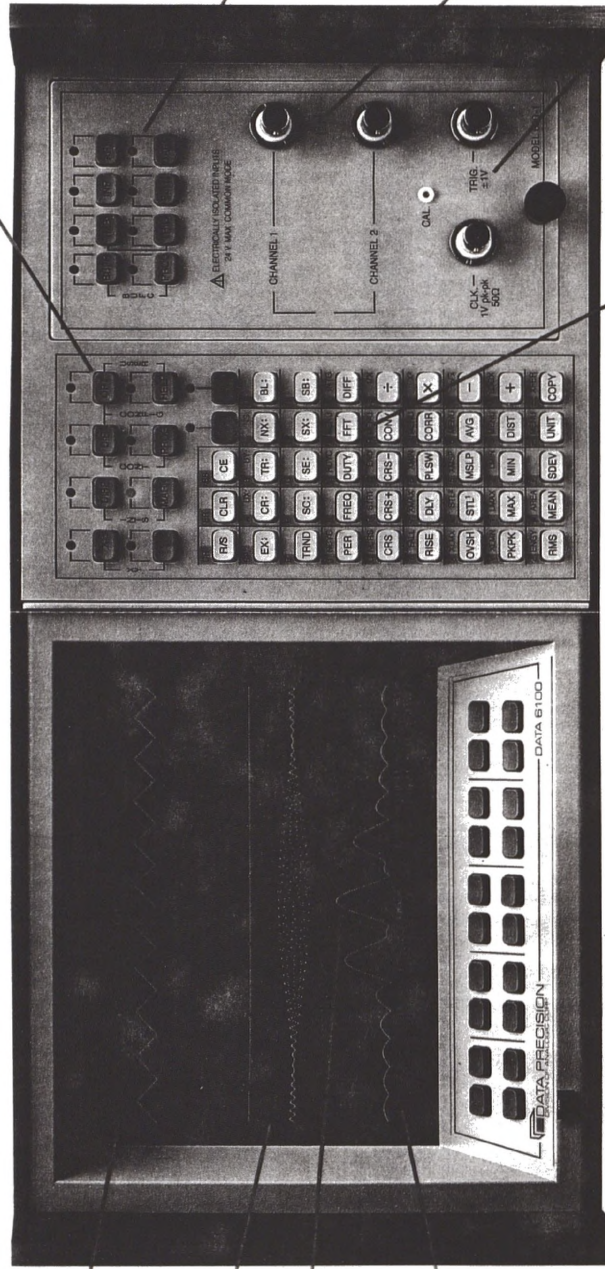
Set up the acquisition for almost unlimited source-to-acquisition conditions

- Choose from 100 MHz, 8-bit sampling up to 1 MHz, 16-bit sampling or 1 GHz equivalent sampling
- Store up to 240,000 16-bit data points
- Select timebase sampling period—with equivalent sampling to 10 ps/data point
- Select up to 16,000 data points of pre-trigger delay and up to 64,000 data points of post-trigger delay (Models 650/652)
- Average up to 32,000 sweeps of live data
- Process input signal with any of 26 preprogrammed filter values

Independently configure analog inputs for each channel

- Single-ended, differential, ac coupling, dc coupling
- +100V continuous without damage (Models 610, 611)
- Up to $\pm 50V$ full-scale measurement ranges (Models 610, 611)

System integrate with external trigger, timebase



Utilize powerful one-key digital signal-processing functions

- Turn on ZOOM CZT for unparallelled spectral resolution—down to a few mHz
- Quickly compute and display any of 18 FFT functions—added by six window functions
- Perform any of 21 record-to-record operations—including Convolution, Auto-correlation, Cross-correlation and two Averaging modes
- Select parts of a waveform and calculate any of 23 scalar results—with 5-decimal-place resolution
- Automatically repeat or chain processing operations—screen will be updated with live data

Fig.9.10- The Analogic Analyser.

Multilevel Help Screens Guide Command, Parameter Entry

Using the 6100 will increase your waveform-processing throughput but not your frustration level. Multilevel HELP screens ensure that help is always only one keystroke away. Pressing the HELP key and any key, immediately flashes a series of screens explaining the set-up and control of the functions governed by that key. Pressing softkeys under displayed data-entry and control fields explains their operation—and allows you to scroll back and forth through the screens. Meanwhile, if you need HELP with any other key's function, simply press that key, display HELP screens for it, and go back automatically to where you left off by pressing HELP again.



Pressing the HELP and PROG keys displays fields controlling the insertion, deletion and renaming of programming instructions. Activating a softkey under the "INSERT" field indicates how to add a line to a 6100 control program.



Plate 9.1- Test beam during construction, showing detail of stirrup location.



Plate 9.2- Completed test beam.

CHAPTER 10

WATER MODEL

10.1- INTRODUCTION

An extensive series of modelling tests has been carried out using a multiprobe array system to examine different samples of steel rods in a water tank. The multiprobe array system consisted of a central transmitting transducer, surrounded by two identical receiving transducers. The scattering effect of concrete was modelled by plastic granulesⁱⁿ some of these experiments.

These tests were performed in order to identify those parts of the received signal which carry information about the condition of the steel. They were successful in locating the position of the steelwork and the presence of cut/broken wire or significant loss of cross section of the wire by corrosion.

10.2- EXPERIMENTATION

Plate 10.1 shows the linear transducer array used in the trials and plate 10.2 shows it in position inside the water tank. The centre transducer acts as the transmitter, with the two outer transducers (channel A and channel B), set 76.2mm from the transmitter (as measured from their mid point), acting as receivers. The array is positioned with the faces of the probes in contact with the surface of the water.

The transducers were selected to be as closely matched as possible with regard to spectral characteristics and sensitivity. Table 10.1 provides some statistics relating to these parameters, inevitably these will not be identical. Figs.10.1 and 10.2 represent the time records and spectra calculated for transducers A and B, in response to a signal sent by the transmitter through water using a 600V spike. The water depth in all experiments was 263mm.

When a 10mm diameter bar is present, it was always at a level of 52mm below the transducers, fig.10.3. At 121kHz (peak frequency), the half-angle of divergence in the far-field for a circular transducer of 25mm diameter in water is 36° . The depth was chosen so that the receivers responded only from the outer edge of the beam reflecting off the mid point of the steel bar, while this reduced the pressure to 28% of that measured from the centre axis, it ensured that the channel separation was maximised with respect to receivers A and B, therefore making signal comparisons more meaningful.

With this system, seven experiments were carried out and analysed. All used a 10mm diameter high tensile steel bar, 950mm in length. These experiments comprised the following:

- 1- Good steel, no defects.
- 2- Steel with saw-cut, 2.5mm width and 5mm depth, position midway between transmitter and channel B.
- 3- As (2), but with saw-cut moved under the right hand edge of

transmitter.

- 4- As (2), but rotated through 90°.
- 5- Bar with force-corroded area, 30mm in length and radial reduction of 1mm, positioned midway between transmitter and channel B.
- 6- Bar left to corrode naturally in tap water for three months.
- 7- Scanning of force-corroded bar as in (5) from right to left.

After the results were obtained with the above samples, the water environment was made less homogeneous by the introduction of irregularly shaped polystyrene beads, with a mean particle diameter of 4mm, see plate 10.3. Polystyrene has a specific gravity of 1.06 and in order to make the beads float in suspension, it was necessary to dissolve salt in the water using a ratio of 16:1 water to salt by mass. This addition has increased the velocity of sound, which was measured at 1542 m/s in comparison to 1480 m/s for fresh water. The speed of sound in polystyrene for compressional waves is 2380 m/s, which gives acoustic impedance of $1649.9E+3 \text{ Kg/m}^2\text{s}$ for water and $25228E+3 \text{ Kg/m}^2\text{s}$ for polystyrene. This difference in the acoustic impedances will cause signal scattering. Since the wavelength will increase if the velocity increases for a given frequency, and hence the beam divergence angle, therefore the depth of the bar in these experiments was adjusted to 50mm.

Experiments performed with this system comprise the following:

- 1- Water with aggregate.
- 2- Good steel with no defects.

3- Scanning of force-corroded bar from right to left.

4- Low-frequency interrogation, 45 kHz transducers.

The final set of water based experiments utilised a 4-channel system, that is, two additional transducers C and D, as shown in fig.10.4. It was intended that these transducers should provide positional information with regard to the steel cable and hence ensure the correct orientation of the transducer array. Experiments carried out were as follows:

1- Examination of bar with force-corroded area.

2- Examination of good bar displaced towards transducer D.

10.3- MODES OF ANALYSIS

The signal rms, and amplitudes at 41 kHz and 121 kHz were calculated for channel B, since the defect, when present was normally located between the transmitter and receiver B (see table 10.2).

In addition, not only channels A and B were compared against each other, but each experiment was compared against the experiment of the good quality bar. In the time domain, this comparison was made by calculating the delay or phase shift for the first $26.4\mu\text{s}$ after the initial echo had been received (each sample point represents $0.1\mu\text{s}$).

Frequency domain analysis was performed by calculating the FFT of the first $36.4\mu\text{s}$ (here each sample point represents $1.0\mu\text{s}$), that

is, up to the point at which an echo was returned from the bottom of the tank. Two readings were therefore required for each experiment, one taken at a sampling speed of 1 MHz, and the other at 10 MHz.

In the scanning experiments, only time-domain i.e. phase change was considered and because these phase changes are of the order of fractions of a microseconds, the sampling speed was increased to 50 MHz

When aggregate was present in the water, spectral analysis was also performed since it is the interaction of steel, aggregate and mortar within the concrete that initiates the frequency changes of the output signal.

For the four channels experiments in water, signal onset times were measured for channels C and D to calculate the bar displacement.

10.4- DISCUSSION

10.4.1- Good Steel v Steel Cut between Transmitter and Channel B

(fig.10.5)

Table 10.3 shows that for the good bar, the reflected signals are in phase i.e. no delay and that there is a high degree of correlation between their spectra (A1, B1). The 121 kHz component exceeds the 41 kHz by 6 times for a good steel bar (table 10.2). Fig.10.5 show the strong echo which is returned from the surface

of the good quality bar.

By contrast, in the case of the cut steel the signal arrives $0.6\mu\text{s}$ later than that of no cut. Although there is a general attenuation of the overall signal the high frequency component is weakened and the ratio HF/LF has fallen to 3.6.

In both cases, the good steel was positioned below receiver A, therefore a comparison of A1 and A2 should yield a high correlation, which is the case. Similarly, a comparison of B1 and B2 should reveal discrepancy, similar in form to the comparison between A2 and B2 (table 10.3).

The attenuation of the high frequency components when a defect is present is readily explained since the shorter wavelengths are more susceptible to scattering at the points of defects or discontinuities. Moreover, the phase change indicates that an echo from a defective area such as a saw-cut actually arrives later than an intact region.

10.4.2- Good Steel v Steel Cut under Right hand Edge of the Transmitter (fig.10.6)

With the cut displaced towards the transmitter it becomes progressively more difficult to make distinctions between the signals arriving at transducer A and B, since the cut is no longer at the point at which the edge of the beam coincides with the cut, bearing in mind it is the echoes of edge of the beam to which the receivers A and B respond.

Table 10.2, still indicates a reduction in the high frequency components which is not as pronounced as when the cut is midway. This could be due to the fact that the surface of the steel bar was not very smooth. Moreover, table 10.4 still indicates a phase change of $0.2\mu\text{s}$ (channels B1, B2). Similarly to the argument above this could be due to the very small irregularities on the surface of the bar.

10.4.3- Good Steel v Cut and Axially Rotated through 90° ,
Midway between Transmitter and Channel B (fig.10.7)

Assuming that the wave front is most affected by the upper surface conditions of the steel bar, it is expected that the results obtained when the bar is axially rotated through 90° contain less contrast than the results in section 10.4.1.

Table 10.2 indicates that the HF/LF ratio has fallen to 4.1 which suggests that part of the high frequency components is scattered. However, table 10.5 suggests that phase difference do exist for channels A2 and B2. This suggests that the system, when it is aligned parallel to the length of the wire, is most sensitive to defects present on the upper surface.

10.4.4- Good Steel v Force-Corroded bar (fig.10.8)

This was a comparatively large defect, involving a 36% reduction in the steel cross-sectional area over a length of 30mm. This feature is readily identified both in time and frequency domains.

Fig.10.8 shows the wavefronts detected by probes A and B, and the significant phase delay which occurs as a result of this defect

The most important aspect of the analysis is the comparison performed in the time domain, which provides a reasonably accurate measure of the reduction in the thickness of the bar. A dimensional change of this kind initiates a phase discrepancy between the wavefronts arriving at channels A2 and B2, since the signal reflected from the defective region takes $0.9\mu\text{s}$ longer to reach the receiver (table 10.6). This when estimated in terms of distance, (with respect to the velocity of sound in water), is 1.3mm. It should be noted that the wavelength of the interrogating signal is at least 12 times greater than the dimension of the flaw detected. This is of crucial relevance with regard to any system developed for concrete, since the frequency must be low enough to minimise the scatter induced by the aggregate, yet high enough to enable dimensional measurements to be made. Moreover, table 10.2 reveals the scattering of the high frequency components in a such case ($\text{HF/LF}=3.75$).

10.4.5- Good Steel v Naturally Corroded Bar (fig.10.9)

In this experiment, the bar was superficially corroded along its entire length through immersion in tap water for a period of 3 months. Table 10.7 indicates that a phase difference exists but it is random since the process involved generate random changes to the surface conditions of the steel (in dimensional terms), from one point to the next. Because the corrosion which has occurred is fairly small, it is estimated that much greater

detail would be required in terms of signal sampling speed, to resolve with certainty any changes to the received waveforms.

10.4.6- Scanning of the Corroded Bar (fig.10.11)

Fig.10.10 illustrates how the bar was scanned from right to left using the linear array system. As the defect passes under the transducers, changes occur in the phase relationships between the signals arriving at transducers A and B. These changes are summarised in the plot shown in fig.10.11, in which the x-axis represents the defect position as measured from the centre point of the transmitter, and the y-axis represents the phase discrepancy between transducers A and B, using A as a reference. The first and last points (-90mm and 90mm) actually lay outside of the range of the system and the readings for this point should, ideally, be zero. At the second point (-61mm), the defect lies under and to the right of transducer A and a slight phase advance occurs, this could be due to slight misalignment of the bar. When the defect lies at a point midway between A and the transmitter, a phase retardation occurs corresponding to the depth of the defect on the upper side of the bar. At zero position i.e. defect under transmitter, the signals are once again nearly in phase. Since the phase changes are always referenced to A, the right hand side of the plot in fig.10.11 should be the inverse of the left hand side. Since this is the case, it strongly suggests that the results derived are not experiment artifacts and further support is given to the conclusion that the kind of system is sensitive to defects where the magnitude of the defect is much smaller than the

interrogating wavelength.

The plot of fig.10.11 essentially provides a continuous record of a sequence of events which can in turn be directly linked to positional data.

10.4.7- Water with Aggregate alone (fig.10.12)

The traces of figs.10.1 and 10.2 were taken with a tank containing clear water, in which the first echo represents reflection from the base of the tank. By contrast, fig.10.12 shows a much noisier signal, this noise or echoes being due to the presence of aggregates (polystyrene beads) in the water. Table 10.8 indicates that the strength of the signal received by the transducers is slightly weaker when the aggregate is present in the water. The spectral comparisons provided by table 10.8 do not however reveal any major changes in frequency composition. Although the aggregate affected the signal amplitude of the latter part of the signal received from the base of the tank, especially after $100\mu\text{s}$ as measured from the wavefront, the initial few microseconds were much less affected, and exhibited virtually no phase changes.

10.4.8- Clear Water with Good Bar v Water with Aggregate and Good Bar

Spectral analysis indicates, as shown in table 10.9, that the presence of aggregate in the water changes the frequency content of the signals reflected from the steel bar. This change is due

partially to the attenuation of the higher harmonics through the processes of scattering and absorption. As it can be seen from table 10.9, this attenuation of the high frequency components is not severe (average 8kHz) because scattering and absorption, in this case, are small.

10.4.9- Scanning of Force-Corroded Bar with Aggregate (fig.10.13)

The trace shown in fig.10.13, which is of the same type as that shown in fig.10.11, reveals a similar phase relationship between transducers A and B as the defect travels under the linear array system. These results are less definitive because of the presence of the aggregate but the trend is nevertheless in evidence.

10.4.10- 4-Channel System in Water

With the addition of two further receiving transducers as shown in plate 10.4, spaced 63.5mm from the central transmitter, bar alignment along the major axis of the array system was made possible. Table 10.10 shows that, as might be expected, the echoes returned to probes C and D are not as strong as those returned to probes A and B. If the bar is displaced towards probe D but kept parallel to the major axis as shown in fig.10.4, the signal strength is enhanced at D and correspondingly weakened at C (table 10.11). More significantly, the signal onset times correspond quite closely to the displacement of the bar.

10.4.11- Low Frequency Analysis

In all the above experimentation the data analysis had two major features:

- 1- The wavelength was short (around 12mm).
- 2- The transducers always emitted a clearly defined beam, the half-angle of divergence being around 36°.

In concrete, neither of these two conditions are attainable using the present model. At 121 kHz, in concrete the wavelength is approximately 35mm and the transducers radiate in all directions. In order to model these features in water, a system was constructed which used transducers with a centre frequency of 45kHz, and a diameter of 25mm. In salt water, the wavelength is 34.2mm and the radiation pattern is in all directions. The transducer spacing was 38mm as measured from their centre points. Despite the obvious presence of surface wave interface, the system was found to have extremely good penetration properties and could readily locate the base of the tank through a dense strata of aggregate in suspension, the depth of the water was 218mm. However the phase discrepancy between the two signals, i.e. the sound bar and the corroded bar, is more difficult to identify because of the presence of the surface wave and moreover, because the wavelength is comparatively long to the dimensions of the defect. It should be emphasised that the 45kHz results in water are equivalent to about 120kHz in concrete.

10.5- SUMMARY

One of the criticisms with regard to these water simulation tests, is that it is too far from the real problem at hand, i.e. the location and identification of defects in steel within concrete bridge beams. However, in order to understand the signal information resulting from defects in the wire and to be able to identify and separate out these signals in the presence of scattering which takes place within the concrete, controlled experiments were necessary in which the level of complexity and the sophistication of the analysis were gradually increased to approximate and validate the model.

The water based experiments were successful in identifying defects, and corroded parts in steel components. The interrogation of the signal response was processed in different ways: onset time, phase, amplitude, or frequency. This has enabled to identify the signal characteristics carrying information about the wire conditions.

Table 10.1- Transducer Characteristics, Water alone.

Channel	rms,V	Peak Frequency,kHz	Estimated Velocity (m/s)
A	0.0755	121	1476.1
B	0.0725	120	1470.8

Table 10.2- RMS and Spectral Change Characteristics, Channel B only

Experiment	rms,V	Amplitude at 41 kHz,V	Amplitude at 121 kHz,V	HF/LF
Good Bar	0.0409	0.0017	0.0102	6
Midway Cut Cut near Transmitter	0.0256	0.0021	0.0076	3.6
Rotated Cut	0.0420	0.0020	0.0100	5
Force-Corr- oded-bar	0.0389	0.0027	0.0110	4.1
Naturally Corroded	0.0139	0.0008	0.0030	3.75
	0.0300	0.0018	0.0100	5.5

Table 10.3- Good Steel v Steel Cut Midway

Channels	Time Domain Time Delay (μ s)	Frequency Domain Spectral Shift (kHz)
A1 B1	in phase	in phase
A2 B2	0.6 (1mm)	in phase
A1 A2	0.05 (0.07mm)	in phase
B1 B2	0.65 (1mm)	in phase

Table 10.4- Good Steel v Steel Cut under R.H. Edge of the Transmitter

Channels	Time Domain Time Delay (μ s)	Frequency Domain Spectral Shift (kHz)
A1 B1	in phase	in phase
A2 B2	0.1 (0.1mm)	in phase
A1 A2	0.1 (0.1mm)	in phase
B1 B2	0.2 (0.2mm)	in phase

Table 10.5- Good Steel v Steel Cut rotated through 90°,
Midway between Transmitter and Channel B

Channels	Time Domain Time Delay (μs)	Frequency Domain Spectral Shift (kHz)
A1 B1	in phase	in phase
A2 B2	0.4 (0.6mm)	in phase
A1 A2	0.1 (0.1mm)	in phase
B1 B2	0.5 (0.7mm)	in phase

Table 10.6- Good Steel v Force Corroded Bar, Midway between
Transmitter and Channel B

Channels	Time Domain Time Delay (μs)	Frequency Domain Spectral Shift (kHz)
A1 B1	in phase	in phase
A2 B2	0.9 (1.3mm)	in phase
A1 A2	0.1 (0.1mm)	in phase
B1 B2	1.0 (1.5mm)	in phase

Table 10.7- Good Steel v Naturally Corroded Bar

Channels	Time Domain Time Delay (μs)	Frequency Domain Spectral Shift (kHz)
A1 B1	in phase	in phase
A2 B2	0.4 (0.6mm)	in phase
A1 A2	0.3 (0.4mm)	in phase
B1 B2	0.7 (1mm)	in phase

Notes to tables 10.1 to 10.7

1- Indice (1) for good bar, indice (2) for the mentioned experiment.

2- Phase changes are indicated by referencing the first channel shown against the second, for example, table 10.7, row 3, channel A2 lags A1 by 0.3 μs .

Table 10.8- Water with Simulated Aggregate

Channel	rms, V	Peak Frequency, kHz	Estimated Velocity (m/s)
A	0.040	117	1538
B	0.052	115	1542.5

Table 10.9- Good Steel in Clear Water v Good Steel in Water with Simulated Aggregate

Channels	Frequency Domain Spectral Shift (kHz)
A1 B1	in phase
A2 B2	4
A1 A2	6
B1 B2	10

Note: Spectral shifts are indicated by referencing the first channel shown against the second, for instance, row 2, the peak frequency in B2 is shifted to the left i.e. less by 4kHz.

Table 10.10- Transducer Characteristics of Four Channel System Interrogating Good Steel in Clear Water

Channel	rms, V	Peak Frequency, KHz
A	0.0755	121
B	0.0725	120
C	0.0448	120
D	0.0454	120

Table 10.11- Transducer Characteristics of four Channel System with Bar Displaced towards Probe D

Channel	rms, V	Peak Frequency, KHz
A	0.0400	120
B	0.0520	120
C	0.0200	120
D	0.0570	120

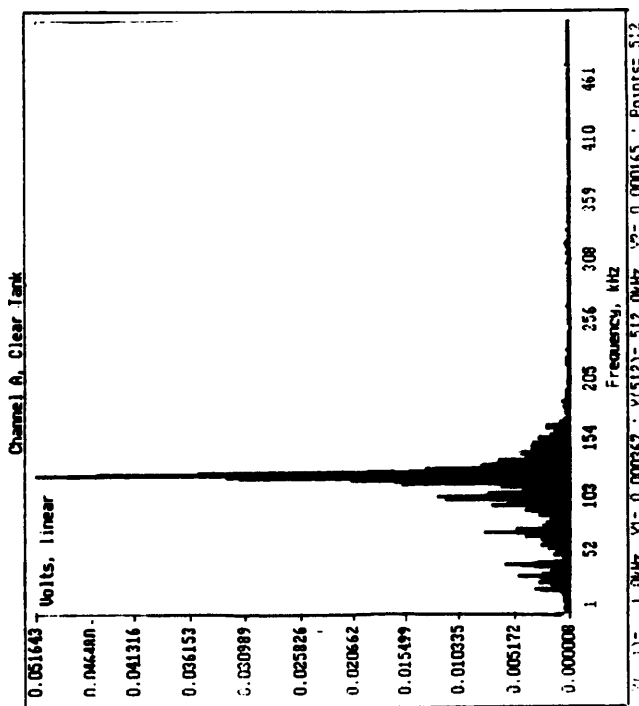
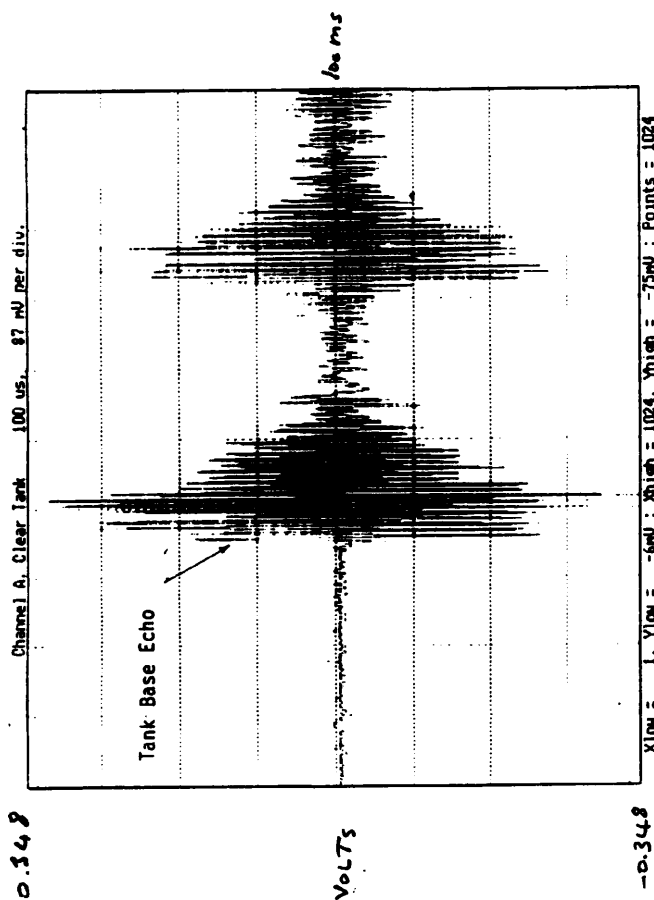
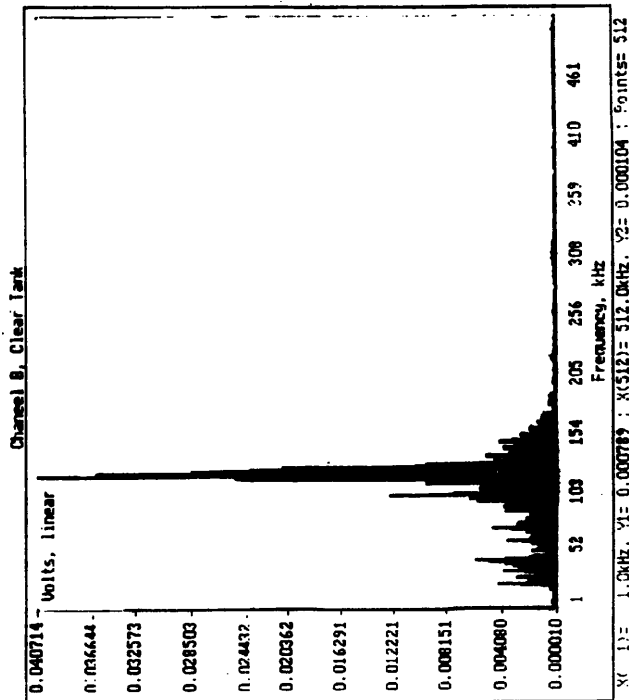
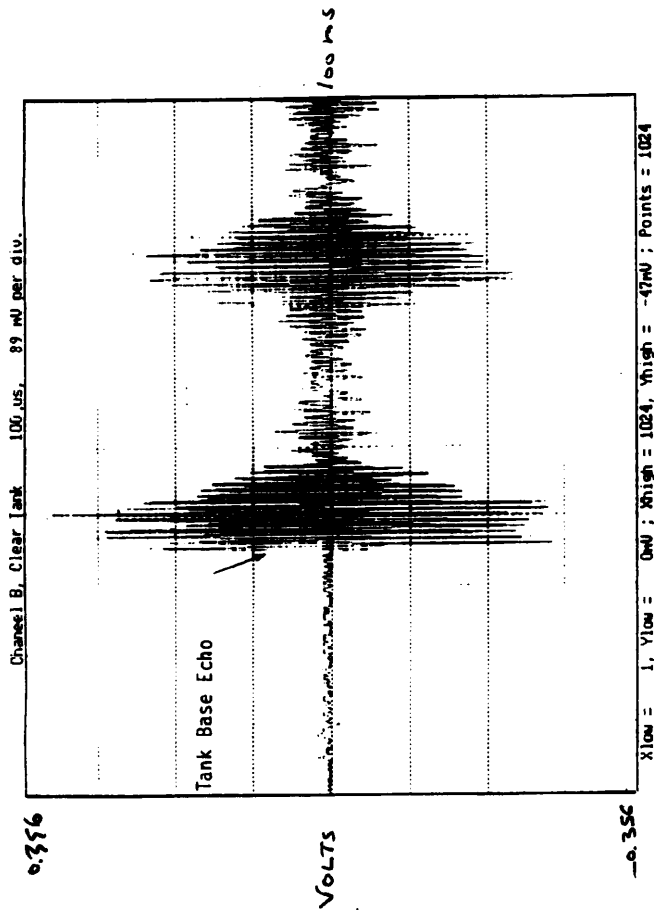


Fig. 10.1- Signal and Frequency Plot for Channel A in Tank containing fresh water only.

Fig. 10.2- Signal and Frequency Plot for Channel B in Tank containing fresh water only.

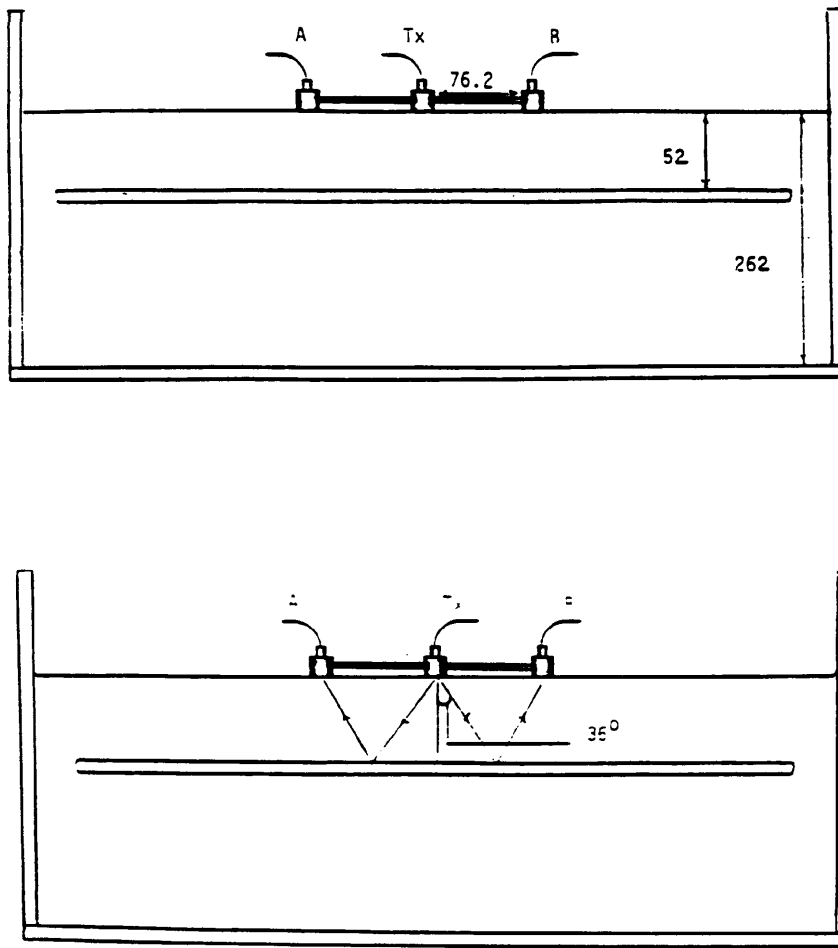


Fig.10.3- Linear Transducer array system used in water showing dimensional specifications.

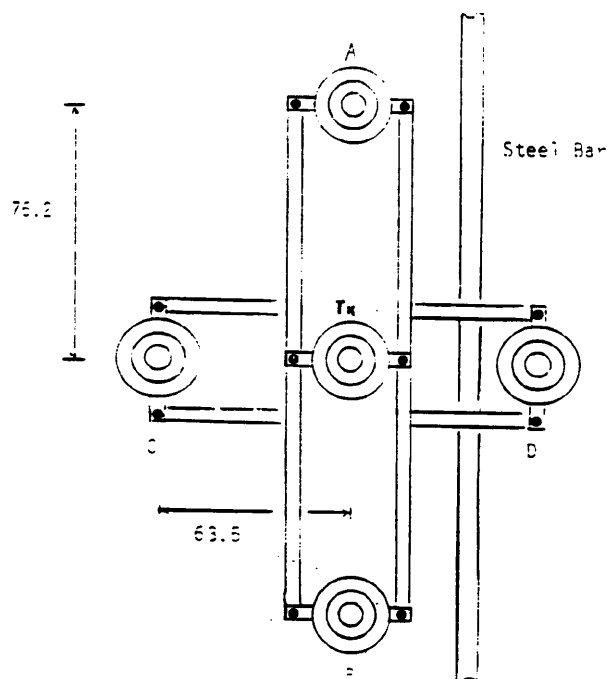


Fig.10.4- 4 channel array in water, with steel bar in parallel to its major axis and displayed towards probe D.

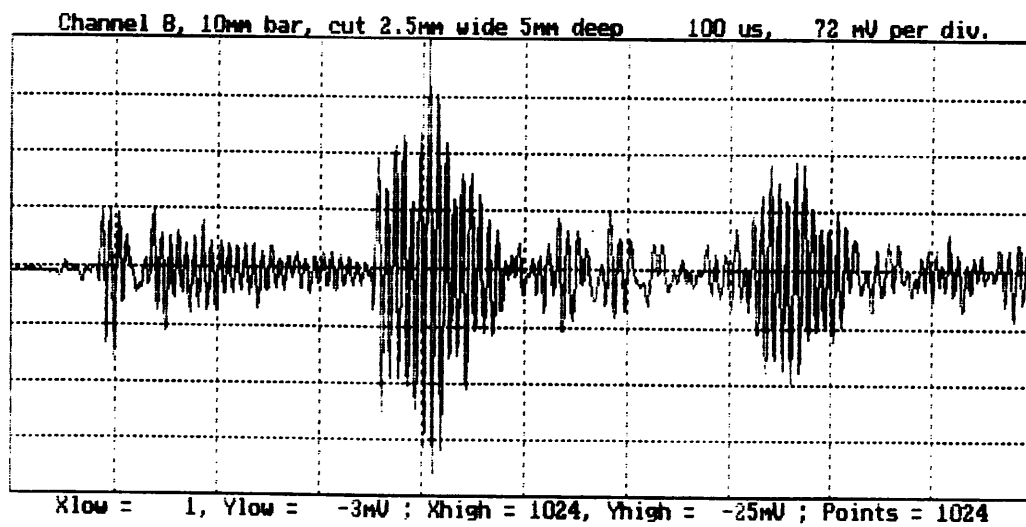
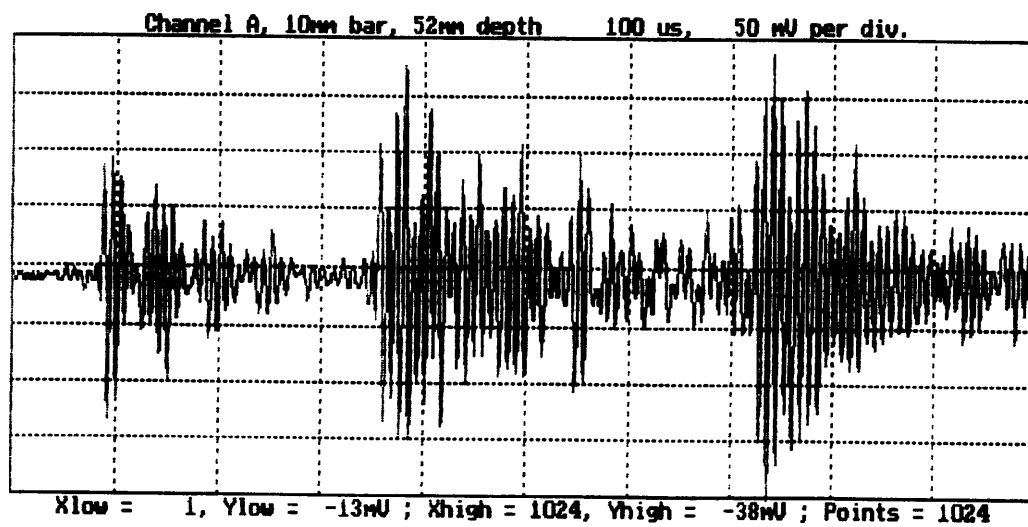


Fig.10.5

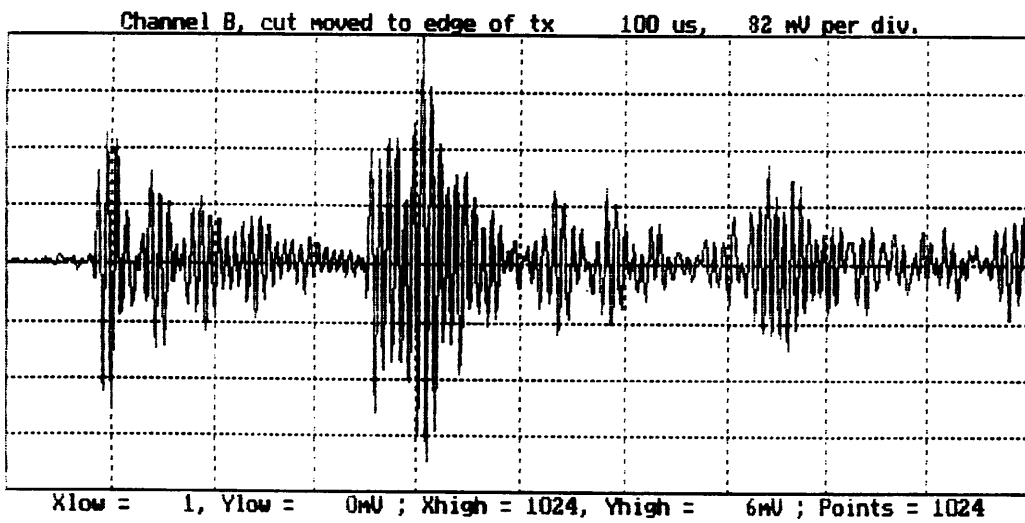
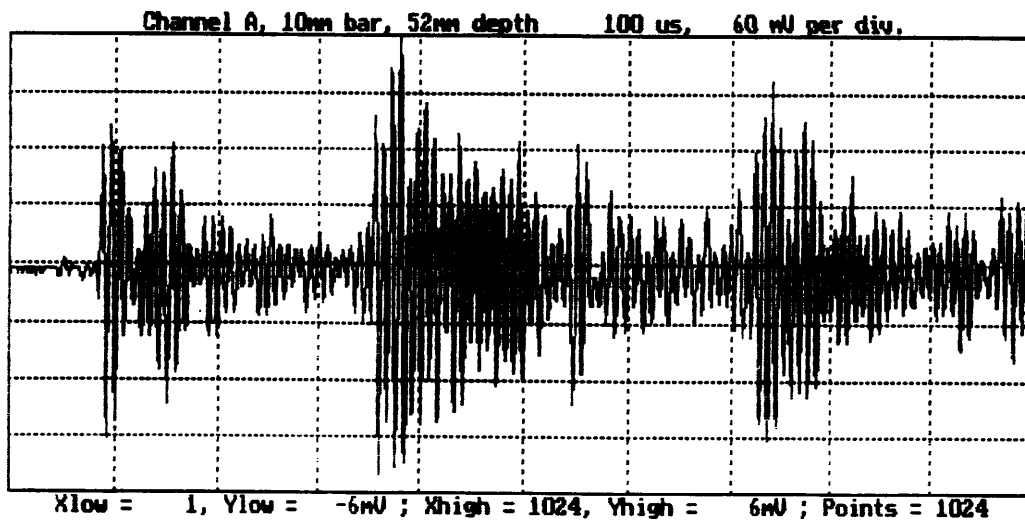


Fig.10.6

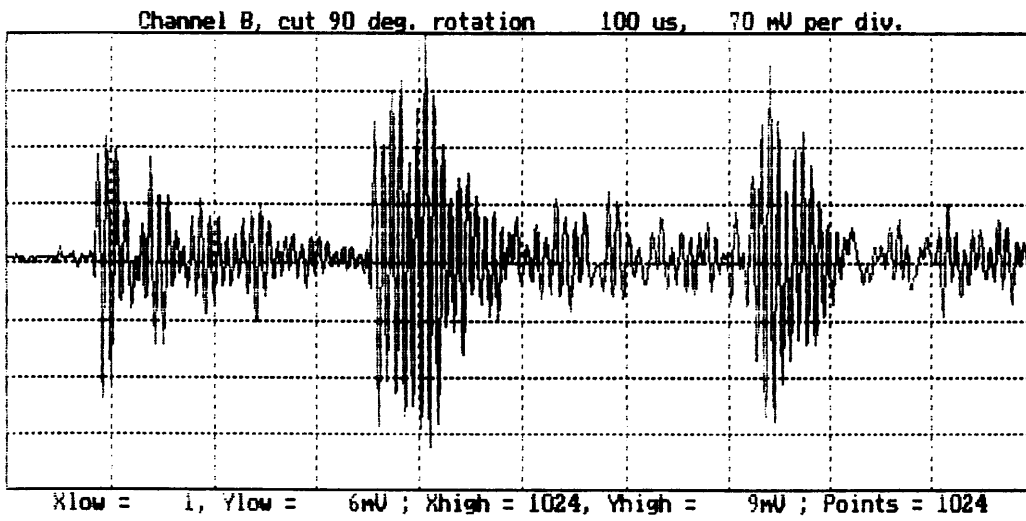
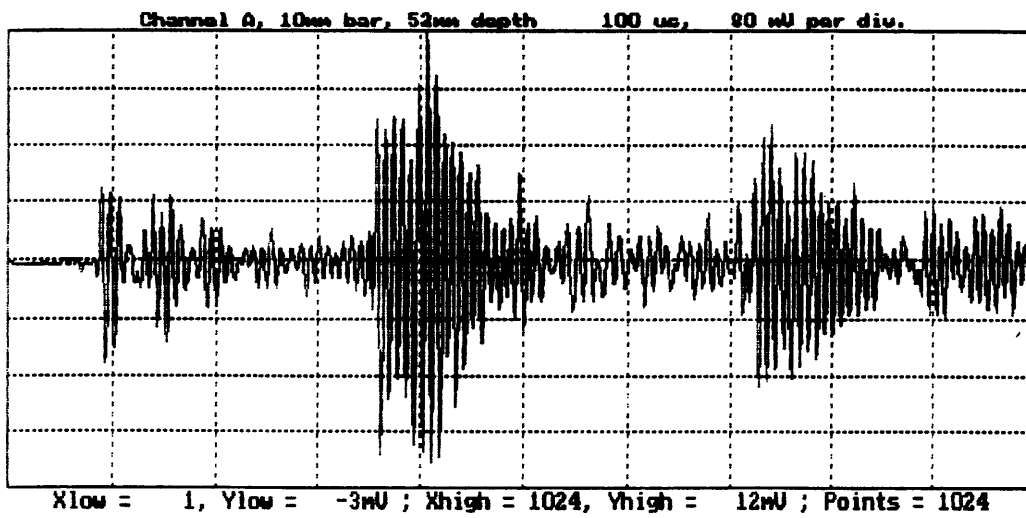


Fig.10.7

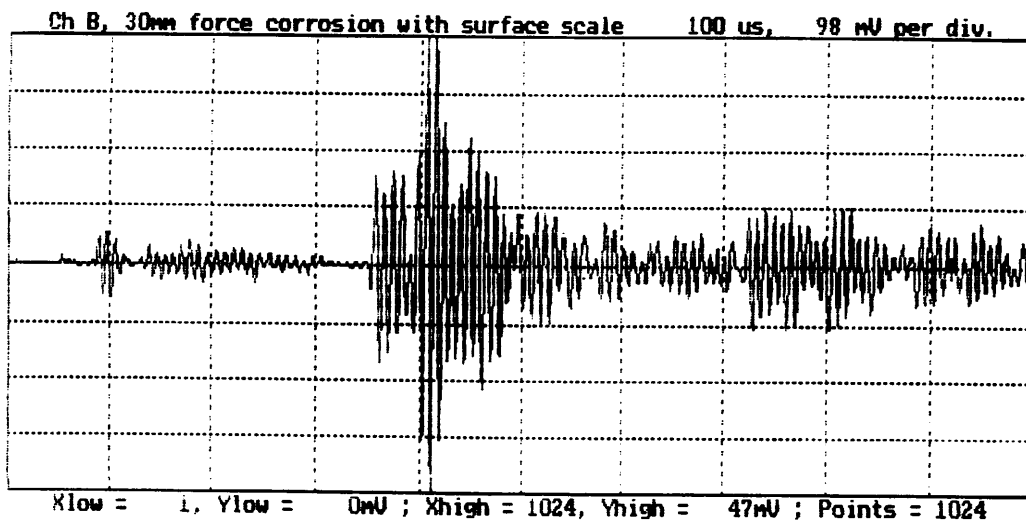
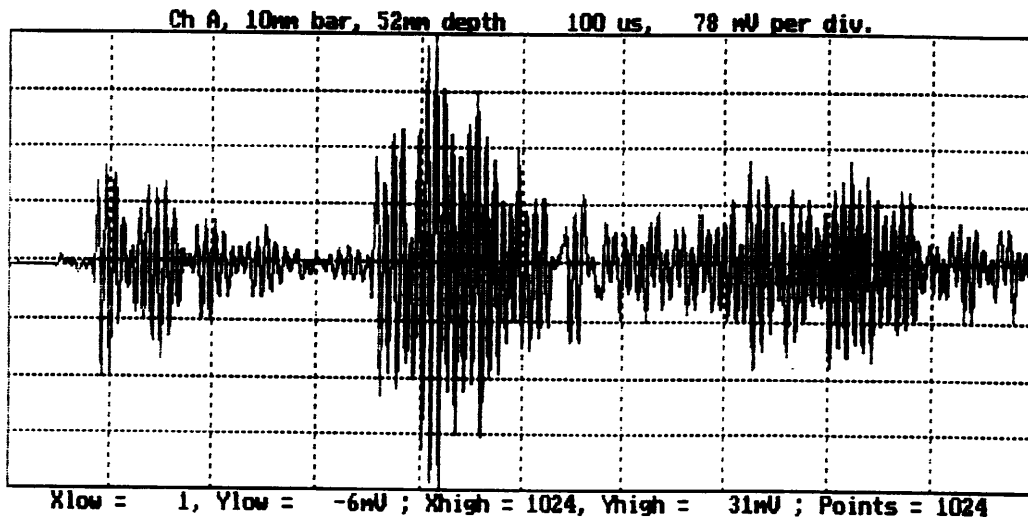


Fig.10.8

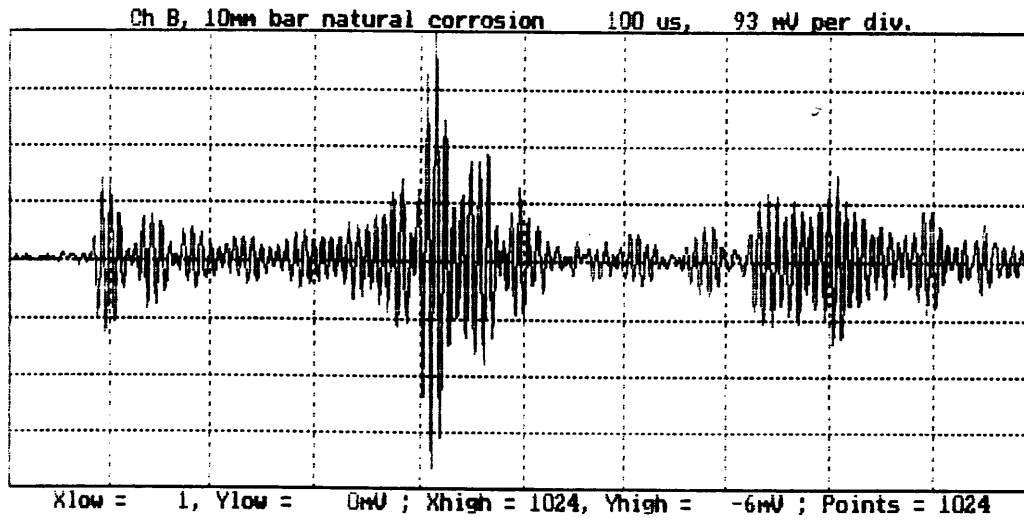
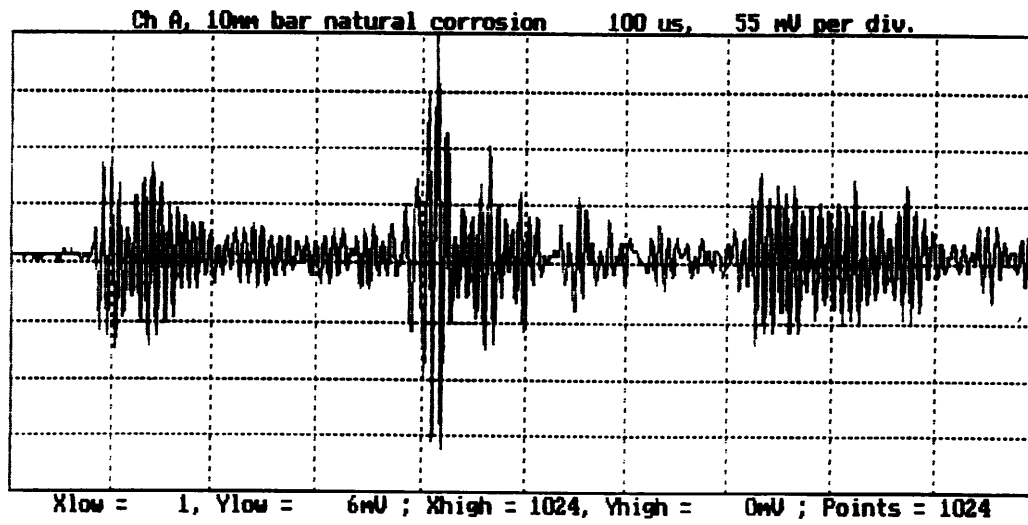


Fig.10.9

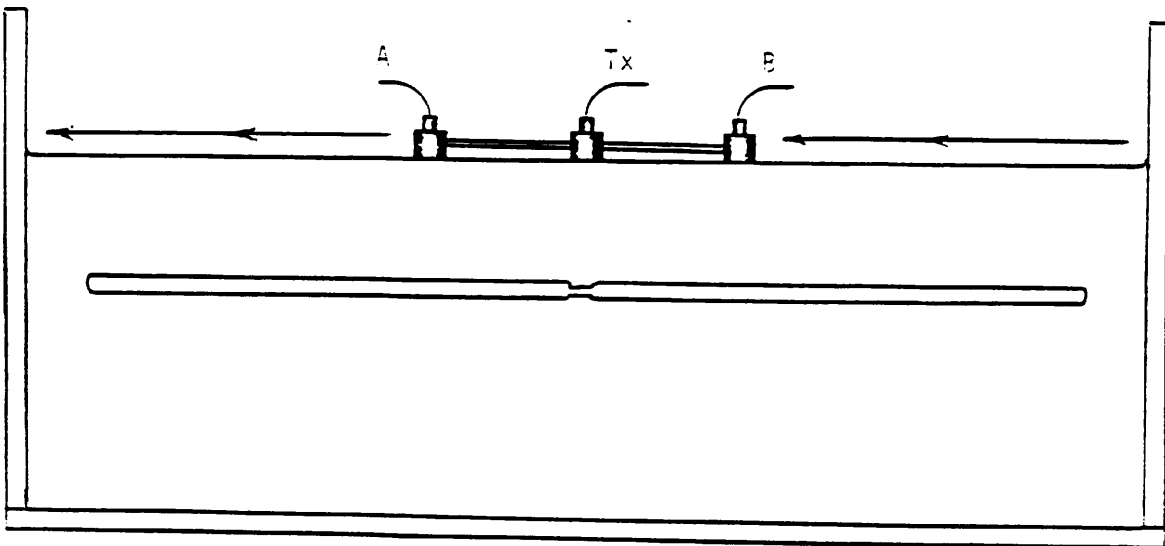


Fig.10.10- Scanning a force corroded section by moving the array along the length of the bar.

Time-delay diagram obtained from
scanning defective bar.

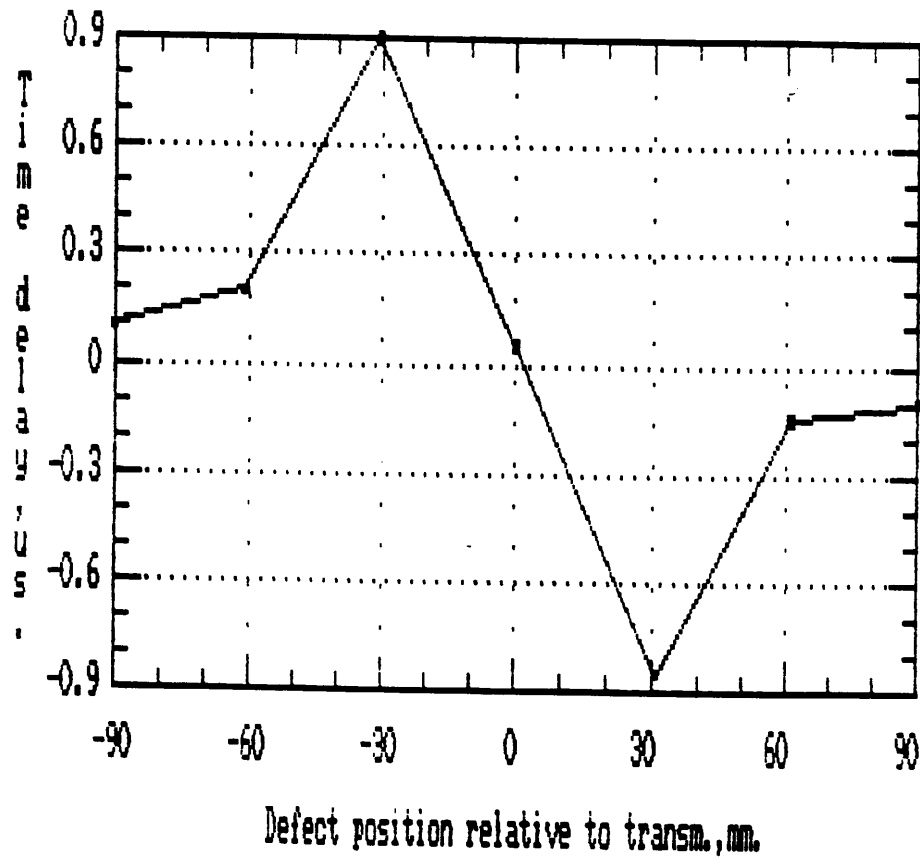


Fig.10.11

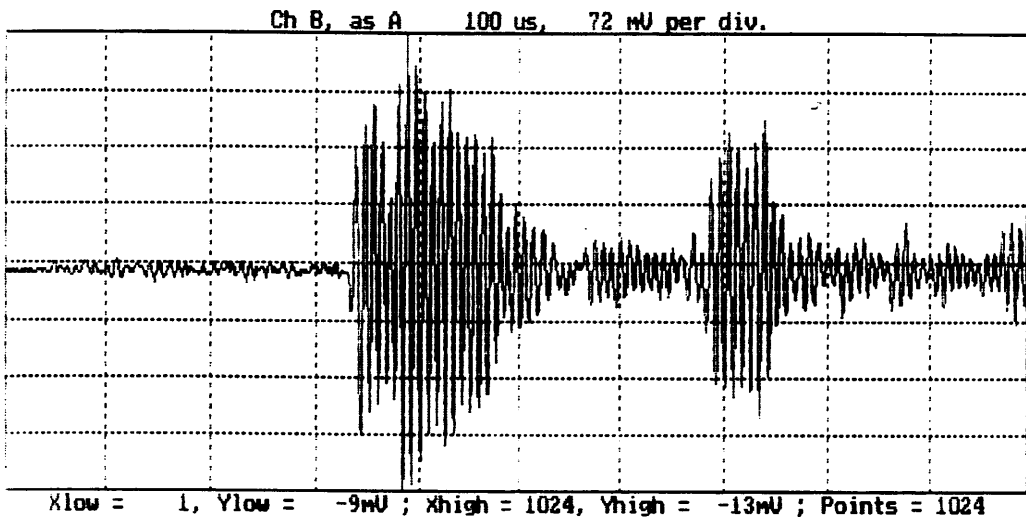
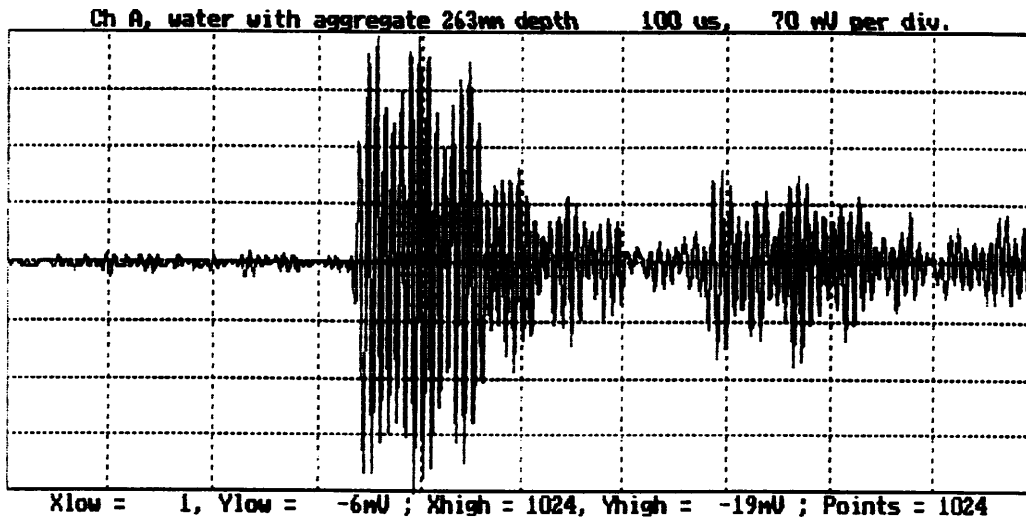


Fig.10.12

Time-delay diagram obtained from scanning defective bar with simul. aggregate.

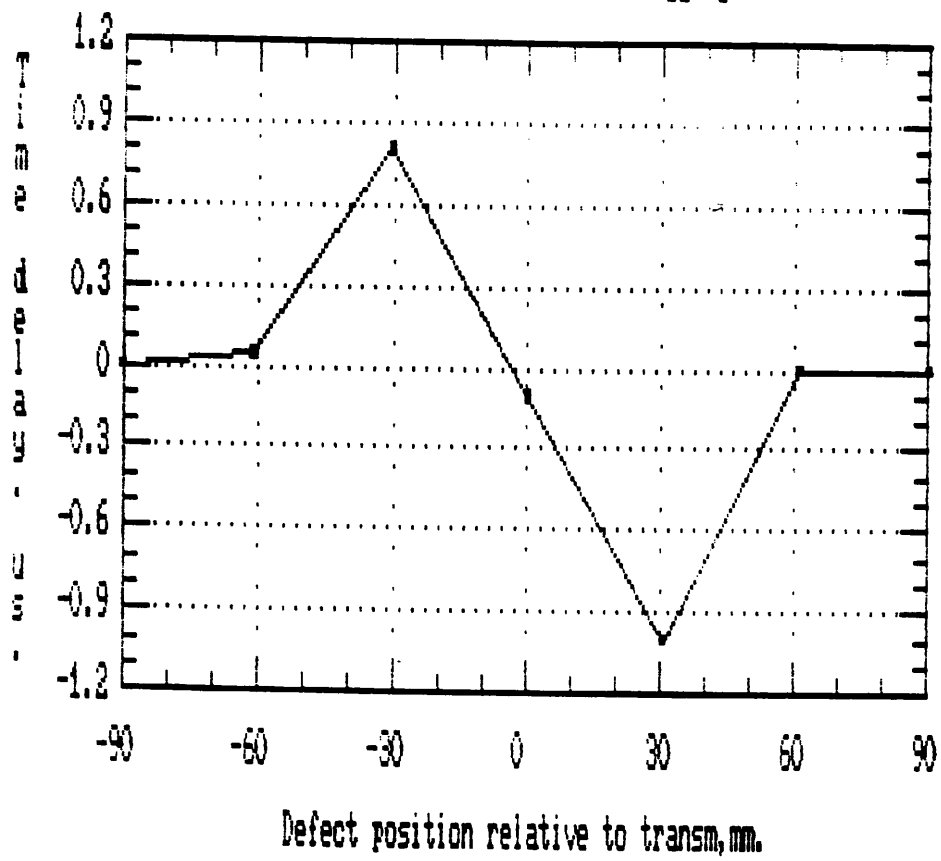


Fig.10.13

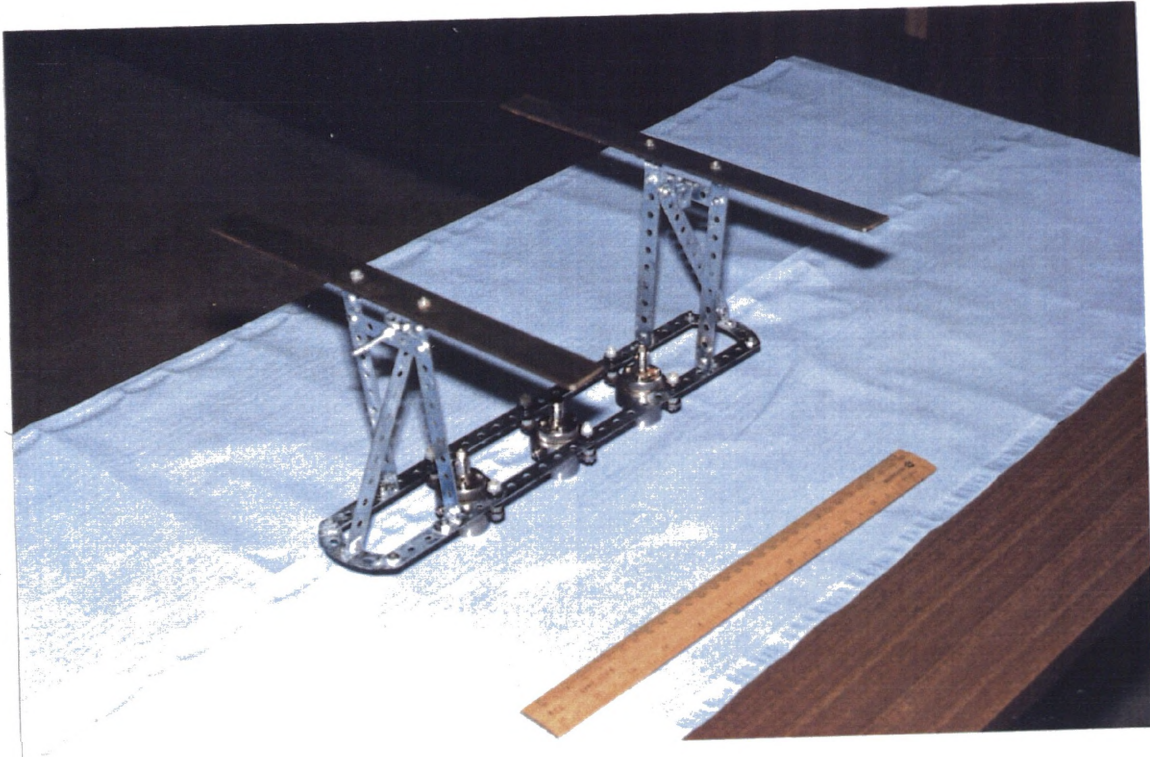


Plate 10.1- Linear transducer array.

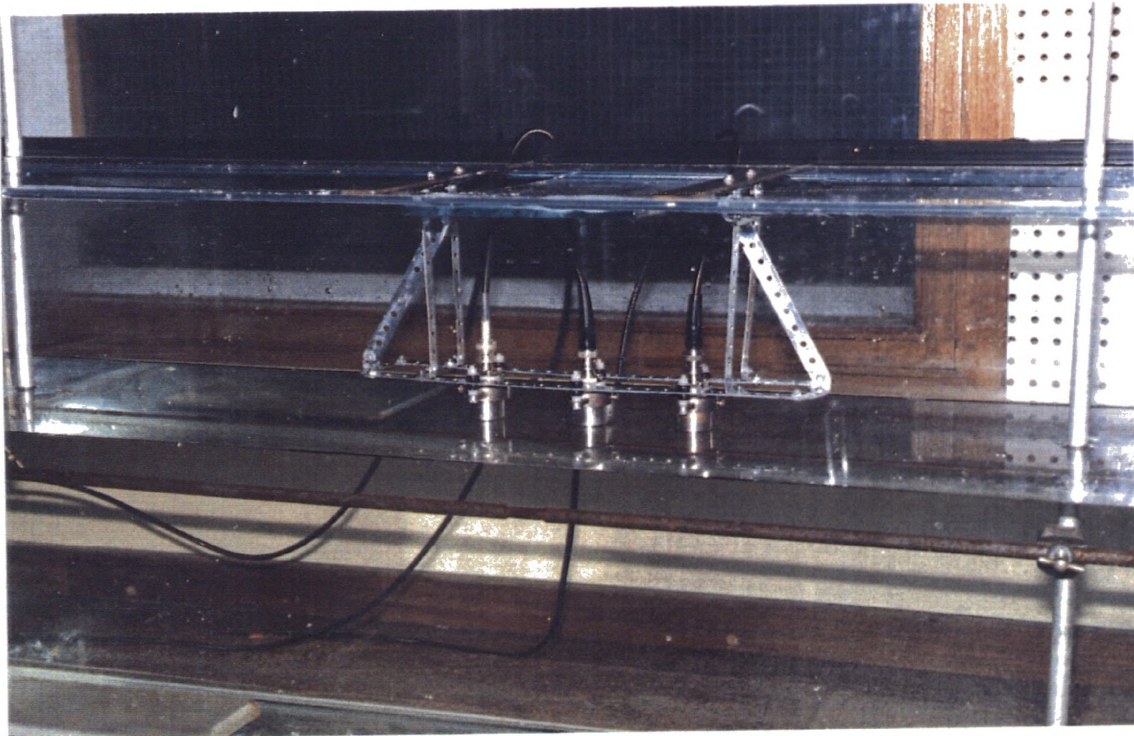


Plate 10,2- Linear transducer array used to investigate defective steel bar.



Plate 10.3- Linear array system with polystyrene beads in suspension used to simulate the effects of aggregate.

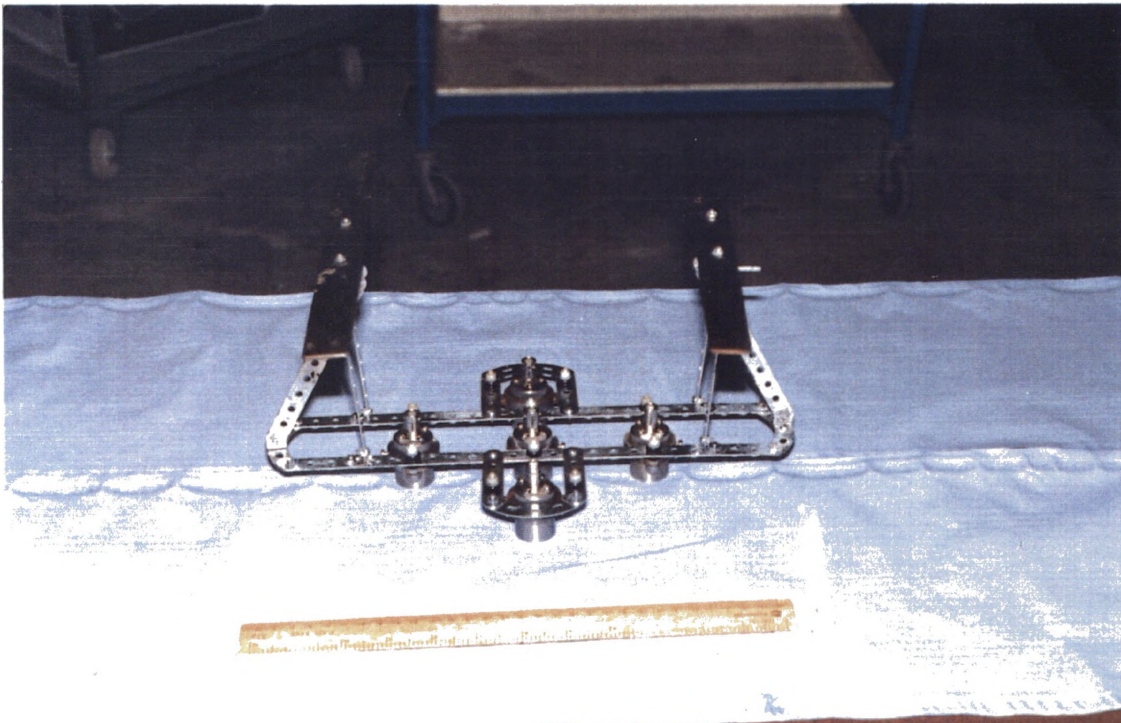


Plate 10.4- 4 Channel system with central transmitting probe.

CHAPTER 11

IMPLEMENTATION OF THE INDIRECT METHOD FOR DETECTION DEFECTS IN REINFORCEMENT EMBEDDED IN CONCRETE

11.1- INTRODUCTION

The experimental phase of this research had the following objectives: (1) to develop a pitch-catch technique (instrumentation and signal acquisition and processing) for finding corrosion or flaws within the reinforcement or prestressing components embedded in concrete, and (2) to confirm the observations and conclusions drawn from the analytical studies of the condition of the components embedded in concrete where it is possible.

This chapter describes the development of an indirect technique (pitch-catch method) for investigation of steel components in concrete (prestressed or reinforced). Results obtained from controlled laboratory studies in plain and reinforced concrete beams are presented. Moreover a new filtering technique was developed which enabled firm detection of major voids and offers the potential of identifying major corrosion parts.

11.2- DEVELOPMENT OF A MEASUREMENT TECHNIQUE

11.2.1- Transducers and Frequency Aspects

In order to detect deterioration in the condition of embedded

components it is firstly necessary to identify a signal returned from the component, and secondly to deduce from this part of the signal differences in response which can be linked to its condition.

The transducers used were compression (longitudinal) wave radiators.

It was established from the analytical and experimental studies (chapters 6, 7, and 10) that for frequencies higher than 300kHz the attenuation through the concrete is so severe that the reflected signal from the reinforcement will be difficult to detect.

When low-frequency transducers were investigated i.e. 45 and 54kHz where the wavelength is 89 and 75mm in concrete respectively, it was found that a strong Rayleigh wave was transmitted by the transmitter which interfered with the reception of the desired echo from the reinforcement although the concrete in this case acts as a homogeneous medium (the wavelength is much larger than the size of the coarse aggregates) in spite of its heterogeneous composition. Moreover, when the wavelength is much greater than the diameter of the component present in the concrete it was demonstrated from the water experiments that the reflected echo from the bar is much smaller. However the key to detecting information about the condition lies in comparing the magnitude/attenuation of that part of the signal reflected from the component at different frequencies, since higher frequency constituents are scattered more by pitted or

irregular surfaces. The frequencies chosen for the experiments were normally between 100-250kHz, therefore the wavelengths were between 40 and 16mm for concrete having 4km/sec longitudinal velocity.

11.2.2- Pulsers

The main pulsers used in the experiments were the one supplied by Steinkamp and the one provided with the PUNDIT. The PUNDIT has a 10Hz pulse repetition and 500 or 1000V pulse voltage. On the other hand the Steinkamp pulser has 1Hz pulse repetition and 600V pulse voltage.

11.2.3- Oscilloscopes

Two scopes were used before the signal analyser became available. These were the 2220 Tektronix 60MHz digital oscilloscope and the 5602 Solarton Enertec 40MHz digital oscilloscope. These oscilloscopes were programmed via a computer (see chapter 9) which facilitated signal processing, and the storage of data on floppy disks. The oscilloscopes could be interfaced with a plotter, or the stored waveforms and frequency spectra could be plotted via the computer using the package described before in chapter 9.

11.2.4- Analyser

The signal analyser used in the later stages was the 6100 Analogic waveform analyser. It has more than 50 waveform

analysis, manipulation, and signal processing functions (refer to chapter 9 for more description concerning its capabilities). The analyser was controlled by a computer program written in PASCAL and the data were stored on a hard disk.

11.2.5- Concrete Specimens

Experimental waveforms were obtained from concrete and mortar specimens cast in the Civil Engineering laboratory at UMIST. These included mortar and concrete beams ($150 \times 150 \times 1000 \text{mm}^3$) plain, reinforced, and chloride contaminated to produce a corrosion environment, two slabs ($150 \times 800 \times 800 \text{mm}^3$), a pre-tensioned concrete beam ($150 \times 300 \times 5000 \text{mm}^3$), and a cracked commercial pre-tensioned T-beam (this was supplied to the department having been rejected on site because of the crack) of 9000mm length and 495mm flange width (refer to chapter 9 for more details about the specimens). It should be mentioned that the T-beam did not have any corroded reinforcement or any major flaws or defects other than the crack present outside (a piece of concrete was broken). Therefore the signals investigated from this beam did not show any change in the time or frequency domains because of no defects present. The results were not therefore included. Fig.11.1 shows some of the samples used in the experiments.

11.2.6- Amplification

A suitable amplifier was used for widely spaced transducers (where the distance exceeded 400mm). The amplifier used was a four channel amplifier. The frequency response was flat from DC

to 1.25MHz, with a -3dB point at 1.5MHz. Each channel could be configured regarding gain to either 40dB or 52dB (x100 or x400).

11.2.7- Multiplexer

In addition to the amplifier, a signal multiplexer was constructed with the help of CAPCIS. The waveform analyser has the capability to handle only 2 channels, but signals are sometimes provided by 4 transducers. The multiplexer is fed by the output of the 4-channel amplifier and alternates its output between channels 1 & 2 and 3 & 4, deriving its synchronization from the trigger signal generated by the pulser unit.

11.2.8- Signal Acquisition and Processing

The test set-up is shown in fig.11.2 and plate 11.1. Data acquisition by the oscilloscope or the analyser was triggered by the voltage produced by the pulser. Once a waveform was acquired, it could be studied in the time-domain or transformed into the frequency domain by the use of the Fast Fourier Transform technique. It should be mentioned that the waves were averaged up to 32 times before they were stored for later interpretation.

In the time domain analysis, the exact time of the start of the signal must be known so that the time of wave arrivals can be determined from the perturbations in the waveform. The longitudinal velocity was first determined using the through-transmission method at any section of the test specimen. The transmitter and the receiver were located on opposite sides of

the test object and the time for an ultrasonic longitudinal wave to travel from transmitter to receiver through the specimen is measured. The velocity was then obtained by dividing the distance between the transducers by the travel time, the transit time being based on detecting the arrival of the leading edge of the pulse. Knowing the velocity of the longitudinal wave in a concrete and the distance between the transmitting and the receiving transducers, the time required for the longitudinal wave to travel from the radiating point to the receiver can be calculated. Moreover the Rayleigh wave arrival can be determined as the Rayleigh speed is approximately equal 0.56 times the longitudinal speed (see chapter 3). Thus for accurate determination of defect depth, the longitudinal velocity should be determined from the through-transmission method on a part of the structure being evaluated where the thickness is known, and this velocity then used to determine the depth of internal interfaces in other parts of this structure. Furthermore calculations of scalar quantities such as rms, energy, dominant frequency, mean voltage, maximum voltage, minimum voltage, and time of occurrence of maximum amplitude can be calculated using the analyser.

After acquiring the data, the time signals were Fourier transformed. Calculations of scalar quantities such as rms, energy, the dominant frequency and the corresponding amplitude were carried out.

The investigation was divided into the following categories:

- 1- Experimentation on mortar (plain and reinforced).

- 2- Experimentation on concrete (plain, reinforced, salted).
- 3- Experimentation on slab with and without simulated void.
- 3- Experimentation on ducted samples (void and grouted).
- 4- Conclusions from small-scale laboratory tests.
- 5- Application of digital filtering techniques to a system for .
flaw and corrosion detection.
- 6- Experimental work using multiple receiving transducers.
- 7- Experimental work using the digital filtering technique.
- 8- Proposal of a system for flaw and and corrosion detection.
- 9- Conclusions.

11.3- EXPERIMENTATION ON MORTAR SAMPLES

Mortar (the constituents were sand+cement+water, refer to chapter 9 for mix proportions) specimens (150x150x1000mm³) were cast with and without reinforcement in an attempt to detect the presence of the reinforcement.

To find the reinforcement in mortar, the problem was tackled in three ways:

- 1- Velocity measurements.
- 2- The energy of the first part of the wave (called the pre-wave) where the echo from the reinforcement is expected.
- 3- Study of the wave characteristics in the frequency domain.

1- Velocity Measurements:

A group of experiments were carried out on two mortar specimens, the first plain, and the second with strand of 15.6mm diameter.

It should be mentioned that the two beams were cast using the same mix, and the strand was positioned in the middle of the beam. However, the average longitudinal velocities (these were derived from the through-transmission method) were slightly different for the two specimens under test, for the plain mortar beam was 3980m/sec, and for the reinforced one 4000m/sec. These tests were carried out with paths directly through concrete, so that there was no influence of embedded steel on the results. The frequency used was 170kHz. Spacings between transmitter and receiver for the main tests were 100, 200, 300, 400, and 500mm. The receiver and the transmitter were put in the middle of the top surface, for example over the strand when the reinforced sample was tested.

Table 11.1 shows the arrival times of the signals for the distances mentioned earlier. It can be seen that in all cases the signal from the reinforced specimen arrived earlier than that of plain sample indicating that the signal was reflected from the strand encased in the mortar.

Table 11.1- Arrival times for the mortar specimens.

Transducer Spacing, mm	Reinforced Beam, μ sec	Mortar Beam, μ sec
100	32.8	34.4
200	55.2	62.4
300	79.2	91.2
400	107.2	117.6
500	132	146.4

2- Energy Calculations

In this investigation, three specimens were cast, the first was plain, the second with 10mm bar, and the third with 32mm bar. The bars were positioned in the middle of the beams. The frequency was 170kHz, and the spacings between the transmitter and the receiver were 100, 200, and 300mm.

After acquiring the time domain signals, 40 μ sec from the start of the signals were windowed for each record and the energy calculations were performed on each of the windowed data. Table 11.2 shows the result. It can be seen that the energy of the pre-wave increases in the presence of the reinforcement. Moreover the energy increases as the bar diameter increases. Fig.11.3 shows the result of 200mm transducer spacing in the case of the reinforced mortar with 10mm bar (fig.11.3.a) and the plain mortar (fig.11.3.b). It can be seen that the pre-wave is much stronger in the presence of the bar. It should be noted that the energy in the plain case is due to the Rayleigh wave.

Table 11.2- Energy calculations for the mortar specimens.

Transducer Spacing, mm	Reinforced Beam with 10mm bar V^2 sec	Mortar Beam with 32mm bar V^2 sec	Plain Mortar V^2 sec
100	0.036	0.0766	0.001
200	0.0339	0.0618	0.005
300	0.0180	0.0480	0.004

3- Frequency Domain Investigation

In the case of mortar, attenuation is mainly due to Rayleigh scattering where the diameter of fine aggregates (<1mm) is much

smaller than the wavelength (22mm) (refer to chapter 7 for more details). Earlier experiments on concrete specimens showed that in the presence of the reinforcement the dominant frequency is higher than the unreinforced specimens (this will be mentioned in the next section), however in the case of mortar the scattering due to grain is not so critical as in the case of concrete (up to 20mm) i.e. the frequency spectra for the mortar experiments had more or less the same peaks. Therefore it was decided to Fourier transform the time signals and record the dominant frequency and its corresponding amplitude.

The experiments were carried on the same specimens as above i.e. plain, reinforced with 10mm and reinforced with 32mm bar. The same transducers were used of 170kHz resonant frequency. The spacings between transmitter and receiver were 100, 200, and 300mm. It was found that all the specimens had the same dominant frequency 169.921kHz, and table 11.3 shows the amplitudes for the distances for each case.

It can be seen from the table 11.3 that as the amount of reinforcement increases (i.e. the diameter of the bar) the amplitude of the dominant frequency increases indicating that in the presence of reinforcement, the amplitude of the dominant frequency is higher from that of a signal with no reinforcement.

Table 11.3- The amplitudes for the dominant frequency for the mortar experiment.

Transducer Spacing, mm	Reinforced Beam with 10mm bar Volt	Mortar Beam with 32mm bar V	Plain Mortar V
100	80.82	88.052	29.0414
200	32.4453	35.732	21.3763
300	23.977	27.185	9.5293

11.3.1- Summary

This group of experiments was carried out on mortar samples to try to examine the effect of the presence of reinforcement on the signal. The signals were studied in the time and Fourier domains. It was found that the signal started earlier when the reinforcement was present and the strength of the first part of the wave (what we call the pre-wave) was stronger than that of a signal captured from a plain mortar. Moreover in the presence of the reinforcement the dominant frequency was found to be stronger.

11.4- EXPERIMENTATION ON CONCRETE

Small concrete beams ($150 \times 150 \times 1000 \text{mm}^3$) plain, reinforced, some with a duct either with voids or grouted, and some beams contaminated with salt to give a corrosion environment, (the description of these specimens could be found in chapter 9), were cast to try to establish a method to check the condition of the embedded components. Work was also carried out later on the large scale test beam ($150 \times 300 \times 5000 \text{mm}^3$) described in chapter 9. Moreover, two unreinforced slabs ($800 \times 800 \times 150 \text{mm}^3$) were cast, one was plain and in the other a polystyrene disk of 200mm diameter and 4mm thickness was inserted in the middle (the time of compaction of this slab was less than the plain case because it was thought that in the presence of a crack the strength would be less) to try to establish the effect of a void on the signal. The purpose of this group of experiments was to study the effects of

steel reinforcement on signal strength, onset time and frequency in relation to transit-time system and the identification of high-frequency components within the total signal.

Again the techniques used in the processing of the signals were as the following:

- 1- Velocity measurements on the plain and reinforced specimens.
- 2- The strength of the pre-wave on the plain and reinforced specimens.
- 3- The frequency spectra for the plain and reinforced specimens.
- 4- The effect of the presence of the chloride.
- 5- The effect of the presence of the void in the two slabs.

1- Velocity Measurements

Tests were carried out on a plain concrete beam, beam reinforced with 15.6mm diameter strand, and beam reinforced with 32mm diameter bar. The same concrete mix was used in three specimens. The frequency of the transducer used was 170kHz, and the spacings between the transmitter and the receiver were 10, 50, 100, 200, and 300mm. The average longitudinal velocities for the three beams were: 4200km/sec for the plain concrete, 4180km/sec for the beam reinforced with the strand, and 4220km/sec for the beam with 32mm diameter bar.

Table 11.4 shows the time of arrivals of the signals for the distances used for each case. It can be seen that for the case of the beam reinforced with the strand and the plain beam the times of arrival of the signals were about the same. This could

be due to two possibilities: a) the scattering from the aggregate (diameter up to 20mm compared to the wavelength 25mm) which could interfere with the start of the signal and mask the echo from the reinforcement which was expected to be small, and b) the presence of the Rayleigh or the surface wave which could arrive before the echo reflected from the reinforcement and could disrupt the start of the signal and make it difficult to distinguish between the two waves i.e. the surface wave and the wave reflected from the reinforcement. However for the case of the beam reinforced with 32mm diameter bar there was a slight advance (earlier arrival) in the signals which could be referred to the higher velocity of the longitudinal wave in the concrete, or it could be due to the diameter of the bar which reflected a bigger amplitude which made it easy to detect the start of the signal, i.e. its amplitude was larger from the Rayleigh wave (it should mentioned that the start of the signals for the cases of plain and reinforced with a strand were not defined as well as for the beam with 32mm bar).

Table 11.4- Time of arrivals for the concrete specimens.

Transducer Spacing, mm	Plain Concrete μ sec	Reinforced with strand, μ sec	Reinforced with 32 mm bar, μ sec
10	11	11	11
50	24	24	22
100	36	37	34
200	59	57	56
300	86	85	83

2- Energy Measurements

Because of the heterogeneous nature of the concrete (composition is gravel+sand+cement+water) it is difficult to gather reproducible data. The variables when two tests were carried out

on the same specimen, using the same transducer spacing, include:

- 1)- the coupling because the contact between the transducer and the concrete surface is difficult to repeat,
- 2)- the volume of aggregates, i.e. gravel, encountered in path of the two signals during the two tests is not the same, and
- 3)- any variability of the strength of the concrete and hence the velocity of sound in the concrete.

A group of experiments was carried out to try to establish the effect of the embedded component on the pre-wave. The experiments given here were extracted from a set of experiments carried out using the same set-up, i.e. same transducers with same spacing, on different concrete beams each reinforced with different bar sizes. The reason is that the strength of the pre-wave did not always increase in the presence of the reinforcement in comparison with the plain specimen, i.e. sometimes the strength of the pre-wave from a reinforced beam was of the same order as the plain case, because of the effect^d the Rayleigh wave and the scattering from the coarse aggregates.

Fig.11.4 shows the two signals captured in the case of plain concrete (fig.11.4.a) and the specimen reinforced with 32mm diameter bar (fig.11.4.b). The frequency used was 250kHz with spacing of 100mm. The strength of the pre-wave on the signal can be seen to be stronger in the case of the 32mm bar.

Fig.11.5 shows the two time signals from plain concrete (fig.11.5.a) and concrete reinforced with a 15.6mm strand (fig.11.5.b). The same frequency was used as before but with

spacing of 250mm. Again the strength of the pre-wave is stronger in the case of the reinforced beam.

Fig.11.6 shows the result from plain concrete (fig.11.6.a), concrete reinforced with 25mm diameter bar (fig.11.6.b), and concrete reinforced with 32mm bar (fig.11.6.c). The frequency used this time was 150kHz with spacing of 150mm. Here it is shown clearly as the diameter of the bar increases the strength of the start of the wave increases, however in the case of the strand it was not possible to detect any change in the strength of the pre-wave.

Another set of experiments was carried out to examine the effect of the reinforcement presence on the rms (rms of the total signal was used) of the signals. The frequency used was 170kHz with spacings 10, 50, and 100mm. Plain and reinforced specimens were used which were cast from the same mix. Table 11.5 gives the result. It can be seen that in the presence of steel reinforcement the rms increases especially if the diameter of the bar is of the same order as the diameter of the transducer (the transducers had 25mm diameters), indicating a shorter path length hence less attenuation. The argument here could be that the attenuation is dependent on the volume and aggregate size and coupling.

Table 11.5- RMS calculations on the total signal records for plain and reinforced concrete.

Transducer Spacing, mm	Plain Concrete Volt	Reinforced with strand, V	Reinforced with 32 mm bar, V
10	123.6	193.18	220.78
50	98.877	114.44	145.11
100	82.55	145.111	150.55

3- Effect of Reinforcement on the Frequency Domain

After acquiring the time domain signals, they were Fourier transformed. Three of the same specimens as before were reanalysed: plain, reinforced with 15.6mm diameter strand, and reinforced with 32mm diameter bar. Data from two frequencies (150 and 170kHz) and three spacings (50, 100, and 200mm) were used.

Table 11.6 shows the result of this investigation. It can be seen that when the reinforcement was present the dominant frequency was higher than that of the plain sample. However for one case the dominant frequency was less than that of the plain beam, i.e. beam reinforced with the strand and where the transducers (170kHz) were spaced 200mm, the reason could be due to the scattering from the aggregates. The draw-back of this comparison is that the frequency spectrum depends on the volume and diameter of aggregate encountered during the propagation of the signal (see chapter 5), and moreover on the coupling between transducer and surface of the concrete.

Table 11.6- The dominant frequencies in the case of reinforced and plain concrete.

150kHz resonant frequency			
Transducer Spacing, mm	Plain Concrete kHz	Reinforced with strand, kHz	Reinforced with 32 mm bar, kHz
50	33.2031	121.093	115.234
100	29.927	121.093	115.234
200	29.927	35.156	113.281
170kHz resonant frequency			
Transducer Spacing, mm	Plain Concrete kHz	Reinforced with strand, kHz	Reinforced with 32 mm bar, kHz
50	166.02	169.921	171.88
100	74.219	167.97	167.97
200	72.266	35.1562	103.52

4- The Effect of the Presence of Chloride on the Signal: Time and Frequency Investigation

The comparison was carried with two specimens ($150 \times 150 \times 1000 \text{mm}^3$): one cast with strand (15.6mm diameter), and the second with the same diameter strand but with addition of (10% of the weight of the cement) salt to the mix used to cast the first specimen. The presence of chloride was intended to reproduce the presence of corrosion on site, moreover its presence would lower the strength of concrete. The contaminated specimen was tested 3 years after casting leaving the corrosion reaction to take place (after this period the strand could easily be seen to be corroded from the two extended ends).

The investigation was carried in three ways:

- 1- Velocity measurements.
- 2- RMS of the total time domain signals.
- 3- Dominant frequency from the total signal for the sound bar and the corroded bar.

Attempts to analyse the signal content of the prewave from these results were unsuccessful and therefore the full time domain signal was used, although it was recognised that the part of this signal reflected from the bar would be very small and difficult to distinguish.

The frequencies used were: 150kHz and 170kHz. The spacings investigated were 50, 100, and 200mm. Table 11.7 shows the arrival times of the time signals i.e. the start of the pre-wave, the rms of the full time domain signals, and the dominant frequencies from the total signal for the frequency spectra for the configuration examined.

Table 11.7- Time of arrivals, rms of the full time signals, and the dominant frequency for a sound and corroded strand in concrete.

Spacing mm	150kHz		170kHz	
	Time of arrivals, μ sec			
	Conc. with Sound Bar	Conc. with Corr. Bar	Conc. with Sound Bar	Conc. with Corr. Bar
50	27	29	24	26
100	40	43	37	42
200	67	84	57	76
	RMS of the full time signals, Volt			
50	161.59	39.368	210.113	42.725
100	124.44	32.196	179.6	34.33
200	117.95	28.076	99.945	14.039
	Dominant frequency, kHz			
50	121.093	25.391	169.921	70.312
100	121.093	27.344	167.97	72.266
200	35.156	27.344	35.1562	31.25

The first conclusion extracted from this study is that the velocity was less in the case of chloride specimen than that of the non-chloride concrete. This effect must be due to the change in properties of the concrete with chloride rather than any corrosion effect on the bar. However, the indication of concrete

deterioration may itself be useful in indicating potential corrosion problems.

The rms of signals for the contaminated specimen were dramatically smaller than for the uncontaminated specimen, and were more affected if large distance and higher frequency are used (in this case 170kHz and 200mm). In this case, both concrete and steel corrosion may affect the results because the higher frequencies are more attenuated due to the dispersive properties of both effects. Since both rms and dominant frequency analyses are based on the whole time domain signal, it would seem that the results are predominantly due to change in concrete condition, with a small contribution only from steel corrosion. To investigate this further, attenuation tests were carried out on both the chloride and non-chloride concrete away from the steel bars, and this showed that the attenuation in the contaminated specimen was substantially higher than the uncontaminated one, which indicated that the reduction of the strength of the received signals from the contaminated concrete is mainly due to the effect of the salt on the concrete itself. Moreover the dominant frequencies for the corroded specimen are all less than the dominant frequencies of the sound specimen for the spacings investigated.

Fig.11.7 shows two time signals and their frequency spectra, fig.11.7.a for the uncontaminated concrete block with sound bar and fig.11.7.b for the chloride concrete block with corroded bar for the spacing of 50mm and frequency 170kHz. It can be seen from this figure that the signal captured from the contaminated

sample (fig.11.7.b) has lost its strength in contrast to fig.11.7.a for the sound sample.

11.5- EXPERIMENTATION ON SLABS WITH AND WITHOUT SIMULATED CRACK

The two slabs were cast from the same mix. The dimensions were $800 \times 800 \times 150 \text{mm}^3$. One was very well compacted, but in the other a polystyrene disk of 200mm diameter was inserted and the time of compaction was reduced to simulate the presence of a flaw in a structure where the strength will be less than that of a sound structure.

Two methods of experimentation were carried out: the through-transmission method and the pitch-catch method (see fig.11.8).

The through-transmission method can be applied only if it is possible to have access to two opposite sides in a concrete structure. Fig.11.9 shows the time signals captured from the two slabs using the through-transmission technique, fig.11.9.a from the sound slab and fig.11.9.b from the slab with flaw. The transducer frequency used was 150kHz. It can be seen that the flaw (the polystyrene disk) obscured the transmission of the signal to the receiver in the other side. This method gives a reliable result for detecting voids if two sides can be accessed.

The pitch-catch method which is under investigation throughout this chapter gives the result shown in fig.11.10. Fig.11.10.a shows the signal from the slab with no void and fig.11.10.b the slab with void. The transducer frequency was 150kHz and the

transducer spacing was 200mm. The experiment was carried out under the disk (simulated flaw). It can be seen that the presence of the disk scattered the signal and due to the shorter compaction time in the case of the flawed slab the signal was more attenuated i.e. the maximum amplitude was 0.040V for the sound slab and for the flawed slab 0.018V. The attenuation could be due to the scattering of the signal which is due to the presence of the disk and due to the reduction in the compaction time which led to a concrete with more voids and therefore less strength.

11.6- EXPERIMENTATION ON DUCTED SAMPLES

Two samples were cast: the first with a 50mm diameter corrugated empty duct embedded in concrete, and the second with a 50mm diameter grouted duct containing one strand of 15.6mm diameter.

Two methods of investigation were studied:

- 1- The strength of the pre-wave.
- 2- the rms of the full time signal.

Fig.11.11.a shows a time signal recorded from an empty ducted sample and fig.11.11.b from a strand in a grouted duct. The configuration was: the transducer frequency was 250kHz spaced 250mm. It can be seen clearly that the signal starts earlier and the strength of the pre-wave is higher.

Moreover Fig.11.12 is for the same set-up but for transducer

frequency of 150kHz (fig.11.12.a is for the void duct embedded in concrete and fig11.12.b is for the grouted duct with strand). Again it can be seen easily that the strength of the pre-wave in the case of the void duct is higher than that of the grouted duct.

A set of experiments was carried out in order to establish the effect of the presence of a void duct compared to a grouted duct. The comparison was examined in the time domain as no major changes in the frequency spectra were obvious. The rms was calculated for the full time records. The frequencies used were 150 and 170kHz. The transducer spacings were 100, 200, and 300. Table 11.8 shows the rms of the configurations mentioned.

Table 11.8- The rms calculated from time domain signals on void and grouted duct specimens.

150kHz		
Transducer Spacing, mm	Void Duct V	Grouted Duct V
100	122.68	108.032
200	86.823	59.357
300	73.242	54.779
170kHz		
Transducer Spacing, mm	Void Duct V	Grouted Duct V
100	136.413	108.8
200	69.4274	50.9643
300	60.425	34.943

The conclusions achieved from these set of experiments are that the pre-wave is stronger in the case of a void duct than that of

a grouted duct. Furthermore, the comparison of the rms of the full time signals from a void duct and that of a grouted duct reinforced with strand through indicates that the path length of the sound or signal is smaller than that of a grouted duct (the rms in the case of the void duct is larger than that of a grouted case). The reason could be that the wave is reflected at the boundary duct/air, in the case of a void duct, giving rise to a high rms, in contrast to the case of a grouted duct where a small amount of energy is reflected at the boundary concrete/mortar which could be due to the difference in the acoustic impedances of mortar and concrete. It should be mentioned that no major reflection occurs at the duct surface because the thickness of the duct is less than 1mm which is much less than the wavelength, about 23mm for 170kHz transducers, therefore the duct acts as a transparent film for the incident signal.

11.7- CONCLUSIONS FROM SMALL-SCALE LABORATORY TESTS

The major conclusions from these tests using time domain and frequency domain analysis were:

1- Signal (apparent) velocity:

This decreases under the following conditions:

- a- Presence of chloride.
- b- Low strength.
- c- Presence of a flaw.
- d- Surface breaking (large path length).

It also increases when steel reinforcement or empty duct is present.

2- Signal amplitude (energy and rms):

This decreases under the following conditions:

- a- Concrete quality variation, especially chloride contamination i.e. severely corroded cables resulting in disbonding at the concrete/steel interface.
- b- Voids or flaws larger than the wavelength.
- c- Cracking

It increases when a void duct or steel reinforcement is present.

3- Signal frequency

The appearance of low-frequency components could possibly be due to the presence of voids or delaminations where the high frequencies are attenuated and scattered. The strengthening of high frequency components could be due to steel components or empty duct. However the weakening of the high frequency components could be referred to damage/fracture of steel reinforcement due to scattering.

The conclusions drawn from these experiment and analysis show limited success because some of them if repeated would not yield the expected result (it should be noted that the experiments

above were carried out with great care, that is, under highly controlled conditions in an attempt to improve reproducibility).

Therefore if the system had to be limited to these conditions, it would not be practical under field conditions.

11.8- APPLICATION OF DIGITAL FILTERING TECHNIQUES TO A SYSTEM FOR FLAW AND CORROSION DETECTION

Having considered the analysis of the whole frequency spectrum in either the time domain or the frequency domain, and considered again the theoretical modelling and analysis, it was clear that the major element missing was the ability to separate out and compare signals at chosen different frequencies. Attempts to obtain or make transducers of discrete narrow band frequencies with very short ringing times had been unsuccessful. A final attempt was therefore made to provide this information in an equivalent way by selective digital filtering technique.

Consider a broad-band ultrasonic pulse containing frequencies up to several hundred kHz, travelling through concrete containing inclusions such as small voids (<20mm diameter) and steel cables, with interface regions between the steel and the concrete. It has been shown before that the high frequency constituents are attenuated more severely due to the heterogeneous nature of the concrete. This of course is undesirable, because it is mainly the higher frequencies which contain information regarding the internal composition of the structure and condition of embedded components. Where these frequencies encounter boundary

conditions (such as voids or interfaces) reflection will occur, the strength being dependent upon the relative acoustic impedances, wavelength, and frequency. At 250kHz for instance, where the wavelength in concrete is approximately 16mm, strong reflections will take place from interfaces or discontinuities whose dimensions can be compared to the wavelength; by contrast these same features will influence frequencies below 100kHz very little.

The total signal that arrives at the receiver will include low frequency components of large amplitude and relatively little information and high frequency components, that do change according to the variations in the material composition through which they propagate and surfaces at which they are reflected, but whose energy is very often of the order of one thousand times weaker than their low frequency counterparts.

For this reason, analysis of the total signal has yielded sometimes a limited success since the frequencies of interest were completely buried in noise. What was needed was a filter which removes the lower portions of the spectra.

The filtering technique was carried out as follows:

- 1- A scan for the sample to be tested was carried out. The chosen frequency was higher than 150kHz (the frequencies used for this technique were 170 and 350kHz) with transducers spaced less than 100mm which was found to give better results because the high frequency components were not as severely attenuated i.e.

smaller path length. The result was a number of time signal records.

2- The time signals were then Fourier transformed.

3- A brick-wall filter was then applied to the frequency spectra. Discrete frequency bands, i.e. band-pass brick-wall filters, were applied. The increment was taken equal to 50kHz, for example for the 170kHz transducers the bands were 0-50kHz, 50-100kHz, 100-150kHz, 150-200kHz. The width of the band was dependent on the transducer frequency, transducer spacing and the digitizing rate. Sometimes only one frequency band was needed i.e. say 100-150kHz.

4- Then the filtered data were inverse Fourier transformed.

5- Calculation of the energy for each of the filtered time signals for the scan for each band was carried out and a trend plot was plotted for these values. Each trend plot for the different bands was then multiplied, for example for the 170kHz transducers carrying out the filtering mentioned in (3) 4 energy trend plots, are obtained, say e_1 , e_2 , e_3 , and e_4 .

6- The individual energy results e_1 , e_2 , e_3 , e_4 , and e_5 , were multiplied together sometimes it was enough to apply one band filter and therefore no need to do this step). The result is a trend plot of the multiplication carried out.

7- In the presence of a void or corroded components a peak occurred in the resultant trend plot showing the presence of high

frequency components compared to the other readings. The explanation for the peak, i.e. stronger high frequency components, is that the received signal has suffered less attenuation due a shorter path length due to reflection at the void interface or at the embedded steel/concrete interface or where the corrosion of the steel components could have caused spalling. Another explanation is that when the probes are positioned over a defect causing the formation of acoustic boundaries, the receiver will detect, in addition to the (random) echoes from the aggregates, more energy reflected from the region of discontinuity. By filtering the signals into frequency bands, determining their energy levels and multiplying these results, the energy relating to one defect is greatly enhanced. This is essentially a form of signal auto-correlation.

11.9- EXPERIMENTAL WORK USING MULTIPLE RECEIVING TRANSDUCERS

11.9.1- Scanning the Large Scale Test Beam

In an attempt to see whether comparative techniques using multiple receiving transducers could deal with the problems of scatter and heterogeneity, a scanning system was tried. A schematic diagram of the scanning system used is illustrated in fig.11.2.

The experimental configuration was as follows:

Scan 1:
No of readings:89
Scan interval: 50mm
Transducer spacing: 50mm
Sample frequency: 1 MHz
Frequency: 170 kHz

Scan 2:
No of readings:89
Scan interval: 50mm
Transducer spacing: 100mm
Sample frequency: 1 MHz
Frequency: 45 kHz

Scan 3:
No of readings:89
Scan interval: 50mm
Transducer spacing: 265mm
Sample frequency: 1 MHz
Frequency: 250 kHz

A number of scans were made of the top surface of the test beam, whose upper internal structure is shown schematically in fig.11.13 (a description of the beam is given in chapter 9). Various faults were incorporated in the beam as shown in fig.11.13. The transducer array was positioned with transducers R1 and R2 over the centre cable B, and transducers R3 and R4 over cables C and A respectively. All transducers were spaced 100mm from the central transmitter. The total length scanned was 4.45m (although the beam was nearly 5m in length).

Fig.11.14 shows the unprocessed waveforms (scan 1) collected by transducer receiver R1 of 170kHz nominal frequency, windowed between $28\mu\text{sec}$ and $92\mu\text{sec}$ for purposes of clarity. Each waveform represents results from one sample position of the transducer R1. Although there is some evidence to suggest that the amplitude decreases over the area containing salts and also decreases over the area containing stirrups, the dominant feature is the lack of coherence between successive waveforms. This suggests that the dominant interrogating wavelength is too small i.e. frequency too high, since it is scattered by the intervening aggregate which is randomly distributed. As a result, the frequency spectrum for this particular case is shown fig.11.15, and contains no

information of significance, and neither does the trend data for the dominant frequency (fig.11.16.a), rms (fig.11.16.b), point in time at which maximum signal amplitude occurs (fig.11.16.c), and dominant frequency calculated in the frequency domain (fig.11.16.d).

Because of the fluctuations in the waveforms, the subtracted data sets (R1 minus R2 and R3 minus R4) also become meaningless. These were intended to eliminate the effects of the surface Rayleigh wave, assumed to be constant, but because of the variability the new waveforms are also random.

The data collected by transducers R2 and R4 also displayed similar variability. As a consequence, a scan (scan 2) was performed along the centre cable using only a transmitter and a receiver (only two transducers) of 45kHz. Fig.11.17 shows the raw waveforms. Immediately it can be seen that there is now considerable coherence between successive signals, which suggests that the effects of scatter have considerably reduced (this is readily understood when we consider that Rayleigh scattering is proportional to f^4). The signal attenuation associated with the region containing the stirrups is now more pronounced, but there is little to indicate the region containing salt.

At this point the data produced have been inconclusive. It was decided therefore to use the filtering technique.

11.10- EXPERIMENTAL WORK USING THE DIGITAL FILTERING TECHNIQUE

11.10.1- Detection of Steel Bar in a Concrete beam

Two concrete beams of dimensions $150 \times 150 \times 1000 \text{mm}^3$, one containing a strand of 15.6mm diameter, and the other plain, (no steel components were embedded), were scanned transversely, i.e. perpendicular to the axis of strand, using two 350kHz rolling transducers, spaced 75mm. Thirteen readings were taken, using a digitizing speed of 1 MHz and a record length of 512 points.

Each record was Fourier transformed for each scan, then discrete brick-wall band-pass filters were applied, of 50kHz bandwidth. Then inverse Fourier transformed, and the energy calculation for each record filtered for the different bands was carried out.

In mathematical terms the calculations were carried for the two scan as follows:

- a- Scan the two beams transversely. The result is 13 time records.
- b- FFT of the 13 readings.
- c- Apply band-pass filters and IFFT each record:
 - Band-pass between 0-50kHz, IFFT the filtered signal, and calculate the energy values, and plot the trend for the 13 records, call it e1.
 - Repeat above for 50-100, 100-150, 150-200, 200-250, 250-300, and 300-350kHz, and call the plots e2, e3, e4, e5, e6, e6, and e7.

d- Multiply $e_1 \times e_2 \times e_3 \times e_4 \times e_5 \times e_6 \times e_7$ and the result is a new trend plot.

Fig.11.18 shows the result for the plain concrete specimen, and fig.11.19 shows the result for the reinforced beam with strand.

From fig.11.18 it can be seen there no evident peak, but rather small peaks indicating that the energy is about the same for all the readings, but in the last reading there is an increase in the energy which could be due to the edge effect. However for the reinforced beam it can be seen very clearly (fig.11.19) that a peak exists in the middle of the plot where the strand is present indicating the detection of the strand.

11.10.2- Detection of Steel Bar in a Grouted Duct

A concrete beam ($150 \times 150 \times 1000 \text{mm}^3$) reinforced with a strand embedded in a grouted duct was scanned with two rolling transducers of 350kHz nominal frequency, spaced 75mm. Thirteen readings were taken, using a digitizing speed of 1 MHz and a record length of 512 points.

The same calculations were carried as (11.10.a). The result is shown in fig.11.20. It can be seen very clearly that the peak in the middle indicates the presence of the duct and the strand. It is not known at this stage, whether the peak could be due to the duct rather than the strand.

In the next section a scan was carried out on a beam with a duct

grouted with a void left in the middle.

11.10.3- Detection of a Void in a Ducted Concrete Beam

In order to check whether the system of looking at narrow frequency bands by digital filtering could detect readily discontinuities of the same order of size as the wavelength associated with grouted ducts, a concrete beam, of dimensions $300 \times 150 \times 800 \text{mm}^3$, containing a 50mm steel corrugated duct lying along its axis was manufactured with a void at its centre point (formed by the insertion of two hollow plastic spheres, diameter 40mm), the remainder of the duct being filled with grout at one end and four 7-wire strands plus grout at the other. The beam was scanned using two probes at this stage, in pitch-catch mode. The frequency used was 170kHz with a probe spacing of 100mm and a scan step of 20mm. A total of 35 readings was taken, using a digitizing speed of 1 MHz and a record length of 512 points.

Each record was then transformed to the frequency domain, high-pass filtered with a lower cut-off point of 150kHz, re-transformed to the time domain and scalar measurements were taken (energy, time of arrival, etc.). Fig.11.21 represents the energy of each reading for all frequencies above 150kHz. The first peak corresponds to the position of the receiver directly over the void, and the second to the position of the transmitter directly over the void. The peak energy about $5 \cdot 10^{-5} \text{ V}^2 \text{sec}$ represents about 1/1000th of the total energy of the unfiltered signal.

11.10.4- Detection of a Flaw in the Large Scale Test Beam

Since the above results clearly held promise, the method was applied to the detection of the void in the large scale test beam (scanned in 11.9.a and described in chapter 9). Fig.11.22 shows the result. In this test a total of only 25 readings were taken with a scan increment of 25mm, over the general vicinity of the void. The same transducers as 11.10.c were used with 100mm spacing. In this case only a single peak is evident, possibly due to the large diameter of the void.

Fig.11.23 shows the trend analysis of the energy values returned when the technique was applied for the centre cable of the above test beam. In this case, the trace represents the processed data obtained from scanning the centre cable of the beam (top surface, see fig.11.15) using the 170kHz transducers (scan 1). The peak corresponds exactly to the point at which the centre cable was deliberately contaminated with chloride before casting.

The technique is not simple nor without problems, as shown by figs.11.24 and 11.25. Again Fig.11.24 represents a scan of the upper centre cable, using the same probes but different digitization rate, i.e. 10MHz instead of 1MHz and a different filtering regime, a 180 to 200kHz band pass filter was applied. This was necessary because the spectral resolution provided by a sample rate of 10MHz and a record length of 512 points (19.53kHz) was too crude with a consequent reduction in energy and increase in noise. However, the peak is still in evidence and since these data were obtained from an entirely separate scan, it showed that

this is not a random coupling improvement.

Fig.11.25 shows what happens when the wrong experimental configuration is used. Again, the centre cable is being scanned (scan 3), but with entirely different probes (nominal frequency 250kHz) a spacing of 265mm rather than 100mm. No amount of signal processing improved these data.

This result suggest two important factors with this level of analysis:

1- The best results are obtained when the probes are as close together as possible. Moreover the greater the transducer spacing, the greater the distance the signal has to travel from transmitter to receiver and the more severe the high frequency attenuation becomes in the concrete, compared to reflection behaviour at embedded components.

2- Linked to the consideration of (1) is the aspect of optimizing the filter bandwidth. If too little low frequency rejection is performed (i.e. low frequencies are included in the energy estimates) the trend data of the energy measurements will be random, similar to fig.11.25. If too high a frequency band is selected, say between 400-500kHz (for the transducers currently used), the data again will be random. This is because there is virtually no energy radiated by the probes in this region and most of what is detected is simply random thermal noise. Similarly, probes that are spaced too far apart will transmit and receive signals with high frequencies so attenuated that they are

of similar magnitude to random thermal electronic noise at that range. Once again, the trend data will be incoherent.

The most critical point is reached when the transmitter is positioned over the region of delamination, salt, etc. The position of the receiver is less important subject to the point about spacing.

In support to the above finding, consider fig.11.26. Here, the transmitter is tracking along the centre cable but the receiver is positioned over a side cable. There is no evidence to suggest that any defects to this side cable are being detected, but the receiver once again registers a large change in high-frequency energy as the transmitter passes over the salt-contaminated region of the centre cable. Moreover, in this experiment the probes had 170kHz nominal frequency and were spaced 80mm.

The most significant feature of the traces presented above is that they represent a body of data, in itself consistent with the notion that real changes are being detected. The next step was to establish if the evidence provided by this method of analysis can form a basis of a reliable practical prototype system. It was decided therefore to re-scan the test-beam using transmitter-receiver pairs tracking over the contaminated areas using rolling transducers.

11.10.5- Using Rolling Transducers to Scan the Test Beam

Because the probes used so far are not suitable for a field prototype (they require considerable attention with regard to coupling), a set of rolling transducer probes were hired from C.N.S. Instruments, having a nominal frequency of 350kHz. These

reduced the problem of coupling and improved the scan speed. The evaluation has been carried out according to the criteria used before for the existing probes with regard to frequencies, bandwidth, and sensitivity.

In order to reduce the random element in signal energies due to coupling, a refined frequency-filtering technique was investigated, in which, instead of relying on absolute energy magnitude, a ratio will be returned of the energies in the high frequency and low frequency bands. The rationale here is that coupling variations will affect both low and high frequency components and hence tend to cancel out, whereas small inclusions, as suggested by the findings in this work will only be revealed by the high frequencies.

Seven scans were carried out on the same test beam as used for (3) above as follows:

Frequency: 350kHz

Spacing : 65mm

Increment: 20mm

Readings : 31, always the middle reading the transmitter will be over a void or corroded strand or cracked strand, i.e. to make it easier to compare the results in the trend plot where the middle reading will show the peak.

Two scans were carried over the two voids (see fig.11.15), three scans over salted regions where corrosion was expected, and two scans over a cracked strand (it is worth mentioning that there is

a good bond between the strand and the concrete in this case whereas in reality where there is a broken wire or bar de-bonding would be expected).

The time signals were Fourier transformed for each scan, and then each spectrum was filtered. The frequency-filtering technique was carried out as the following:

1- Applying a filter between 0-50kHz on the initial time signal records, then IFFT the filtered spectra, and finally plot the energy trend for the filtered signals and call the result e1.

2- Repeat 1 but with filtering between 50-100kHz, and call the energy trend plot e2.

3- Repeat 1 with filtering between 100-150kHz, and call the energy trend plot e3.

4- Repeat 1 with filtering between 150-200kHz, and call the energy trend plot e4.

5- Repeat 1 with filtering between 200-250kHz, and call the energy trend plot e5.

6- Repeat 1 with filtering between 250-300kHz, and call the energy trend plot e6.

7- Repeat 1 with filtering between 300-350kHz, and call the energy trend plot e7.

8- Repeat 1 with filtering between 350-400kHz, and call the energy trend plot e8.

Then the ratio (R_{CC}) was derived using the following equation:

$$R_{CC} = e8 / (e1.e2.e3.e4.e5.e6.e7)$$

By dividing e8 by (e1.e2.e3.e4.e5.e6.e7) the coupling variations which will affect the low and high frequency tend to cancel out, leaving the features which are affected by particular bands of frequencies to be revealed. However the multiplication (e1.e2.e3.e4.e5.e6.e7.e8) was enough sometimes to reveal the presence of the defects.

Figs.11.27, and 11.28 are the results from the scans over the voids using the technique explained before i.e. the ratio was used. The voids are very well detected.

Figs.11.29, 11.30, and 11.31 are the results from the scans over the salted regions. The regions are shown clearly. Here the multiplication was used.

Figs.11.32, and 11.33 are the output from the scans over the two cracked strands using the filtering bands technique illustrated before. The results are here doubtful, this is because no voids were left when the beam was cast between the strand and the surrounding concrete.

The evidence again has shown that this technique can be a basis for detection of flaws and major corrosion in pre-stressed and reinforced concrete.

11.11- PROPOSAL OF A SYSTEM FOR FLAW AND CORROSION DETECTION

At its present stage of development, the system is very much a laboratory prototype system. To make it a practical system which could^{be} suitable for field testing, a prototype scanning system is proposed, a schematic diagram is shown in fig.11.2. The analysis of the data is performed entirely by the analyser, which operates on the data collected by the four receiving rolling probes (see fig.11.7) where a central rolling probe is used as transmitter. It performs the following functions:

a- Display of the collected waveform for each rolling transducer R1 to R4, in the time domain for each scan position. Fig.11.14 shows an example of this. Each line represents the signal received by transducer R1 within the period 28-29 μ sec, and all the signals are displayed in a sequence corresponding to this position along the length of the beam. This form of presentation is known as a waterfall display which enables rapid identification of any differences between the signals.

b- Calculation of the frequency spectrum for each scan waveform, R1 to R4, and display in waterfall mode, for each scan position. An example of this presentation of the frequency domain information is given in fig.11.15.

c- Calculation of scalar quantities for each reading, to enable trends to be determined and displayed as plots. In such plots the x-axis represents position along the beam, and the y-axis the

calculated signal quantity. Up to eleven scalar quantities may be computed using the analyser from any individual signal including rms, dominant frequency, average period, cycle number, mean voltage, energy, peak-to-peak voltage, maximum voltage, minimum voltage, and time of occurrence of maximum amplitude. An example of a set of four trend plots is shown in fig.11.16.

d- Applying a brick-wall filter to the frequency spectrum for each scan waveform, R1 to R4, and then IFFT (Inverse Fourier Transform) of the filtered data, and then calculation of scalar quantities (trends) on the filtered time signals, and then display these as plots.

e- Calculation and display of waveforms derived by subtracting signal R2 from signal R1, and signal R4 from signal R3, and subsequent calculation of time domain, frequency domain and trend data on these new data sets.

The entire system, control of the analyser, and data storage is supervised by a computer program.

Practical testing of this proposed system has not been possible with the timescale and limitations of this Ph.D. research. Further development work on practical aspects of the scanning system is expected to lead to field trials followed by commercial applications.

11.12- CONCLUSIONS

The pitch-catch technique has been used for investigation of components in concrete (prestressed or reinforced). A system has been developed using this technique (instrumentation and signal processing) for finding defects in concrete.

From the experiments of the small samples it was clear that it was necessary to separate out and compare signals at chosen different frequencies by applying digital filtering.

The application of digital filtering techniques in the frequency domain has allowed the high frequency signal content to be separated out. This in turn has enabled firm detection of major voids and offers the potential of identifying major corrosion or cable/breaks (on the condition that Δ -bonding exists between the surrounded concrete).

The use of rolling probes proved to reduce the problem of coupling and improve the scan speed.

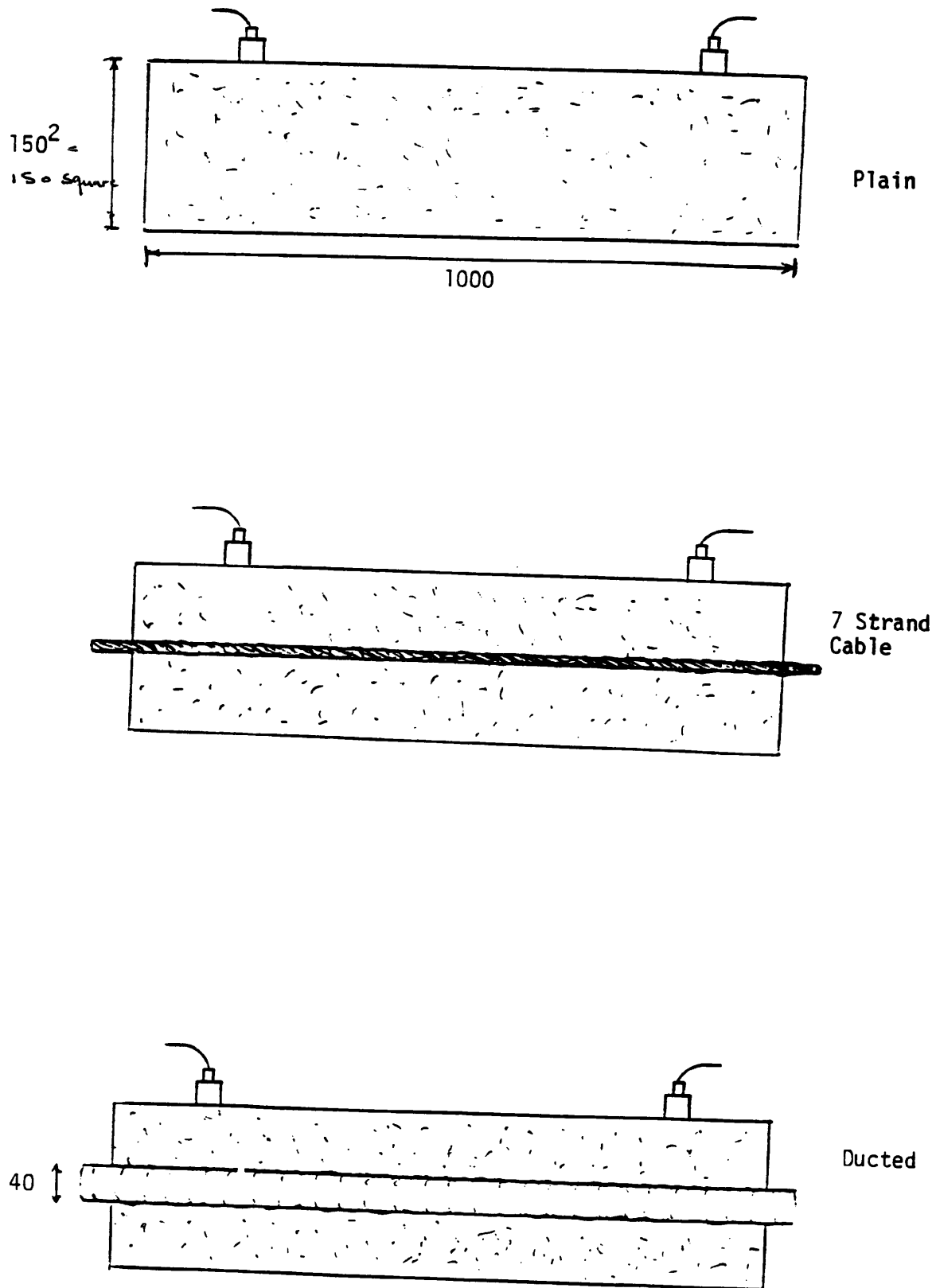
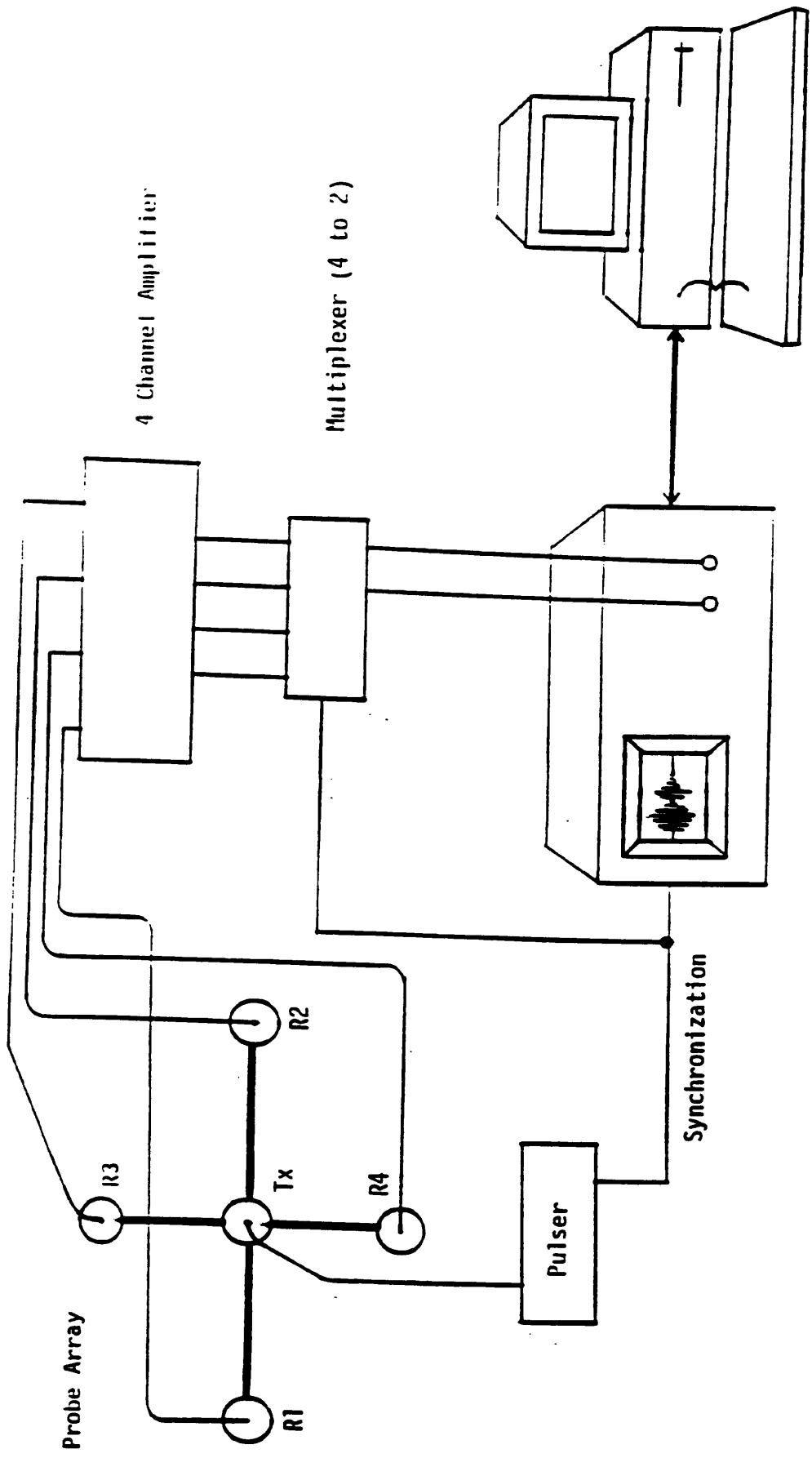


Fig.11.1- Samples used in the experiments.

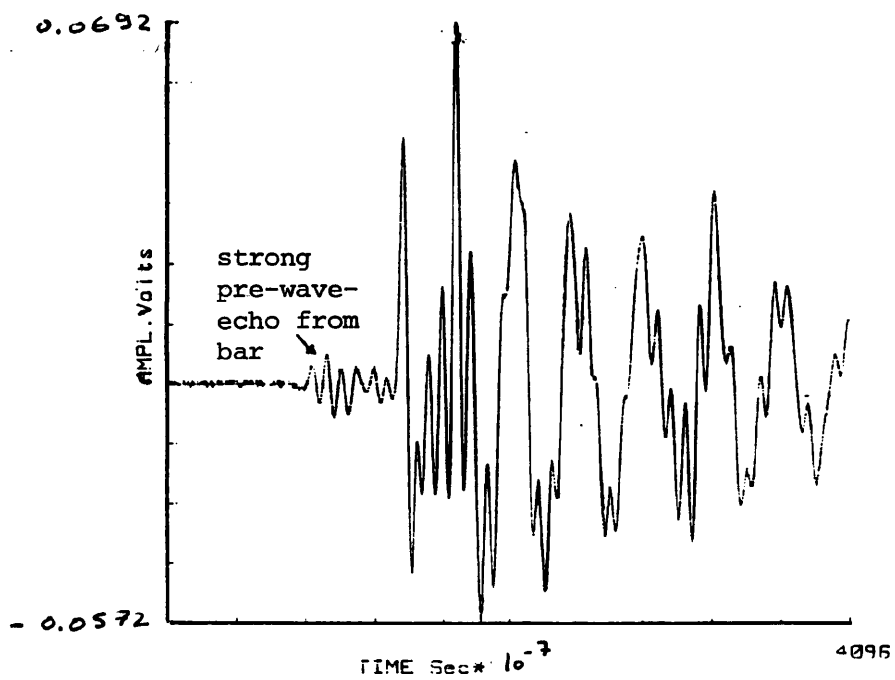


Waveform Analyser

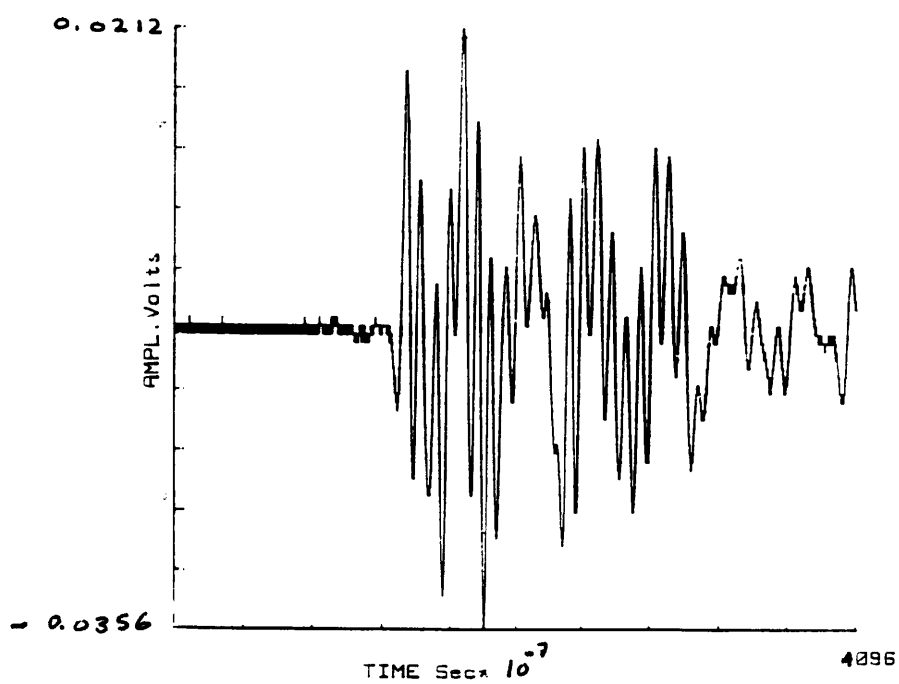
(Programming analyser, data storage and retrieval)

Fig.11.2- Schematic diagram for the scanning system used.

Fig.11.3

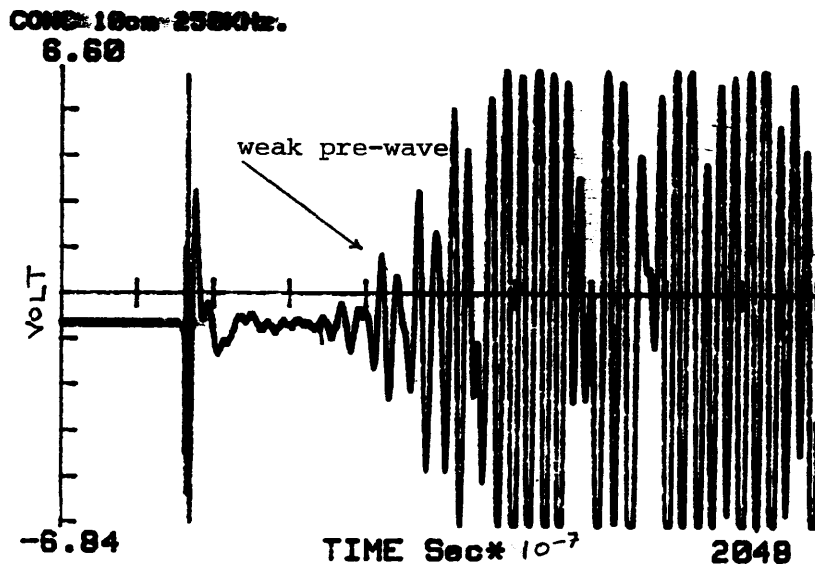


a- Mortar with 10mm diam. bar through.

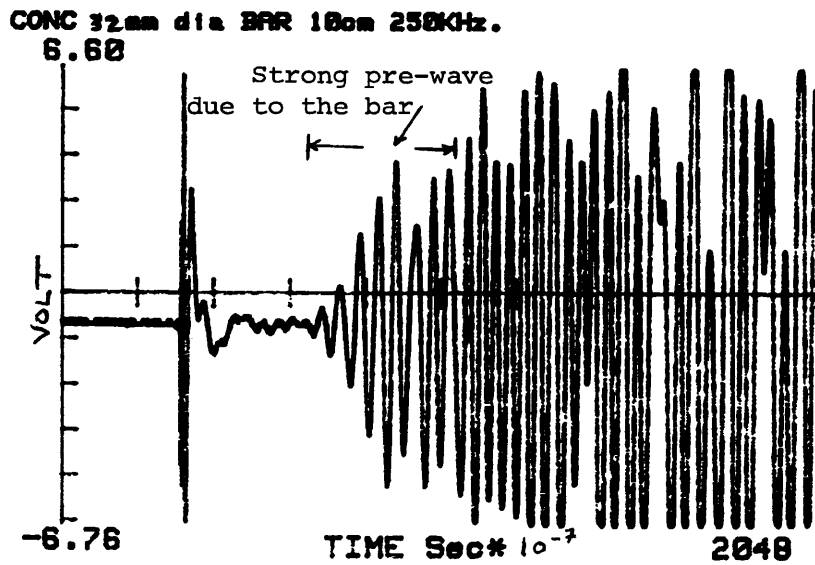


b- Plain mortar.

Fig. 11.4

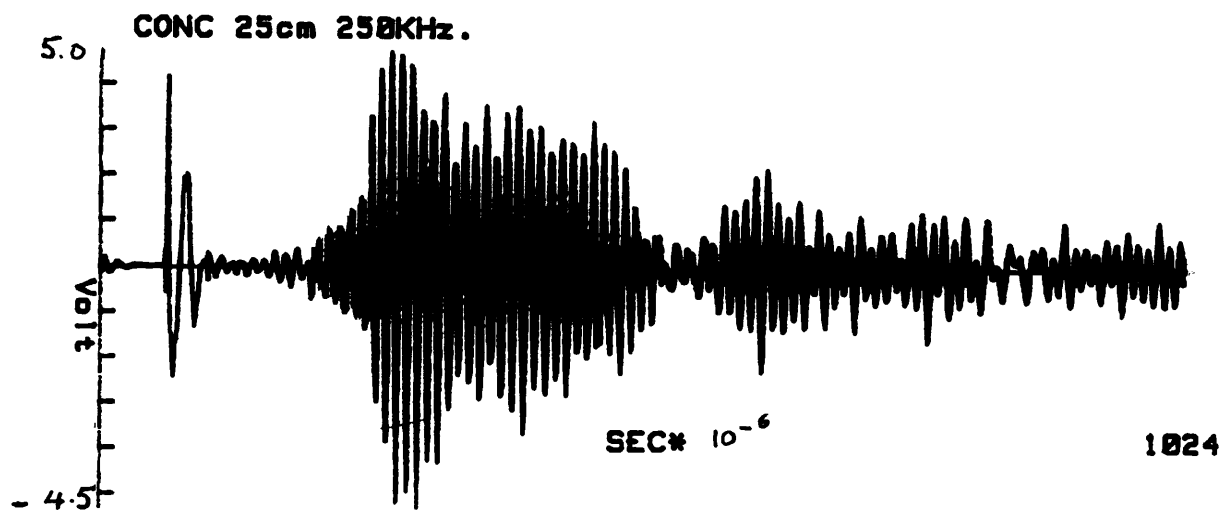


(a)

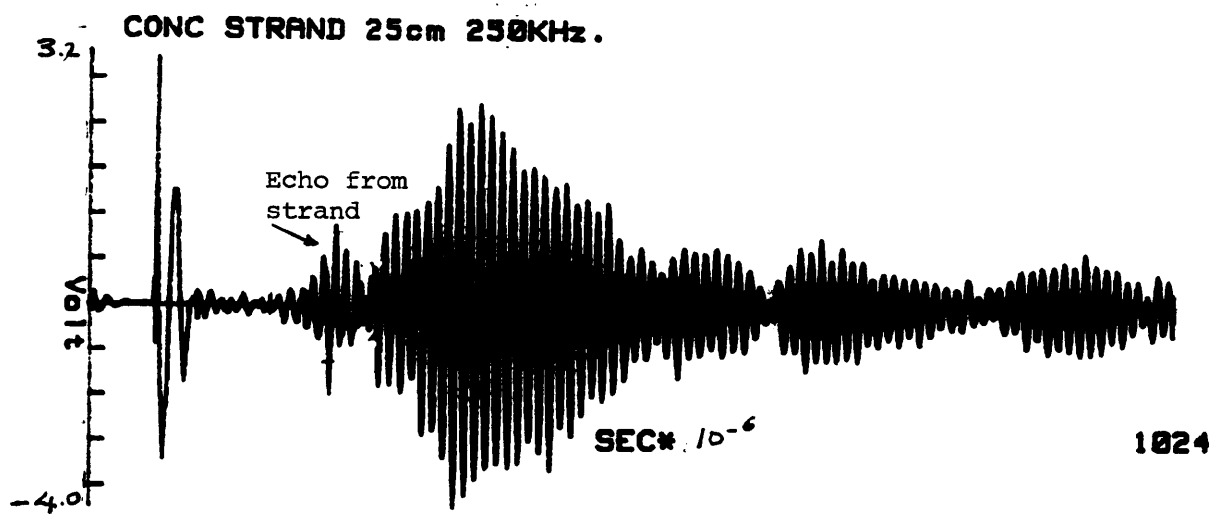


(b)

Fig.11.5



(a)



(b)

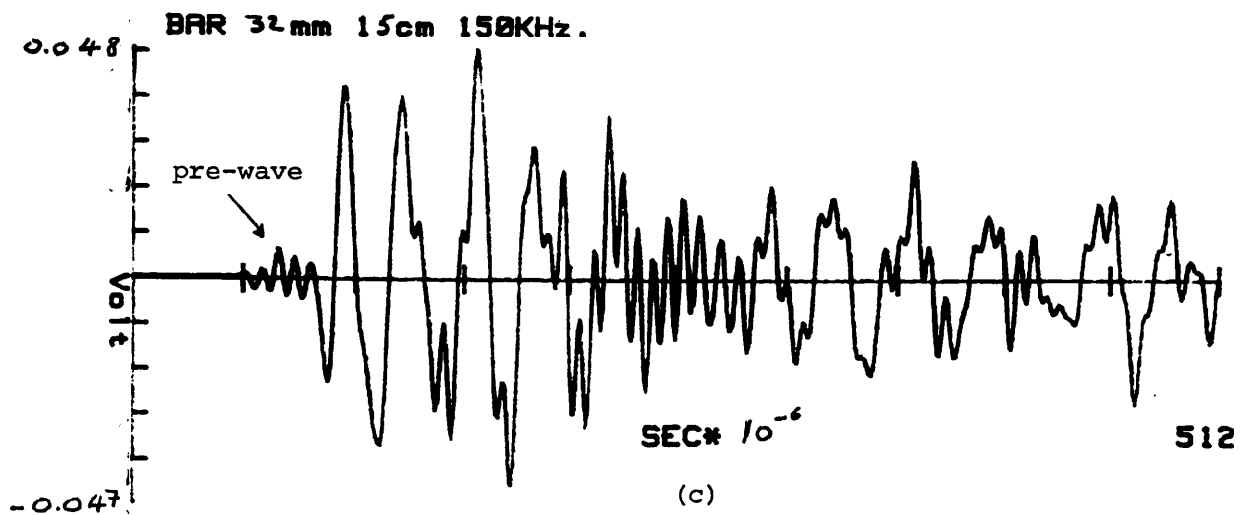
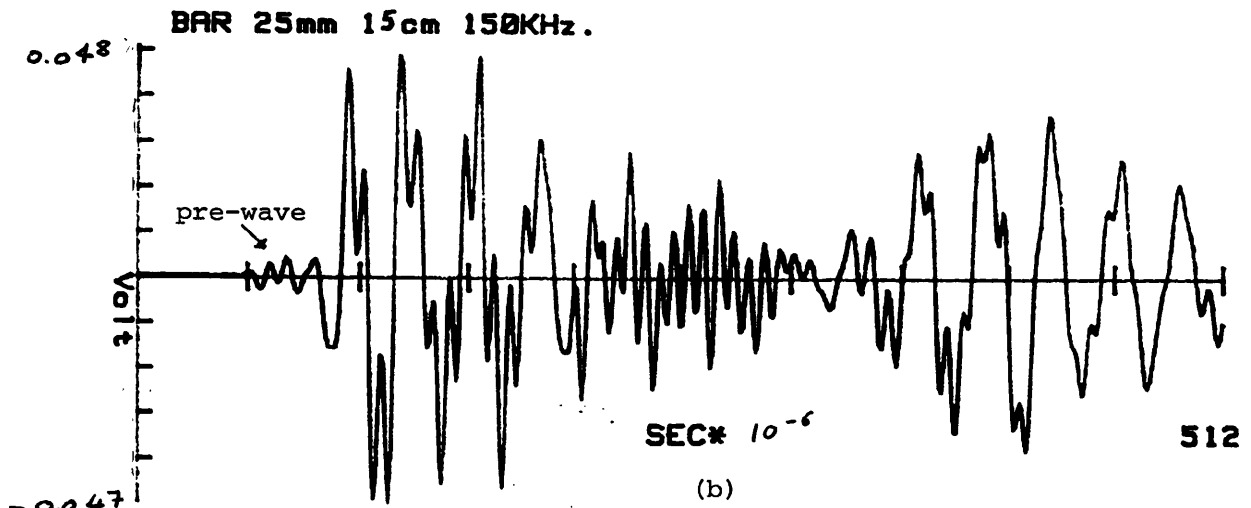
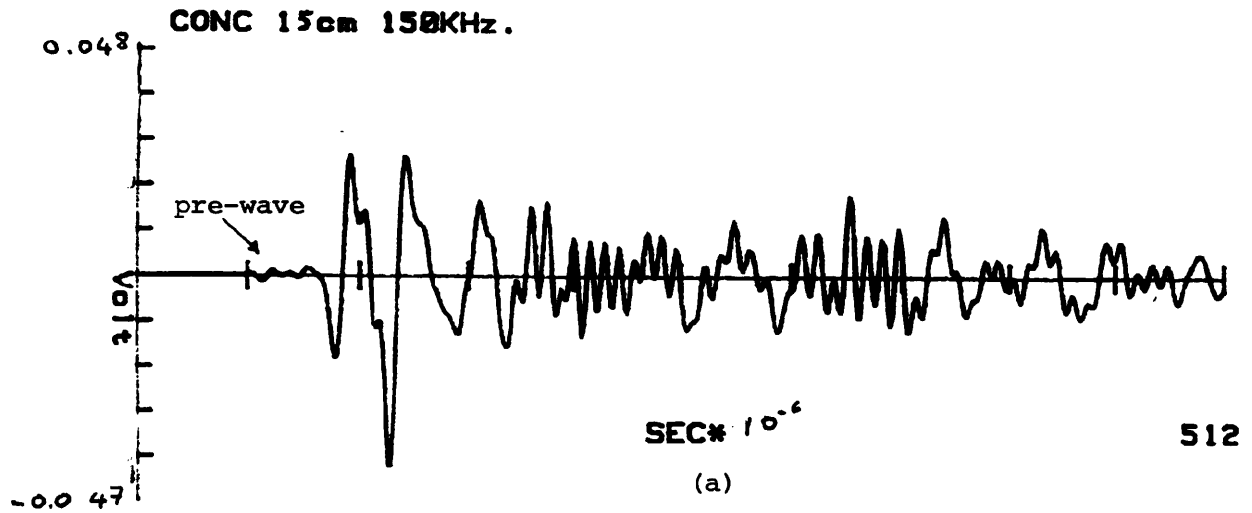
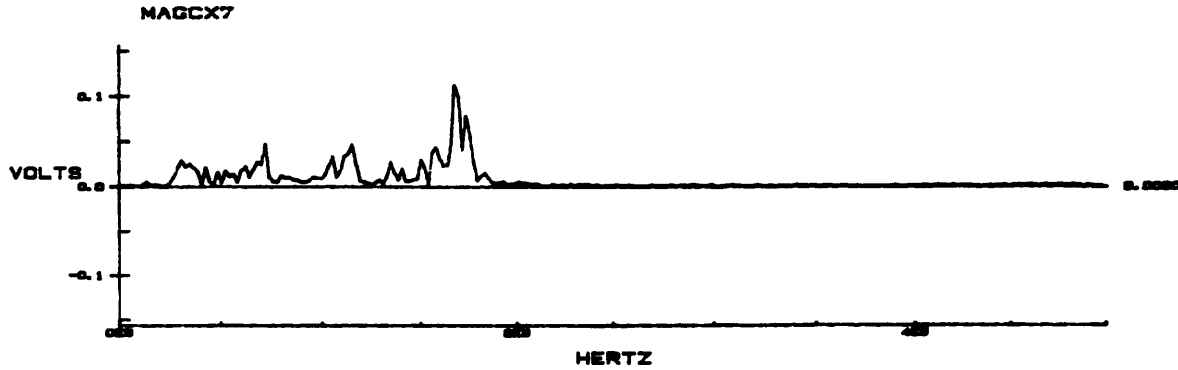
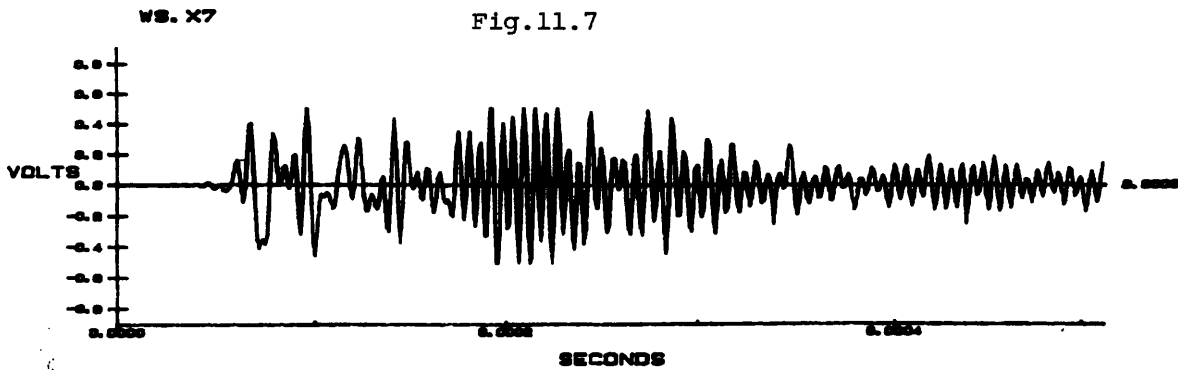
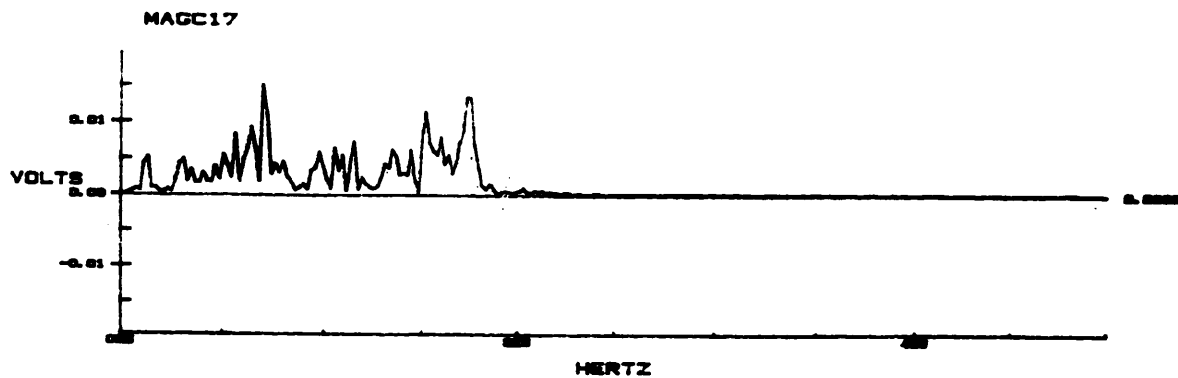
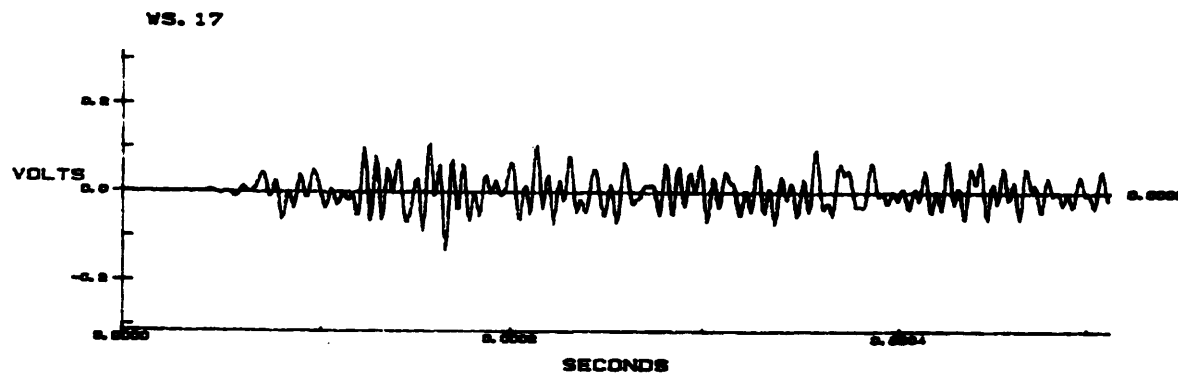


Fig.11.6- Notice how the pre-wave increases with bar diameter.

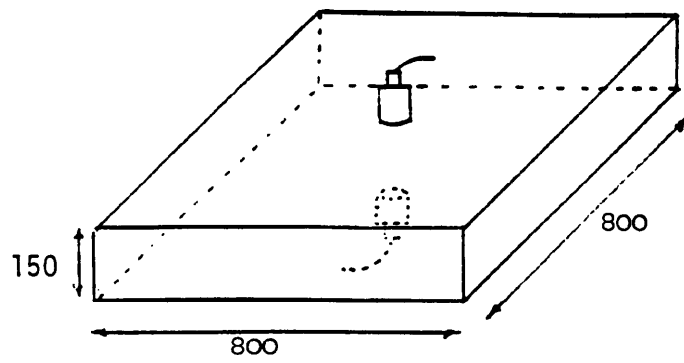


a- Signal and its spectrum from uncontaminated concrete block with sound bar.



b- Signal and its spectrum from chloride concrete with corroded bar; notice how the signal is weaker compared to (a).

Direct Transmission



Indirect Transmission

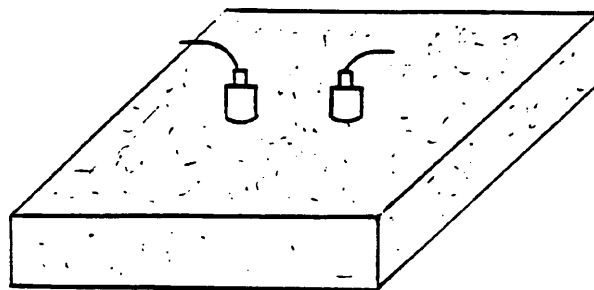
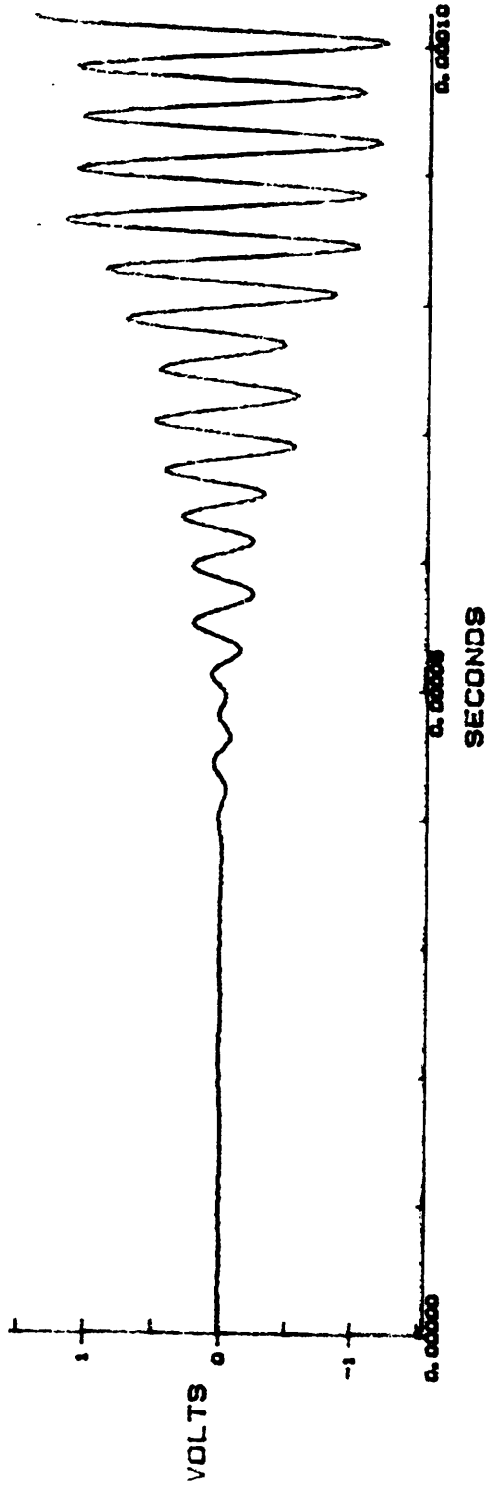
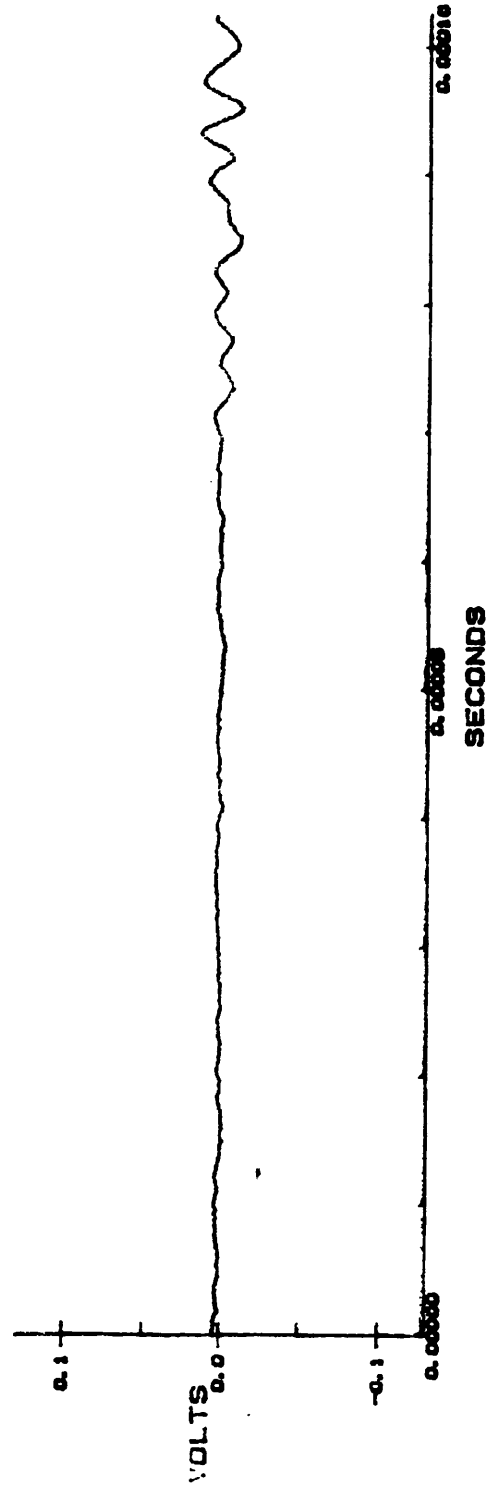


Fig.11.8



a- Through transmission testing for the slab with no disk.



b- Through transmission testing where polystyrene disk is between the transmitter and the receiver; notice how the disk obscures the transmission of the signal.

Fig.11.9

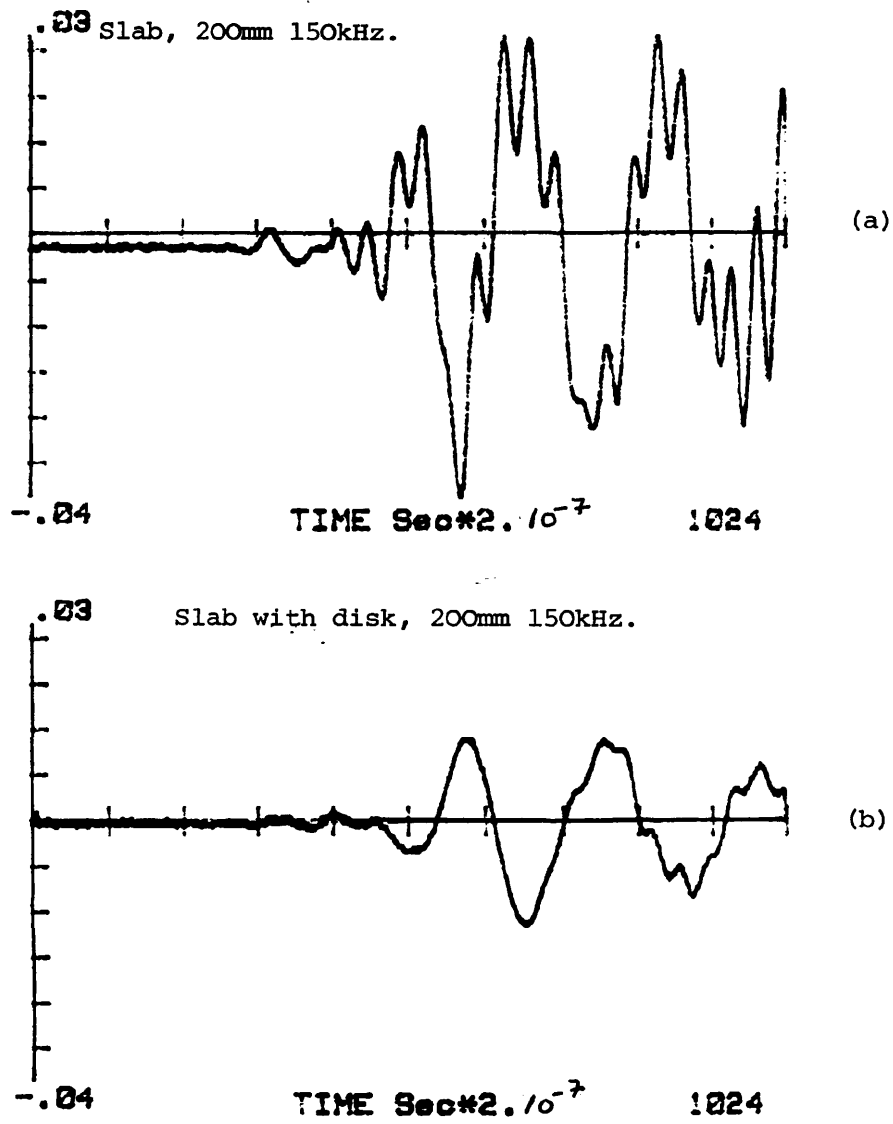


Fig.11.10- Indirect testing of the two slabs; notice how improper compaction decreases the strength of the signal.

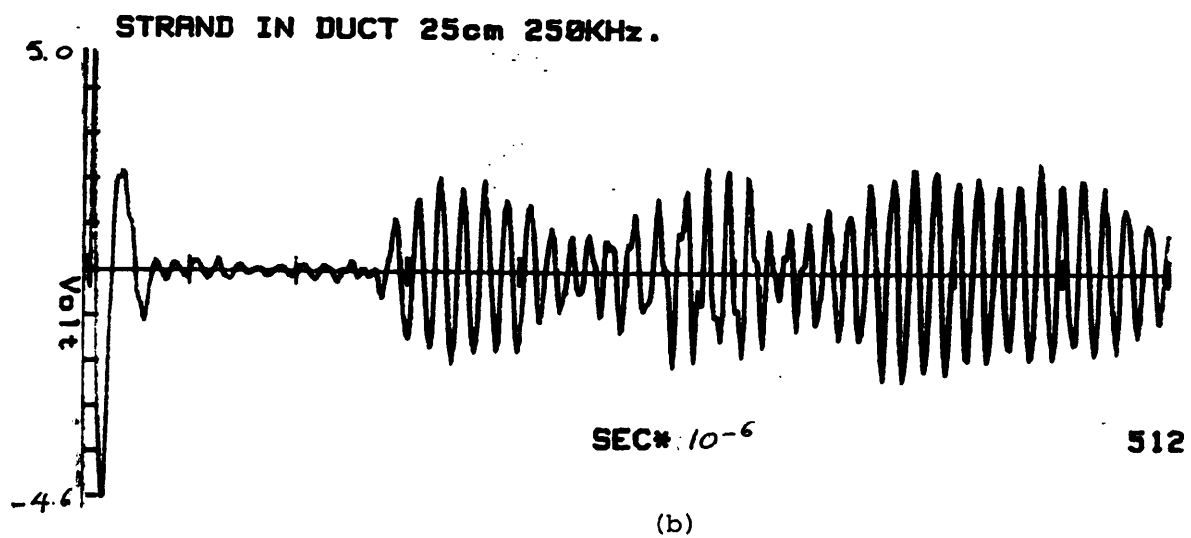
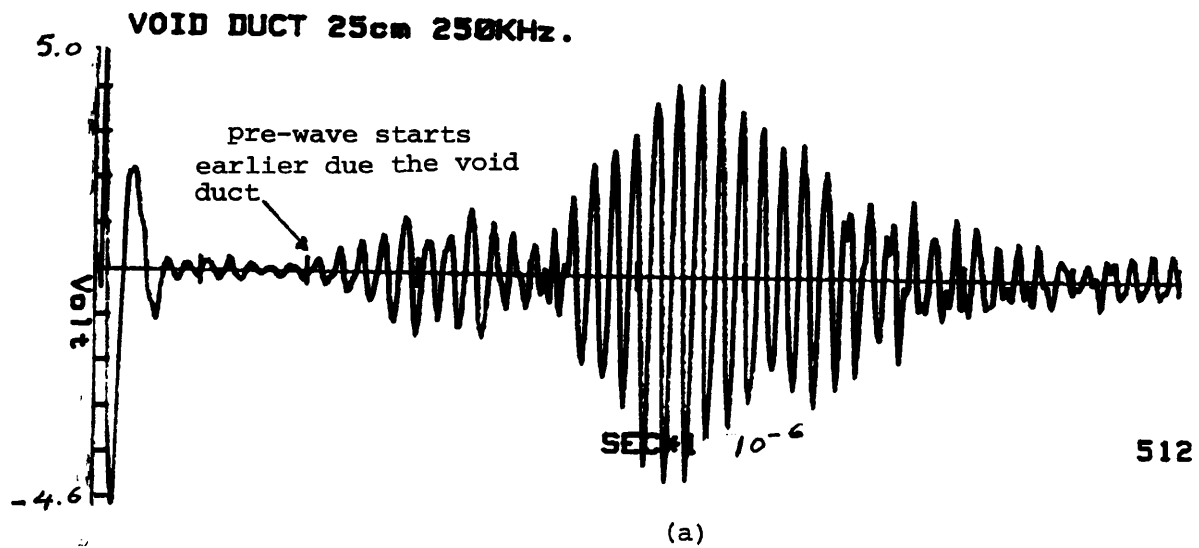


Fig.11.11

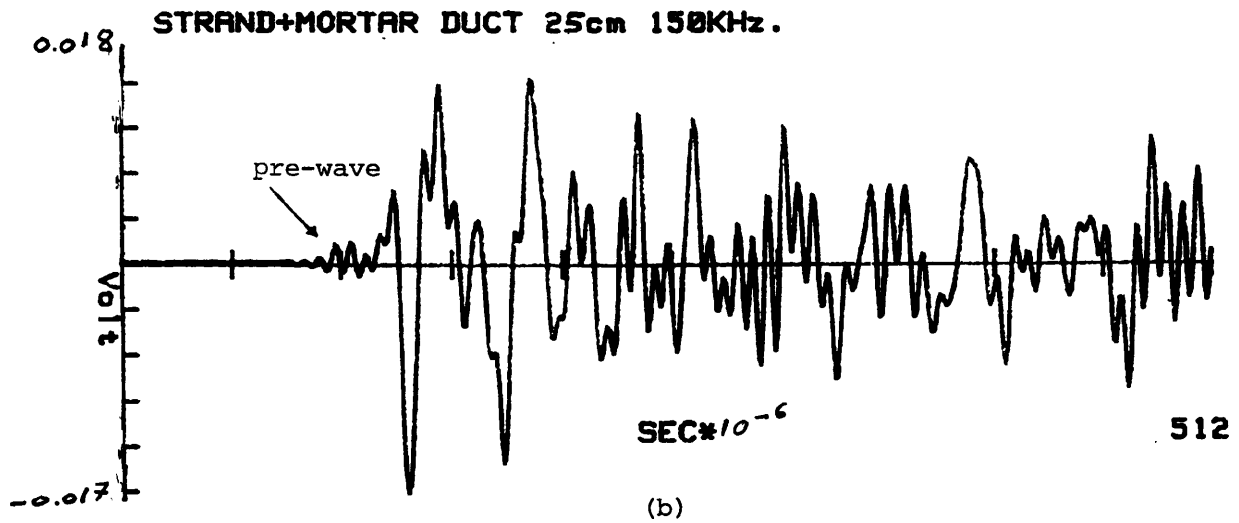
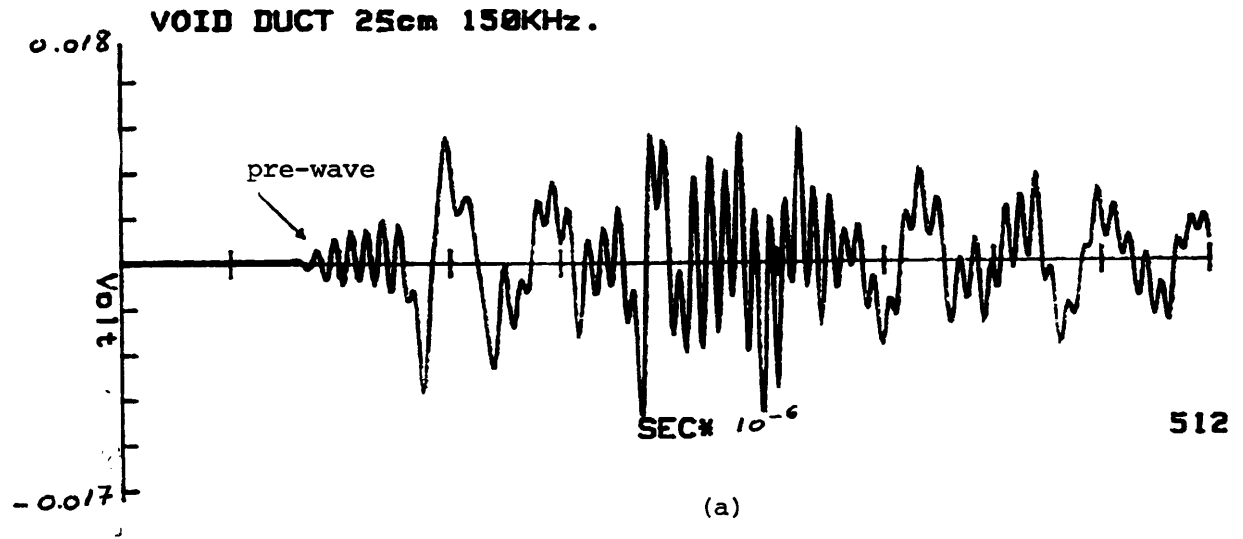


Fig.11.12- Notice how the pre-wave is stronger in the presence of a void duct.

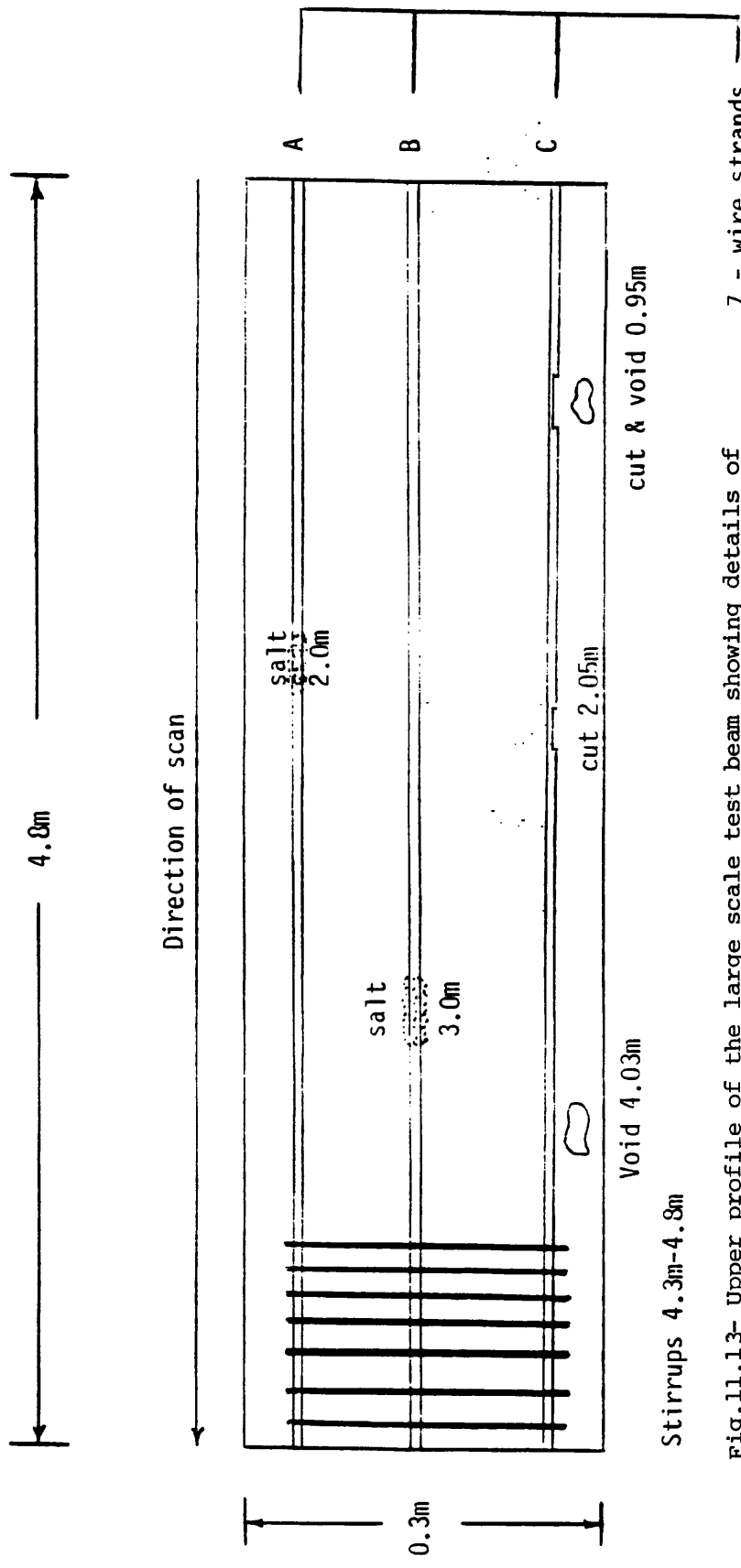


Fig.11.13- Upper profile of the large scale test beam showing details of inclusions.

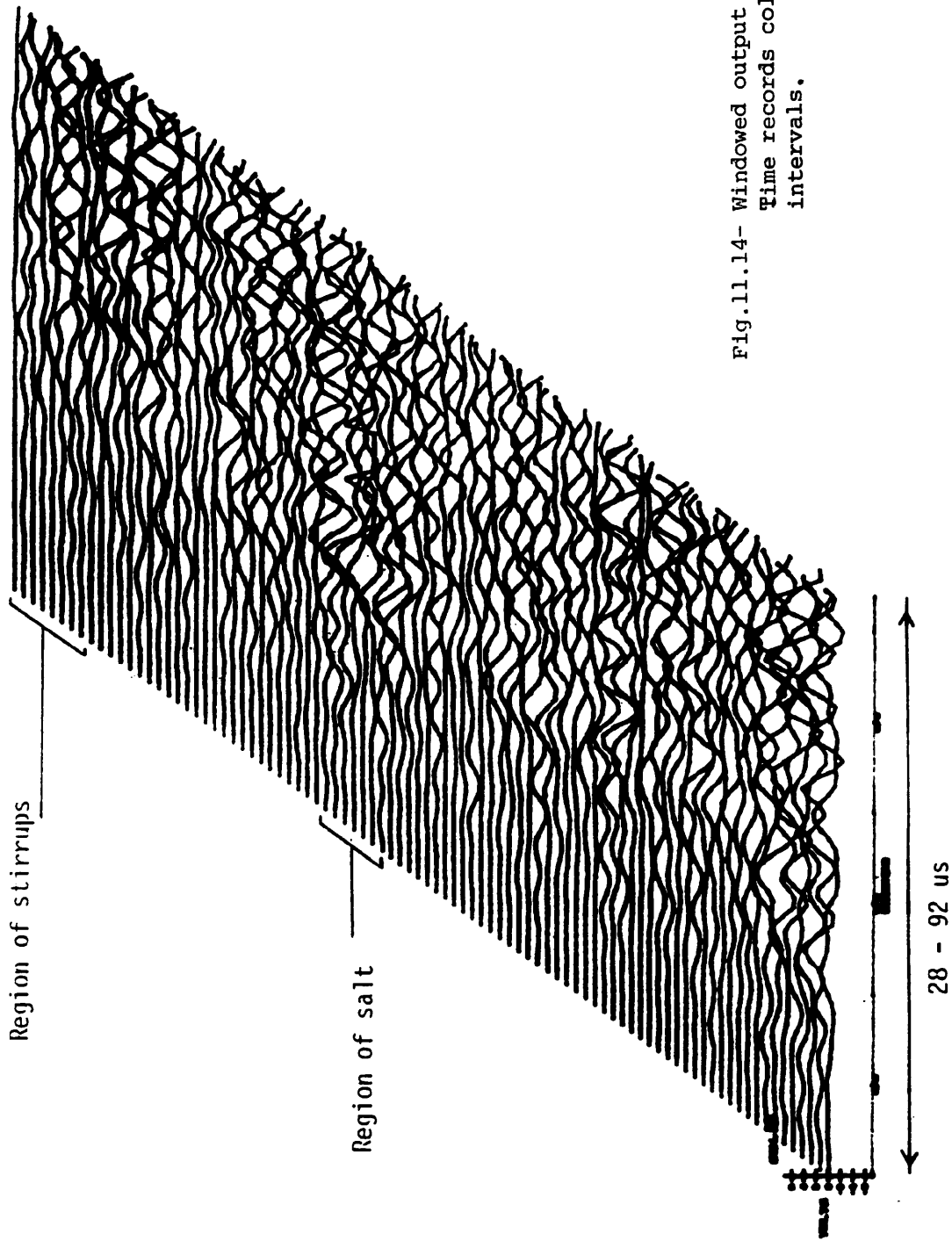


Fig.11.14- Windowed output of receiver R1.
Time records collected at 50mm
intervals.

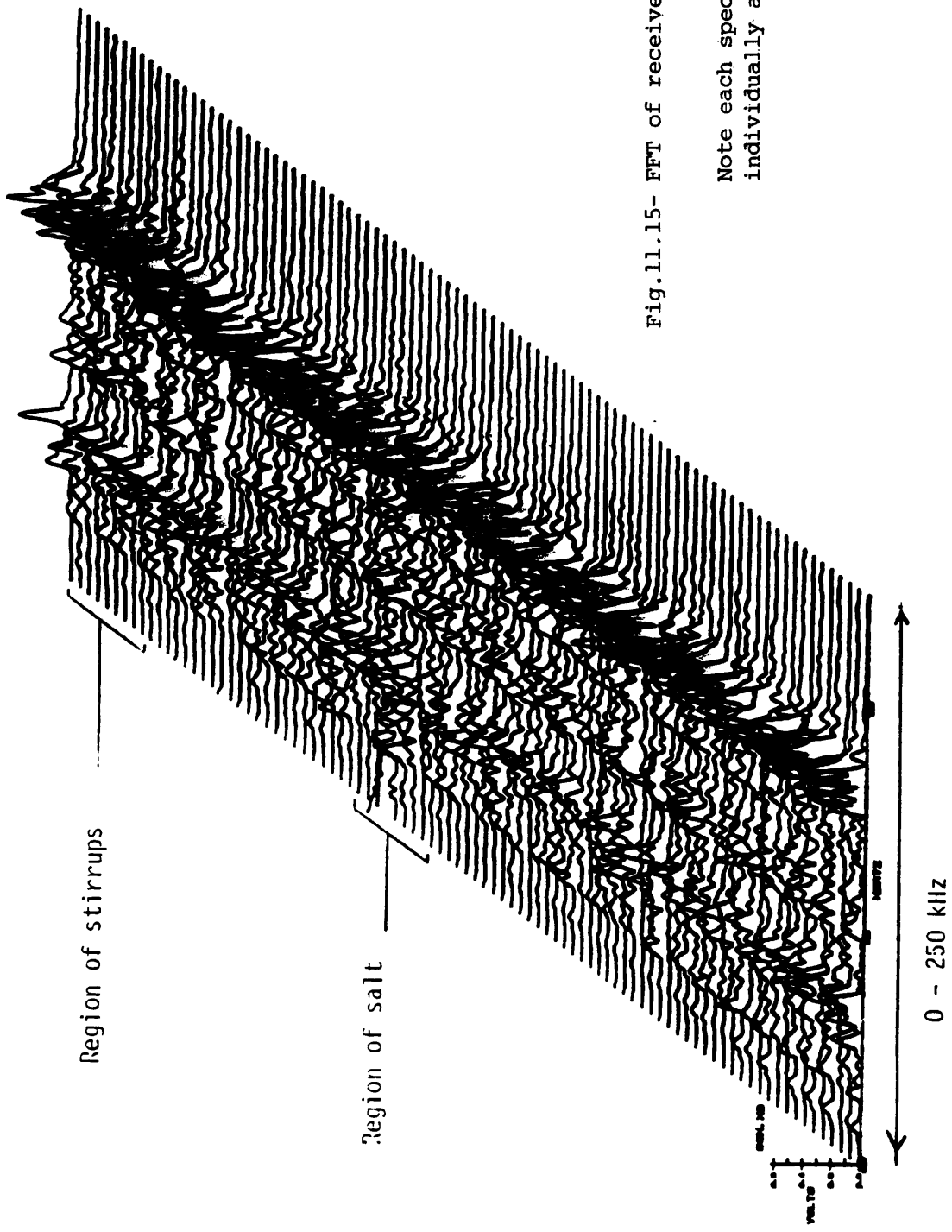


Fig.11.15- FFT of receiver R1,

Note each spectrum has been individually auto-scaled.

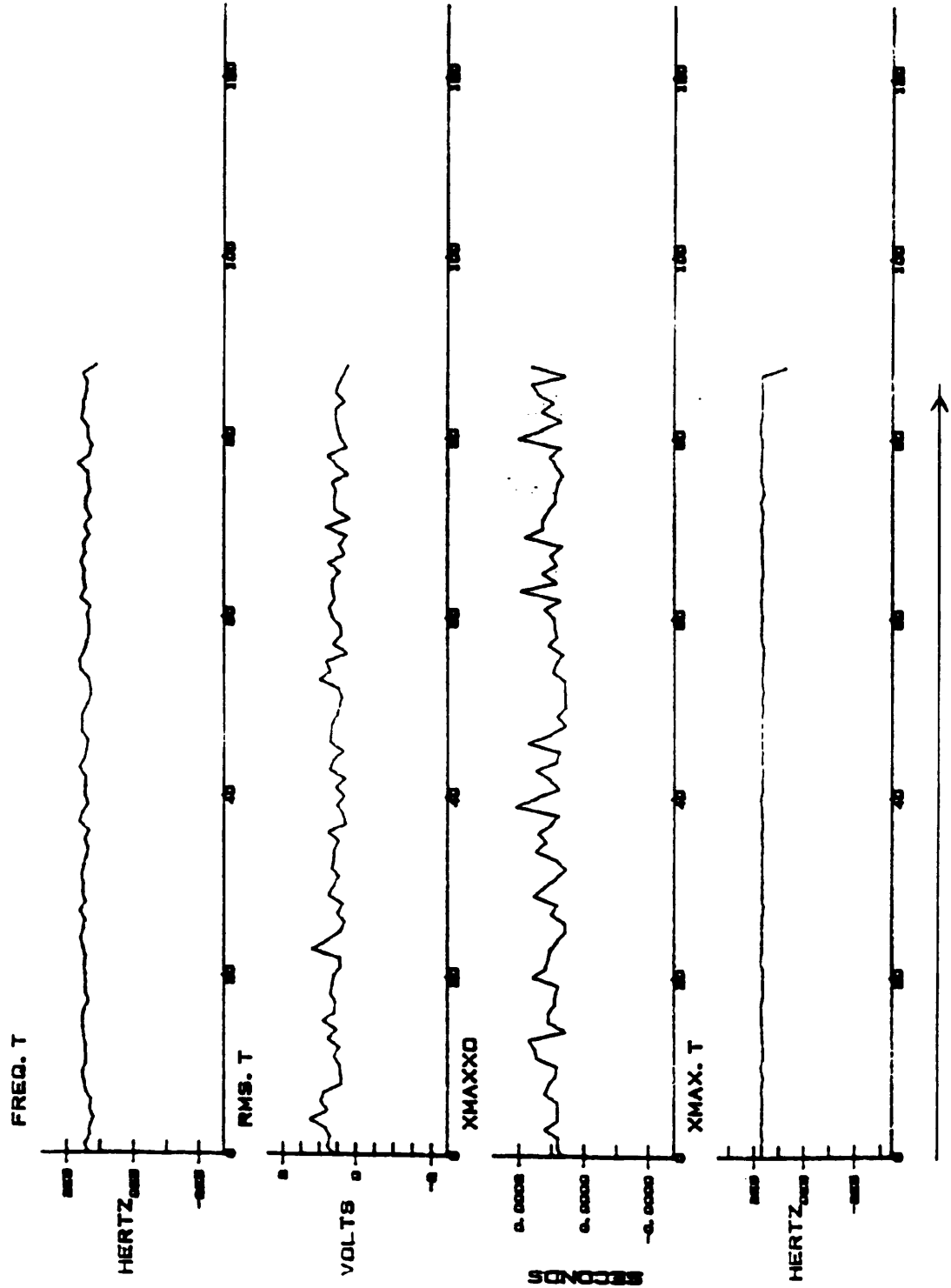


Fig.11.16-

Trend data, showing the following:

- a. Dominant frequency, calculated in the time domain.
- b. Signal RMS.
- c. Point in time at which maximum signal amplitude occurs.
- d. Dominant frequency, calculated in the frequency domain.

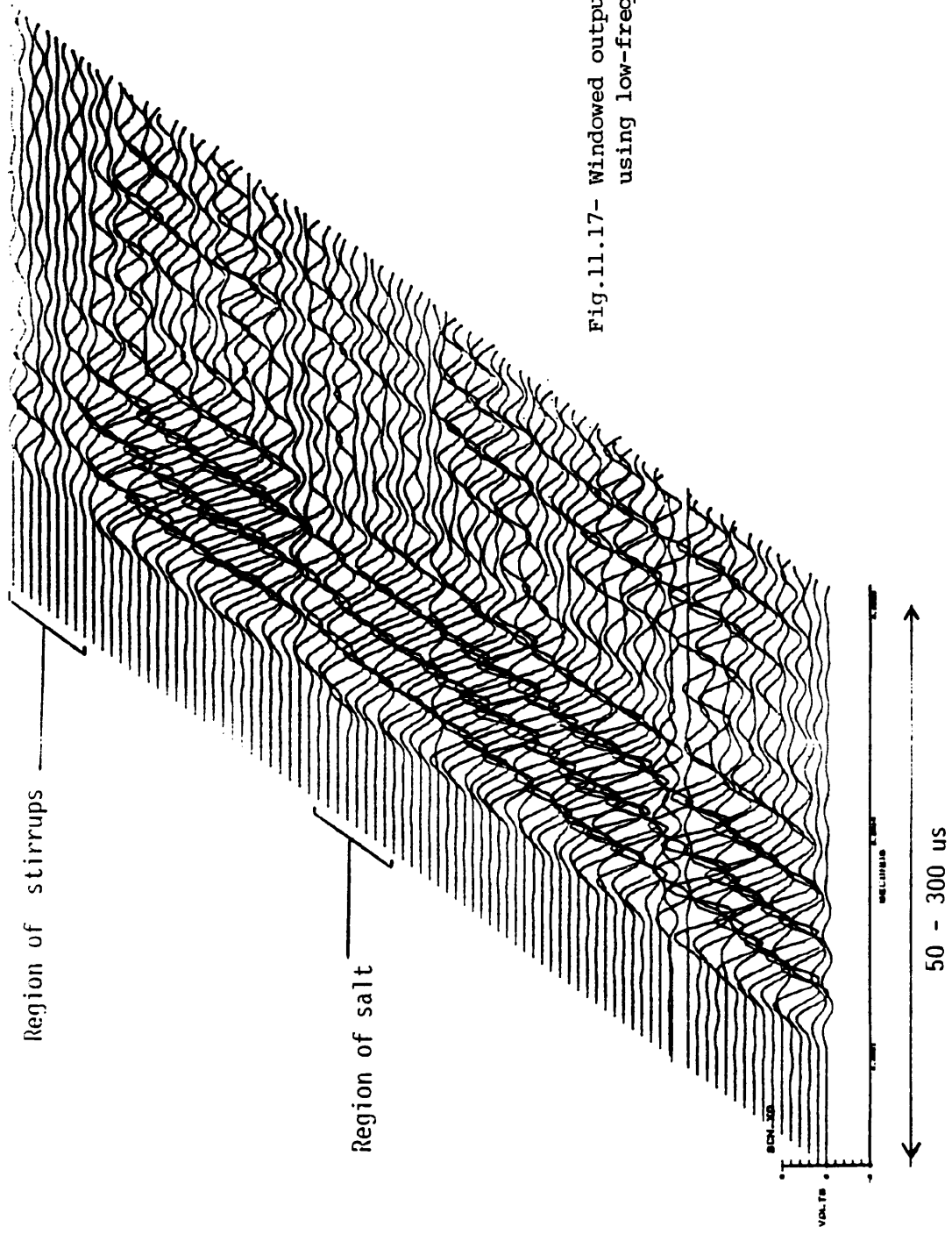


Fig.11.17- Windowed output of receiver R1 using low-frequency (45kHz) probes.

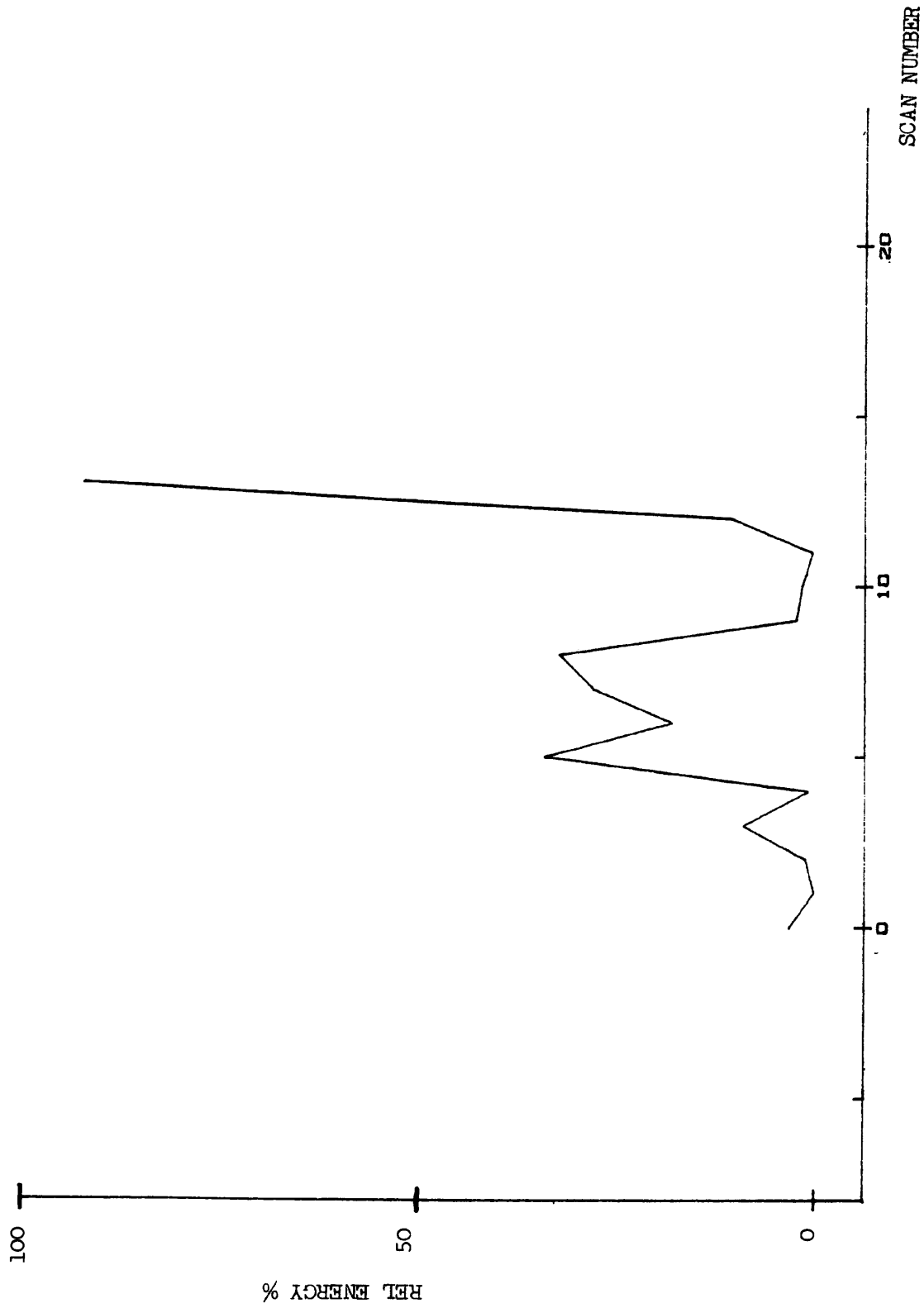


Fig.11.18- The trend energy plot from a plain concrete block; notice no evident peak is present.

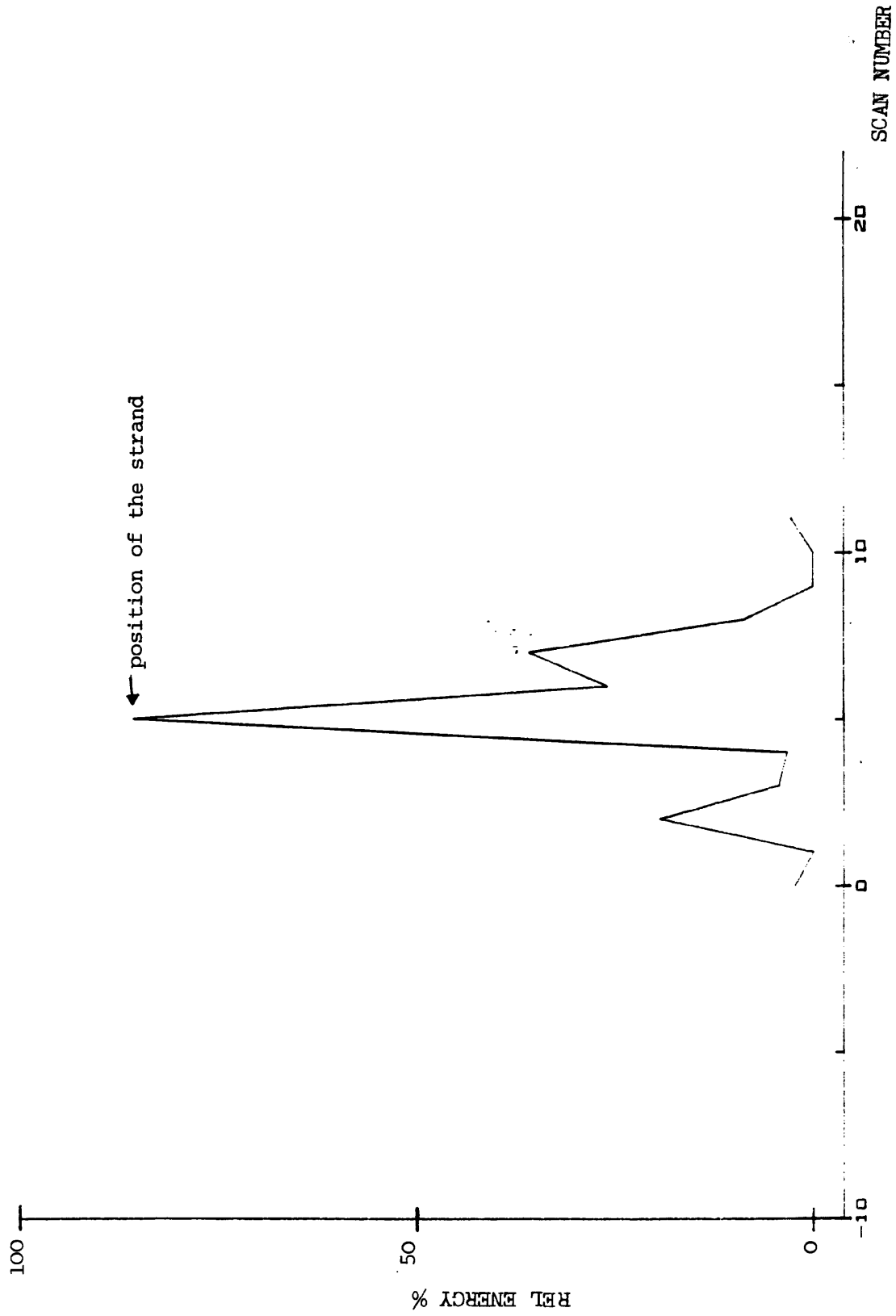


Fig.11.19- The trend energy plot from a reinforced block with a 7-wire strand; the peak indicates the position of the strand.

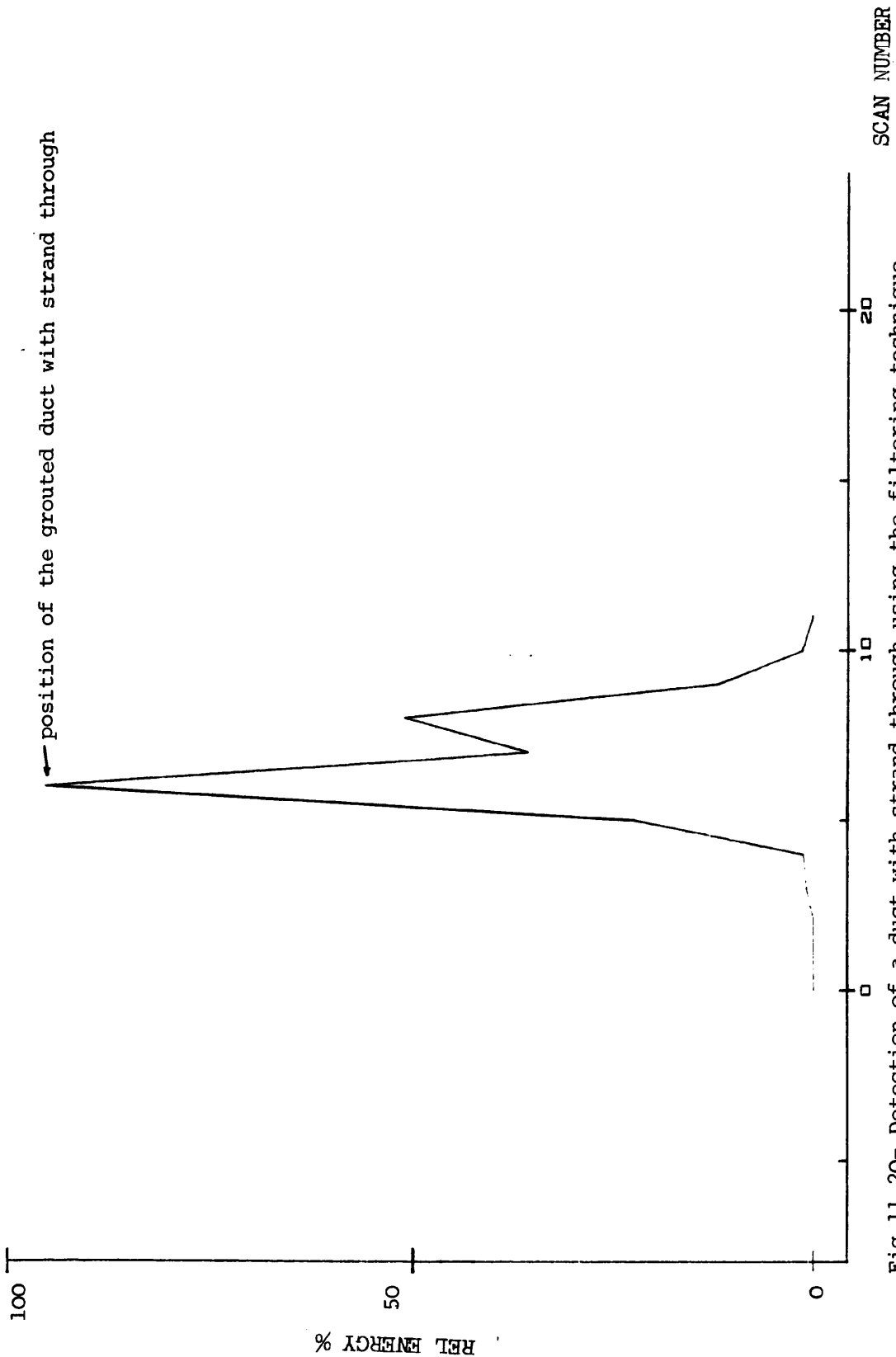


Fig.11.20- Detection of a duct with strand through using the filtering technique.

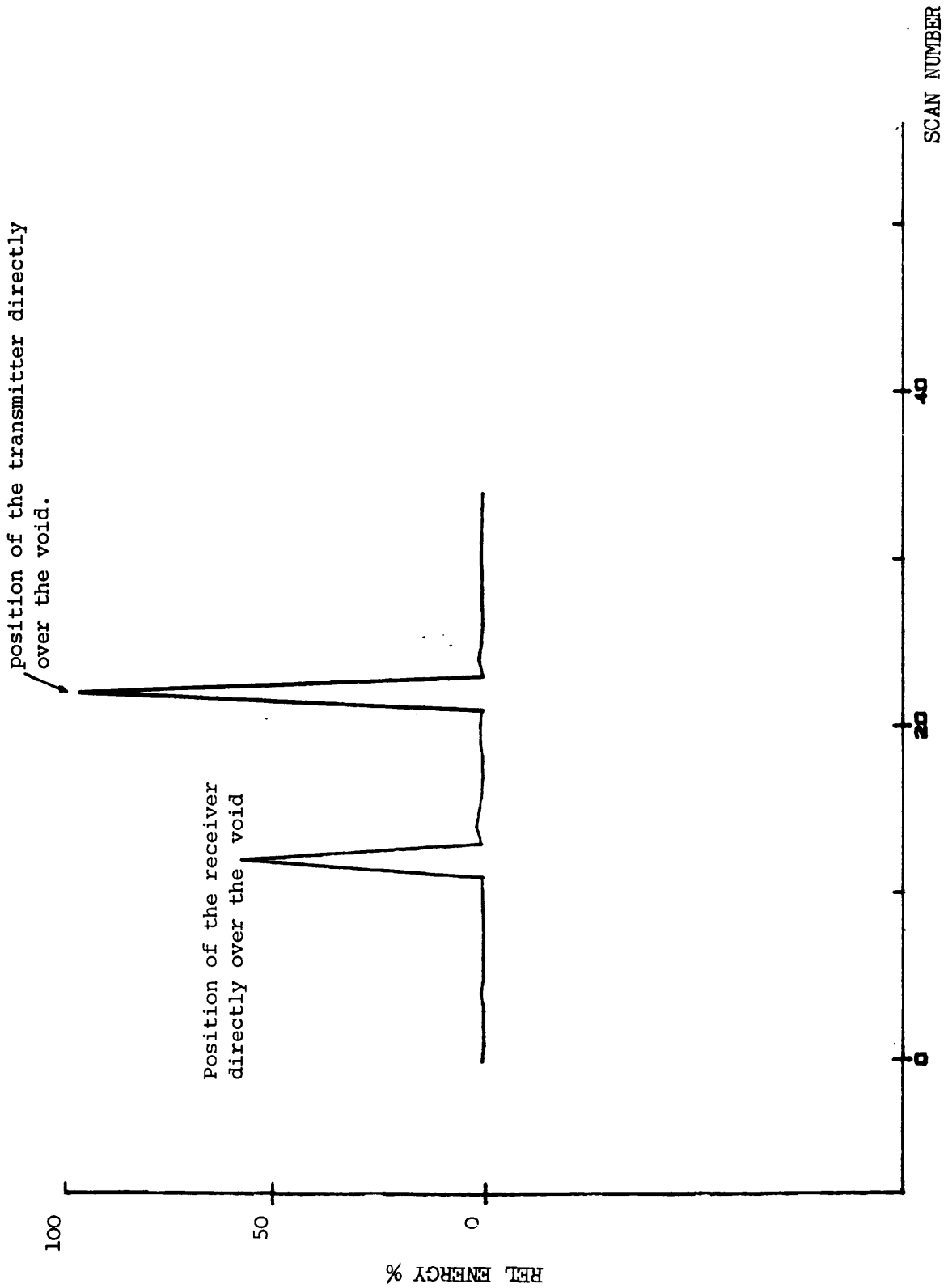
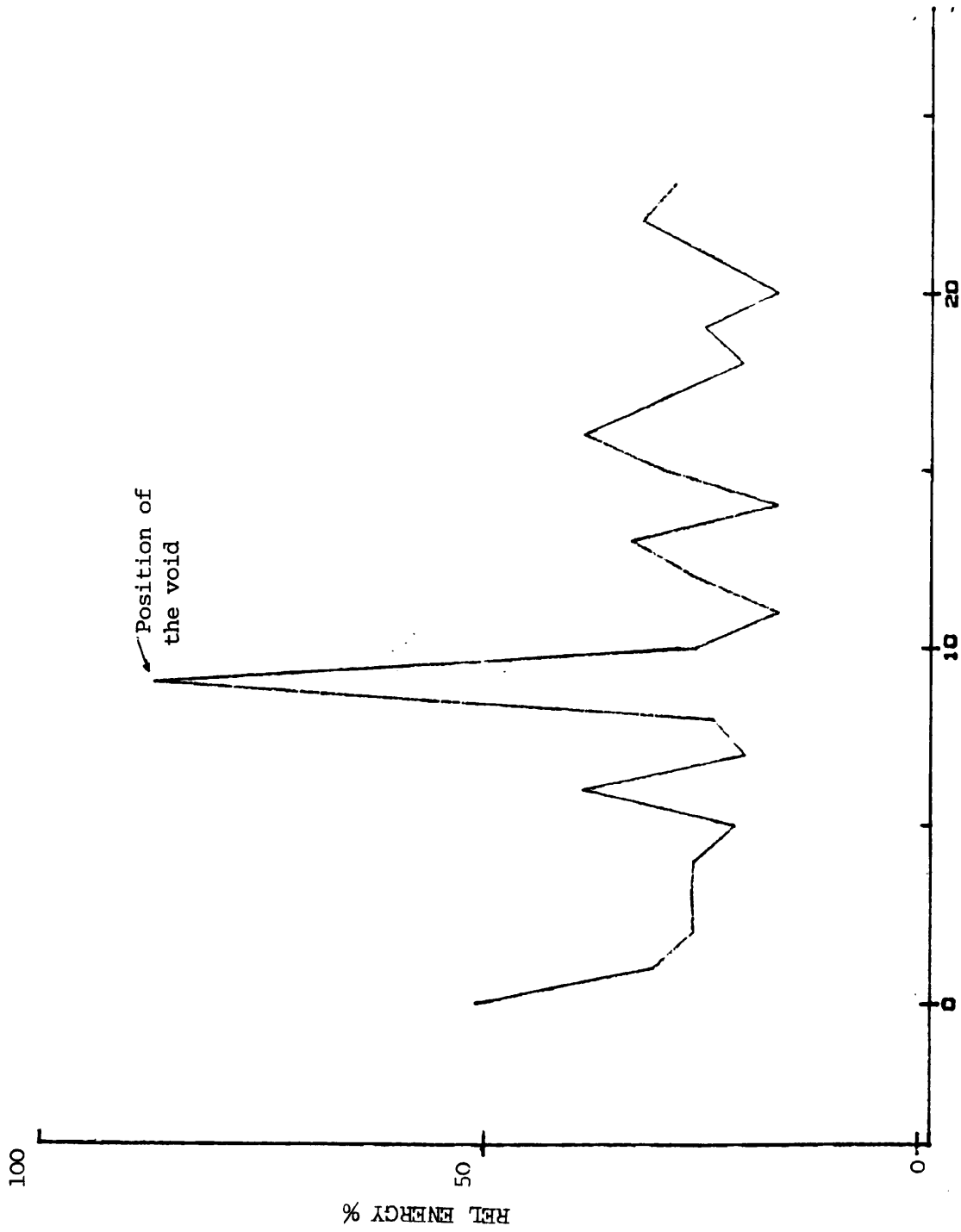


Fig.11.21- Void-detection: energy of filtered high frequency components.



SCAN NUMBER

Fig.11.22- Void-detection: location estimate of void in test beam using high frequency filtering technique.

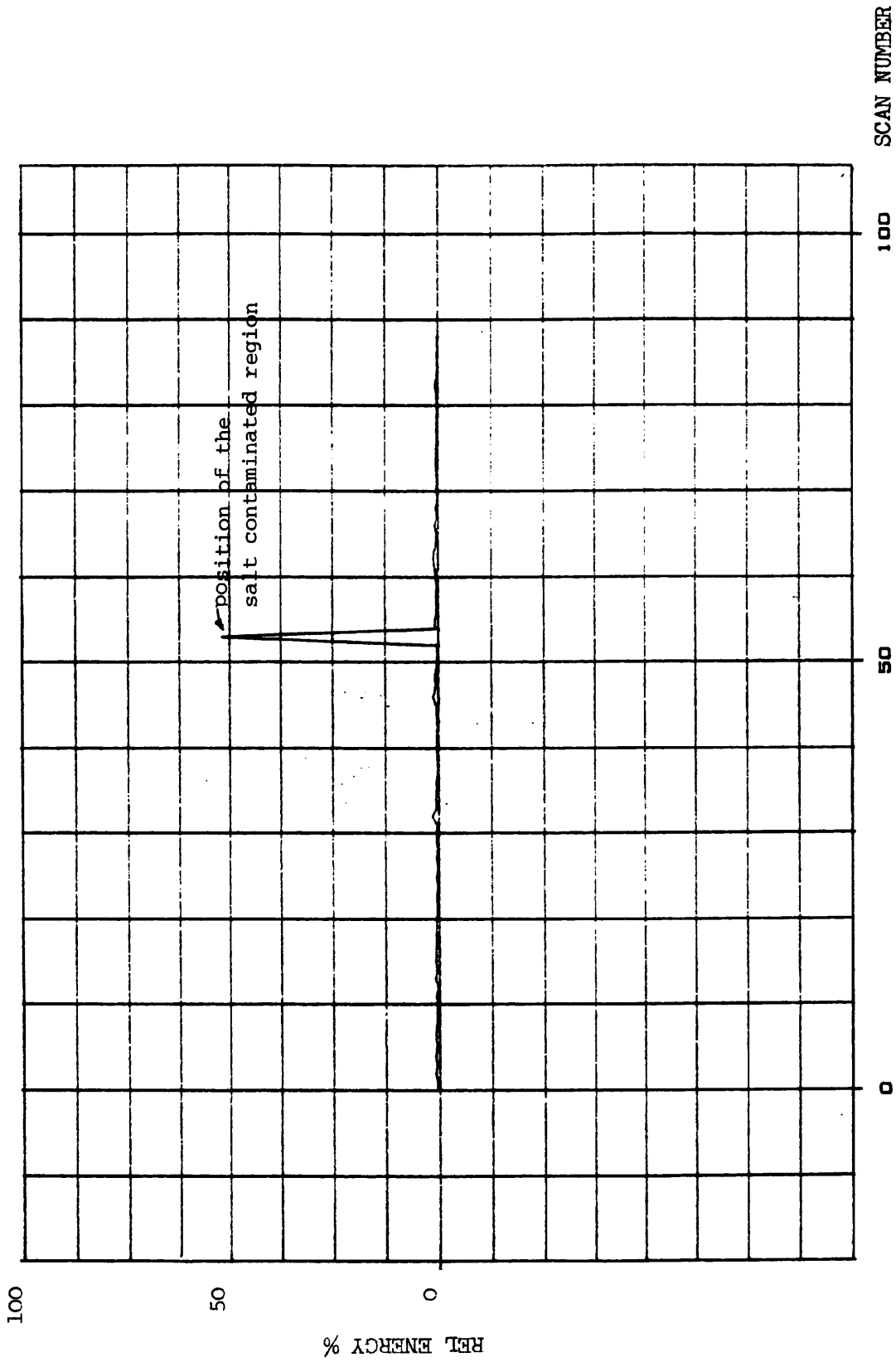


Fig.11.23- Detection of salt-contaminated region of 7-wire strand using probes spaced at 100mm using filtering technique; with high pass filter, with lower cut-off of 300kHz.

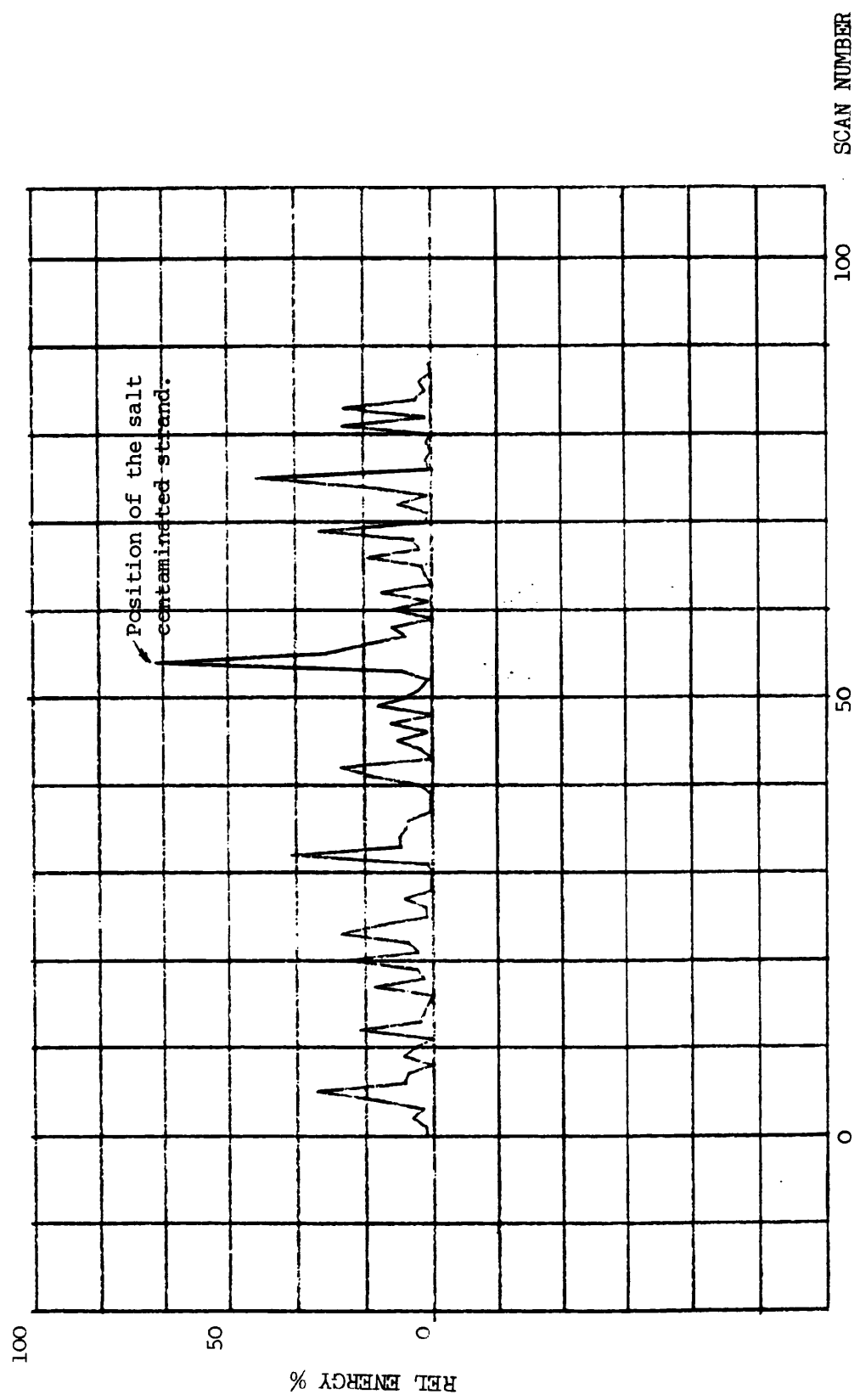


Fig.11.24- Detection of salt-contaminated region of 7-wire strand using probes as fig.11.23 but with 10MHz digitization rate and band-pass filtered between 180-200kHz.

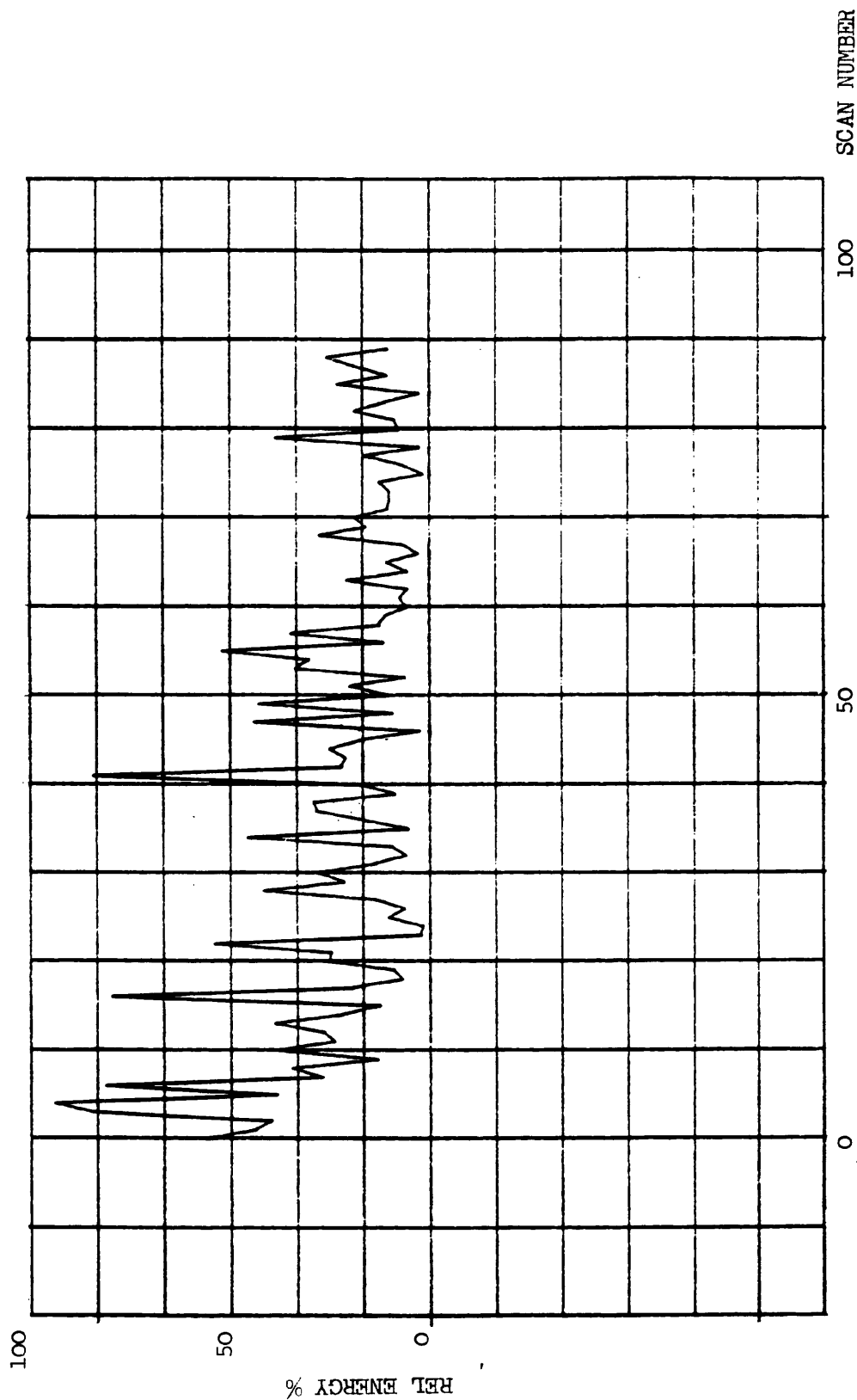


Fig.11.25- Detection failure: Random noise due to great probe spacing (264mm) resulting in high frequency components being of the same magnitude as thermal noise.

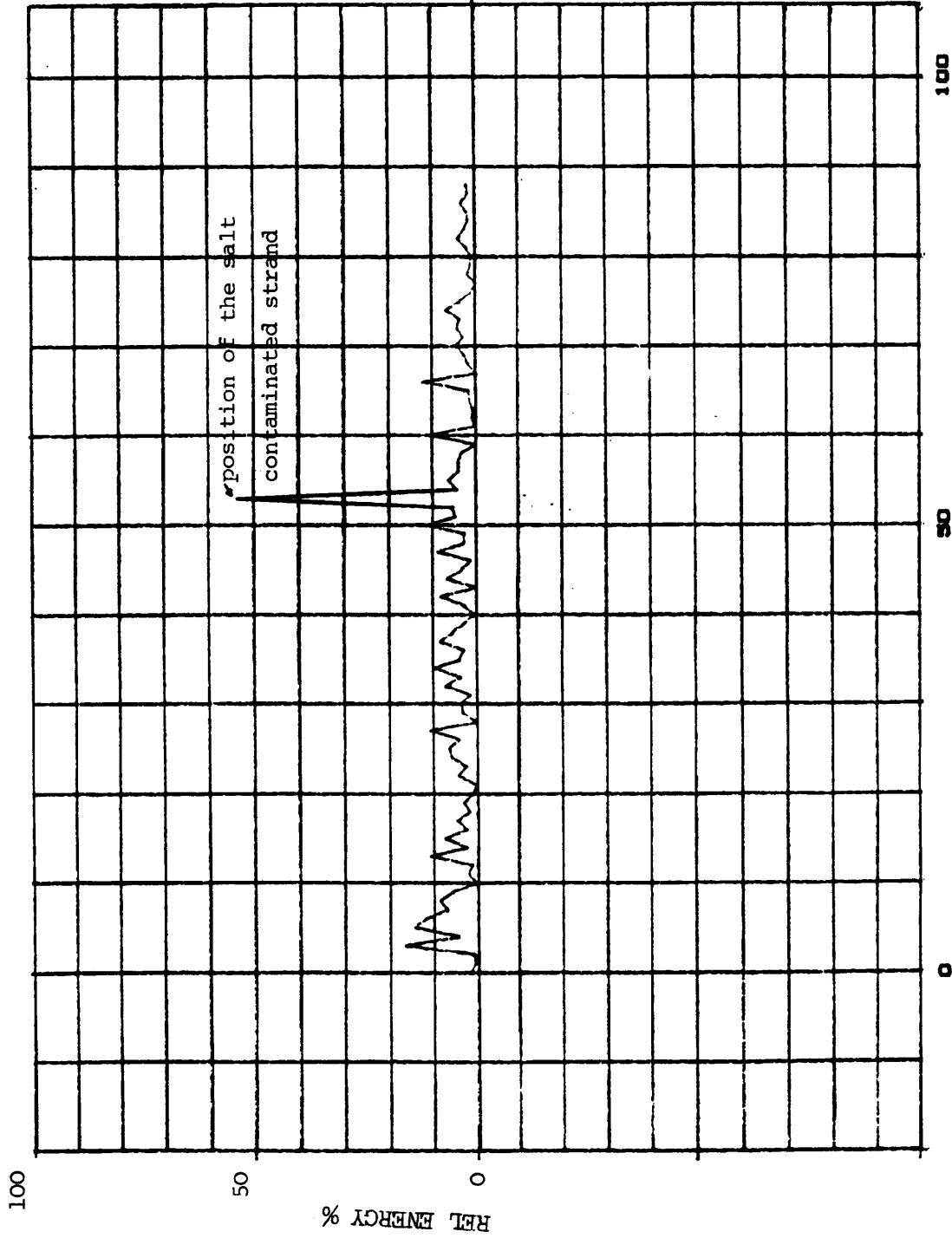


Fig.11.26- Detection of salt-contaminated region of 7-wire strand by laterally mounted probe receiver, suggesting position of transmitter is critical. 100-200kHz band-pass filter.

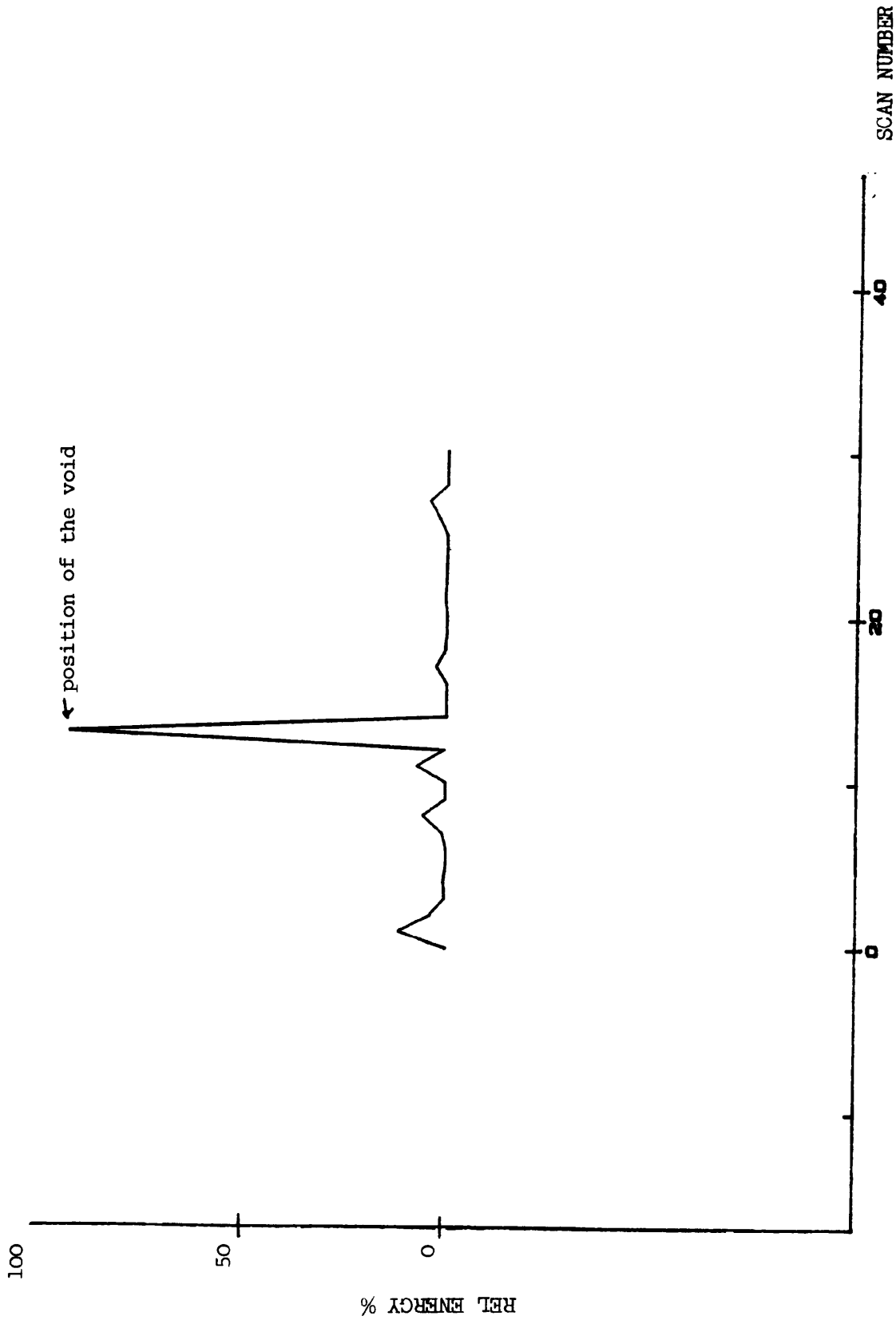


Fig.11.27- Detection of the first void in large test beam using the rolling probes and the filtering technique.

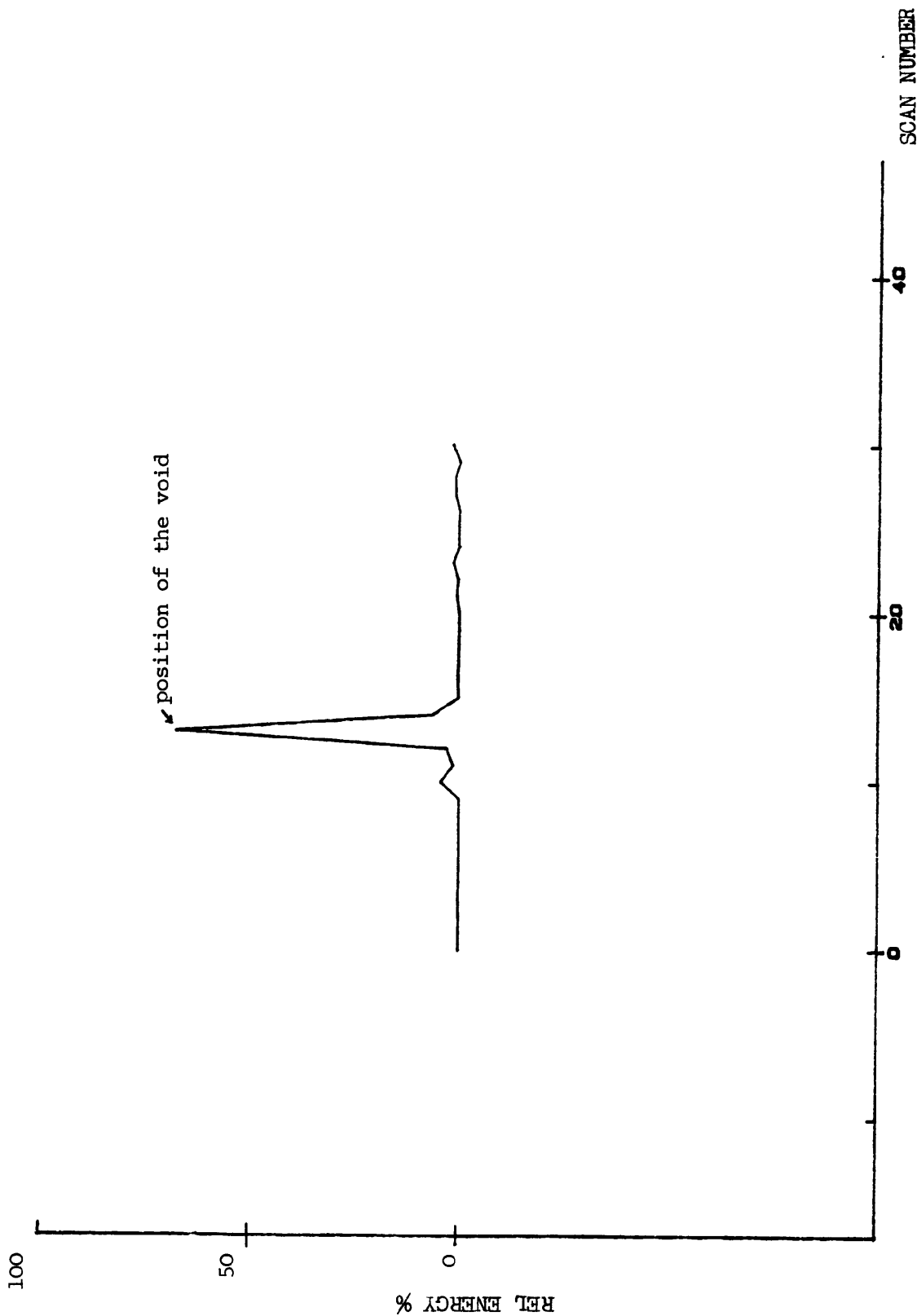
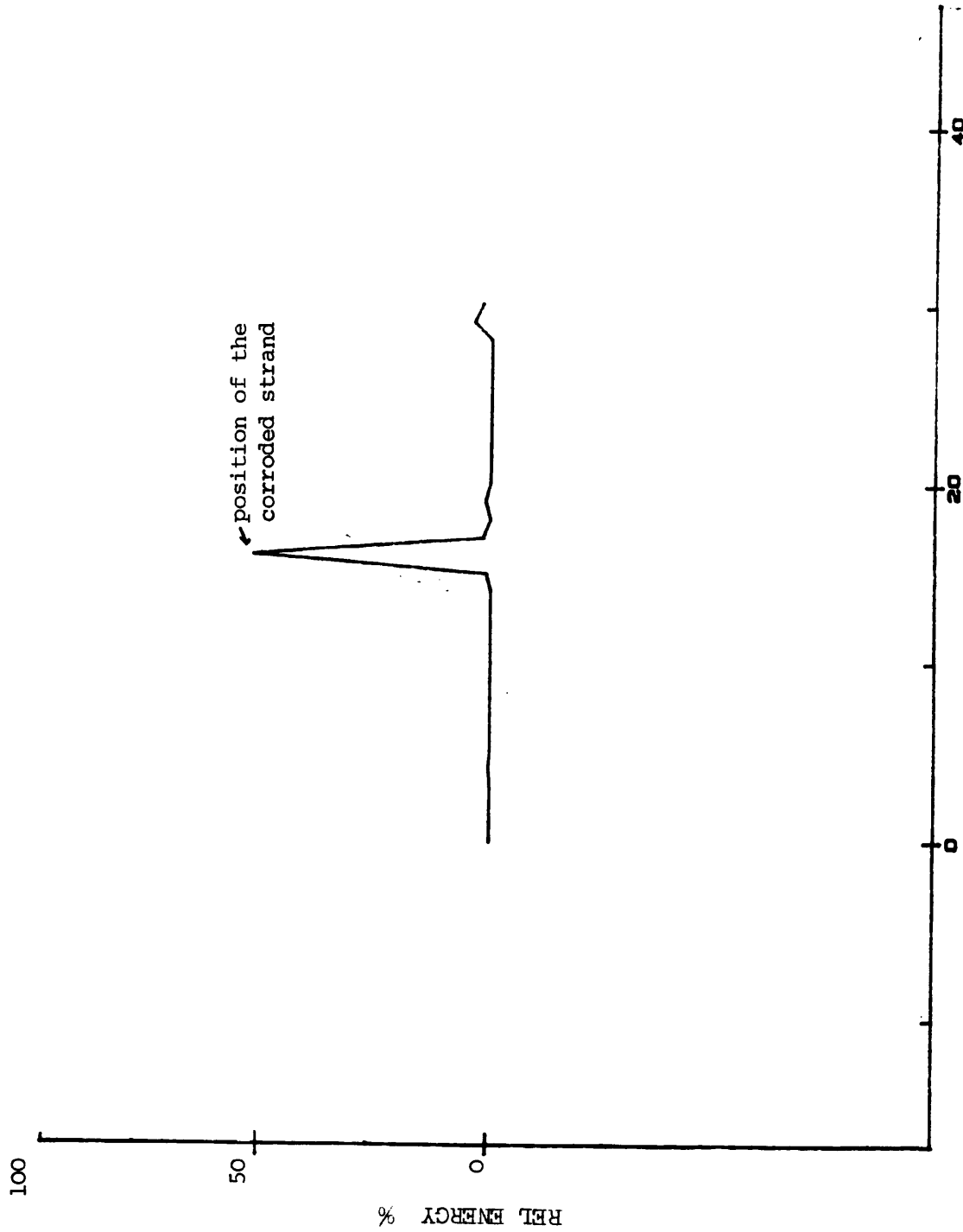


Fig.11.28- Detection of the second void in large test beam using the rolling probes and the filtering technique.



SCAN NUMBER

Fig.11.29- Detection of the middle corroded strand in the large test beam using rolling probes and the filtering technique.

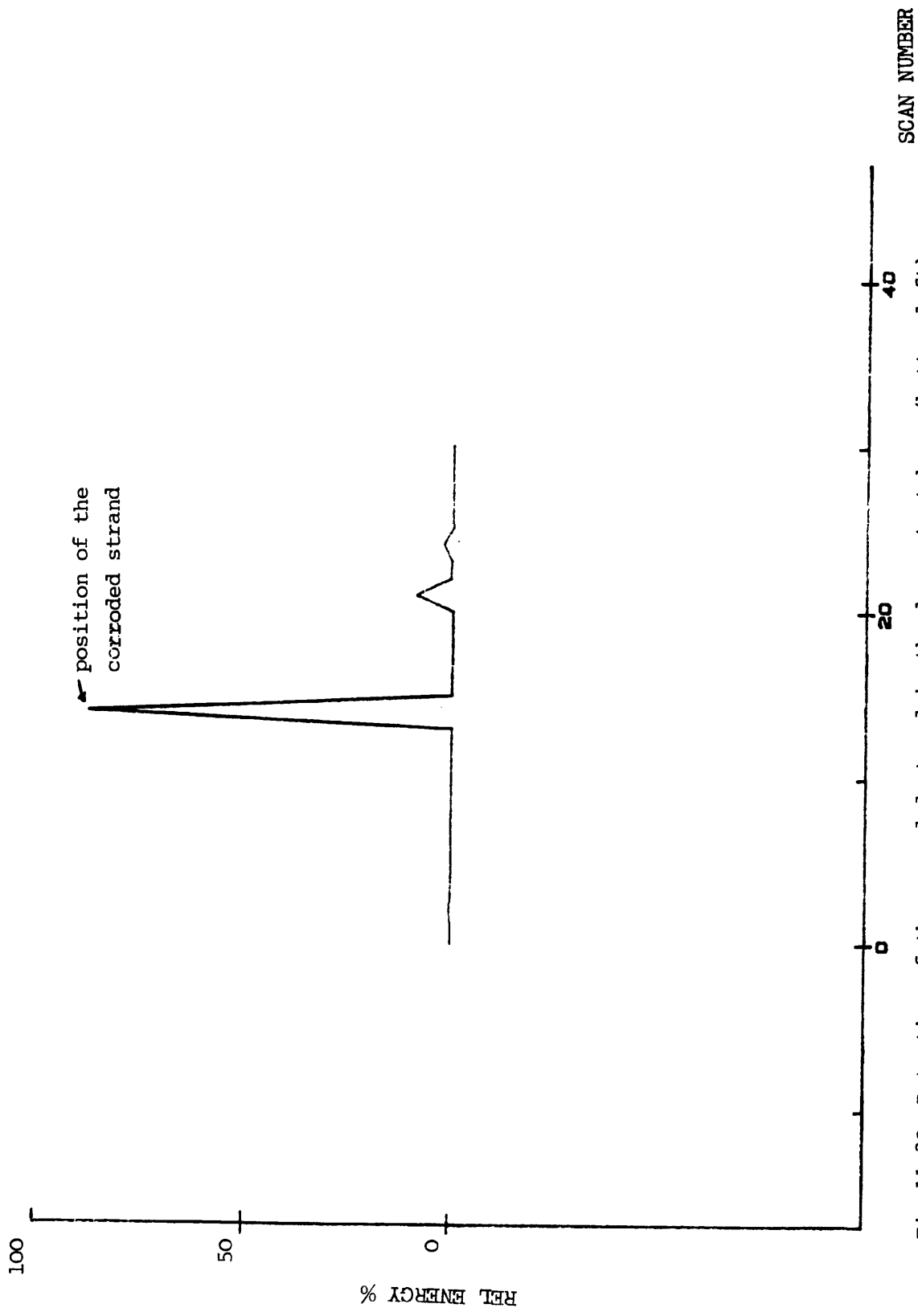
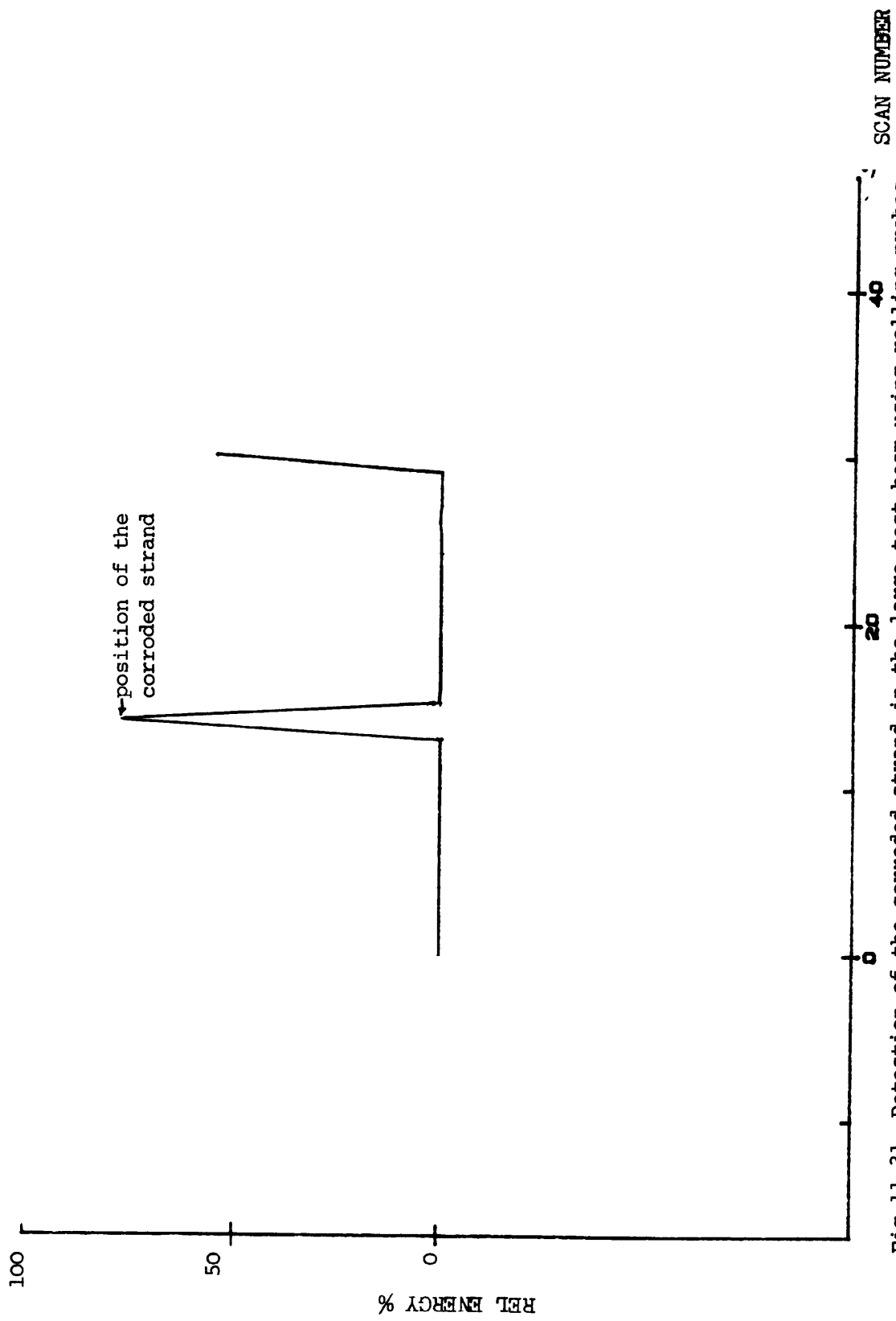


Fig.11.30- Detection of the corroded strand in the large test beam (bottom left) using high filtering technique.



SCAN NUMBER

Fig.11.31- Detection of the corroded strand in the large test beam using rolling probes.

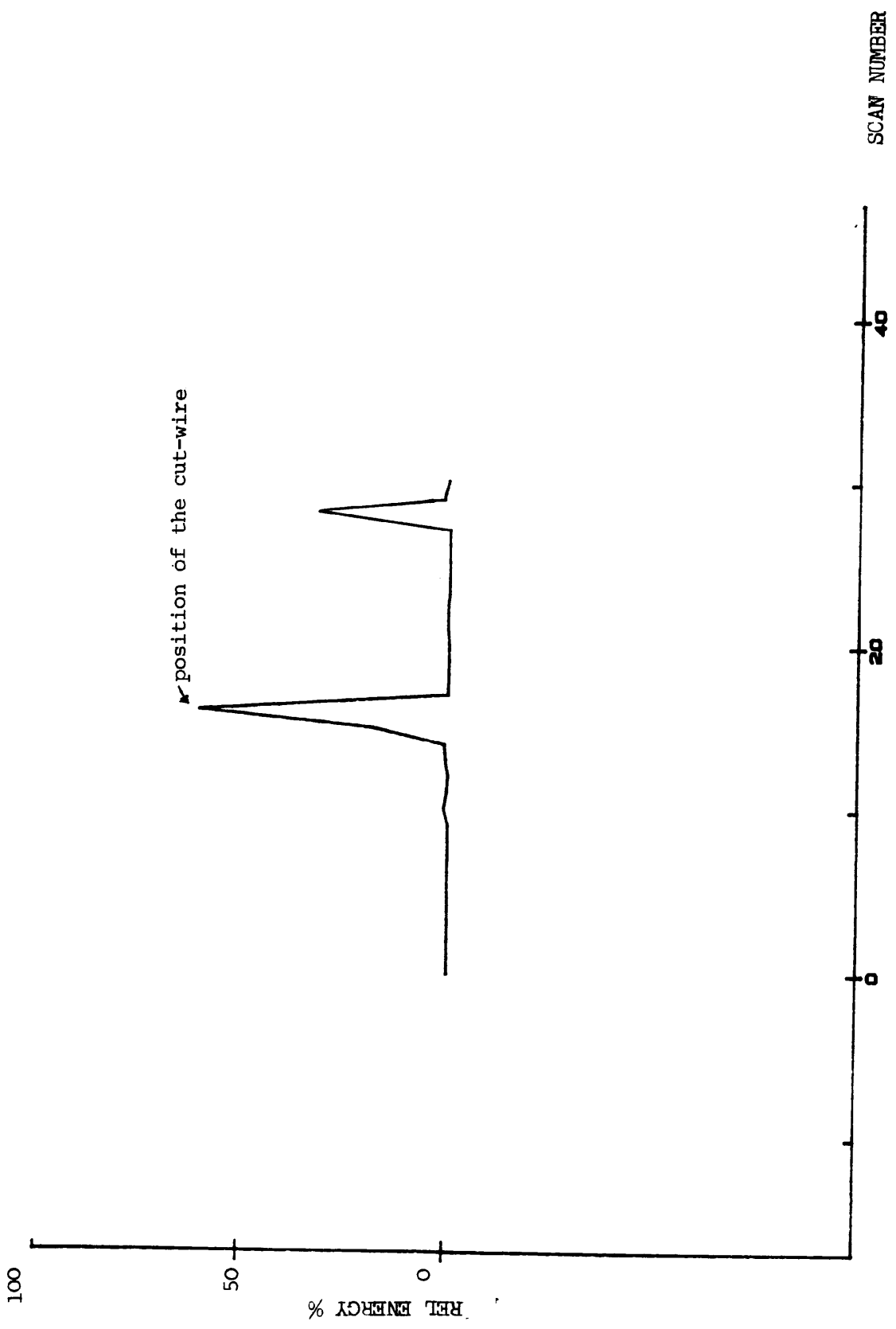
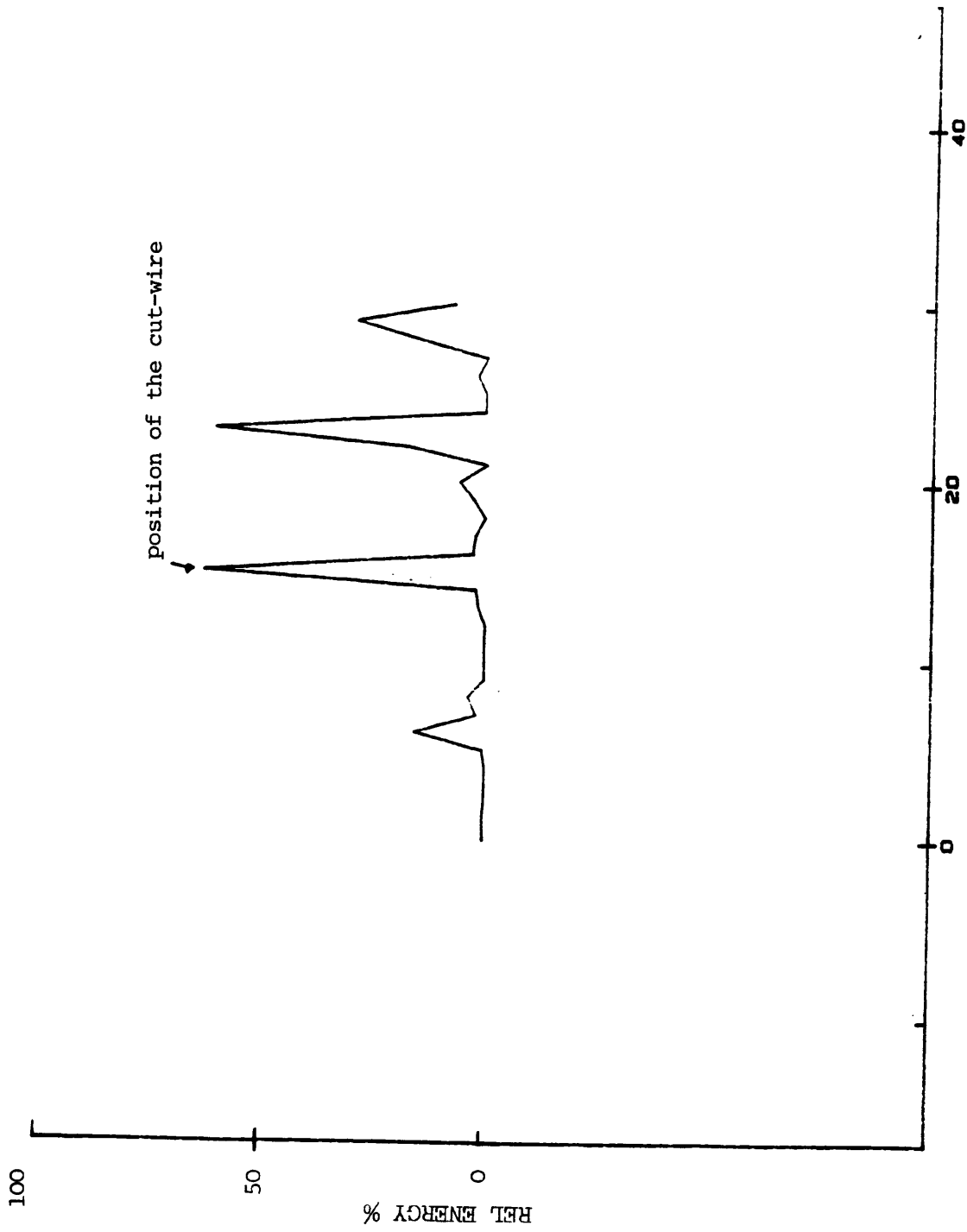


Fig.11.32- Detection of a cut-wire in the large test beam using the filtering technique.



SCAN NUMBER

Fig.11.33- Detection of the second cut-wire in the test beam using the rolling probes.

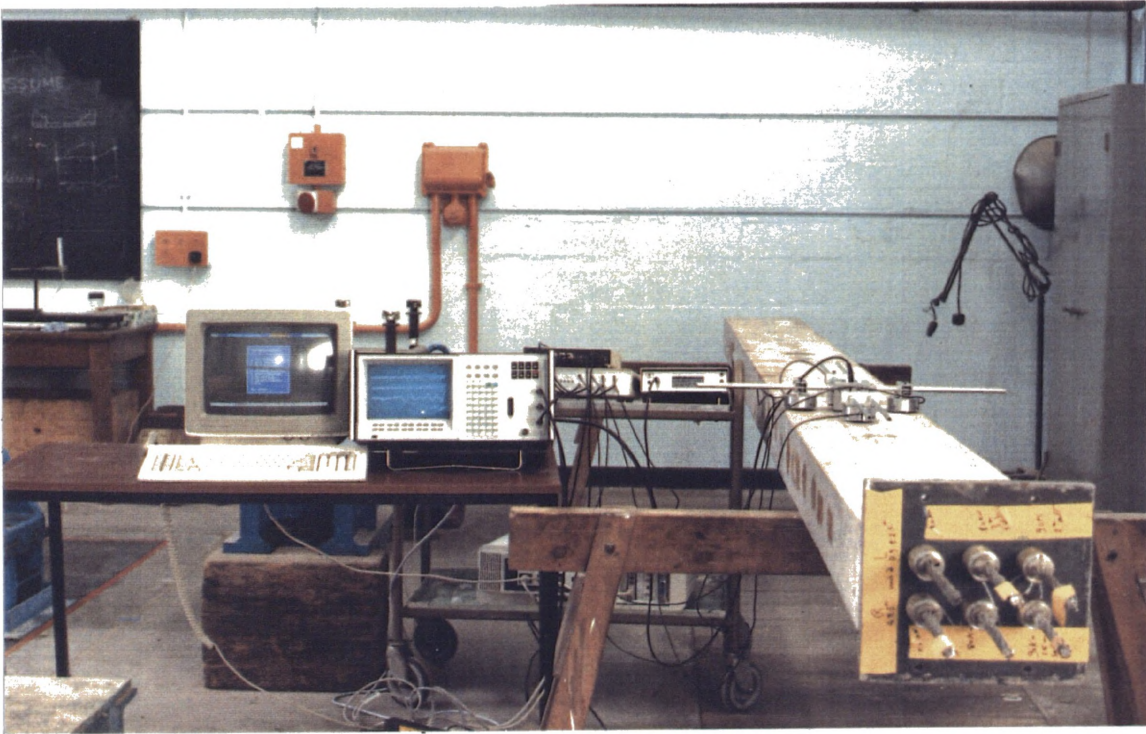


Plate 11.1- Prototype system used to scan the large scale test beam.

CHAPTER 12SUMMARY, CONCLUSIONS, AND FUTURE RESEARCH12.1- SUMMARY

This study has presented theoretical and laboratory studies of ultrasonic wave propagation in concrete. These were undertaken to develop a basis for using the transient stress wave propagation as a technique for corrosion and flaw detection in an heterogeneous material such as concrete.

Computer synthesis was used to simulate the effect of the bar size, its depth in the material, surface condition i.e. sound, corroded, or cracked, and transducer frequency, on the signals received from steel components embedded in concrete. A comparison was carried out using experiments with components in water and concrete samples.

Attenuation losses due to scattering and absorption of ultrasonic waves have been studied. An equation based on experimental results was derived for high strength concrete. Moreover a review of the methods used in concrete testing has been given. A theoretical model of a pulse-echo system (where one transducer acts as a transmitter and a receiver in the same time) for a sound and corroded bar embedded in concrete has been given, with a comparison of such system for a bar immersed in water.

Laboratory results obtained from using the transit time on concrete specimens (reinforced and pretensioned) containing corrosion and flaws have been presented. Observations and conclusions drawn from the theoretical study were used to aid interpreting some of the experimental results specially in water.

The development of an experimental pitch-catch technique for finding corrosion and flaws within reinforced concrete has been described. This enabled proposals for a prototype testing system to be put forward. The key features of the technique are as follows:

1- Five rolling transducers are required (one transmitter and four receivers) with nominal frequencies between 150-300kHz. The transmitter should be mounted at the centre and the four receivers in a rectangular array surrounding the transmitter. The spacing should not be more than 100mm.

2- A pulser to excite the transducer transmitter.

3- Scanning of the specimen over the region where embedded components are under the transmitter.

4- The received signals should be transformed to give the frequency spectra, then application of a brick-wall filter on the FFT to leave a chosen frequency bandwidth, and then IFFT of the filtered signal. The energy trend of the scan after filtering is carried out. These techniques can be achieved by using an oscilloscope and a computer or by using an analyser, in this

research both methods were used.

12.2- CONCLUSIONS

A programme of research has been carried out to investigate the use of a pitch-catch method (the indirect method) in detection of corrosion and flaws in reinforced or prestressed concrete. One objective was to investigate experimentally the effects of scattering and absorption of the ultrasound with different frequencies in concrete to be able to detect the presence and condition of embedded components including salt presence, component size, a void duct, a flaw, and corroded conditions or breaks in wires. A second objective was to construct a computer program to predict the amplitude of the received signal when the pitch catch method is used for different frequencies and surrounding media (water and concrete).

The significant conclusions reached as a result of the studies presented in this work are stated in the following sections:

12.2.1- Theoretical Studies

Two models were carried out: a model using the pulse-echo technique, and a model using the pitch catch method to estimate the strength of the echo reflected from a bar embedded in concrete.

The following conclusions were drawn from the parameter studies of different frequency waveforms obtained from beams containing

sound, corroded, and cracked bars:

1- The strength of the signal, in general, is more attenuated as the frequency increases, mainly due to scattering and absorption effects.

2- The strength of the echo reflected from a bar embedded in concrete increases with increase of the bar size.

3- The attenuation for a corroded bar is greater than a sound bar, but the difference is frequency dependent.

4- The signal captured from corroded reinforcement is frequency dependent i.e. the reflected signal from a corroded bar loses strength as the frequency increases.

5- As the roughness height of the corroded surface of the bar increases, the reflected wave from the bar is more attenuated.

6- If a crack is present in a bar, the amplitude of the reflected signal from the reinforcement is less than that of a sound one, the reduction being greater as the gap between broken ends increases.

7- The strength of the echo reflected from a bar drops as the bar is embedded deeper in concrete.

8- As the distance between the transmitter and the receiver increases the reflected signal, in general, will lose strength

because of the increased path length.

12.2.2- Experimental Studies

The signals were interpreted in the time and the frequency domains. Fast Fourier transform and filtering techniques simplify signal interpretation.

The main conclusions reached as a result of this experimental work were as follows for steel components embedded in concrete:

1- The ultrasonic signal is affected by scatter and damping because of the heterogeneous composition of the concrete. The concrete is composed of materials with different elastic properties which can cause difference in sound velocities and energy propagation in different directions.

2- The apparent velocity of the signal is greater where a large steel component is present compared to plain concrete specimen.

3- High frequency components are found where reinforcement is present compared to signal with no steel components.

4- The energy of the pre-wave (the start of the wave) increases as the bar size increases.

5- The energy of the signal reflected from a bar where corrosion has occurred is less than that where no corrosion exists.

6- The energy transmitted through a concrete specimen which is not well compacted (where flaws are expected) is much less than that of well compacted one.

7- The apparent velocity of the signal received from a void duct was found to be greater compared to a fully grouted duct, due to the shorter path length associated with the reflection from the void interface.

8- The energy reflected from a void duct is much more from that of a fully grouted duct.

9- The presence of steel components embedded in concrete and the presence of voids in duct or hardened concrete and corrosion areas can be determined from the peaks of the energy trend for a scan carried out on the specimen under investigation. The technique was carried out by Fourier transform of the time signals, then filtering to a chosen frequency bandwidth, then IFFT of the frequency records, and then energy trend plot of the filtered time signals. This method can filter out the variability of the coupling effects which were found to be important. It is worth mentioning that uniform coupling between the transducer and the concrete surface was difficult to achieve and if voids were present in the surface contact area between the transducer and the concrete the signal captured was different in energy and frequency contents.

Results of the filtering technique showed that the pitch-catch method has the potential for: determining the presence of

corroded strands, distinguishing hollow ducts from fully grouted ducts, and determining the presence of flaws in concrete.

These studies have demonstrated that the pitch-catch method has the potential to become a reliable field technique for detecting flaws and condition of embedded components within concrete structures.

12.3- FUTURE RESEARCH

The following general recommendations are made for future work:

1- The availability of supercomputers should make it possible to study a wide variety of nondestructive testing related problems modelling closely physical phenomena which could not be studied using other existing analytical methods.

2- The concrete modelled in this study was assumed to be homogeneous, therefore further work should be carried out to model the heterogeneity of concrete (i.e. gravel, sand, and cement) and its effect on scatter and dispersion.

3- The model given in this study was for bars, future work should model strands and the shape of any reinforcement which could be found in reinforced concrete. Moreover the corrosion of the bar modelled in this research was taken as a pitted surface, further work could be to study the effect of spalling of concrete due to corrosion on the signal using computer models.

4- The model studies in this research have been restricted to a beam-like structures with one bar through. Therefore further studies of other structural elements, such as round columns and plate structures with different reinforcement must be carried out.

5- Future analytical work should be carried out to model planar flaws in concrete structures which were not present in this research.

6- Strong Rayleigh wave generation is primarily responsible for obscuring the reflection from the embedded components in concrete. One way to improve the detection of the echo is to reduce the interference due to Rayleigh wave by proper transducer design. Therefore further development would be to investigate the transducer design.

7- The ability of the pitch-catch method to detect other types of artefacts needs to be investigated. For example, a common type of flaw in concrete structures is honeycombing (concrete that is not fully consolidated).

8- Field testing of the proposed pitch-catch method is essential. A practical and efficient field system must be assembled and evaluated under actual field conditions. The key component of this field system will be the development of rugged rolling transducers that can be easily coupled to vertical as well as horizontal surfaces.

9- It was found that the results depend on the equipment used such as transducers, amplification system, gains, quality of the electronics, etc. Therefore further work should investigate this.

It is hoped that the work presented in this thesis will form the basis for the development of a nondestructive test method that will be used for routine evaluation of reinforced and prestressed concrete structures. Moreover when this method of testing is used with other methods such as potential measurements, the accuracy and reliability of the results will be increased.

REFERENCES

- 1- Detection of Flaw in Reinforcing Steel in Prestressed Concrete Bridge Members, Signal Enhancement and Interpretation
F.N. Kusenberger, R.S. Birkelbach
Southwest Research Inst., San Antonio, Texas, Nov. 1983.
- 2- Reinforcement Corrosion and the Durability of Concrete Bridges
P. Vassie
Proc. Instn. Civ. Engs., Part 1, Vol.76, 1984, pp.713-723.
- 3- Prestressing Steels
K.W. Longbottom and G.P. Malett
The Structural Engineer, Vol.51, No 12, 1973, pp.455-471.
- 4- Construction of Prestressed Concrete Structures
b. Gerwick
John Wiley & Sons, 1971
- 5- Stress Corrosion in British Prestressing Wire
J. Gilchrist
Prestressed Concrete Development Group, Research Note PCR 1, 1965.
- 6- Cases of Damage Concrete Due to Corrosion of Prestressed Steel
Netherlands Committee for Concrete Research, Report No 49, July 1971.
- 7- FIP Commission on Durability
D. A. Andrews
Concrete, June 1971.
- 8- Corrosion of Reinforcement: an Assessment of Twelve Concrete Bridges after 50 Years Service
P.R. Vassie
TRRL Research report 78, Transport and Road Research, 1984.
- 9- Non-Destructive Methods for Field Inspection of Embedded or Encased High Strength Steel Rods and Cables
Prof. F.M. Burdekin
CAPCIS/UMIST, Phase 1, Rep. 851214, May 1986.
- 10- Metal Corrosion in Civil Engineering and Building
C. Hall
Building Course, UMIST, 1981.
- 11- Steel in Concrete: Part I, A Review of the Electrochemical and Thermodynamic Aspects
K.K. Sagoe-Crentsil, F.P. Glasser
MCR, Vol.41, No 149, 1989, pp 205-212.
- 12- Prestressing Steels
K.W. Longbottom and G.P. Malett
The Structural Engineer, Vol.51, No 12, 1973, pp.455-471.

- 13- Application of Acoustic Emission for Detection of Reinforcing Steel Corrosion in Concrete
M.S. Weng, S.E. Dunn, W.H. Hartt, and R.P. Brown
Corrosion-NACE, Vol.38, No 1, Jan.1982, pp. 9-14 .
- 14- Reinforcement Corrosion and the Durability of Concrete Bridges
P. Vassie
Proc. Instn. Civ. Engs., Part 1, Vol.76, 1984, pp 713-723.
- 15- Inspecting Concrete Bridges
R.J. Woodward
Physics Bulletin, Vol.35, No 4, 1984, pp 149-151.
- 16- Rapid Measurement of Concrete Cover on Bridge Decks
K.R. Moore
Public Roads, Sep. 1975, pp. 48-52.
- 17- The Magnetic Method for Measuring the Diameter and the Depth of Reinforcement Below the Surface of Concrete
L. Brukarski and A. Karminski
The 7th Int. Conf. on NDT, Paper No D-28, June 1973, pp 253-254.
- 18- Detection of Flaws in Reinforcing Steel in Prestressed Concrete Bridge Members
F.N. Kusenberger, J.R. Barton
Southwest Research Institute, Texas, 1981.
- 19- Study on Detection of Buried Steel Bar in Concrete with Electromagnetic Impact Driving Method
S. Motooka and M. Okujima
Jap. J. Appl. Phy., Vol.21, 1982, pp. 144-146.
- 20- Inspection and Monitoring of Concrete Structures for Steel Corrosion
R.D. Browne, P.L. Domone, and M.P. Geophagan
9th Offshore Technology Conference, Vol.1, Texas, 1977, pp. 571-572.
- 21- Electrochemistry of Steel Corrosion in Concrete
M. Stearn and A.L. Geary
J. Electrochem. Soc., Vol.104, No 56, 1957.
- 22- Electrochemistry of Steel Corrosion in Concrete Compared to its Response in Pore Solution
J.L. Dawson and P.E. Langford
Presented ASTM Meeting, Feb. 1986.
- 23- Application of Novel Techniques to the In-Site Inspection of Reinforcing Steel in Concrete
D.G. John et al
Presented at Science Symposium, NACE Corrosion/84, New Orleans, 1984.
- 24- Measuring the Corrosion Rate of Reinforcing Steel in Concrete
E. Escanlante et al
Report No FHWA/RD-84/0777 U.S. Department of Commerce, April 1984.

- 25- Application of AC Impedance Technique to Steel in Concrete
J.L. Dawson, L.M. Callow, K. Hladky, and J.A. Richardson
NACE Corrosion/79, 1979, p. 20.
- 26- On-Line Monitoring of Continuous Process Plant
J.L. Dawson, K. Hladky, and D.A. Eden
in D.W. Butcher (Ed), Ellis Horwood, 1983.
- 27- Use of AC Impedance Technique in Studies on Steel in
Concrete in Immersed Conditions
D.G. John, P.C. Searson, and J.L. Dawson
Br. Corr. J., Vol.16, No 2, 1981, pp. 102-106.
- 28- Radar as Applied to the Evaluation of Bridge Decks
T.R. Cantor and C.P. Kneetor
Transp. Res. Rec., No 853, 1982.
- 29- Review of Penetrating Radar as Applied to the NDT of
Concrete
T.R. Cantor
ACI SP 82-29, Detroit, 1984, pp 581-602.
- 30- Concrete Evaluation by Radar: Theoretical Analysis
A.V. Alongi, T.R. Cantor, and C.P. Kneetor
Transp. Res. Rec., No 853, 1982.
- 31- Location of Reinforcement by Induction Thermography
B. Hillemeir
SPIE, Vol.520, Nov.1984.
- 32- Experimental Study of the Capabilities and the Optimum
Parameters of Eddy Current Transducers for ND Inspection of
Structural Steel Ties
V.I. Karpov and N.N. Zatsepin
Trans. Defektoskopiya
Sov. J. NDT (USA), Vol.15, No 12, 1979, pp. 52-57.
- 33- A New NDT Method for Structural Integrity assessment
R.J. Savage and P.C. Hewlett
NDT International, April 1978, pp. 61-67.
- 34- Flaw Detection in Concrete by Frequency Spectrum Analysis of
Impact-Echo Waveforms
N. Carino, M. Sansalone, and N. Hsu
Int. Advances in NDT, Vol.12, 1986, pp 117-146.
- 35- Zur Frage der Fortplanzung Ultraakustischer Schwingungen
in Verschiedenen Korpern
S.Ya. Sokolov
ENT 6, 1929, pp. 454-461.
Means for Indicating Flaws in Materials
U.S. Pat.2, 164,125, 1937.

- 36- Improvements in or Relating for Flaw Detection and Velocity Measurement by Ultrasonic Echo Methods
D.O. Sproule
Brit. Pat.774675, 1952.
and Surface and Shear Wave Method and Apparatus
F.A. Firestone
U.S. Pat.2,439,139, 1943.
- 37- A Sonic Method to Determine Pavement Thickness
R. Muenow
J. of the PCA Research and development Laboratories, Vol.5,
No 3, 1963, pp. 8-21.
- 38- An Investigation of the Applicability of Acoustic Pulse Velocity Measurements to the Evaluation of the Quality of Concrete in Bridge decks
G. Swift et al
Texas Transportation Inst., College Station, RR 1307, 1971, pp. 29-39
- 39- Determining the Thickness of Concrete Pavements by Mechanical Wave: Directed Beam Method
G. Bradfield and E. Gatfield
Magazine of Concrete Research, Vol.16, No 46, 1964, pp. 31-34.
- 40- Pavement Thickness Measurement Using Ultrasonic Techniques
H. Mailer
Highway Res. Record, Vol.378, 1972, pp. 20-28.
- 41- Detecting Honeycombing, Depth of Surface Breaking Cracks and UngROUTED Ducts: An Impact-Echo Method
M. Sansalone and N. Carino
Concrete International: Design and Construction, ACI, April 1988.
- 42- Initial Studies of Ultrasonic Testing of Prestressing Wires
W.T. Damaj
M.Sc. Dissertation, UMIST, 1986.
- 43- Laboratory Evaluation of Ultrasonics for Crack Detection in Concrete
L.I. Knab, G.V. Blessing, and J.R. Clifton
ACI J., Jan.-Feb. 1983, pp. 17-27.
- 44- Assessing Fire Damage of Concrete by the Ultrasonic Pulse Technique
H.W. Chung and K.S. Law
The American Society for Testing and Materials, 1985, pp 84-89.
- 45- Inspection of Prestressing Cables in Bridges
No author
Indian Concrete J., Vol.61, No 2, Feb. 1987.
- 46- A Sonic Method for the Detection of Deep Cracks in Large Structures
K. Nand et al
Indian Concrete J., March 1974, pp. 99-102.

- 47- Caisson Evaluation by Stress Wave Propagation Method
H. Steinbach and E. Vey
J. Geotechnical Eng. Div., ASCE, Vol.101, GT4, April 1975, pp.361-372
- 48- The detection of Voids in Concrete Piles Using Sonic Methods
I. Fegen, M.C. Forde, and H.W. Whithington
Proc. 4th Colloque Int. sur les Methodes de Control Non-Destructif, Grenolbe, Sep. 1979, pp. 40-46.
- 49- Les Possibilites d'application de L'analyse Frequentielle au Controle Non-Destructif par Ultrasons
J. Dory, C 24, pp.385-390.
- 50- Erosion Rate Measurements Using an Acoustic Technique
H. Sutherland and L. Kent
Rev. Scientific Instruments, Vol.48, No 8, Aug.1977, pp.1010-1016.
- 51- Development of Ultrasonic Methods for the ND Inspection of Concrete
T. Claytor and W. Ellington
Ultrasonics Symposium Proc., Halifax, Nova Scotia, July 1983, 8pp.
- 52- The Use of Surface Scanning Waves to Detect Opening Cracks in Concrete
R. Smith
Pres. at Int. Conf. on In Situ/NDT of Concrete, Ottawa, 1984.
- 53- The Use of Sonic Non-Destructive Techniques for Masonry Structures
F.K. Birjandi
Ph.D. Thesis, Edinburgh University, 1986.
- 54- Low Frequency NDT Testing of Historic Structures
M.C. Forde and A.J. Batchelor
3rd European Conference on NDT Testing, Florence, 1984, p.316-324
- 55- Acoustic Emission on Wire Ropes
T. Casey and J. Taylor
Ph.D. Thesis, University College, Swansea, Wales, 1984.
- 56- A Report on The Pulsed Acoustic Emission Technique Applied to Masonry
J.D. Leaird
J. Acoustic Emission, Vol.3, No 4, pp. 204 - 210.
- 57- Application of Acoustic Emission to Detection of Reinforcing Steel Corrosion in Concrete
M.S. Wang et al
Corrosion-NACE, Vol.38, No 1, 1982, pp.9-14.
- 58- Acoustic Emission Characterization of Corrosion Induced Damage in RC
S.E. Dunn et al
NACE/Corrosion/84, New Orleans, 1984, pp. 339 - 347.
- 59- Survey of Structures by Using Acoustic Emission Monitoring
J.L. Robert and M.B. Rolland
IABSE Reports, No 39, 1982, pp 33-38.

- 60- An Appreciation of the Schmidt Rebound Hammer
J. Kolek
MCR, No 28, 1958, and ICE, NDT of Concrete and Timber, 1970, pp. 19-22.
- 61- Utilisation of the Electron Probe Microanalyser in Highway Materials Analysis
W.T. Parry and C. Chahas
Feasibility Study State Dep. of Highways Salt Lake City, Rep..
No UTAH-RR-500-992-PB-227 447/0, 1973.
- 62- New Method for Detecting Cracks in Concrete Using Fibre Optics
P. Rossi and F. Lemaou
Materials and Structures, Jan. 1989.
- 63- In-Situ of the Permeability of Concrete to Chloride Permeability
D. Whiting
ACI SP-82, 1984, and Materials Performance, Vol. 17, No. 12, 1978, p. 9.
- 64- On-Site Rapid Air Permeability Test for Concrete
Y. Kasai et al
ACI, Sp-82, 1984.
- 65- Evaluation of Techniques for Investigating the Corrosion of Steel in Concrete
P.R. Vassie
TRRL Supplementary Report 397, 1978.
- 66- Acoustic Inspection and Monitoring of Prestressing Tendons and Bars in Concrete Structures
Cur-Gouda (Ed)
Centre for Civil Engineering Research, Codes and Specification, in-House Publishing, Netherlands, 1986.
- 67- Ultrasonic Testing of Materials
J. Krautkrammer and H. Krautkrammer
Springer Verlag, 1983.
- 68- Wave Propagation Theory for Ultrasonic Testing
R.A. Nickerson
7th Int. Conf. on NDT, Warszawa, Paper C-14, 1973, pp. 295-308.
- 69- Non-Destructive Testing of Concrete
R. Jones
Cambridge University Press, 1962, pp 104.
- 70- Ultrasonic Testing
J. Szilard (Ed)
John Wiley and Sons, N.Y. 1982.
- 71- User Handbook for the Ultrasonic Test Instrument Type BPV
G. Steinkamp
Steinkamp Company, 1988.

- 72- Electronic Signals and Systems
P.A. Lynn
MacMillan Education, London, 1986.
- 73- Determination of the Geometry of Hidden Defects by
Ultrasonic Pulse Analysis Testing
O.R. Gericke
JASA, Vol.35, 1963, pp 364-368.
- 74- Ultrasonic Frequency Analysis
H.L. Whaley and K.V. Cook ^{pp. 61-66}
Mater. Eva., Vol.28, 1970, ^{and Vol.29, 1971, p. 182.}
- 75- Ultrasonic Frequency Analysis in NDT
L. Adler and H.L. Whaley
in Proc. 8th Int. Congress on Acoustics, London, 1974, pp. 416.
- 76- Ultrasonic Spectroscopy of a solid Inclusion in an Elastic
Solid
F. Bifulco and W. Sachse
Ultrasonics, May 1975.
- 77- Ultrasonic Spectroscopy of a Fluid-Filled Cavity in an
Elastic Solid
W. Sachse
JASA, Vol.54, 1974.
- 78- Measurements of Scattering from Bulk Defects
Proc. of the DARPA/AFWAL Review of Progress in Quantitative
NDE, Technical Rep. AFWAL-TR-81-4080, 1980.
- 79- Ultrasonic Characterization of Rough Cracks
L. Adler, and K. Lewis
in New Procedures in NDT
P. Holler (Ed), Springer-Verlag, 1983.
- 80- Spectral Analysis Technique of Ultrasonic NDT of Advanced
Composite Materials
F.H. Chang et al
NDT, 1974, Vol.7, No 4, p. 104.
- 81- Characterization of Periodic Rough Surfaces by Ultrasonic
Spectroscopy
F. Cohen, G. Quentin et al
8th World Conf. on NDT, Cannes, 1976, 3 F4, 8 pages.
- 82- Sizing Crack-Like Defects by Ultrasonic Means
M. Silk
in Reseach techniques in NDT, Vol.3, R. Sharpe (Ed)
Academic Press, New York, 1977, pp 51-98.
- 83- Frequency Dependent Interaction of Ultrasonic Waves with
Surface Breaking Cracks
D.W. Fitting and L. Adler
in New Procedures in NDT, P. Holler (Ed.), Springer-Verlag,
1983.

- 84- Ultrasonic Attenuation as a Measure of Void Content in Carbon-Fibre Reinforced Plastics
E.W. Stone, B. Clarke
NDT, June 1975, pp 137 - 145.
- 85- Testing Concrete by an Ultrasonic Pulse Technique
R. Jones and E.N. Gatfield
Road Research Technical Paper No 34, 1965, London.
- 86- A review of the NDT of Concrete
R. Jones
Symposium on NDT on Concrete and Timber, ICE, London, 1970, pp.1-7.
- 87- NDT of Concrete
R.H. Elvery and J.A. Forester
Progress in Construction Science and Technology, Medical and Technical Pub., 1971, pp 175 - 216.
- 88- NDT of Structural Concrete by the Pulse Technique
T.N. Ackroyd and R. Jones
Proc. 4th Int. Conf. on NDT, Butterworths, 1964, pp. 230-234.
- 89- NDE Technique for Detection and Characterization of Porosity
D.O. Thompson et al
in New Procedures in NDT
P. Holler (Ed), Springer-Verlag, N.Y. 1983.
- 90- Acoustic and Vibration NDT Testing of Piles in Glacial Tills
M.C. Forde, H.F. Chan, and A.J. Batchelor, pp. 243-251, 1982.
- 91- Sonic Investigation of Shear Failed Reinforced Brick Masonary Walls
F.K. Birjandi, M.C. Forde, and H.W. Whittington
Masonry International, Nov. 1984.
- 92- Model 6100, Universal Waveform Analyser
ANALOGIC
Volume I: Users Guide.
- 93- Utility of Split-Spectrum Processing in Ultrasonic ND Evaluation
J.L. Rose, P. Karpur, and V.L. Newhouse
Materials Evaluation, Vol.46, Jan.1988, pp. 114 - 123.
- 94- Digital Filters
M.H. Ackroyd
Butterworths, London, 1973.
- 95- Digital Signal Processing
A. Peled and B. Liu
John Wiley & Sons, 1976.
- 96- BASIC Digital Signal Processing
G.B. Lockhart and B.M.G. Gheetham
butterworths, 1989.

- 97- Mathematical Treatment on the Decay of a Vibrating System Due to the Emission of Sound Wave into the Surrounding Medium
Z. Sakadi and E. Takizawa
J. Phys. Soc. Jap., Vol 31, 1948, pp 235-241.
- 98- Etude Vibratoire des Pieux en Baton; Response Harmoniques et Impulsionnelle, Application au Controle
J. Paquet
Annales Inst. Tech. Batim., 21st year, No 245, May 1968, pp 789-801
- 99- Propagation of Longitudinal Waves and Shear Waves in Cylindrical Rods at High Frequencies
H.J. McSkimin
JASA, Vol.28, No 3, May 1956, pp 484 - 494.
- 100- Dispersion of Ultrasonic Pulse Velocity in Cylindrical Rods
L.Y. Tu and J.N. Brennan
JASA, Vol.27, No 3, 1955, pp. 550 - 555.
- 101- Testing of Concrete Structures (in)
J.H. Bungey
Surrey University Press, 1989.
- 102- Effects of Embedded Steel Bars upon Ultrasonic Testing on Concrete
H.W. Chung
Magazine of Concrete Research, Vol.30, No 102, March 1978, pp 19-25
- 103- Structure-Borne Sound
L. Cremer, M. Heckel, and E.E. Ungar
Springer-Verlag, 1973.
- 104- NDT of Concrete in Romania
I. Facaoru
Symposium on NDT on Concrete and Timber, ICE, London, 1970, pp 39-41
- 105- Ultrasonic Material Property Determinations
S. Serabian
in Materials Analysis by Ultrasonics, A. Vary (Ed.),
NDC, 1987, pp. 211 - 224.
- 106- Energy Losses of Sound Waves in Metals Due to Scattering and Diffusion
W.P. Mason and H.J. McSkimin
J. of Appl. Physics, Vol.37, Oct. 1948, pp. 940 - 946.
- 107- Ultrasonic Spectral Analysis for ND Evaluation
D. Fitting and L. Adler
Plenum Press, 1981.
- 108- Wave Propagation and Scattering in Random Media
A. Ishimaru
Academic Press, Vol.1 & 2, 1978.
- 109- The Scattering of Electromagnetic Waves from Rough Surfaces
P. Beckmann and A. Spizzichino
Macmillan, 1963.

- 110- Elastic Waves in Solids, with Applications to NDT of Pipelines
A.H. Harker
British Gas, Eyre & Spottiswoode ltd, 1988.
- 111- Quantitative Measurements of Laser-Generated Acoustic Waveforms
R.J. Dewhurst, D.A. Hutchins and C.B. Scruby
J. Appl. Phys, Vol.53, No 6, June 1982, pp. 4064 - 4071.
- 112- A Laser-Generated Standard Acoustic Emission Source
C.B. Scruby, H.N.G. Wadley, R.J. Dewhurst, and D.A. Hutchins
Materials Evaluation, Vol.39, No 13, 1981, pp. 1250 - 1254.
- 113- Laser-Generation as a Standard Acoustic Source in Metals
D.A. Hutchins, R.J. Dewhurst, S.B. Palmer, and S.B. Palmer
Appl. Phys. Lett., Vol.38, No 9, 1981, pp. 677 - 679.
- 114- Ultrasonic Waves and their Applications
S. Sokolov
Zhur. Tekh. Fiz., Vol.2, 1935, pp. 522 - 544.
- 115- Methods for the Computer Modelling of Ultrasonic Waves in Solids
L. Bond
in Reseach techniques in NDT, Vol.6, R. Sharpe (Ed) , pp. 107 - 147,
Academic Press, New York.
- 116- Mathematical Modelling in NDT
M. Blackemore and G.A. Georgiou (Eds)
Institute of Mathematics & Its Applications Conference Series
Oxford University Press, 1988.
- 117- Simulation of Transducer-Couplant Effects on Broadband Ultrasonic Signals
A. Vary
International Advances in NDT, Vol.8, 1981, pp. 167 - 200.
- 118- Acoustic Emission energy and Mechanisms of Plastic Deformation and Fracture
M. Mirabile
NDT, April 1975, pp. 77 - 85.
- 119- Acoustic Emission and Transient Waves in an Elastic Plate
Y.E. Pao and R.R. Ceranoglu
JASA, Vol.65, 1979, pp. 96 - 105.
- 120- Acoustic Emission Measurements on Reactor Pressure Vessel Steel
I.G. Palmer
Materials Science and Engineering, No 11, 1973, pp. 227.
- 121- Spectrum Analysis of Acoustic Emission
G. Curtis
NDT, April 1974.

- 122- Assessment of Structural Integrity by acoustic Emission
P.H. Hutton and D.L. Parry
Materials Res. and Standards, March 1971, pp. 25 - 32.
- 123- Identification of the Physical Mechanisms Underlying
Acoustic Emissions During the Cracking of Concrete
P. Rossi et al
Materials and Structures, Vol.22, 1989, pp. 194 - 198.
- 124- Acoustic Emission Applied to Study Crack Propagation in
Concrete
P. Rossi et al
Materials and Structures, Vol.22, 1989, pp 374 - 384 .
- 125- Application of Acoustic Emission to the Field of Concrete
Engineering
T. Uomoto
J. Acoustic Emission, Vol.6, No 3, 1987, pp. 137 - 144 .
- 126- Radar and Acoustic Emission Applied to Study of Bridge Decks
Suspension Cables and Masonry Tunnel
T. Cantor and C. Kneetor
Transp. Res. Rec., No 676, 1978.
- 127- Some Aspects of Defect Location and Assessment in Pressure
Vessels Using Acoustic Emission Techniques
D. Birchon, R. Dukes, and Mrs. J. Taylor
Second Int. Conf. Press. Vessel Tech., Vol.2, ASME, 1973.
- 128- Acoustic Emission Techniques Applied to Civil Engineering
Structures
R. Laloux et al
Bulletin de Liaison des Laboratoires des Ponts et Chousses,
No 139.
- 129- Acoustic Emission Characteristics in Concrete Diagnostic
Applications
M. Ohtsu
J. Acoustic Emission, Vol.6, No 2, 1987.
- 130- Acoustic Emission Methods for Flaw Detection in Steel in
Highway Bridges Phase I & II
P.H. Hutton and J.R. Skorpik
Fed. Highw. Adm., Rep. No FHWA-RD-78-97 & 98, 1978.
- 131- Damping Characteristics of AE Propagating through Concrete
K. Yamada and Y. Kosaka
J. of the Society of Material Science, Vol.36, July 1987.
- 132- Ultrasound in the Production and Inspection of Concrete
Part I: Applications
T.E. Kornilovich et al
Trans. from the Russian by T.S. Wood, 1965.
- 133- Sonic Testing of Reinforced Concrete
P.X. Bellini
Ohio Dept. of Transportation, Columbus, Ohio, Rep. no. DT 0174,
1973.

- 134- Detecting Defects and Detrioration in Highway Structures
CAPCIS/UMIST NCHRP 20-5, Jan. 1985.
- 135- The Influence of Reinforcement on Ultrasonic Pulse Velocity Testing
J.H. Bungey
In Situ/ Non-Destructive Testing of Concrete, ACI SP-82, 1984,
pp 229-24
- 136- Effects of Steel on Ultrasonic Measurements for Concrete Members
J.H. Bungey
IABSE, Venice Symposium, 1983, pp. 83-100.
- 137- Recommendations for Measurement of Velocity of Ultrasonic Pulses in Concrete
British Standards Institution
BS 1881: Part 203, London.
- 138- Estimate of Concrete Strength by Ultrasonic Pulse Velocity and Damping Constant
A. Galan
J. Am. Concr. Inst., Vol.64, Oct. 1967, pp 678-684.
- 139- Ultrasonic Pulse Attenuation as a Measure of Damage Growth during Cyclic Loading of Concrete
W. Suaris and V. Fernando
ACI Materials J., May/June 1987, pp. 185-193.
- 140- A Point Source-Point Receiver, Pulse-Echo Technique for Flaw Detection in Concrete
J. Carino, M. Sansalone, and N. Hsu
ACI J., Proceedings Vol.83, No 2, 1986, pp 199-208.
- 141- Pulse Velocity as a Measure of Concrete Compressive Strength
V. Sturupp et al
In Situ/NDT of Concrete, Sp-82, ACI, Detroit, 1984.
- 142- Ultrasonic Wave Velocities in Concrete
W.N. Reynolds et al
Magazine of Concrete Research, Vol.30, No 104, 1978, pp. 139-144.
- 143- The propagation of Ultrasonic Waves in Carbon Fibre Reinforced Plastics
S.J. Wilkinson, W.N. Reynolds
J. Physics, D: Applied Physics, Vol.7, 1974, pp.50-57.
- 144- Investigation of Applicability of Acoustic Pulse Velocity Measurements to Evaluation of Quality of Concrete in Bridge Decks
G. Swift and W.M. Moore
Highway Res. Record, Vol.378, 1972, and Vol. 451, 1973, pp. 44-52.
- 145- Laboratory Study of Flaw Detection in Concrete by the Pulse-Echo Method
N.J. Carino
In Situ/NDT of Concrete, ACI, Detroit, 1984, pp.557-579.

- 146- Acoustic Pulsing—a Technique for Remote Defect Monitoring
P.M. Bartle et al
The Welding Inst. Res. Bulletin, Sep. 1983, pp. 292-294.
- 147- Damage-Detection Monitoring Method for Offshore Platforms is Field-Tested
H. Crohas and P. Lepert
Oil and Gas Journal, Feb. 1982, pp.94-103.
- 148- Standard Test Method for Pulse Velocity Through Concrete
Americam Society for Testing and Materials
ASTM C597, Philadelphia.
- 149- ND Evaluation of Concrete Structures- Method and Applicability of NDT
Y. Kasai and T. Fuji
Nippon University, Japan Inst. Technology Inspection, 1988.
- 150- Verification of Strength Properties of Concrete Structures by NDT
K. Orantie and E. Punakallio
ESPOO (Finland): In-House Publishing, 1986.
- 151- Measurements of the Thickness of In-Place Concrete with Microwave Reflection
G.G. Clemena and R.E. Steele
Virginia Transportation Research Council, April 1985.
- 152- Vibration Measurements on Prestressed Concrete Bridges: A Study with a ND Test Method
K. Gylltoft and L. Kopp
Statens Provningsanstalt, Boras, Sweden, 1986.
- 153- Determining the Extent of Damage Due to Fire in Concrete Structures by Ultrasonic Velocity Measurements
K. Mani
Indian Concerte J., Vol.60, No 7, July 1986.
- 154- On Relations between Compressive Strength, Pulse Velocity, Dynamic E, and Lograthmic Decrement of Concrete
S. Ohgishi
The 5th Japan Congress on Testing Materials Non-Metallic Materials, pp. 123-126.
- 155- A Proposed Ultrasonic Inspection for Offshore Structures
M.D. Fuller et al
Materials Evaluation, Vol.41, April 1983.
- 156- In-Situ/NDT of Concrete, A Global Review
V.M. Malhorta
In-Situ/NDT of Concrete, SP-82, 1984, pp.1-17.
- 157- Diagnosing in Situ Concrete by Ultrasonic Pulse Technique
H.W. Chung and K.S. Law
Concrete International, Oct.1983, pp. 42-49.

- 158- Acoustic Inspection and Monitoring of Prestressing Tendons and Bars in Concrete Structures
W.R. De Sitter et al
Inst. of Applied Physics Tno-Th, Netherlands, April 1986.
- 159- The ND Physical Analysis of Concrete
W.N. Reynolds and S.J. Wilkinson
Br. J. OF NDT, Jan.1979, pp. 35-39 .
- 160- An Appraisal of the Ultrasonic Pulse Technique for Detecting Voids in Concrete
H.W. Chung
Concrete, Nov. 1978, pp 25-28.
- 162- Laboratory Evaluation of Ultrasonics for Crack Detection in Concrete
V.R. Knabb et al
J. of ACI, Vol.80, 1983, pp 17-27 .
- 163- Detecting Delaminations in Concrete Slabs with and without Overlays Using the Impact-Echo Method
N.J. Carino
ACI Materials J., March/April 1989, pp. 175-184.
- 164- Investigation of Prestressed Concrete Box Beam of an Elevated Expressway
A. Tork
Int. Conf. on Short and Mid Span Bridges, Toronto, 1982, Session 7.
- 165- Conditions within Ducts in Post-Tensioned Prestressed Concrete Bridges
R.J. Woodward
TRRL Laboratory Report 980, 1981.
- 166- The Capability of Ultrasonic Method for Fine Art Stone Object Investigation
J. Gembal
5th Int. Congress on Detrioration and Conservation of Stone, Lausanne, Vol.1, 1985, pp. 49-65.
- 167- Proceedings of the International Conference on NDT
H. Whittington, B. Topping, and M.C. Forde
London, 1983.
- 168- Methods to Investigate Prestressing Reinforcement
H.G. Kniess
Mitteilungsblatt Der Bundesaunstaly fur Wasserbrau, Vol.58, 1988.
- 169- Detecting Defects and Deterioration in Highway Structures
National Cooperative Highway Research Program
NCHRP Project 20-5, Topic 15-03, Sponsored by American Association of State Highway and Transportation.
- 170- A Sonic Method for the Detection of Deep Cracks in Large Structures
K. Nand et al
Inadian Concrete J., March 1974, pp. 99-102 .

- 171- Pavement Thickness Measurement Using Ultrasonic Techniques
S. Howkins et al
Highway Res. Rec., No 378, 1972, pp. 20-28.
- 172- Rapid Measurement of Concrete Pavement Thickness and
Reinforcement Location- Field Evaluation of ND Systems
National Cooperative Highway Research Program
NCHRP Report 168, Wash. D.C., 1976.
- 173- ND Evaluation of Pavements
F.B. Holt and J.W. Eales
Concrete Int. J., Vol.9, No 6, 1987.
- 174- Pavement Thickness Measurement Using Ultrasonic Pulses
M.J. Golis
Highway Res. Record, Vol.218, 1968, pp. 40-48.
- 175- Integrity Testing of Piles by the Shock Method
J. Higgs
Concrete, Oct. 1979, pp. 31-33.
- 176- From Theory to Field Experience with the ND Vibration Testing
of Piles
A.G. Davis, C.S. Dunn
Proc. Inst. Civ. Engrs., Part 2, Dec. 1974, pp. 571-593.
- 177- Drilled Shaft Integrity by Wave Propagation Method
T. Hearne et al
J. Geot. Eng. Div., ASCE, Vol.107, Oct. 1981, pp. 1327-1344.
- 178- Case Histories, Evaluation of Drilled Pier Integrity by the
Stress Wave Propagation Method
in Drilled Piers and Caissons, Vol II
C. Baker (Ed), ASCE, 1985.
- 179- Tomographic Analysis of Structural Materials
H. Ellinger, I.L. Morgan, R. Klinksiek, and F. Hopkins
SPIE, 1982.
- 180- ND Inspection of Overlaid Bridge Decks with Ground-
Penetrating Radar
G.G. Clemena
Transportation Res. Rec., No 899, 1983.
- 181- Gamma Radiography of Concrete
J.A. Forrester
Symposium on NDT on Concrete and Timber, ICE, London, 1970, pp. 1-13
- 182- Radiographic Inspection of Prestressed Concrete up to 1600mm
Wall Thickness Using a 9 Mev Linear Accelerator
F. Niehues et al
Int. Commit. NDT, Vol.1, Columbus, USA, 1985.

- 183- Television Inspection System Using High-Energy Radiation for NDT of Prestressed Concrete Bridges
J.C. Dufay
Deuteteche Gesellschaft fur Zerstorungsfreie Materialprufung,
Mainz, 1978.
- 184- Television Systems Using High Energy Radiation for NDT in Prestressed Concrete Bridges
J. Dufay
9th World Conf. NDT, Melbourne, Paper 5A-3, Nov. 1979, pp. 13-23.
- 185- The X-Ray Examination of Concrete
L. Mullins and H.M. Pearson
Civil Engineering and Public Works Rev., Vol.44, No 515, 1949.
- 186- Radiographic Inspection of prestressed Concrete up to 1600mm Wall Thickness Using a 9 Me Linear Accelerator
F. Niehues
Report For World Conference on NDT in Las Vegas 1985.
- 187- The application of Infrared Thermography in the Detection of Delamination in Bridge Decks
G.G. Clemena, and W.T. McKeel
Highway & Transp. Res. Council, Rep. No VHTRC-78-R27, 1977.
- 188- Using Microwaves in Industry
J. Allison
Engineering, Vol.21, No 4, 1972.
- 189- Detecting defects and Deterioration in Highway Structures
D.G. Manning (Ed)
NCHRP, Synthesis of Highway practice No 118, USA, 1985.
- 190- A New Method for Structural Integrity Assessment (SHRIMP Method)
J.R. Smith and J.L. Franks
NDT Int., Vol.11, No 2, 1978.
- 191- Temperature and Strain Fields Measurements in NDT
L.M. Rogers
Br. J. of NDT, July 1977.
- 192- Earth Resistivity Tests Applied as a ND Procedure for Determining Thickness of Concrete Pavements
Highway Res. Rec., No 218, 1968.
- 193- An Electrical Method for Evaluating Bridge Deck Coatings
D.L. Spellman and R.F. Stratfull
Highway Res. Rec., No 357, 1971.
- 194- In-Situ Determination of the Chloride Content of Portland Cement Concrete Bridge Decks
J.R. Rhodes et al
Federal Highway Administration, Rep. No FHWA/RD-80/030, 1981.
- 195- Factors Influencing Electrode Potential in Concrete
G. Grimide et al
Br. Corros. J., Vol.21, No 1, 1986, pp. 55-62.

- 196- Opportunities for NDT of Highway Structures
C. Galambos and C. McGoney
Materials Evaluation, July 1975.
- 197- The Practical Use of Ultrasonic Pulse Velocity Measurements
in the Assessment of Concrete Quality
H.N. Tomsett
MCR, Vol.32, March 1980, pp 7-16.
- 198- Application of Acoustical Holography to the Inspection of
Offshore Platforms
A. Stankoff et al
10th Offshore Technology Conf., Houston, 1978, pp. 2435-2440.
- 199- Cathodic Protection- Arresting Active Corrosion
A. Buttfield
Civil Eng., Aug.1987, pp. 39-42.
- 200- Corrosion Monitoring in Process Plant using advanced
Electrochemical Techniques
J.L. Dawson, W.M. Cox, D.A. Eden, K. Hladky.
Pres. 2nd Int. Conf. On-Line Surveillance and Monitoring,
Venice, May 1986.
- 201- Comments on Electrochemical Measurements of the Rate of
Corrosion of Steel in Concrete
C.M. Hansson
Cement and Concrete Research, Vol.14, 1984.
- 202- Measuring Steel-in-Concrete Corrosion with an Electrical
Resistance Probe
J.T. Keldsen
NACE Corrosion/123, 1978.
- 203- Half Cell Potentials and the Corrosion of Steel in Concrete
R.F. Stratfull
Calif. State Div. of Highways, Material and Research Dev.,
Rep. No CAS-HYMR-5116-7-72-PB-218-720/1
- 204- AC Impedance and Electrochemical Noise Measurements on
Reinforcing Bars in Concrete
P.C. Pearson et al
Paper Presented at "Electrochemical Methods in Corrosion
Testing and Research", Manchester, 1982.
- 205- An AC Impedance Study of Steel in Concrete
P. Lay et al
J. Appl. Electrochemistry, Sep. 1985.
- 206- The Significance of Carbonation Tests and Chloride Level
Determination in Assessing the Durability of Reinforced
Concrete
J.P. Theophilis and M. Bailey
Int. Conf. on Durability of Building Materials and
Components, Vol.3, Aug.1984.

- 207- Laboratory Testing and Monitoring of Stay Current Corrosion of Prestressed Concrete in Seawater
D. Cornet et al
ASTM Conf., 1980.
- 208- A Comparison of Linear Polarization and AC Impedance in the Determination of Corrosion Rates of Reinforcements Embedded in Concrete
J.A. Gonzalez et al
NACE Corrosion/85, 1985.
- 209- Electromagnetic screening by RC
J.A. Battilana
MCR, Vol.41, No 148, Sep.1989, pp. 163-169.
- 210- An Electromagnetic Method of Checking Reinforcements in Concrete (Position, Cover Thickness and Diameter of Reinforcements)
P.R. Rajagopalan
Research and Industry, Vol.28, No 4, 1983.
- 211- Electromagnetic Methods of Testing Metals
R. Hochschild
Progress in NDT, Vol.1, Heyood & Company, 1958.
- 212- ND Electromagnetic Testing of Corrosion of Reinforcing Rods in Concrete
L.Y. Frenkel
Trans. from Zashchita Metallov
Sov. J. NDT (USA), Vol.16, No 3, 1980, pp. 377-378.
- 213- Metal Corrosion
T.K. Ross
Oxford University Press, 1977.
- 214- Corrosion of Reinforcement and Prestressing Tendons
P.E. Halstead
Materiaux et Contructions, 1976.
- 215- Corrosion of Steel and its Monitoring in Concrete
Dep. of Industry, Guide to Practice in Corrosion Control No 7
HMSO, 1981.
- 216- The Corrosion of Steel in Environments Simulating the Liquid Phase of Concrete
P.R. Vassie
TRRL Supplementary Report 396, TRRL 1978.
- 217- Chlorides and Bridge Deck Deterioration
D. Spellman and R. Stratfull
Materials and Research Dep., California Div. of Highways,
1969, pp.38 - 49.
- 218- Corrosion Processes
K.N. Parkins (Ed.)
Applied Sciences, 1982.

- 219- Corrosion for Students of Science and Engineering
K.R. Trethewey and J. Chamberlain
Longman, 1988.
- 220- Corrosion of RC in Marine Environments- Methods of Inspection
L. Lemoine et al
Centre Francais de la Corrosion, Societe de Chimie
Industrielle, Paris.
- 221- Sorting Tests for Stress Corrosion Resistance of Cold Drawn
Prestressing Tendon
K.F. McGuinn and M. Elices
Br. Corr. J., Vol.16, No 3, 1981, pp. 132-139.
- 222- Corrosion of Prestressed Wire in Concrete
G.E. Monfore and G.J. Verback
J. ACI, Nov.1960, pp 491 - 515.
- 223- A Survey of Site Tests for the Assessment of Corrosion in RC
P.R. Vassie
TRRL Laboratory Report 953, 1980.
- 224- A Study of Prestressing Steel Effect of Stress Metallurgical
Structure and Environment
D.T. Klodt
Proceedings of 24th NACE Conference.
- 225- Exploratory Tests of Corrosion of Reinforcing Steel in
Concrete by X-Radiography
I. Sekine and M. Fujiuawa
Materials Evaluation, Vol.42, Jan.1984.
- 226- Corrosion of Reinforcement in Coverete Construction
E. Alan and P. Frame
Corrosion Monitoring of Steel in Coverete, 1983.
- 227- The Durability of Steel in Concrete
K.W. Treadway and C.L. Page
Anti-Corr. Methods and Materials, Vol.32, No 1, Jan.1985.
- 228- Field Test of Reinforcement Corrosion in Concrete
P. Fidjestol and N. Nilsen
Performance of Concrete in Marine Environment
SP 65-12, ACI, 1984.
- 229- Corrosion and Electrical Impedance in Concrete
B.B. Hope et al
Cement and Concrete Research, Vol.15, 1985, pp. 525-534.
- 230- Corrosion Monitoring of Steel in Concrete
J.L. Dawson
Corr. of Reinforcement in Concrete Construction,
A.P. Crane and E. Alan (Eds), Ellis Howood, 1983, pp. 175-191.
- 231- The Durability of Steel in Concrete: Part 2, Diagnosis and
Assessment of Corrosion-Cracked Concrete
Building Res. Establishment Digest, Digest 264, Aug.1982.

- 232- Corrosion of Metals in Concrete and Masonry Buildings
R. Heidersback and L. Lloyd
NACE Corrosion/85, 1985.
- 233- The Role of Hydrogen in Corrosion Cracking of Reinforcing Steel
V.G. Gavriilyuk et al
Trans. Fiziko-Khimicheskaya Mekhanika Materialov, Vol.17, No 1, Jan.1981, Plenum Pub. Corp. 1981, pp.38-41.
- 234- Corrosion Monitoring Using EMATS
B.J. Smith
Welding and Metal Fabrication, Aug./Sep. 1985, pp.256-257.
- 235- The Radiation Pattern from a Rationally Symmetric Stress Source on a Semi-Infinite Solid
R.L. Roderick
Metals Res. Rep., Brown University, 1950.
- 236- A Reappraisal of the Variability of Ultrasonic Transducers
B.H. Lidington and M.G. Silk
NDT, Aug. 1974, pp. 204 - 208.
- 237- Electromagnetic Acoustic Transducer for In-Plane and Plane-Normal Velocity Measurements
A. Arora and W.J. Pardee
J. NDE, Vol.3, No 2, 1982, pp. 85-91.
- 238- Measurements of Long. and Trans. Waves Radiated by a Compressional Source into Elastic Semispace
L. Fillipczynski
Proceedings of Vibration Problems, Warsaw, Vol.5, 1964, pp 89-93.
- 239- Some Factors which Affect the Performance of Ultrasonic Transducers
Br. J. NDT, Vol.22, No 15, 1980.
- 240- Sound Beam Directivity: a Frequency-Dependent Variable
T. Cross
NDT, April 1971, pp. 119-125.
- 241- Optimizing the Parameters of an Acoustic Locator
V.M. Morozov and V.I. Malyshev
Trans. in Sov. J. NDT (USA), March/April 1973, pp. 170-173.
- 242- Characteristical Sound Field Data of Angle Probes: Possibilities for their Theoretical and Experimental Determination
H. Wustenburg
The 7th Int. Conf. on NDT, Warazawa, 1973, Paper H03.
- 243- Interaction of Surface Waves with Surface Defects
R.F. Lumb et al
Mater. Evalth Vol.36, No 10, 1978, p.57.
and Proc. 7th Int. Conf. on NDT, Warsaw, 1973.

- 244- Scattering of Elastic Waves by Small Inhomogeneities
L. Knopoff and J.A. Hudson
JASA, Vol.36, No 2, Feb. 1964, pp. 338-343.
- 245- Ultrasonic Attenuation Caused by Scattering in Polycrystalline Metals
E.M. Papadakis
JASA, Vol.37, No 4, April 1965, pp. 711-717.
- 246- Revised Grain-Scattering Formulas and Tables
E.M. Papadakis
JASA, Vol.37, No 4, April 1965, pp 703-710.
- 247- Multiple Scattering of Elastic Waves by Cylinders of Arbitrary Cross Section, 1- SH Waves
V.K. Vardan et al
JASA, Vol.63, No 5, May 1978, pp 1310-1319.
- 248- Notes and References for the Measurement of Elastic Moduli by Means of Ultrasonic Waves
H.J. McSkimin
JASA, Vol.33, No 5, May 1961, pp 606-615.
- 249- Surface Waves at Ultrasonic Frequencies
E.G. Cook and H.E. VanValkenburg
ASTM Bulletin, May 1954, pp. 81-84.
- 250- Time-Frequency Domain Formulation of Ultrasonic Frequency Analysis
W.A. Simpson Jr.
JASA, Vol.56, No 6, Dec. 1974, pp 1776-1781.
- 251- Scattering of Elastic Waves in an Inhomogeneous Solid
T.S. Chow
JASA, Vol 56, No 4, Oct 1974, pp 1049-1051.
- 252- Ultrasonic Attenuation and Velocity in Two-Phase Microstructures
R.H. Latiff and N.F. Flore
JASA, Vol.56, No 6, Part II, June 1975, pp 1441-1447.
- 253- Long-Wavelength Scattering by Hard Spheroids
J.E. Burke
JASA, April 1966, pp 325-330.
- 254- Grain-Size Distribution in Metals and its Influence on Ultrasonic Attenuation Measurements
E.M. Papadakis
JASA, Vol.33, No 11, 1961, pp 1616-1621.
- 255- Scattering of Elastic Waves by Small Inhomogeneties
L. Knopoff and J. Hudson
JASA, Vol.36, No 2, 1964, pp 338-343.
- 256- Scattering of High-Frequency Sound Waves in Polycrystalline Materilas
A.B. Bhatia
JASA, Vol.31, No 1, 1959, pp 16-23, 1140-1142.

- 257- Single and Multiple Scattering of Elastic Waves in Two Dimensions
JASA, Vol.74, No 3, 1983.
- 258- Elastic Wave Dispersion in a Cylindrical Rod by a Wide-Band Short-Duration Pulse Technique
J. Oliver
JASA, Vol.29, No 2, 1957, pp. 189-194.
- 259- Dispersion of Ultrasonic Pulse Velocity in Cylindrical Rods
L.Y. Yu et al
JASA, Vol.27, No 3, March 1955, pp 550-555.
- 260- Elastic Waves and Vibrations of Thin Rods
J. Prescott
Phil. Mag., Vol.33, Oct. 1942.
- 261- Elastic Wave Scattering at a Cylindrical Discontinuity in a Solid
R.M. White
JASA, Vol.30, No 8, Aug. 1985, pp 771-779.
- 262- Waves Profiles Generated in Rods by a Short Shock Pulse
A.G. Ivanov et al
Sov. Phys. Acoust., Vol.23, No 2, March/April 1977, pp 182-183.
- 263- Transmission of Elastic Pulses in Metal Rods
D.S. Hughes et al
Phy. Review, Vol.75, No 10, 1949, pp 1552-1556.
- 264- Sound Scattering by Elastic Cylinders of Finite Length
I.B. Andreeva and V.G. Samovol'kin
Sov. Phys. Acoust., Vol.22, No 5, 1976, pp. 361-364.
- 265- Dispersion Relations of Waves in a Rod Embedded in an Elastic Medium
R. Parnes
J. of Sound and Vibration, Vol.76, No 1, 1981, pp. 65-75.
- 266- Ultrasonic Frequency Analysis
L. Adler, K.V. Cook, and W.A. Simpson
in Research Techniques in NDT, Vol. III
R.S. Sharpe (Ed.), Academic Press, 1977.
- 267- Frequency Dependent Interaction of Ultrasonic Waves with Surface-Breaking Cracks
D.W. Fitting and L. Adler
in New Procedures in NDT
P. Holler (Ed), Springer-Verlag, N.Y. 1983.
- 268- Ultrasonic Correlation Techniques
V.L. Newhouse and E.S. Furgason
in Research Techniques in NDT, Vol. III
R.S. Sharpe (Ed.), Academic Press, 1977.

- 269- Dispersion Effects in Ultrasonic Waveguides and their Importance in the Measurement of Attenuation
M. Redwood
Proc. Phys. Soc., Vol.B-70, 1957, pp 721 - 738.
- 270- Application of Elastic Scattering Theory for Smooth Flat Cracks to the Quantitative Prediction of Ultrasonic Defect Detection and Sizing
J.M. Coffey and R.K. Chapman
Nucl. Energy, No 22, 1983, p.319 - 333.
- 271- A Review of Current Ultrasonic NDT Developments in the UK
G.J. Curtis
NDT Centre, AERE, Harwell, Feb. 1975.
- 272- Numerical Filtering of Ultrasonic Backscattered Signals
H.J. Pongratz et al
in New Procedures in NDT
P. Holler (Ed), Springer-Verlag, 1983.
- 273- Acousto-Ultrasonics: Theory and Applications
J.C. Duke (Ed)
Plenum Press, 1988.
- 274- Spectral Analysis and its Application
G.M. Jenkins and D.G. Watts
Holden-Day, 1968.
- 275- Elastic Waves in Layered Media
Ewing et al
McGraw-Hill Book Company, 1957.
- 276- Fundamentals of Ultrasonics
J. Blitz
Butterworths, 1967.
- 277- Geophysical Signal Analysis
E.A. Robinson and S. Treitel
Prentice Hall, 1980.
- 278- Basic Digital Signal Processing
G.B. Lockhart and B.M.G. Cheetham
Butterworths, 1989.
- 279- Ultrasound: Principles and Practice
Short Course, DIAS, UMIST, 1985.
- 280- The Theory of Elastic Waves and Waveguides
J. Miklowitz
North-Holland, 1980.
- 281- Analytical Acoustics
F.B. Stumpf
Ann Arbor Science, Butterworth Group, 1980.
- 282- Mechanical Waveguides
M. Redwood
Pergamon Press, 1960.

- 283- Physical Acoustics and the Properties of Solids
W.P. Mason
Van Nostrand, 1958.
- 284- Sound Waves in Solids
H.F. Pollard
Pion ltd, 1977.
- 285- Shock and Vibration Handbook
C.M. Harris and C.E. Crede
McGraw-Hill Book Company, Sec. Ed., 1976.
- 286- Schlieren and Computer Studies of the Interaction of
Ultrasound with Defects
V.M. Baborovsky et al
NDT, Aug. 1973, p.200-207.
- 287- Ray Methods for Waves in Elastic Solids
J.D. Achenbach
Pitman, 1982.
- 288- Deconvolution of Geophysical Time Series in the Exploration
for Oil and Natural Gas
M.T. Silvia and E.A. Robinson
Elsevier, Amsterdam, 1978.
- 289- Multichannel Time Series Analysis with Computer Programs
E.A. Robinson
Goose Pond Press, Second Ed., 1983.
- 290- Longitudinal Impact of a Semi-Infinite Circular Elastic Bar
R. Skalak,
J. Appl. Mechanics, March 1957, pp 59-64.
- 291- Stress Pulse in Bar with Neck or Swell
H.C. Fisher
Appl. Science Res., Vol.4, 1954, pp 317-328.
- 292- Reflections and Transmission of Elastic Pulses in a Bar at a
Discontinuity in Cross Section
E.A. Ripperger and H.N. Abramson
Proc. Third Midwestern Conf. on Solid Mech., 1957, pp 135-145.
- 293- Properties of Cylindrical Boreholes as Reference Defects in
Ultrasonic Inspection
H. Wastenberg and E. Mundry
NDT, Aug.1971, pp.260-265.
- 294- Use of Ultrasonic Models in the Design and Validation of New
NDE Techniques
R.B. Thompson and T.A. Gray
Phil. Trans. R. Soc., A320, London, 1986, pp 169-179.
- 295- The analysis of Ultrasonic Wave Attenuation Spectra in Metals
W.N. Reynolds and R.L. Smith
Br. J. NDT, Sep. 1985, p. 291-294.

- 296- Basic Principles of the NDT of Metals
L. Weidman and P.M. Reynolds
The Metallurgist and Materials Technologist, July 1976, pp 373-382
- 297- Quality Control of Steel Products by Determination of Sound Attenuation
E. Kraiper
Proc. 4th Int. Conf. on NDT, Butterworths, 1964.
- 298- Determination of the RMS value h of the roughness of randomly rough surfaces
M. De Billy, B. Delmas, and J. Doucet
8th World Conf. on NDT, Cannes, 1976, 3 F^o, 8 pages.

ProQuest Number: U028311

INFORMATION TO ALL USERS

The quality and completeness of this reproduction is dependent on the quality and completeness of the copy made available to ProQuest.



Distributed by ProQuest LLC (2022).

Copyright of the Dissertation is held by the Author unless otherwise noted.

This work may be used in accordance with the terms of the Creative Commons license or other rights statement, as indicated in the copyright statement or in the metadata associated with this work. Unless otherwise specified in the copyright statement or the metadata, all rights are reserved by the copyright holder.

This work is protected against unauthorized copying under Title 17, United States Code and other applicable copyright laws.

Microform Edition where available © ProQuest LLC. No reproduction or digitization of the Microform Edition is authorized without permission of ProQuest LLC.

ProQuest LLC
789 East Eisenhower Parkway
P.O. Box 1346
Ann Arbor, MI 48106 - 1346 USA